Low Power IoT based Automated Manhole Cover Monitoring System as a Smart City application

A thesis submitted in partial fulfilment of the requirement of Staffordshire University for the degree of Doctor of Philosophy

Hesham Hamdy Gaber Ahmed Aly

11020838

School of Creative Arts and Engineering

Staffordshire University

March 2019

ACKNOWLEDGEMENTS

ABSTRACT

With the increased population in the big cities, Internet of Things (IoT) devices to be used as automated monitoring systems are required in many of the Smart city's applications. Monitoring road infrastructure such as a manhole cover (MC) is one of these applications. Automating monitoring manhole cover structure has become more demanding, especially when the number of MC failure increases rapidly: it affects the safety, security and the economy of the society. Only 30% of the current MC monitoring systems are automated with short lifetime in comparison to the lifetime of the MC, without monitoring all the MC issues and without discussing the challenges of the design from IoT device design point of view. Extending the lifetime of a fully automated IoT-based MC monitoring system from circuit design point of view was studied and addressed in this research. The main circuit that consumes more power in the IoT-based MC monitoring system is the analogue to digital converter (ADC) found at the data acquisition module (DAQ).

In several applications, the compressive sensing (CS) technique proved its capability to reduce the power consumption for ADC. In this research, CS has been investigated and studied deeply to reach the aim of the research. CS based ADC is named analogue to information converter (AIC). Because the heart of the AIC is the pseudorandom number generator (PRNG), several researchers have used it as a key to secure the data, which makes AIC more suitable for IoT device design. Most of these PRNG designs for AIC are hardware implemented in the digital circuit design. The presence of digital PRNG at the AIC analogue front end requires: a) isolating digital and analogue parts, and b) using two different power supplies and grounds for analogue and digital parts. On the other hand, analogue circuit design becomes more demanding for the sake of the power consumption, especially after merging the analogue circuit design with other fields such as neural networks and neuroscience.

This has motivated the researcher to propose two low-power analogue chaotic oscillators to replace digital PRNG using opamp Schmitt Trigger. The proposed systems are based on a coupling oscillator concept. The design of the proposed systems is based on: First, two new modifications for the well-known astable multivibrator using opamp Schmitt trigger. Second, the waveshaping design technique is presented to design analogue chaotic oscillators instead of starting with complex differential equations as it is the case for most of the chaotic oscillator designs. This technique helps to find easy steps and understanding of building analogue chaotic oscillators for electronic circuit designers.

The proposed systems used off the shelf components as a proof of concept. The proposed systems were validated based on: a) the range of the temperature found beneath a manhole cover, and b) the signal reconstruction under the presence and the absence of noise.

The results show decent performance of the proposed system from the power consumption point of view, as it can exceed the lifetime of similar two opamps based Jerk chaotic oscillators by almost one year for long lifetime applications such as monitoring MC using Li-Ion battery. Furthermore, in comparison to PRNG output sequence generated by a software algorithm used in AIC framework in the presence of the noise, the first proposed system output sequence improved the signal reconstruction by 6.94%, while the second system improved the signal reconstruction by 17.83%

CONTENTS

List of Figures

List of Tables

Abbreviations

Abbreviations	Explanation
MC	Manhole cover
PZT	Piezoelectric Transducer (Lead Zirconate Titanate)
ADC	Analogue to digital converter
AIC	Analogue to information converter
PRNG	Pseudorandom Number Generator
FPAA	Field Programmable Analogue Array
IoT	Internet of Things
LFSR	Linear Feedback Shift Register
SHM	Structural Health Monitoring
NR	Negative Resistance
DAQ	Data Acquisition
SC	Smart City
CS	Compressive Sensing
FPGA	Field Programmable Gate Array
PGA	Power Gain Amplifier
LNA	Low Noise Amplifier
CU	Control Unit
MUX	Multiplexer
WSN	Wireless Sensor Network
WSNN	Wireless Sensor Network Node
SCADA	Supervisory Control and Data Acquisition
TRNG	True Random Number Generator
HRNG	Hybrid random number Generator
VOA	Voltage opamp
CFOA	Current feedback opamp
RD	Random demodulator
CTSS	Continuous-Time Spectrally-Sparse Sampling
OMP algorithm	Orthogonal Matching Pursuit

Chapter 1
Introduction

1- INTRODUCTION

Urban cities have been attracting people to live in. Due to the growth of the population, cities utilities and resources are suffering from the rising number of utilities failure and resources consumption. Modern governments normally monitor these utilities and resources to overcome the population growth effect by using new monitoring technologies.

Monitoring and controlling the city utilities, resources and the services using the new monitoring technologies is a strategy named "Smart City". To clear this point, smart city can be defined as mentioned in [1]: " Smart City is a city which functions in a sustainable and intelligent way, by integrating all its infrastructures and services into a cohesive whole and using intelligent devices for monitoring and control, to ensure sustainability and efficiency". Smart City has many branches from the sensing technology viewpoint as shown in Figure 1-1.
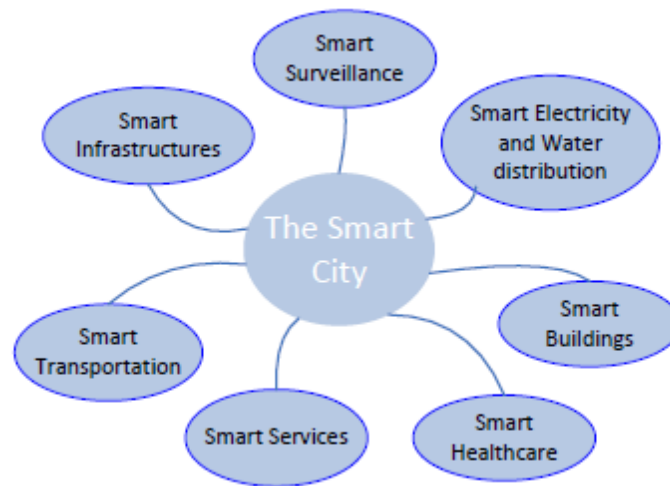
Figure 1-1 Smart City [1]

Due to the huge developments in the communication systems technologies and the internet, the goal now in the smart city concept is to connect the infrastructures and the services via the internet cloud.

Smart city communication based on internet of things (IoT) cloud is still in the early stages; it is starting to appear in several smart city applications. For example, smart healthcare using wearable medical devices connected to the internet is starting to spread very fast and extending from monitoring patients to being used for monitoring the human health in daily life from several perspectives. When monitoring devices are connected to the cloud, they are called IoT devices. This connection adds more challenges to the monitoring system design like security, privacy, big data, and more.

As reported in [1], smart infrastructures are one of the smart city fields for which applications are required. Infrastructures include underground utilities, which are considered as the vein for any city [2] because most of these infrastructures are commonly used by the people like electrical, water/sewer, natural gas systems, etc. These utilities are designed to be accessed and monitored via a room called "manhole".

Manholes are composed of many structures[3]. One of these structures is the manhole cover (MC). MC is like a door between two different environments: Upper ground and underground environment. As manhole locations can be found all over the cities, MC structure can be affected, and its failure affects the safety, security and the economy of the cities.

Generally, monitoring utilities have two types: automatic and manual. Automatic type means that no human effort has to be done to monitor these utilities; however, the monitoring system is designed to send the data via wireless or wired systems. The other type is manual monitoring, which is based on a human effort to go to the utility location for monitoring regardless of the technologies used to monitor. Automated monitoring systems cost less and are very fast in comparison to the manual ones. However, they are still in the early stages because of several challenges. It is noteworthy that monitoring systems based on IoT cloud which is used for Smart city applications are called nowadays "IoT device". The IoT device for monitoring MC normally needs to be placed beneath the MC to prevent any harm to pedestrians or the traffic and is connected to the base station then to the cloud. Information is then transferred to the organisation that is concerned about the manhole cover and the utilities under it.

The IoT based automated MC monitoring system is composed mainly of Sensors, Data Acquisition system (DAQ), Control Unit (CU), Communication unit, and Power unit as shown in Figure 1-2. Based on the study done by the researcher, power consumption is one of the main challenges for designing the IoT based automated MC monitoring system. An analogue to digital converter (ADC) found in the DAQ unit is the circuit with the highest power consumption which needs to be redesigned to reduce the amount of power consumed.
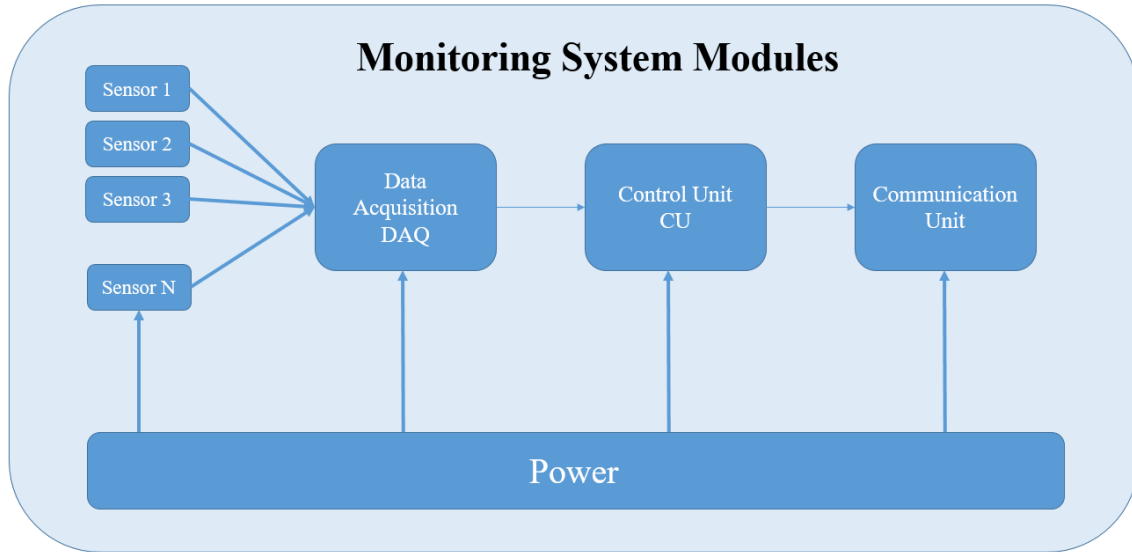
Figure 1-2 IoT device based automated MC monitoring system

While most of the designs of IoT devices is based on digital circuit design techniques because it is robust to noise and easy to program, analogue circuit design can be considered as another route to overcome the same challenges with significant results especially for power consumption and security [4].

From this point of view, the research is focusing on designing a low-power, secured ADC based on analogue circuit design techniques to be used in the DAQ unit for the IoT based automated MC monitoring system. The research uses the off-shelf components and a design using a printed circuit board (PCB) for the sake of simplicity and to achieve an optimum design with acceptable low cost.

The main reason that makes an ADC circuit the unit which consumes more power is using a high sampling rate as it will be shown later. The sampling rate for a traditional ADC is based on the bandwidth of the signal which is for the DAQ unit the sensors signal bandwidth. Based on the study done by the researcher as will be introduced at the end of Chapter 2, the sensors' signal can reach 5 MHz frequency range. The minimum required sampling rate for the traditional ADC is at least double the signal bandwidth (Nyquist Shannon sampling theorem).

On the other hand, an IoT device designer needs to take all the design challenges into his/her considerations. There are several challenges besides the power consumption which must be considered like security, huge data, and cost, etc. Several techniques have been addressed to optimise these challenges. However, the compressive sensing technique is more attractive because of its basic design which has the ability to reduce the power consumption and the amount of data at the same time.

Compressive Sensing (CS) theory introduced in 2002 claims that sampling rate of the ADC can be reduced to less than the Nyquist Shannon rate if the signal has a sparse representation in one of the known domains like the frequency domain. Fortunately, most of the sensor signals are sparse in some domains like the frequency domain [5]. The sparse representation means that the signal is sparse in a specific domain if most of its values in this domain are equal to zero. Another advantage of reducing the sampling rate is the reduction of the memory size because the number of bits needed to represent the analogue signal will be reduced.

Compressive Sensing based ADC is called Analogue to Information Converter (AIC). The reason for this name is that CS is targeting the information in the signal more than its bandwidth. As for sparse signals, the information content is less than the bandwidth; the ADC sampling rate requirement will be reduced in comparison without reducing the sensor signal bandwidth. AIC has several architectures like Random Demodulation (RD), Random Modulator Pre-Integrator (RMPI), Xampling…etc. This research will focus on RD only because of its simplicity.

The central part of most of the AIC architecture is the random number generator (RNG). RNG has to generate random (-1, 1) or (0,1) sequence with a rate equal to or more than Nyquist Shannon rate. Most of the RNG used in AIC is a pseudorandom generator (PRNG) designed by linear shift register (LFSR) technique. LFSR is a very well-known digital circuit that generates PRNG. However, this digital circuit is found in the analogue front end of the AIC, which means isolation is required between the analogue and digital parts to prevent crosstalk and noise. Another disadvantage of using LFSR in AIC analogue front end is the security factor. While LFSR generates random signals, it suffers from the lack of security. This point is very important from the IoT device design viewpoint and motivated several researchers to develop the CS to make it acceptable from the security point of view.

However, most of these efforts were based on digital circuit design by developing or replacing LFSR with more complex digital design and mainly based on digital chaotic oscillator design. Chaotic oscillators can be presented in an analogue and digital manner. Because chaotic oscillators are based on differential equations that model the dynamic behaviour of the oscillators, an analogue hardware implementation for chaotic oscillators consumes less power than digital hardware implementation as will be shown later in this research. Furthermore, analogue circuit design becomes more attractive from the power consumption point of view through merging the analogue circuit design with other fields like neuroscience and biology. This point was highly motivating to study and investigate the ability

to design low power analogue chaotic oscillator to replace LFSR taking into consideration the security issue.

As a starting point of the research, an analogue Chua circuit chaotic oscillator will be tested in AIC framework as it is considered as the basic circuit to implement chaos theory. The motivation for using the Chua circuit is the simplicity with few numbers of components required. Chua circuit is one of the mostly used circuits in communication applications for encryption and is used to generate random numbers in some applications [6].

The chaotic sequence has been studied before in the CS theory and shows good performance for signal reconstruction. However, implementing the analogue chaotic circuit in AIC framework has not been performed until now to the knowledge of the author. This has motivated the researcher to study the use of the analogue chaotic oscillator circuit to identify the hardware limitations and the design trade-off.

The proposed systems are based on coupling oscillators. The coupling oscillators concept is starting to get more attention from the scientists as it can be used in several fields like neuroscience, neuromorphic engineering and analogue circuit design. Generally, a chaotic oscillators design starts from modelling the chaotic system in differential equations form to model the dynamic behaviour. In this research, another circuit design technique will be presented which is the waveshaping technique.

The waveshaping technique is well known for design relaxation oscillators. This technique is based on studying the effect of charging and discharging the energy storage elements in the presence of the resistors and/or diodes to reshape the input signals. The technique is very easy to understand and does not require extensive differential equation analysis as in the traditional chaotic oscillator design and analysis.

The relaxation oscillator circuit design can be implemented by means of transistors or opamp. The Opamp Schmitt trigger-based relaxation oscillator will be used for implementing the proposed systems. The two main motivations to use opamp Schmitt trigger are:

1- The simplicity of the design.
2- Schmitt trigger is one of the main blocks for designing field programmable analogue array (FPAA), which gives the advantage of controlling the analogue design by programming. This point is more important when the hardware implementation of the compressive sensing is based on FPAA, which has been done before and still promising for more development especially after applying the neuromorphic engineering concept on analogue design as will be shown later.

In this thesis, two modifications are presented for an opamp Schmitt trigger. These modifications mimic the effect of coupling oscillators between two biological oscillators which leads to chaotic behaviour which is the main target of the design.

PSpice software was used for simulating the analogue Chua circuit and the proposed systems. Hence, the output of the PSpice will be fed to Random Demodulation based AIC framework implanted in Matlab software. Besides the simulation, hardware implementation takes place by using the Texas Instrument Analog System Lab Kit which shows the simplicity of designing the proposed systems.

The proposed systems are simulated based on: a) the range of the temperature found beneath MC (-30ºC – 60ºC), and b) the presence and the absence of the noise. The proposed systems are also validated by comparing them with a Jerk chaotic oscillator using two opamps which has the same number of the active elements. The validation results show the good performance of the proposed systems from the power consumption and the signal reconstruction viewpoints especially the second proposed system.

The proposed systems can be found in the same PCB or IC with using only two opamps. This point is very attractive from the security perspective because of the fewer resources required. Because the study uses off the shelf components, it is expected to develop for what is now called open source hardware to be used for the IoT hardware design.

1.1. Aim

This research aims to investigate and design a low-power IoT-based manhole cover (MC) monitoring system to be used for smart city applications taking into consideration the IoT device design requirements and challenges.

1.2. Objectives

To reach the aims mentioned above, several points need to be achieved as follows:

- Critically surveying the existing problems and researches for the Manhole Cover and its monitoring systems (literature review). The results and analysis from this survey are used to identify and list the main challenges for designing automated MC monitoring system from the Smart city and IoT point of view (Chapter 2)

- Investigating Compressive sensing and the analogue circuit design techniques to reduce the power consumption for IoT -based manhole cover monitoring system (Chapters 3 and 4).

- Developing an improved performance technique suitable for reducing the power consumption of the IoT -based manhole cover monitoring system (Chapters 5 and 6)

- Validating the developed technique using simulation results and hardware implementation and examining the power consumption and the thermal effect of the signal reconstruction for the proposed systems, based on the range of the temperature found beneath the manhole cover. (Chapter 6)

1.3. Thesis Contributions

1- This research proposed a new detailed classification for manhole cover issues and the current monitoring systems. The proposed classification covers the influence of the environment found beneath or above the manhole cover. This classification is recommended to be used by the modern governments which seek the development of their societies from the smart city point of view. Furthermore, the classification shows the lack of using the automated monitoring systems for manhole cover and how much damages and losses can be avoided by changing the monitoring systems from manual to automated systems.

2- This research studies for the first time replacing complex digital pseudorandom number generator (PRNG) found in the analogue information converter (AIC) analogue front end, for the sake of the power consumption and the security. This study leads to the use of analogue chaotic oscillators, which exhibits more enhancement for the AIC analogue frontend design from the perspective of power consumption and security compared with digital design.

3- The research proposed the use of the waveshape design concept to design analogue chaotic oscillators without the need to start by complex differential equations which describe the behavior of the dynamic systems of the chaotic oscillators. In this research, the waveshaping design concept was thus used to design analogue chaotic oscillators based on coupling oscillators found in neuroscience, with few steps which can be widely used for neuromorphic oscillators design.

4- This research proposed a new vision for design by using an opamp Schmitt trigger which mimic biological oscillators. Furthermore, as an opamp Schmitt trigger is one of the main blocks of the field programmable analogue array (FPAA), the proposed vision can be easily implemented and re-programmed which gives more richness to using an opamp Schmitt trigger.

5- This research proposed two low-power analogue chaotic oscillators using 2 opamps Schmitt trigger based on coupling oscillators. The proposed systems design offers an innovative analytical and methodological approach based on contributions 3 and 4. The design of the proposed systems combines between new vision of analogue chaotic oscillator design based on neuromorphic engineering with hardware implementation and software simulation. The proposed systems are implemented to replace the traditional digital PRNG found in the AIC analogue frontend. The proposed systems have been implemented and simulated under the temperature range found beneath the manhole cover. The validation takes place by comparing the proposed systems with another 2 opamps based Jerk chaotic oscillators. The validation proved the good performance of the proposed systems, especially the second system from the power consumption and the security point of view. The validation extends to compare between the output chaotic sequence from the proposed systems and the random sequence based on numerical algorithm that can be implemented using digital circuit. This comparison shows the ability of the proposed systems to reconstruct the original signal more accurately than the numerical algorithm in the absence and the presence of the noise.

6- As the proposed systems were implemented using off the shelf components, it is expected that the proposed systems will enhance the IoT device based on open source hardware from the power consumption point of view which is the main disadvantage found in these devices. Furthermore, the proposed systems developed an IoT device based on open source hardware using neuromorphic engineering which is still in its early stage and is expected to be widely used in the near future.

1.4. Outline

Based on the aim of this research and the previous objectives, this thesis is organised as follows: Chapter 2 covers the first point of the objectives. It shows the MC issues by survey and deep analysis with new classification attached to the current automated monitoring system used.

Chapter 3 covers the third point in the objectives and introduces the basics of the CS theory and the need for using the random signal with a brief introduction for the AIC and the analogue Chua circuit.

Chapter 4 gives an extension for the third objective by presenting the simulation study with analysis of implementing the analogue Chua circuit in the AIC framework. This Chapter

16

introduces the analogue chaotic oscillator for the first time to the knowledge of the author to the AIC analogue front end design.

Chapter 5 is the foundation of the proposed systems presented in the following chapter and covers the fourth objective. It gives a brief introduction to the coupling oscillators, followed by the new modifications for the opamp Schmitt trigger.

Chapter 6 presents the proposed systems and the design validation with a discussion of the results from the power consumption and signal recovery points of view.

Chapter 7 presents the conclusions and future work.

1.5. Publications

1- Hesham H. Aly, Abdel Hamid Soliman, Mansour Mouniri., "Towards a Fully Automated Monitoring System for Manhole Cover," IEEE First Int. Conf. Smart Cities, 2015. [Published]

2- Hesham H. Aly, Abdel Hamid Soliman, and Mansour Mouniri. "Analogue to information converter design using analogue Chua circuit for IoT devices." In Proceedings of the Second International Conference on Internet of things, Data and Cloud Computing. ACM, 2017. [Published]

Chapter 2

Manhole Cover Issues and Current Monitoring Systems

2. MANHOLE COVER ISSUES AND CURRENT MONITORING SYSTEMS

This chapter discusses the manhole cover (MC) issues and the current monitoring systems. First, the need of automated MC monitoring system is highlighted, and the effect of MC structure failure impact on the society from the safety, security and economy point of view is also discussed. MC issues are classified based on the environmental effect on the MC structure.

The classification identifies the current automated and manual monitoring systems used to monitor MC issues. Hence, a discussion is presented to evaluate the current automated monitoring MC techniques and identify the main challenges and requirements to design an IoT -based automated MC monitoring system.

Power consumption is the main challenge facing the design of an IoT based automated MC monitoring system. The data acquisition (DAQ) module is the main source of consuming power as will be shown later in this chapter. Analogue to digital converter (ADC) is the circuit which is responsible for increasing the power consumption of the DAQ module. This is because of the high sampling rate for the ADC and the need to activate the DAQ module most of the time in comparison to other modules. Several techniques can be used to design low power consumption for the ADC circuit.

Based on the study done by the researcher, compressive sensing (CS) theory is promising to give acceptable results to design low power ADC. Furthermore, the CS framework is very attractive to design an automated monitoring system based on IoT device design requirements.

Besides, an intensive study is presented in this chapter and extended in Appendix I to identify the sensor types and bandwidth required for fully automated MC monitoring system. This point is very essential to address the sampling rate required for the ADC found in the DAQ module.

This chapter is organised as follows: First, the MC structure failure impact on the society will be discussed. Classification of MC issues and the available monitoring systems is shown in the second section of this chapter. Analysis and discussion of the MC issues and identifying the requirements and the challenges for designing IoT based automated MC monitoring system takes place in the third section. The fourth section discusses the sensor

type selection as a first step to design a low power ADC circuit in the DAQ module for IoT based automated monitoring system. The last section is the conclusion of this chapter.

2.1.   Manhole Cover and its failure's impact

MC, as mentioned before, is like a door between two different environments. Each environment affects the MC structure and this effect differs according to the MC material types. Generally, MC can be fabricated from several materials like cast iron or composite like fibre reinforced plastics and other materials as shown in Figure 2-1. The type mostly used all over the world and found intensively in the roads is the cast iron.
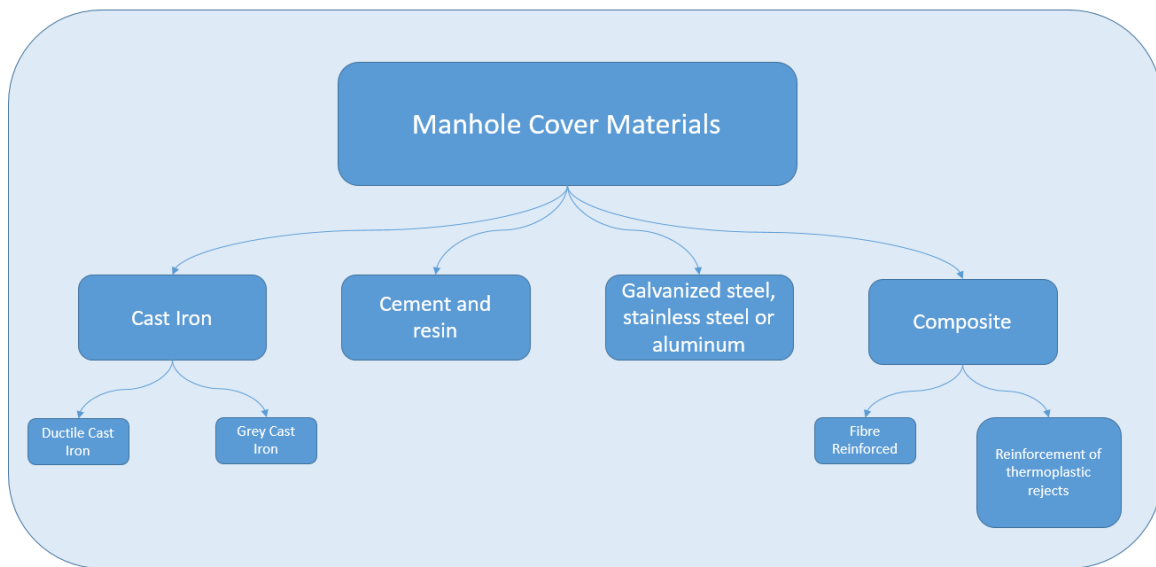
Figure 2-1 MC materials

Besides, any MC design has to follow the country's specifications. For example, in the UK, BSI British Standards is the UK's national standards organisation that produces standards and information of products that promote and share best practice. The code which begins with "BS EN 124" is the code for gully tops and manhole tops for vehicular and pedestrian areas. Based on the location of manhole it is classified into several classes as shown in Figure 2-2. The type that will be considered in this study mainly is Group 4 which includes carriage and roads (heavy duty) which is called BS EN124 Class D400.
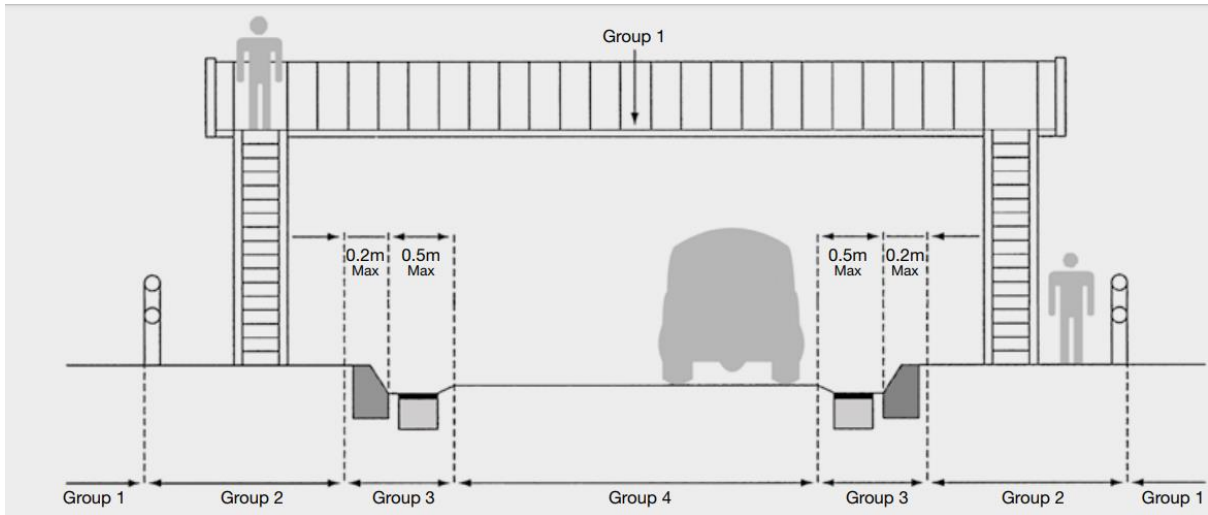
Figure 2-2 British Standard BS EN124 Specs

MCs are mainly located on the road. This location makes it attached to the pedestrians and any failure of its structure harms people, especially motorbikes and bikes riders. The Motorcycle Action Group (MAG) has mentioned on its website [7] several problems of the MC structure. MC structure defects can cause injuries and accidents.

The UK government reported the statistical release for the road casualties for 10 years as shown in Figure 2-3[8]. For 10 years the motorcycle accidents approximately did not change in comparison with the car accidents that have been rapidly reduced within the same period, while the cyclist accidents have slightly risen in the same period. Accident sources are several, one of them is the MC structure failure. Automating the monitoring of MC will contribute in fast warning about any MC failure or defects that cause accidents which will improve the safety and security of people.

Metallic MC especially the cast iron is very valuable. This makes it very attractive to be stolen. This makes the pedestrians more prone to fall into manholes, which causes injuries and lets the underground utilities be more susceptible to be facing any terrorist attack, besides the cost of replacing the MC.

In [9] it is reported that MC is one of the common metal thefts that cost millions of pounds every year besides the harm of underground utilities like electrical cables and national heritage. On the other hand, the work in [10] mentioned that WRC (Water Research Centre) found that many Manhole Covers in the UK have failed and caused hazards which cost almost 40 million pounds. Table 2-1 shows examples of the MC failure impact on the society and economy in the UK[10],[11].

Chart RAS45013: Reported killed or seriously injured (KSI) road casualties by road users, rolling four quarter totals: GB Q1 2003 – Q1 2012
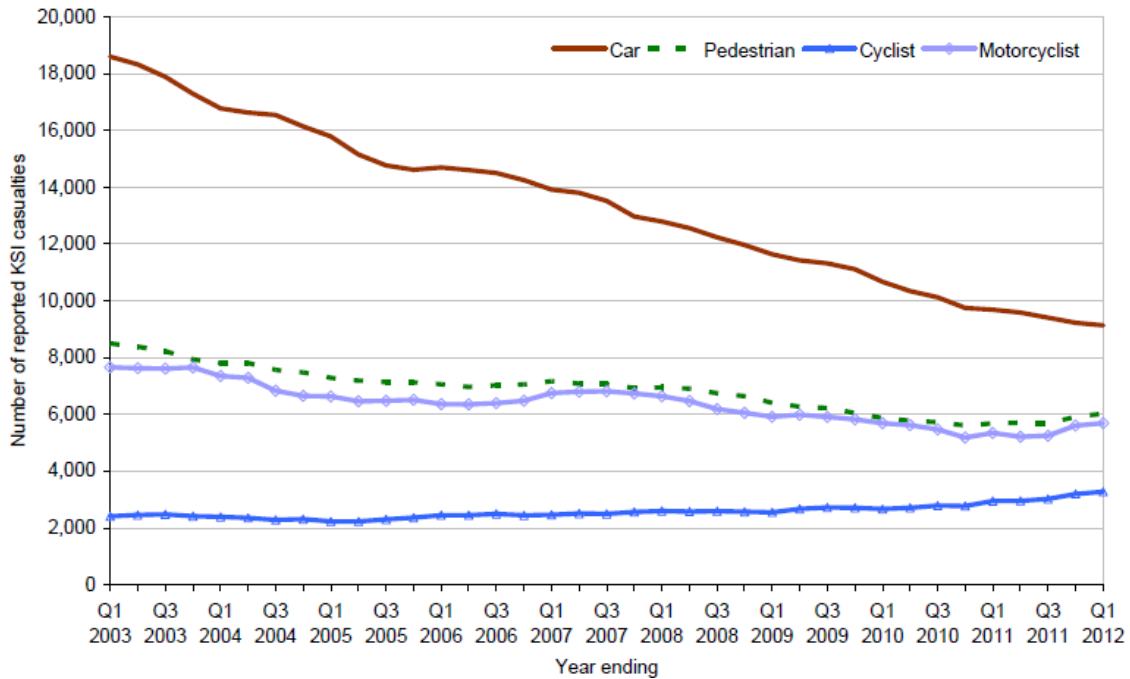
Figure 2-3 Killed or seriously injured (KSI) road casualties by road users in the UK[8]

Table 2-1 Examples of MC failure cost [10],[11]

Example	Cost	Comment
Installation	£1000	1MC with labour cost
Premature MC Failure	£1600-£2000	1 MC in the first year of installation
Stolen MC	£500,000	Yorkshire Council pays in one year
Replacing failure MC for water utilities	£40 M/year	
Human cost	£40,000/year	Injuries to staff handling MC
Potholes	£91M on fixing potholes	MC is one of the main reasons for potholes

From all the information mentioned, it can be concluded that MC failure affects the safety, security and the economy of the society. Current automated MC monitoring systems are not monitoring all the issues that affect MC. The need for automated MC monitoring system has increased by the rapidly increasing MC structure failure which dramatically affects the security, safety and economy of the society, especially in the UK. Besides, the design of the automated MC monitoring system needs to be developed based on the smart city requirements. One of these requirements is to connect this automated monitoring system to the internet cloud. In other words, an automated MC monitoring system needs to be designed as an IoT device.

22

2.2. MC Classifications Issues

The available monitoring systems for MC are not all automated and the automated types are not monitoring all the MC issues. Most of the current monitoring systems monitor one or few of MC issues and are based on partial classification or study. The partial study of the MC issues has limited capabilities to address the wider automation problems, and this leads to a high probability of inaccurate monitoring. For example, in [12], authors designed an automated monitoring system that monitors the security of the MC by monitoring the tilting of the MC; this system is very sufficient but the data from their proposed system can be misleading because MC structure can be tilted because of several sources like the soil moving or traffic pressure and not only because of unauthorised intrusion. Another example is in [13], where authors used high-resolution images to identify the location of the MC and their methods detect only 40% of MC while their study was not concerned about the MC structural degradation issue which may affect their results.

It can be concluded that the reasons for the surge to find an IoT based automated monitoring system for MC can be summarised as follows:

- Reducing any delay that can happen after any failure of the MC that may harm pedestrians or traffic.
- Reducing the cost of using labours and protect the labours from being harmed from the harsh environment beneath the MC.
- Integrating with other infrastructures within a smart city based on IoT.

To reach an IoT based automated MC monitoring system, the MC issues and the current monitoring systems used for these issues have to be addressed first. The target of this section and the chapter is to assign the manual monitoring methods that need to be replaced by the automated methods to reach an IoT based automated system.
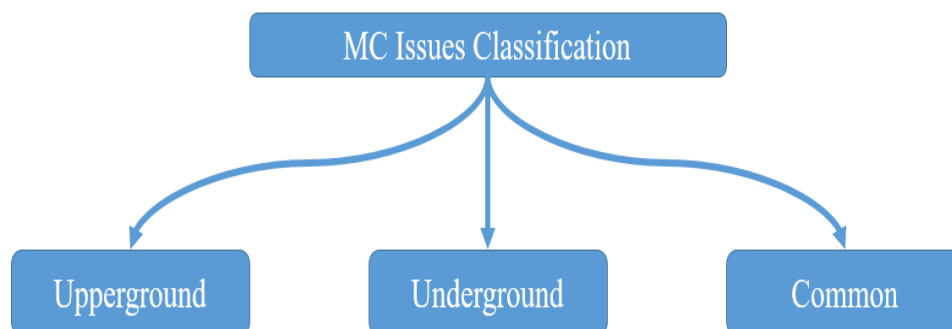
Figure 2-4 MC Issues Classification

MC issues are caused by the ambient underground or upperground environments. Some of these issues are common in both environments. For this reason, the classification is branching to three main branches: Upper ground, Underground and Common, as shown in Figure 2-4.

One of the contributions of this study is that it shows most of the issues and the current monitoring MC systems, which have not been gathered before in one reference. This classification can be used by the government, industry and researchers to develop in several fields like smart city, Internet of Things, underground monitoring and much more. Most of the references used in this chapter are from companies' websites. These kinds of references may not explain in detail the monitoring systems used for marketing reasons. This makes it difficult to gather all of the information. However, by comparing and reading from different resources, complete classification based on the criteria mentioned before (environment effect-based classification) is suggested.

Before starting the MC issues classification, first, the definition of "MC issue" has to be cleared. MC issue can be defined as "the issue which causes MC structure failure, or it is the issue resulting from the MC structure itself". As the classification is based on the environmental effect as mentioned before, MC issues can be classified into three types: a- Upper ground MC Issues: MC issues based on the effect of the upperground environment only, b- Underground MC issues: MC issues based on the effect of the underground environment only, and c- Common MC Issues: which are common between the upperground environment and underground environment effects. However, the influence of each environment on the MC structure may differ.

Table 2-2 MC Issues Classification based on the type of the environment

MC Issues	Upperground MC Issues	Security
		Detection
		Skid resistance
	Underground MC Issues	Stray/Contact
		Explosion
		Noise
	Common MC Issues	Corrosion
		Structure degradation
		Misalignment/Moving

Table 2-2 shows the MC issues classifications based on the type of the environment. It is shown that each type of environmental effect on the MC structure is responsible for three kinds of MC issues.

The available monitoring techniques for the upperground MC issues, underground MC issues, and the common MC issues are summarised in Figure 2-5. Based on upperground effect, three main issues are highlighted: security, detection and skid resistance. The security issue is the only issue for which automated monitoring system is used based on several techniques: mechanical, fibre optics, magnetic sensor, infra-red (IR) sensor, closed circuit television (CCTV), and accelerometer sensors. The first five techniques are summarised and their functionality is detailed in [14]. Accelerometer sensor is used for measuring the tilting of the MC as mentioned in [12].

MC detection is one of the main issues for MC in some countries like Taiwan which uses buried MC. However, this issue is still monitored by manual techniques like radio-frequency identification (RFID), digital camera, or mobile laser scanning [13], [15]–[19]. Because of the high population and the increase of transportation vehicles, MC structure failure has increased and has affected society. The need for using an automated system for monitoring structure degradation is becoming one of the modern societies' demands. Skid resistance is one of the main reasons for most of the bikes and motorbikes accidents. However, this issue is still monitored by using a manual system like Pendulum scale. The average of decreasing the percentage of the skid resistance of MC can reach less than half in 12 months.

As for the upperground environment effect on the MC structure, three main issues are found based on the type of underground utility found beneath the MC, namely stray/contact, explosion and noise. The stray takes place normally if there is no isolation between the cables and the MC. Isolation may be not working, which also generates the stray voltage leading to the contact voltage. One company has mentioned that it designed and fabricated an automated system for the stray/contact issue. However, no technical data has been known for this system [20].

Explosion issue mainly takes place with the gas or electric utilities. For the electric utility, some companies like ABB has used some automated monitoring systems as mentioned in [2], [22], [23]. For the gas utility, the manual monitoring system is still used till now. Noise or sound coming from MC has been accounted to be an issue, however, this issue is very rare and it is monitored manually only based on the claims of the people [24]. Some of MC issues can take place from either upperground or underground, and these are classified as the common issues, these include corrosion, structure degradation and misalignment/moving. Corrosion issue is the first one, it has increased because of acidic environment found in the sewer utility or if the MC is found near to the sea coast. Corrosion issue is still monitored manually by the digital camera and by human inspection [25]–[28].

Structure degradation is one of the main issues for MC. However, this issue is still monitored by manual techniques like vacuum tester or digital camera [29]. Movement of the MC structure can happen because of the pressure of the transportation vehicles or moving the soil. In both cases monitoring the movement of the MC is done manually.

To conclude this section, MC issues have been classified based on the type of the environment that affects the MC structure. The classification divides the issues into three categories: Upper ground environment effects, Underground environment effects and common issues that can be based on the upperground environment or the underground effects. The classification identifies also the type of current monitoring systems used to monitor these issues. In the next section, discussion and analysis based on this classification will be done to identify the challenges and the requirement for designing IoT based automated MC monitoring system.
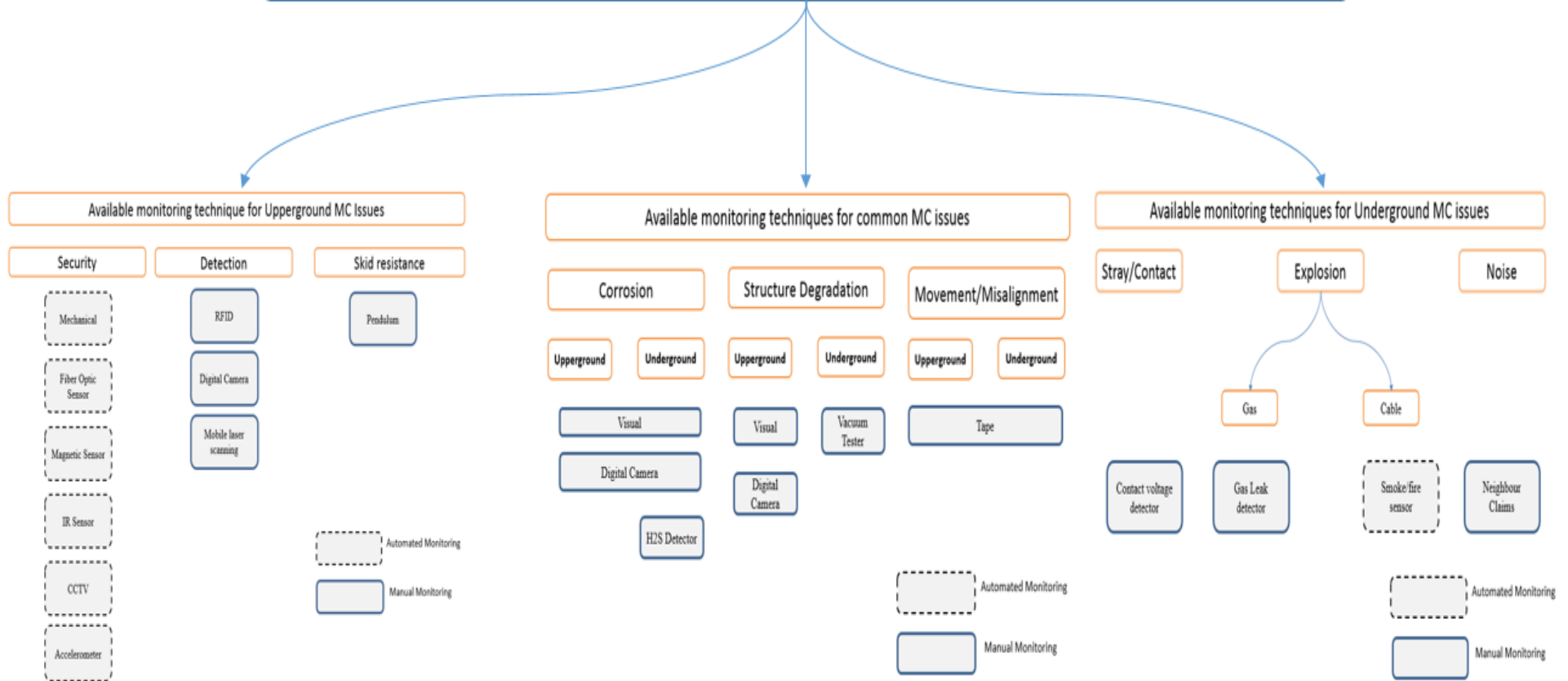
Figure 2-5 MC Issues and the available monitoring technique

2.3. Discussion and analysis of MC classification issues

This section discusses and analyses the MC classification issues explained in the previous section and the available monitoring systems for MC to design an IoT based automated monitoring system for MC. Most of the MC issues are monitored manually and some monitoring systems are based on a recording camera to capture an image of the MC attached to the regular inspection report [28]. Regular manual inspection is mainly based on underground utilities [22] and may take from several times per month to several times per year. However, long time without inspection and monitoring can result in sudden MC failure or stealing which badly affects society and could cause several unwanted hazardous effects. To evaluate the overall monitoring systems to assign the need to design an IoT based automated monitoring system for MC, the analysis will be presented in this section.

Based on the previous section, the available automated MC monitoring systems cover only 30% of the MC issues found. Table 2-3 and Figure 2-6 identify the automated systems used for MC issues and the percentage of these automated systems to the manual ones respectively.

Besides, from the survey, and by addressing and analysing the effect of each underground environmental utilities on the health of the MC structure, it is found that Water/Sewer underground utilities are the utility mostly affecting the MC structure by causing most MC issues. Figure 2-7 represents the percentages of the MC issues caused by the different types of underground utilities based on this survey.

Using automated systems to monitor the MC issues is needed for the safety and security of the society. However, designing an IoT based automated MC monitoring system faces several challenges and needs to be reliable to the smart city and IoT concepts, which are used by modern governments to protect the society. From the study done by the researcher, there are mainly four big challenges facing the design of the IoT based automated MC monitoring system: power consumption, platform cost, data security and memory size required to store the information.

Table 2-3 MC Issues and the available automated monitoring systems used.

MC Issues	Available automated monitoring systems
Security	✓
Detection	✗
Skid resistance	✗
Stray/Contact	✓
Explosion (Gas)	✗
Explosion (cable)	✓
Noise	✗
Corrosion	✗
Structure degradation	✗
Misalignment/Moving	✗

MC Issues Monitoring System

■ Automating Monitoring system   ■ Manual Monitoring system
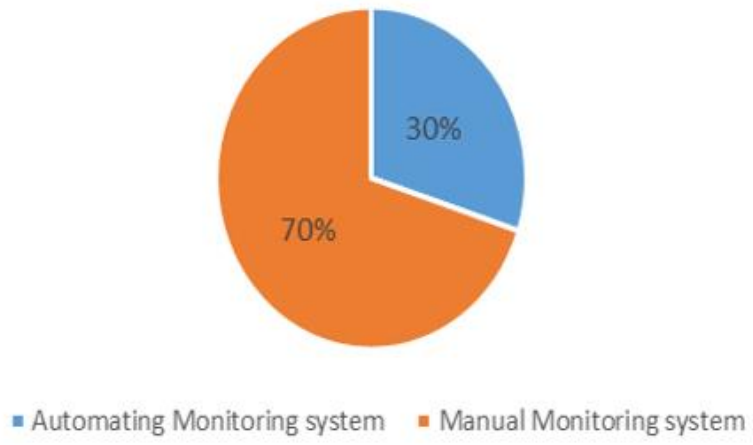
Figure 2-6 Percentages of the automated and the manual monitoring systems available for monitoring the MC issues

Effect of the underground utilities type on the MC structure failure
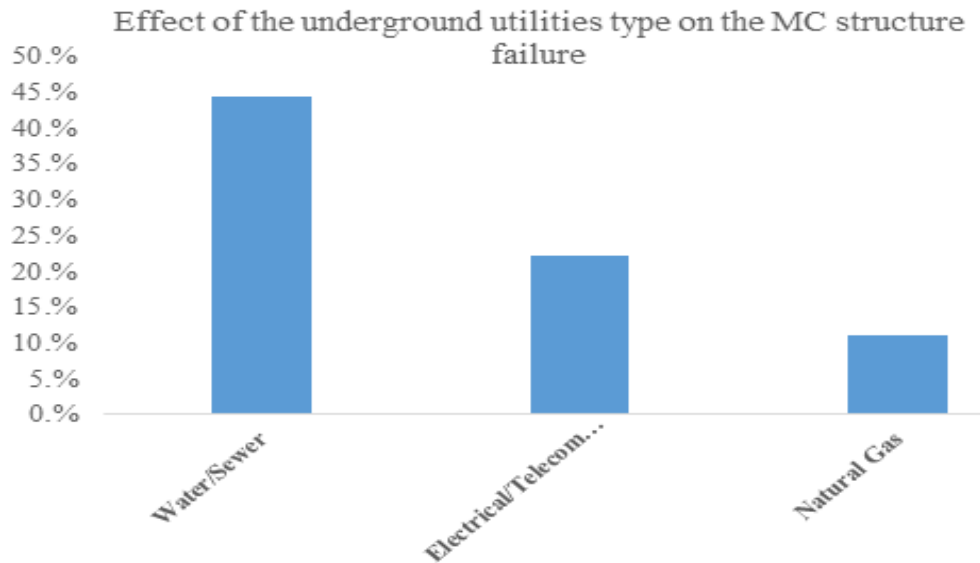
Figure. 2-7 Effect of underground utilities-type on MC structure

i. Power

The power consumption challenge is very essential because the automated system lifetime is mainly based on the battery lifetime. Replacing the battery several times during the MC lifetime is not reliable or sufficient from the cost point of view. This point is very critical, especially that the maximum number of MC issues that are monitored automatically in one system is only two issues and the lifetime is about only one year.

Reducing the power consumption has debatable aspects [30]. However, as the IoT based automated cast iron MC monitoring system is not found until now, the sensor type selection needs to be addressed first because using active sensors may affect the power consumption of the monitoring system (intensive study in the selection of the sensors type is presented later in this chapter).

According to several references like [31], the DAQ module needs to be activated more than any module of the wireless monitoring system regardless of the concept of the monitoring strategy (Trigger- Driven or Scheduled-Driven) as shown in Table 2-4 [31] and by using some types of active sensors, the power consumption will increase more [32]. However, because of the different types of underground utilities, it can be concluded that the IoT based automated MC monitoring system is not universal and depends on the type of underground utilities.

30

Table 2-4 Power states for wireless monitoring system [31]

Mode	Trigger-Driven			Schedule- Driven		
	DAQ	Control Unit (CU)	Communication	DAQ	Control Unit (CU)	Communication
S_0	-	-	-	off	off	Off
S_1	Off	Off	Off	-	-	-
S_2	On	On	Off	On	On	Off
S_3	On	On	Transmit	On	On	Transmit
S_4	On	Idle	Off	On	Idle	Off
S_5	On	On	Receive	On	On	Receive

Generally, several techniques had been developed by several researchers to reduce power consumption. In Table 2-5, selected examples of these techniques used to reduce the power consumption are shown. However, power consumption is still one of the biggest challenges for designing automated monitoring systems.

In addition to these techniques, analogue circuit design starts to attract the researchers for low power consumption applications. Merging analogue circuit design with other fields like neuroscience, opens a new route for designing low power IoT device [33]–[62] especially with the development in Machine Learning algorithms [63], [64].

Table 2-5 Selected Techniques used to reduce power consumption

Power consumption techniques	Method of the technique	Comment
Battery	a high capacity battery such as D batteries (15000 mAh) instead of widely used AA batteries (2000-2400 mAh)[65]	the sensor nodes' lifetime can be extended about 7 times longer.
Energy harvesting	Using piezoelectric (PZT) sensor to harvest energy from traffic vibrations [66]	Not efficient till now to the knowledge of the authors
Low sampling rate ADC	Compressive sensing[67]	Relaxes the ADC sampling rate requirement and can be used for both DAQ and Communication Modules
Monitoring in low sampling time rate	Monitoring every 6 hours[68]	Reduces the need for activating the monitoring systems for a long time, hence structure failure takes a long time.
Energy management algorithms	Adaptive Sampling Algorithm (ASA)[32]	This method depends on the specific sensor, whose power consumption is significantly larger than that of the Communication Module

ii.   Platform cost

Another challenge is the cost of the monitoring system platform itself. By entering the smart city (SC) and IoT era, monitoring systems need to be of low cost and suitable to be controlled and managed via the internet. From the survey, available MC monitoring systems from one side and smart city and IoT from the other side were not mentioned in any reference before now, to the knowledge of the author. This opens a new research field to investigate. Besides that, some of the monitoring systems used in several applications including some current automated MC monitoring, off-shelf monitoring systems hardware platform like Imote2, Waspmote (which is called also motes) and by using open source software cloud, controlling these motes via internet is used and has become more easy and reliable [69]. However, the cost of these modules is still high. On the other hand, a new hardware technology is spreading very fast, which is open source hardware like Beaglebone, Raspberry Pi [70]. These systems are very promising and proved suitable to be used in several smart cities and IoT applications, because of the low cost and the ease with which they can be programmed. However, open source hardware suffers from the high power consumption with respect to the off shelf motes mentioned before [70].
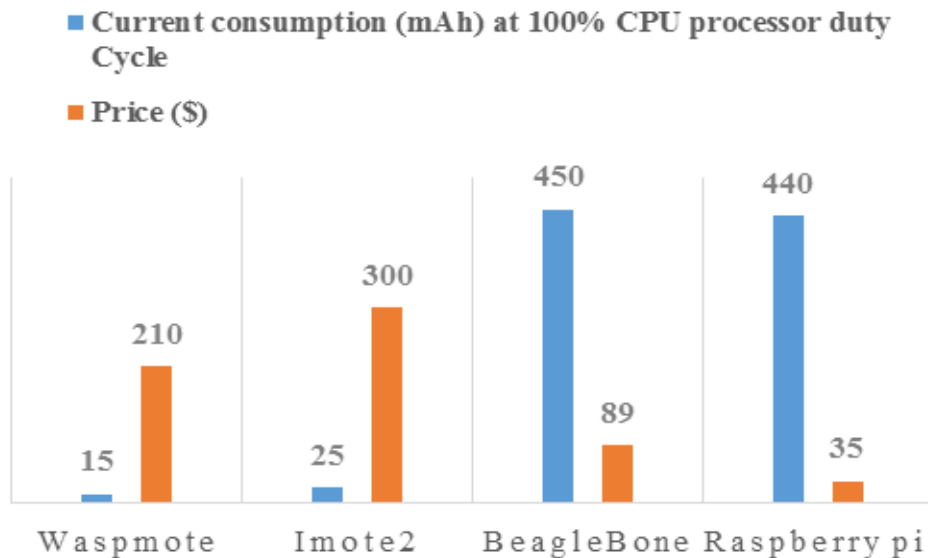
Figure 2-8 Example of current consumption and price for off shelf mote and open source hardware [40]

Figure 2-8 shows examples of the current consumption and price of selected motes and open source hardware [70]. Open source hardware opens a new gate for research in several monitoring

32

applications like IoT based automated MC monitoring system by redesigning it to be less power consuming and to be used for smart city and IoT applications.

iii. Security

Another challenge facing the design of the IoT based automated monitoring systems is the security. IoT based monitoring systems can be wired like supervisory control and data acquisition (SCADA) or wireless like wireless sensor network nodes (WSNN). Wired monitoring systems have the advantage of the security over the wireless systems. However, wired systems are very expensive if compared with the wireless systems[71].

This problem leads to looking further to design WSNN with a high security system. Also, in the internet of things (IoT) era which is based on connecting or communicating all the monitoring systems under the internet cloud, even wired monitoring systems like SCADA will face the security issues in internet security [72].

In some studies, the combination of the two methods (SCADA and WSNN) takes place to get the advantages of both systems [72], [73]. However, this concludes that both systems will be facing mainly the same security issues, but they differ in the cost which makes WSNN monitoring systems replace the wired monitoring system in the future for monitoring most of the city utilities [71].

Another challenge for a secured IoT device design is the power consumption [74]–[78]. The tradeoffs between the power consumption and the security has become a hot spot for the current IoT device designs for several applications. Moreover, hardware design is more demanding as it consumes less power if compared to software-based security system like in [78].

While most of the current design for the secured IoT devices is based on digital circuit design, analogue circuit design starts to improve the secured IoT device hardware design from a power consumption point of view [79]. The improvement of the analogue circuit design for the power consumption has been mentioned above.

iv. Big Data

By increasing the number of sensors and networks, the size of memory required needs to be increased, which was not reached till now. This problem is still in development in several scales from the smart city point of view[80].

It can be observed from the previous discussion that the design of an IoT based automated monitoring system for MC needs more effort, especially with the lack in the current automated monitoring systems to monitor all of the MC issues. It is clear that this system will have to include the uppergound MC issues monitoring techniques, common MC issues and has the ability to attach other sensing techniques for underground MC issues based on the type of the utility beneath the MC.

Most of the automated monitoring systems for underground utilities, use the MC as a holder to monitor these utilities [81]–[84]. This means that the design of an IoT based automated monitoring system for MC should also be able to attach more sensors that can be used to monitor the underground utilities. This will need more care in the design as it will be more complex and therefore more power consumption is expected.

To conclude, this section analyses the proposed classification of the MC issues and shows the gap area in the research for the design of an IoT based automated monitoring system for MC. It extends to identify the expected challenges that face this design. The effect of the type of underground utilities on the MC structure was also mentioned in this section.

2.4. Power consumption challenge for IoT based automated MC monitoring system design

Designing an IoT based automated MC monitoring system faces several challenges as shown before. The present research focuses on reducing the power consumption of the system. However, the IoT device designer needs to take into consideration all the previous challenges. As shown also, active sensors and DAQ are the main parts that consume more power in the system. To be more focused, this research will consider reducing the power consumption of the DAQ module by reducing the power of the most consuming circuit in the DAQ which is ADC. The first step to reduce the ADC power consumption is to identify the sensors types to determine the required bandwidth and the power required for the ADC to work. For this reason, the next section will propose a study to identify the sensors types required for the IoT based automated MC monitoring system. This will help to assign the power requirements for the DAQ.

A DAQ module consists mainly of [86] :

i-   Sensor Signal conditioning circuit: which reads the variation of the sensor signal based on its function.

ii-   A multiplexer (MUX): MUX is one of the most sensitive parts in the design of the DAQ system. It is important for accurate sampling of multi-input channels. A MUX typically consists of several switches connecting all of the input channels to the output end of the MUX.

iii- Amplifier: is mainly a Programmable Gain Amplifier (PGA), Low Noise Amplifier (LNA), or Charge Amplifier.

iv-   Filter: to activate the essential bandwidth of interest. The filter mainly is Low Pass Filter.

v-   Analogue to digital converter (ADC): to transfer the analogue signal into the digital domain which converts the analogue signal to a digital value. ADC function is to deliver the processed analogue signal to the CU module to process and store.

The ADC is the circuit which consumes the most power in the DAQ module. This is because it needs to sample the sensor signal at least double its bandwidth (Nyquist Shannon theorem). By increasing the bandwidth of the sensor signal, the sampling rate increases. For the purposes of designing an IoT based automated MC monitoring system, reducing the sampling rate is one of the main targets to reduce the power consumption in the DAQ module.

Choosing the ADC architecture is one of the solutions to reduce the power consumption. Several architectures have been designed to achieve optimal power consumption for different sampling rate and resolution (resolution indicates the number of the discrete values it can produce over the range of the analogue values) as shown in Figure 2-9 [51]. However, the selection of the type of an ADC architecture will be cleared after choosing the sensor type in the next section.
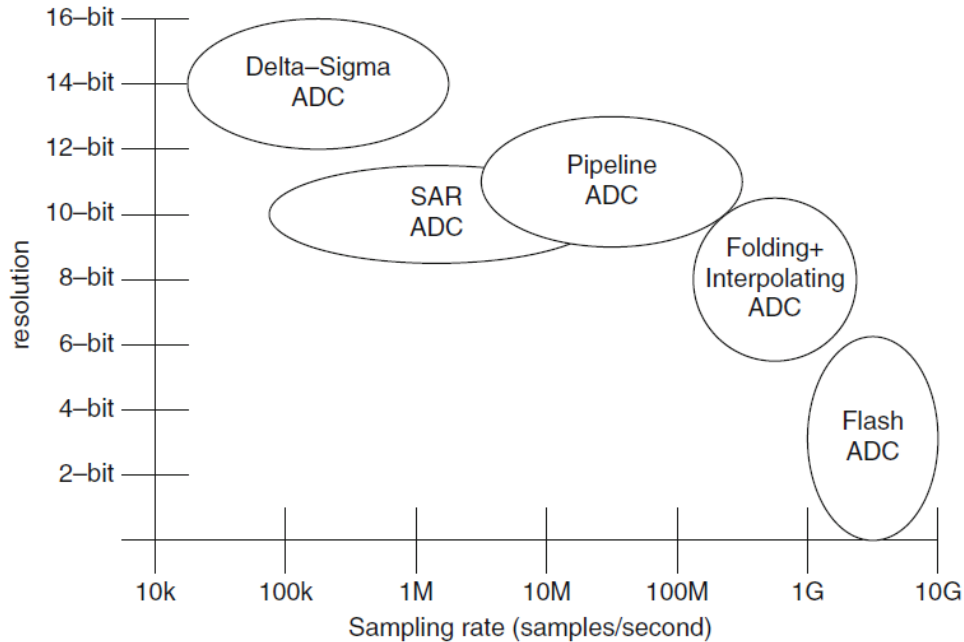
Figure 2-9 ADC Architectures [51]

On the other hand, an ADC architecture is not the only optimum solution to reduce the power consumption for designing low-power IoT based automated MC monitoring system. It is mentioned in [87] that one of the new approaches to reduce the power consumption of sensor nodes in IoT is to add analogue processing before the ADC as shown in Figure 2-10.
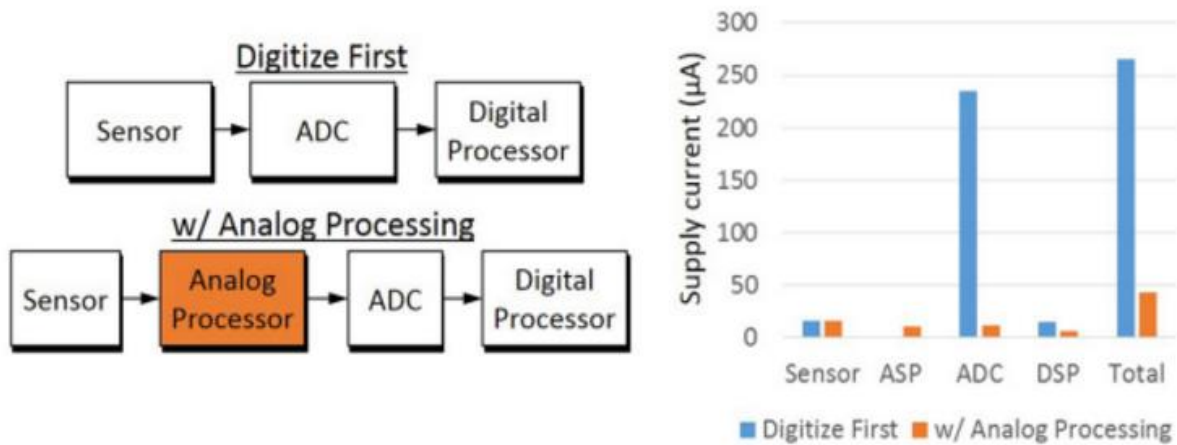
Figure 2-10 Comparison of the dominant power consumers in a traditional sensor system and a sensor system that incorporates an analogue processor [87]

Compressive Sensing (CS) based hardware implementation is called analogue to information converter (AIC) [37], [53]– [66]. AIC is already following the approach of using an analogue preprocessor before the ADC as mentioned in [87]. CS concept takes place if the original signal is sparse in one domain like frequency or time which is the case for most of the sensor signals [5].

While CS or AIC can improve the reduction of ADC power consumption, it reduces also the size of the data. However, as mentioned before, IoT device designer needs to take all the IoT device design challenges into consideration especially if the IoT devices need to be located in harsh or difficult to reach environments.

Because the heart of the AIC is the pseudorandom generator (PRNG), this attracted researchers to use it at the same time for the data security. The traditional hardware designs for AIC used the digital linear feedback shift register (LFSR) for generating PRNG. However, LFSR is not recommended for security[102], [138]–[141]. Hence, researchers started to replace LFSR with another digital PRNG with more security capability. Most of these efforts are done by using digital circuit design. Digital hardware implementations add more complexity for the AIC which consumes more power. This point will be discussed in more details in the next chapter.

From this point of view, the present research focuses on studying the use of AIC to design a low-power secured IoT based automated MC monitoring system. The study extends to enhance the AIC circuit design by replacing the digital part in the AIC analogue front end to make this part pure analogue for power consumption issue and to overcome any need of isolation between digital and analogue circuits as will be shown later. This study is expected to contribute to monitoring MC, monitoring underground utilities and extends to contribute in several fields used in smart city concepts and develop in the design of IoT devices.

To conclude, this section focuses on power consumption as the main challenge to design a secured IoT based automated MC monitoring system. It was shown in this section that the ADC circuit is the main circuit consuming more power. Compressive sensing theory is targeting reducing the power consumption of the ADC by reducing the sampling rate which is the main reason for

increasing the power consumption for the ADC. Hence, this study will focus on developing CS based ADC which is called analogue to information converter (AIC).

2.5. Types of Sensors needed for IoT based automated Manhole Cover Monitoring System

Before proceeding in the ADC design, sensor types need to be identified first. This section is very important for designing the required ADC. However, several challenges were found to identify the sensor types for an IoT based automated Manhole Cover monitoring system. The first challenge is that not all the available monitoring systems are automated; hence, the type that can be used for automated systems should be identified. The second challenge is that an issue like skid resistance has special kind of monitoring which is the pendulum. This kind of monitoring is very rare, and it also does not use an electronic circuit to monitor but uses a mechanical ruler and the user has to read it. This means an intensive study needs to identify the type of sensor that can be used to replace this manual method and to be efficient.

While the sensor design is not the aim of this study, the selection of the sensor type is very essential to identify the required bandwidth for the system. Hence the ADC requirement will be determined, and to be specific the sampling rate for the ADC will be identified.

From the survey in this chapter, it can be observed that the IoT based automated Manhole cover monitoring system is not universal, but it depends on the underground utility beneath the Manhole Cover. In other words, IoT based automated monitoring system for the Manhole cover is a multisensor monitoring system which has the ability to add more sensors based on the underground utility type.

Based on this observation, the Manhole Cover issues and the monitoring system can be divided into two branches: the first one is fixed which includes the upperground and the common issues, while the second branch includes the underground issues. The physical phenomenon to be measured by each branch needs to be recognized to identify the sensor type. By observation of the MC issues classifications, the physical phenomenon that needs to be monitored can be classified as shown in Figure 2-11 to four different classes which are: orientation, structure degradation, electrification and explosion. To be more specific about sensor type selection, the physical phenomenon can be classified into two categories: first for upperground and common issues; the

38

second is for the underground utility type. For each class, one or more sensors can be used to monitor the related MC issues.

It has to be mentioned that two issues have been omitted from the study in this section from the Manhole Cover issues. The first one is the detection phenomenon, because generally most of the automated monitoring systems need to send information including the location or system identification. Hence, it has to be found in the design by several ways like adding the location to the information content. The other issue is the noise or, in other words, sound phenomenon. The noise issue as mentioned before is rare and also depends on several aspects like the design of the Manhole Cover or sometimes results from the structure degradation which needs to be monitored.
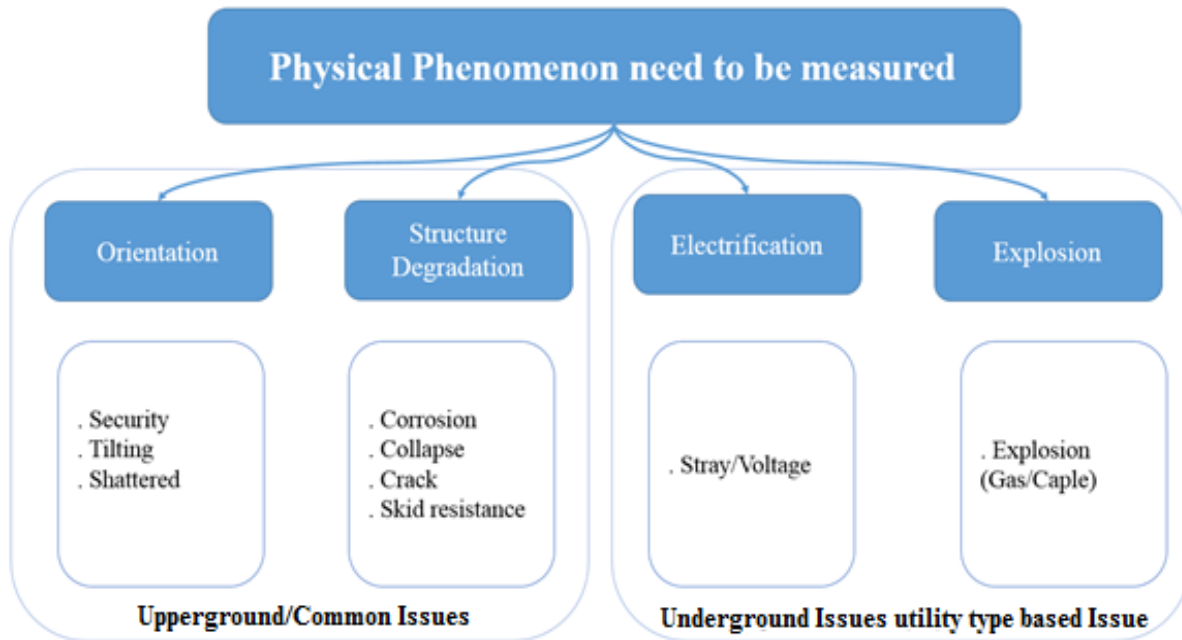
Figure 2-11 Physical phenomenon needed to be measured for IoT based automated Manhole Cover monitoring system

Sensor type selection was very challenging and required to study the sensing techniques from several fields like civil engineering and aerospace. Besides, the selection of the sensor type needs to satisfy the need for low power consumption for the sensors. Based on the survey done by the researcher and by the investigation from several references [103][104]–[120], Table 2-6 shows the sensor type selection for IoT based automated Manhole Cover monitoring system. More details about this study are found in Appendix 1.

It is shown from Table 2-6, that the maximum sensor bandwidth is 5 MHz for the PZT which required at least 10 MHz for sampling (it has to be mentioned that in [109] authors use the PZT sensor with sampling rate 100MHz to avoid noise).

To conclude, this section presents the sensor selection required for the IoT based automated Manhole Cover monitoring system. The selection was based on the available techniques for the automated system besides the sensing techniques from other fields like civil engineering. The target of this section is to identify the maximum sensor bandwidth needed for IoT based automated Manhole Cover monitoring which shows the minimum sampling rate required for traditional ADC.

Table 2-6 Sensor Type Selection for IoT based automated Manhole Cover monitoring system

Sensor	MC Issues				Frequency
Inertial Measurement Unit (IMU) (Accelerometer-Gyroscope)	Security	tilting	Shattered (Structure Degradation)	Collapsed (Structure Degradation)	350 Hz-17kHz
Piezoelectric sensor (PZT)	Crack (Structure Degradation)	Corrosion	Skid resistance (expected)		Few hundreds of Hz- MHz (≈5MHz)
Voltage sensor (Electrical/Telecommunication utilities only)	Stray/contact (expected)				≈60Hz
Smoke/fire sensor (Electrical/Telecommunication utilities only)	Explosion				ON/OFF switch or IR gas

2.6.   Conclusion

In this chapter, MC types and issues have been highlighted and a new classification of these issues has been presented in view of the available monitoring systems. The outcome of this classification shows that 70% of the monitoring systems for the Manhole cover is based on manual technique. With the increasing failure of the Manhole Cover because of various issues and the effect of this failure on the society from the security, safety, and economy sides, the need to design an IoT based automated Manhole Cover monitoring system has increased.

Based on the analysis and the observations from this chapter, power consumption is the main challenge to reach to a fully automated manhole cover monitoring system based on IoT device design requirements. It was shown that the main source of consuming the power in the IoT is the analogue to digital converter (ADC) found in the DAQ module. However, IoT device design cannot ignore the other challenges like security or cost from the design point of view.

The investigation in this research extends to study the sensing types required to design fully automated manhole cover monitoring system. This study gives the main requirements for the ADC specifications that is required to design IoT based manhole cover monitoring systems. This point shows the minimum sampling rate of the ADC required which is very essential for the power consumption calculation. Based on this study, the sampling rate for the ADC can reach to 10-100MHz. Using traditional ADC circuit design with the sampling rate mentioned before, will not be suitable for monitoring manhole cover like cast iron manhole cover which has life time of 20-25 years. Hence, this chapter studies several techniques and scenarios that can extend the lifetime of the DAQ module in comparison with the manhole cover lifetime.

It was shown from several references the ability of the analogue circuit design to overcome several design challenges like power consumption. It was not mentioned in any reference to the knowledge of the author, the use of analogue circuit design to enhance the manhole cover monitoring circuit design. This motivates the researcher to do more investigation about the analogue circuit techniques that can develop in the manhole cover circuit design from the power consumption point of view.

Based on the investigation done by the researcher, a compressive sensing technique will be studied thoroughly in the next chapter to identify its suitability to be used for the IoT -based manhole cover monitoring system.

Chapter 3

Analogue to Information Converter (AIC) and Chua circuit

3. ANALOGUE TO INFORMATION CONVERTER (AIC) AND CHUA CIRCUIT

3.1. Introduction

In Chapter 2, it was concluded from the research done by the author that ADC is the circuit which consumes most power in the DAQ module which is the module with the highest power consumption in the IoT based automated MC monitoring system. At the end of Chapter 2, it was concluded that PZT sensors are the highest frequency (5 MHz) used sensors in the IoT based automated MC monitoring system which needs at least 10 MHz sampling rate based on Nyquist Shannon criteria. As the target of this research is to design and develop an IoT based automated MC monitoring system, the research is focusing on designing a low-power ADC.

Several techniques have been mentioned in Chapter 2 to reduce ADC power consumption. However, compressive sensing (CS) proved to be the most efficient technique that can be used for an IoT based MC monitoring system to reduce ADC power consumption. The reason for this is that the CS framework can overcome the ADC power consumption, with a reduction of the signal size which reduces the size of the memory required to store data. Furthermore, the heart of the CS framework is the pseudorandom generator (PRNG), which attracted the researcher to use it for the data security at the same time. However, this point affects the power consumption due to the digital implementation of the secured PRNG.

This chapter and the rest of the thesis are focused on the ability to design a low-power, secured ADC using compressive sensing by means of the analogue chaotic oscillator. The motivation of this is the ability of the analogue chaotic oscillator to enhance power consumption and at the same time the security as will be shown later.

This chapter is considered as the first step to study and investigate the ability of the analogue chaotic oscillator to work within the CS framework or analogue to information converter (AIC) framework (AIC is the CS based ADC). An analogue Chua circuit will be highlighted as it will be used in the AIC framework with several implementations in the next chapter. Chua circuit is one of the fundamental or the first hardware implementation for chaotic oscillators

The target of this chapter is to give an overview of the fundamentals and the backgrounds of the AIC, PRNG circuit and Chua circuit. This chapter is organised as follows: First, ADC power consumption and CS solutions will be highlighted. The compressive sensing background and the

AIC circuit will be overviewed. The AIC power consumption and security trade-offs will be presented after that, followed by PRNG circuit design and Chua circuit background.

3.2. Analogue to Digital converter and Compressive sensing

The main idea of ADC is to deliver the analogue signal to the Control Unit module in digital form. This process is done in three steps: a) Sample and Hold, b) Quantising, and c) Coding. The signal delivering process by ADC is mainly consuming more power with comparison to the other components. ADC is based on sampling the signal by the sample and hold process at equal or more than double of the analogue signal bandwidth, which is called Nyquist Shannon rate criteria. After that, the quantising process takes place by assigning each sample amplitude of the sampling signal to a specific level. Coding assigns the digital code that represents the signal at each quantised level.

Two observation points affect the ADC. The first is the high sampling rate required if the analogue signal has very high bandwidth; second is the memory required. Figure 3-1 shows the effect of the sampling rate on some of the off-shelf ADC [121]. Regarding the memory issue, it was convenient to reduce the memory requirements by applying compression technique in the CU. This means that another overhead task for the CU to reduce the size of the data is needed. From this point, researchers started to address these observations to reach optimum methods to reduce both the power consumption and the memory size required for the data.
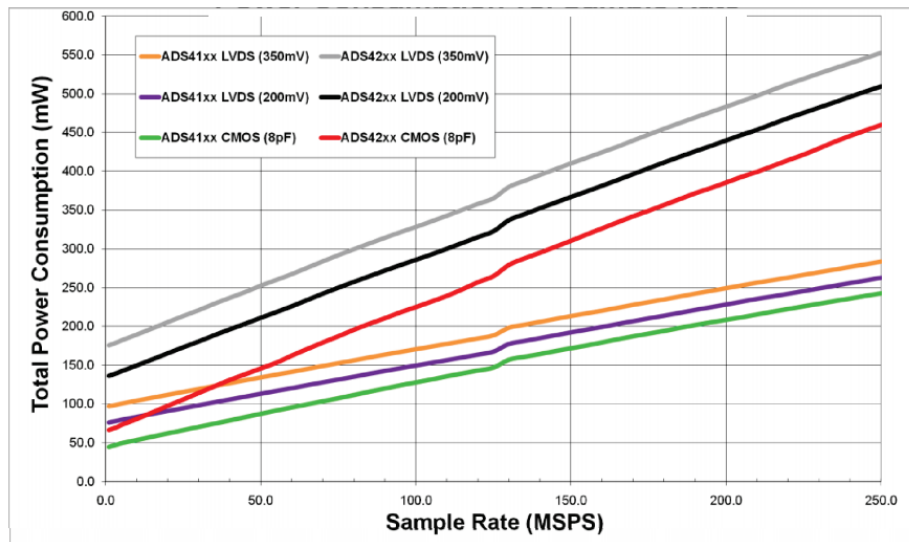
Figure 3-1 ADC Sampling Rate versus Power Consumption for ADS4xxx Family of ADCs[121]

One of the efforts done by researchers is using the Compressive sensing (CS) technique. CS is dealing with both issues (high sampling rate and memory size) at the same time. CS is briefly based on the fact" that if the signal is sparse in some domain like frequency domain, this means that sampling process based on Nyquist and Shannon theory is sampled more than the information content of the analogue signal". From this point of view, compressive sensing (CS) theory is targeting only the information content of the signal especially if it is only sparse in some domain as mentioned above. Fortunately, most of the sensors' signals are sparse in some domain. Hence, the number of required bits will be less than the traditional technique which reduces the size of the memory required. CS based ADC is named analogue to information converter (AIC).

AIC generally consists of two blocks: first is the pre-processing block to reduce the size of the original signal which leads to the use of traditional ADC with less sampling rate; the second block is nonlinear algorithm to reconstruct the signal. One of the main circuits that are used to construct the pre-processing block is the pseudorandom number generator (PRNG). While the PRNG is found in the analogue front end of the AIC, most of the researchers (to the knowledge of the author) use the digital circuit to PRNG. Using digital circuit in analogue frontend needs critical design, and from the PCB circuit design viewpoint, it needs good isolation to prevent any crosstalk or noise. Generating random signal using analogue circuit can overcome this issue.

In the signal processing and circuit design fields, chaotic signal generators can generate PRNG based on analogue or digital circuit design. Chaotic signal generator attracts several researchers especially in the telecommunication field for encryption purposes. While it is used mainly for encryption, it can also be used for other applications. Chua circuit is the first circuit to demonstrate the chaotic signal with a very simple design. The pseudorandom sequence generated from the Chua circuit has been tested for CS algorithms and shows very good results. However, implementing analogue Chua circuit based PRNG in AIC framework has not been studied before from the circuit limitations and power consumption viewpoints.

3.3. Compressive Sensing Background

Compressive Sensing (CS) theory deals with signals which have a sparse representation in a domain [37], [53]– [66] . It is known that a signal can be sampled at a rate called Nyquist and Shannon rate. The main idea of using CS is that most of the practical signals collected by the sensors or antennas have a sparse representation in a specific domain.

In [97] the CS theory is explained as: consider a vector N × 1 signal f represented as follows

$$f = \Psi x \tag{3-1}$$

where x is the coefficient vector of f that is expanded on the basis $\Psi \in R^{N \times N}$. The signal is sparse when most of its coefficients are zero or small enough to be ignored. In Figure 3-2, the N-dimensional input signal f is compressed to a vector M × 1 signal y where M ≪ N by the following relation

$$y = \Phi f \tag{3-2}$$

Where $\Phi \in R^{M \times N}$, $f \in R^{N \times 1}$. The vector N × 1 signal f can be reconstructed from the vector M × 1 signal y, one must solve the following relation.

$$\min_{x \in R^n} \|x\|_{l_o} \quad subject\ to\ y = \Phi \Psi x \tag{3-3}$$
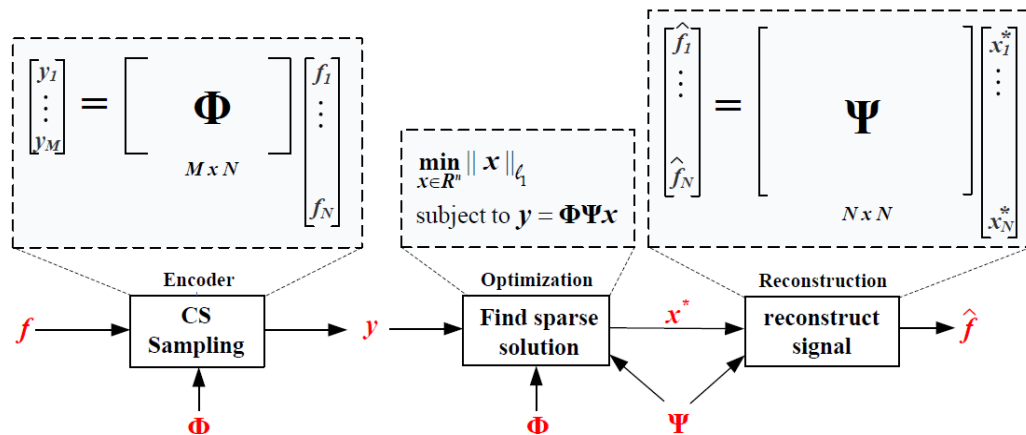
Figure 3-2 Compressive sensing technique [62]

Where lo is norm zero which means the count of nonzero entries of the vector. This reconstruction method is a very difficult problem to solve. Instead, several optimisation methods have been studied to recover this problem by using norm1 (norm1 is the summation of the absolute values of the signal) [95]. The reconstruction algorithms used in CS are summarised in Figure 3-3 below [95]. It has to be mentioned that in [5] it is shown that if the original signal is well known then matching filter can be used instead of the nonlinear operation for reconstruction.

FOCUSS

Iterative Re-weighted Least Squares

Sparse Bayesian Learning Algorithms

Monte-Carlo based Algorithms

Non-convex minimization Algorithms

Chaining Pursuits

Heavy hitters on Steroids (HHS)

Fourier Sampling Algorithms

Combinatorial/ Sublinear Algorithms

Expander Matching Pursuit (EMP)

Sparse Matching Pusrsut (SMP)

equential SMP

Belief Propogation

Message Passing Algorithms

Iterative Soft Thresholding (IST)

Iterative Hard Thresholding (IHT)

Iterative Thresholding Algorithms

Compressive Sensing Reconstruction Algorithms

Convex Relaxation

Basis Pursuit (BP)

Basis Pursuit De-noising (BPDN)

Modified BPDN

LASSO

Nuclear Norm minimization

Greedy Iterative Algorithms

Matching Pursuit (MP)

Orthogonal Matching Pursuit (OMP)

CoSAMP

Subspace Pursuit

Tree Matching Pursuit

Gradient Pursuit

Regularized OMP

Orthogonal Multiple Matching Pursuit

Stagewise OMP

Bregman Iterative Algorithms

Figure 3-3 CS Reconstruction Algorithms[95]

Based on the theory of CS, Φ must be incoherent with basis Ψ. Incoherence means that the rows φ_j of the matrix Φ cannot sparsely represent the elements of the sparsity-inducing basis ψ_i and vice versa. In the signal processing theory, Φ has to be random with independent and identically-distributed (i.i.d) entries, e.g. Gaussian or +/- binary entries, to obey this rule [122]. From this point, Φ is implemented in hardware as a random signal generator or to be specific pseudorandom number generator (PRNG) to generate random sequence {-1,1} to satisfy the requirements for the CS theory to be used in several applications.

CS has several applications like medical imaging, Radar, and Analogue to information converter (AIC). AIC is based on adding a pre-processing block to reduce the sampling required then adding traditional ADC with low sampling rate. It was mainly targeting the high-frequency applications in communication receiver because high frequency (high MHz and GHz) need very high sampling rate ADC which increases the power consumption. Besides that, AIC showed very good performance in low-mid frequency applications for low power applications. The last point has motivated the author to investigate and study the performance of replacing ADC in DAQ module by AIC for an IoT based automated MC monitoring system.

On the other hand, using an analogue circuit design for sake of the power consumption is starting to attract the attention of the researchers, especially with merging the analogue circuit designs with other fields like neuroscience and biology, as will be shown later in this research. Besides that, while signal reconstruction algorithms are mainly implemented in a digital hardware

manner, it is reported in [123]–[127] several sparse algorithms have been implemented by field programmable analogue array (FPAA) and showed the good performance with low power consumption.

However, most of the analogue AIC frontend uses a digital circuit like linear feedback shift register (LFSR) [128] to generate the random sequence required for AIC. Combining analogue and digital circuits in the same PCB required good isolation between them to avoid crosstalk and noise [129]. Hence, the research focuses on replacing the digital circuit by analogue with low power consumption design.

Designing low-power analogue circuits has several approaches, like the technology, the number of elements used to reconstruct the circuit, some circuit design techniques and more. From this point, the research investigates more about the design of low-power analogue circuits that generates a random sequence.

One of the methods used to generate a random sequence using analogue circuits is based on the chaos theory. While the chaos theory has several methods to design chaotic oscillator like Chua, Lorenz, etc. Chua circuit is selected as a first step to study the analogue chaotic oscillator in AIC framework. This is because of the simplicity of design with few numbers of components which satisfies one of the power consumption design needs as mentioned before.

Fortunately, chaotic sequence generated from the mathematical model (discrete presentation not continuous) like Chua circuit has been studied to use in CS theory like in [130] and shows good performance. However, to the knowledge of the researcher, using a chaotic oscillator in AIC framework has not been addressed before from the circuit design viewpoint.

The study will test the performance, the limitations, the trade-off and the requirements of applying analogue Chua circuit in AIC framework by simulation which will be shown in the next chapter. The rest of this chapter will show a brief background about the AIC and the analogue Chua circuit that will be used in the study in the next chapter.

3.4. Analogue to Information Converter (AIC)

Analogue to information converter is one of the main applications of CS. AIC as mentioned before consists of two major blocks: pre-processing before using traditional low sampling ADC (AIC analogue frontend) and signal reconstruction. AIC analogue frontend is a pre-processing step to reduce the size of the original signal if it is sparse in a well-known domain. The basic idea can be shown in one of the simple AIC topologies which is called Random Demodulation (RD) shown

in Figure 3-4. Simply, RD frontend consists of a multiplier which multiplies the input signal (*f(t)*)with random signal generator (*Pc(t)*) {-1, 1} or in other words chipping sequence then integrated and sampled by n samples. The random signal represents the random matrix Φ mentioned in the previous section. Hence the output of the multiplier feeds the integrator which is followed by a low rate sampler or low sampling ADC.
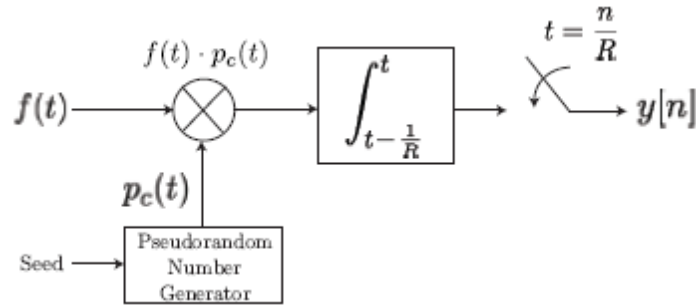
Figure 3-4 AIC using Random Demodulation topology[122]

To analyse the RD topology first, the signal is multiplied by the random signal generator with Nyquist rate or more to repeat the spectrum of the input signal because of the convolution process (convolution is the frequency representation of the multiplication process). Applying the integrator or low pass filter (LPF) on the multiplier output will capture the input signal at the baseband which needs less sampling rate in comparison to the spectrum of the input signal. This process is shown in Figure 3-5 [122].
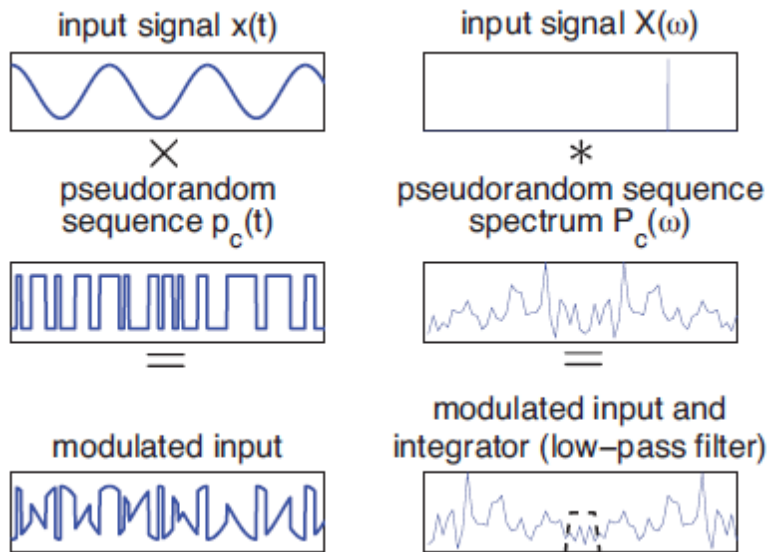
Figure 3-5 AIC analogue frontend pre-processing[122]

AIC has several topologies like non-uniform sampling, random modulation pre-integration (RMPI), Xampling, and more [5], [128], [131]. However, RD is considered to be the basic topology for most of these topologies. For this reason, this research will focus on the RD topology because of the simplicity.

Generating the random sequence or PRNG is the heart of the AIC design. As mentioned before, most of the researchers use digital implementation to generate PRNG like linear feedback shift register (LFSR) which required very good isolation between the analogue part and digital part to avoid any crosstalk or noise. Hence it is clear that to overcome the need of the good isolation, the AIC analogue frontend needs to be a completely analogue or analogue and mixed circuit. Hence, it is required to replace the digital PRNG with analogue PRNG. Another motivation to replace LFSR by an analogue circuit design is the data security. The next section will highlight this motivation.

3.5. AIC security Vs power consumption

As mentioned in Chapter2, MC affects the society in mainly three points: security, safety, and economy. For this reason, the data of the MC structure has to be secured to increase security. This becomes more demanding based on the underground utility found beneath the MC. Besides that, designing a monitoring system for MC structure as an IoT device requires special care for the data security issues. However, adding a security system to the IoT device increases the power consumption.

While CS has proved the ability to reduce the power consumption and the big data challenge, it has also become attractive to the researchers from the security point of view. As the PRNG is the heart of the CS, it also became the key for encryption at the same time, as mentioned in [132]–[139].

In the AIC analogue front end, most of the efforts were focusing on developing LFSR digital circuit which is not acceptable from the security prospective[140]–[143]. Another approach mentioned in [138], the authors secured the data using the user password before sending it to the cloud. This approach adds more hardware to the IoT device itself.

Developing LFSR by another digital manner is acceptable from a security point of view with some concerns about the power consumption. As mentioned before, analogue circuit design has become more attractive for the power consumption applications. Moreover, while fields like machine learning and deep learning-based hardware implementation seem to be pure digital, it is proved that analogue hardware for these algorithms will be efficient from the power consumption point of view. This motivated the researcher to study replacing the digital LFSR with low-power analogue oscillators.

In Chapter 2, an example of the power consumption-security issue was presented. In this section, more examples will be presented to highlight this point and to make it clearer. Xingbin Liu et.al mentioned encryption algorithm based on compressive sensing (CS) and chaos in the fractional Fourier[144]. They claim that they use simple chaotic map algorithm which was software implemented. However, a similar algorithm was used in [145], the hardware design is presented in Figure 3-6 followed by the number of resources required shown in Table 3-2. This type is also mentioned in [146] to secure compressive sensing.
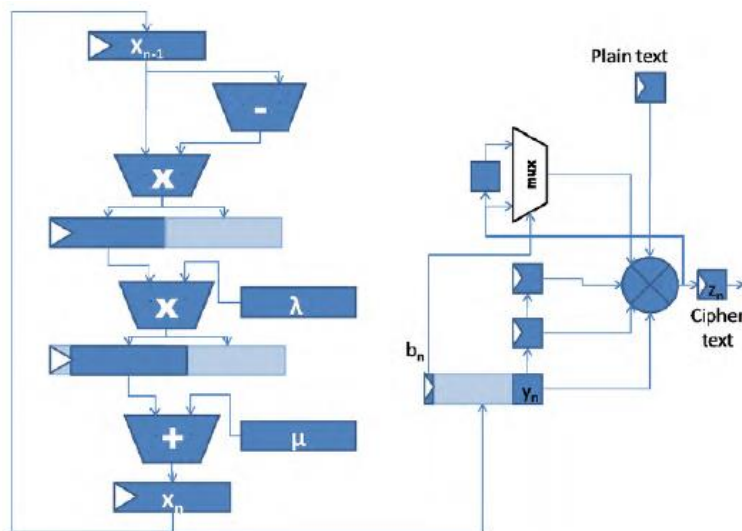
Figure 3-6 FPGA encryption hardware mentioned in [145]

Table 3-1 Resources required for FPGA encryption shown in Figure 3-6 [145]

Resources	Original Design	Optimum Design
Clock Frequency (MHz)	69	93
No. DSP48E1 slices	23	16
No. Slice Register	228	160
No. Slice LUT	354	643

To show the complexity, the authors in [145] used look up table (LUT) with FPGA, [147] and [148] show several architectures of LUT used in PRNG by means of FPGA Processor as shown in Figure 3-7.
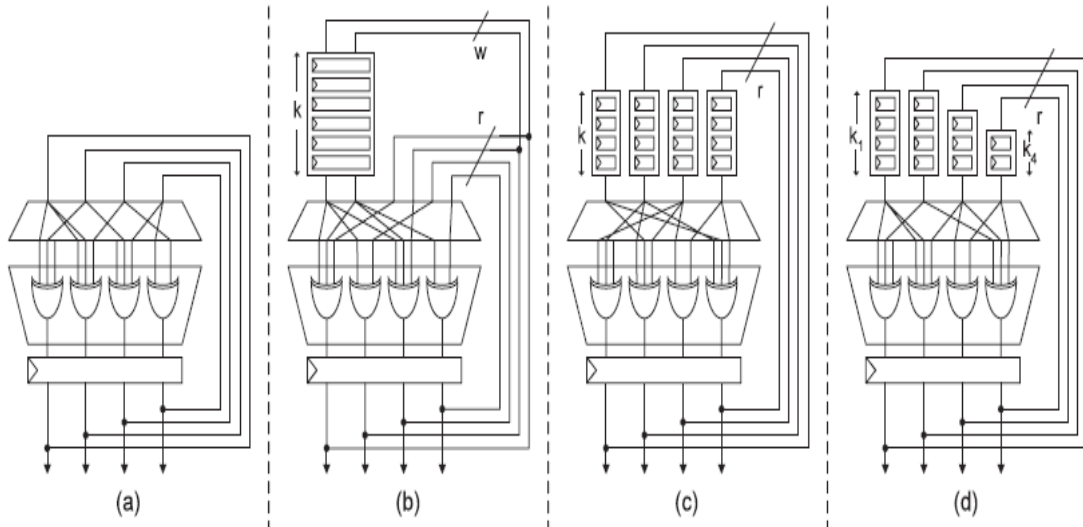
Figure 3-7 LUT types for FPGA mentioned in [150] and [151]

In [133], the authors use the following Double Random Phase Encoding (DRPE) which is used only for optical applications and image applications as mentioned in [149]
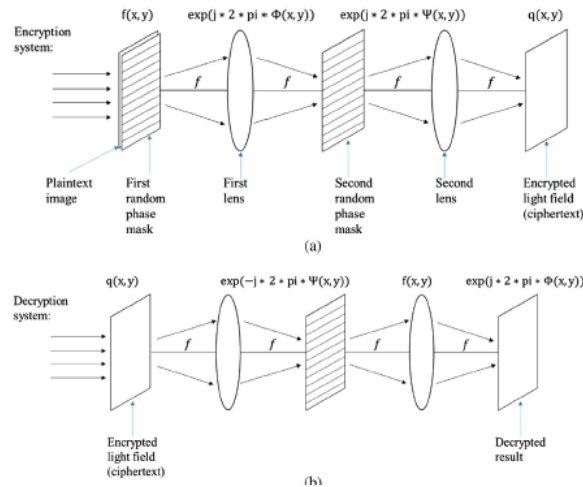
Figure 3-8 Double random phase encoding (DRPE) [133]

Jinho Choi in [150] considered an encryption scheme based on compressive sensing for multicarrier systems, where artificial noise is selectively transmitted together with a sparse message signal in the frequency domain to make an adversary's attack difficult.

52

To conclude, this section gives a brief view of the trade-offs between security and power consumption. Hardware implementation for security systems consumes less power than software. Furthermore, analogue hardware implementations consume less power if compared to digital implementations for the same security system.

3.6. Chipping Sequence or Pseudorandom number generator (PRNG)

It can be concluded from the two previous sections that the random signal sequence in the AIC and CS theory is highly important. The random signal has a random sequence of {-1, 1}. It also has to follow some rules: a) it needs to satisfy restricted isometry property (RIP) criteria, b) independent and identically-distributed (i.i.d) rule, and c) incoherence fact. The pseudorandom sequence can satisfy all of these rules.

Two scenarios can be used to implement the pseudorandom sequence. The first is to store the sequence in memory and recall it when needed. The second is to implement a pseudorandom generator (PRNG). The first solution has a very bad effect on power consumption. For example, as mentioned in [151], if we need to store 1024 bit, then at each cycle we will activate 1024 flip-flop and some extra circuits. This can result in high power consumption and can make the random sequence circuit exceed the power consumption of the ADC.

The other solution is more convenient, which is to use a PRNG circuit. Most of the previous architectures use a linear feedback shift register (LFSR). This circuit consists of a few numbers of flip flops and generates the required pseudorandom sequence of {-1, 1}. Other techniques use phase shift with a random controller. While both techniques reduce the power consumption of the PRNG, they intrude a digital circuit in an analogue frontend. Using analogue and digital circuits in the same systems requires isolation or partitioning between the two different types of the circuit to prevent the cross talk or noise. Three questions need to be asked:

1- Is there any analogue circuit that can generate the pseudorandom sequence?
2- Will this circuit consume more power than traditional LFSR or not?
3- What will be the performance of the signal reconstruction if the previous questions were positively answered?

To answer these questions, first, random number generators (RNG) types need to be identified. Then, a critical study needs to be done based on signal processing and circuit design to

know the capabilities to design an analogue circuit to generate a random signal including the hardware limitations.

Generally, a random number generator consists of three types: Pseudorandom (PRNG), True Random (TRNG), and Hybrid Random (HRNG) as shown in Figure 3-9. PRNG is deterministic and based on input seeds to generate random sequence and is mainly designed based on Linear Feedback Shift Register (LFSR) digital design concept. TRNG is based on capturing random physical quantity like thermal or chemical to generate the random signal. HRNG is a combination of both PRNG and TRNG.
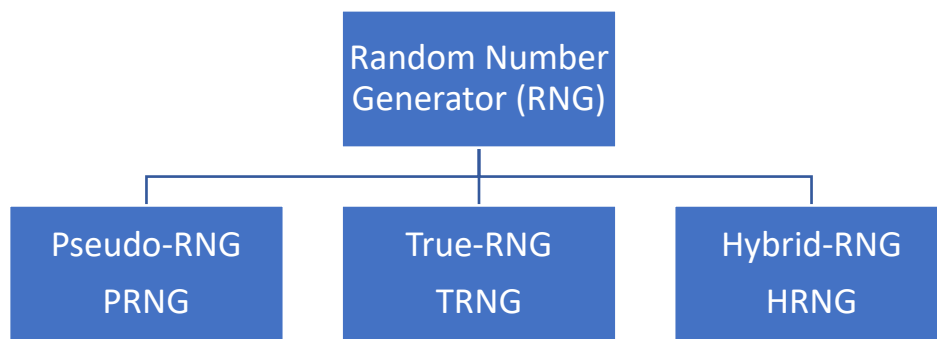
Figure 3-9 Types of Random Number Generator

PRNG is the most commonly used family in an AIC framework. This is because it is easy to be generated in hardware or software for both sides in the capturing and reconstruction of the signal. However, PRNG is not sufficient for security which is essential to the design of IoT devices.

In the signal processing filed, chaotic signals represent a potentially rich class of signals both for detecting and characterising physical phenomena and in synthesising new classes of signals for telecommunication and other signal processing applications. [152]

Chaotic signals are deterministic; they are not predictable in any practical sense in that even with the generating dynamics known, and estimation of prior or future values from a segment of the signal or from the state at a given time is highly ill-conditioned. These signals appear mainly to be noise-like. Chaotic signals can be analysed and processed using classical techniques for stochastic signals.

Comparing the power consumption for implementing the same system by an analogue circuit or digital circuit is very debatable. For example, low dynamic range makes the analogue

circuit more suitable than digital for some common CMOS technologies[153] as shown in Figure 3-10.

Generally, implementing the same system with the same specification by the analogue circuit is less power consuming than digital. However, analogue circuits suffer from noise and the possibility of crosstalk. Digital circuits are more reliable for design in several applications because of the suitability to be reconfigurable. Hence, analogue and mixed circuit design which is mainly based on an analogue circuit design that is controlled by digital controller appear to have the benefits of the analogue and the digital circuit design.
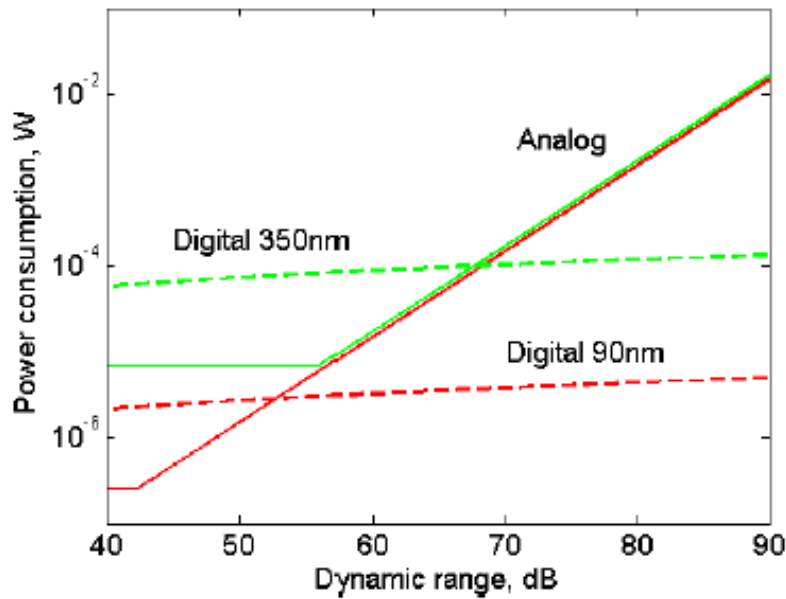
Figure 3-10 Analogue Vs Digital for Power consumption [153]

However, in the present research, an analogue chaotic oscillator will be addressed to replace the traditional digital PRNG and to overcome any isolation required between the analogue circuits and the digital circuits to implement the analogue frontend of the AIC. As this research is targeting PCB circuit design for implementing a low-power IoT based automated MC monitoring system, the evaluation of the power consumption will be based on using the off-shelf components.

On the other hand, the noise effect is very important to be addressed for using analogue chaotic based PRNG in AIC framework. In the next chapter, the noise effect will be shown based on the observation of the simulation results.

Before proceeding, it has to be mentioned that chaotic oscillator can be implemented by an analogue or digital circuit. However, because chaotic oscillators are based on differential

equations, digital implementation is more consuming to power and requires more size from IC design point of view. As an example, Figure 3- 11 shows the conceptual Digital chaotic circuit implementation [154]. The number of resources required to be used if we use DSP Processor or FPGA to implement the system shown in Figure 3-8 is detailed in Table 3-3, while Table 3-4 shows the resources used for implementing three different chaotic oscillators families by FPGA [155]. It is very clear that the huge amount of resources required increases the complexity and leads to consumption of more power. On the other hand, an analogue chaotic oscillation design can vary from using few numbers of active elements like transistors or opamps to very complicated analogue design based on the application as will be shown later in this research.
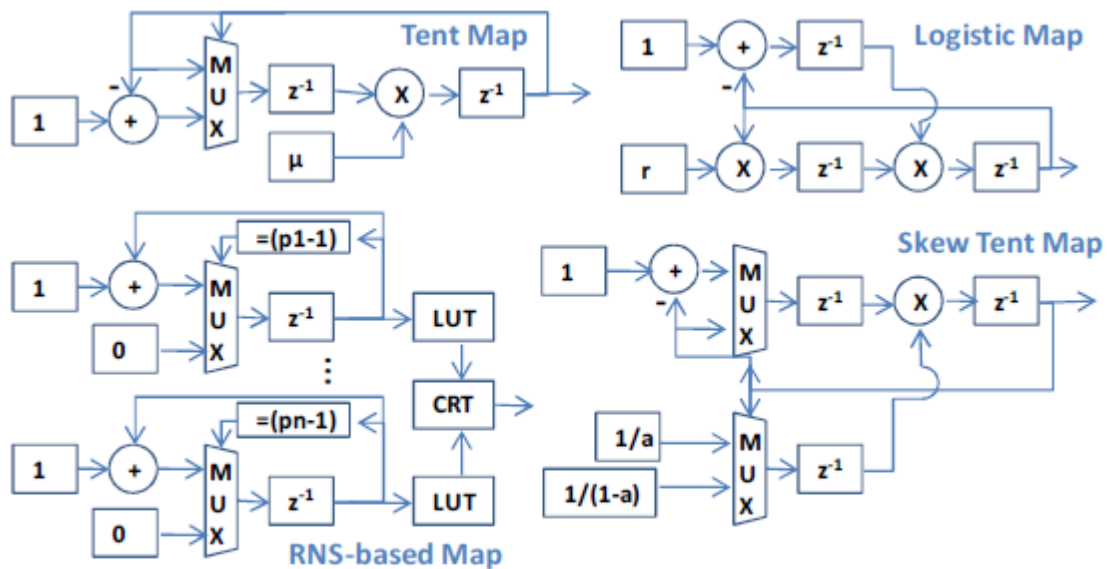
Figure 3-11 Conceptual digital chaotic circuit implementaions [154]

Table 3-2 Computational complexity comparison [154]

Chaotic Map	DSP Resources		FPGA Resources				
	Clock Cycles/Stamp	Memory (bytes)	Registers	Look Up Table (LUT)	Multiplier	Maximum Clock Frequency (MHz)	Pipeline factor
Tent Map	114	44	302	765	12	70	2
Skew Tent Map	1225	8	302	823	12	70	2
Logistic Map	183	4	169	1468	24	51	2
RNS Cubic Map	154	4908	222	4712	0	134	1

Table 3-3 Implementation of three chaotic oscillators families by FPGA [155]

Chaotic Oscillator	Number of Reg.	Number of LUTS	Number of Occupied slices	Max Clock Frequency (MHz)
Euler-Based	9196	7822	2482	436143
Heun-Based	19721	16591	5848	463.688
RK4-Based	42021	39309	11390	373.094

56

The three questions mentioned in this section can be properly answered with a discussion of the limitations after implementing the analogue Chua circuit as a chaotic based PRNG for AIC framework in the next chapter. But before proceeding to introduce the Chua circuit, using chaotic algorithms in CS will be addressed in the next two paragraphs.

In CS theory, using chaos theory-based algorithms to generate random sequence is not new. However, two important points are missing in this usage. Chaotic AIC mentioned in [156]and shown in Figure 3-12, no hardware implementation by analogue or digital was presented.

(a) Measurement Subsystem
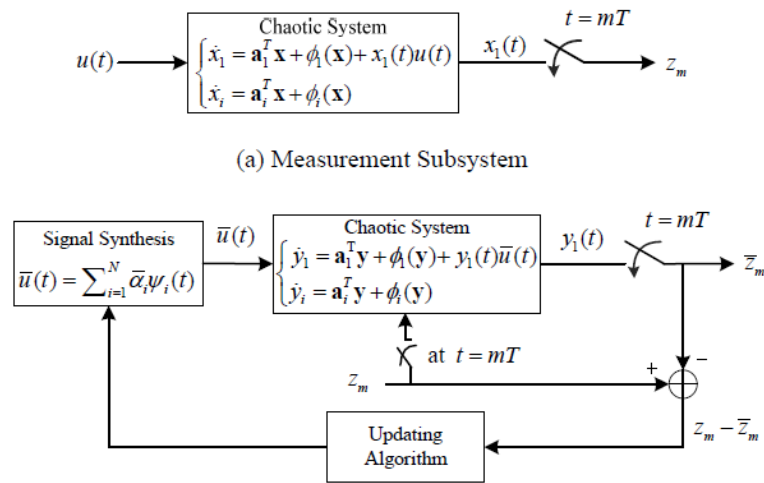
Figure 3-12 Chaotic AIC [156]

Based on these facts, this research is focused on replacing the digital PRNG with a low-power analogue chaotic PRNG to prevent any need of isolation. In the next section, the Chua circuit will be introduced. Then, the output of the Chua circuit will be tested in the AIC framework in the next chapter.

At the end of this section, generating PRNG using an analogue circuit to be found in the AIC framework is one of the targets of this research to design a pure analogue AIC analogue frontend. Analogue chaotic based PRNG is promising to replace the traditional digital based PRNG which is generally found in most of the AIC analogue frontend. Analogue Chua circuit is chosen as a first step to test the analogue circuit oscillator behaviour because of its simplicity in design and the analysis as will be shown in more detail in the next section.

3.7. Chua Circuit background

Hardware implementation for chaos signal was introduced by Leon Chua in 1983 by using a nonlinear circuit. This circuit consists of LC oscillator, an RC coupling circuit and nonlinear

negative resistance as shown in Figure 3-13. Chua's circuit demonstrates dynamical systems as found in mechanical or thermal systems and generates a random sequence. The concept of this circuit has spread in many fields especially in encryption of communication systems.
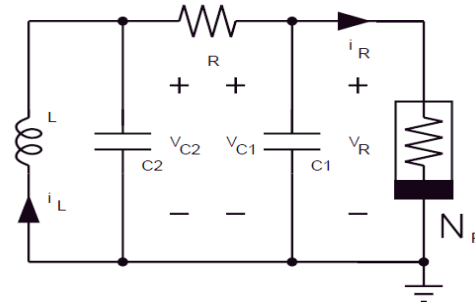
Figure 3-13 Chua Circuit

By applying simple electric circuit analysis, we found that Chua circuit state equations are:

$$C_1 \frac{dvc_1}{dt} = \frac{1}{R}(vc_2 - vc_1) - g(vc_1) \tag{3-4}$$

$$C_1 \frac{dvc_2}{dt} = \frac{1}{R}(vc_1 - vc_2) + i_L \tag{3-5}$$

$$L \frac{di_L}{dt} = -vc_2 \tag{3-6}$$

Where $g(v_R) = m_o v_R + 0.5(m_1 - m_0)[|v_R + B_p| - |v_R - B_p|]$

m_0, m_1 are the outer slope for the I-V characteristics for the negative resistance (NR)

B_p is the break point, as shown in Figure 3-14
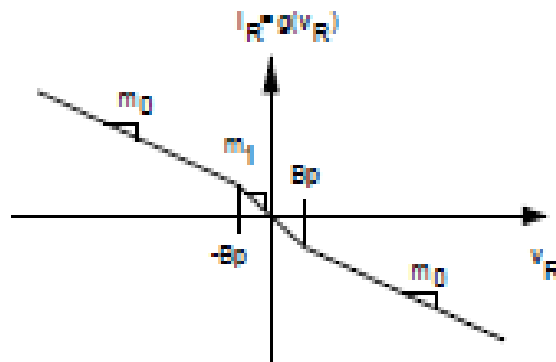
Figure 3-14 I-V characteristics for the negative resistance (NR)

As mentioned before, the Chua circuit is composed of three sub-circuits: First is the oscillator, second is the RC coupling circuit, and the third circuit is the negative resistance (NR)

[157]. From the design point of view, at least one of these circuits has to be active. Several implementations for Chua circuit have been done and summarised in Figure 3-15.

Researchers implement the NR circuits based on active circuits by means of diodes, op-amps or transistors [158]. HP Company has announced that they designed a Memristor device that has NR properties [159]. On the other hand, using Memristor as NR is still at the research level and will be commercially used soon; hence it will not be tested in this study. In this study, op-amp presentation will be used which is easier to design.

An opamp based NR implementation has three ways based on op amp functionality: Voltage operation amplifier (VOA), current feedback operational amplifier (CFOA) or operation trans-conductance amplifier (OTA). In this chapter, VOA implementation will be used as a first step to test the Chua circuit while the other implementations will be considered as future work.
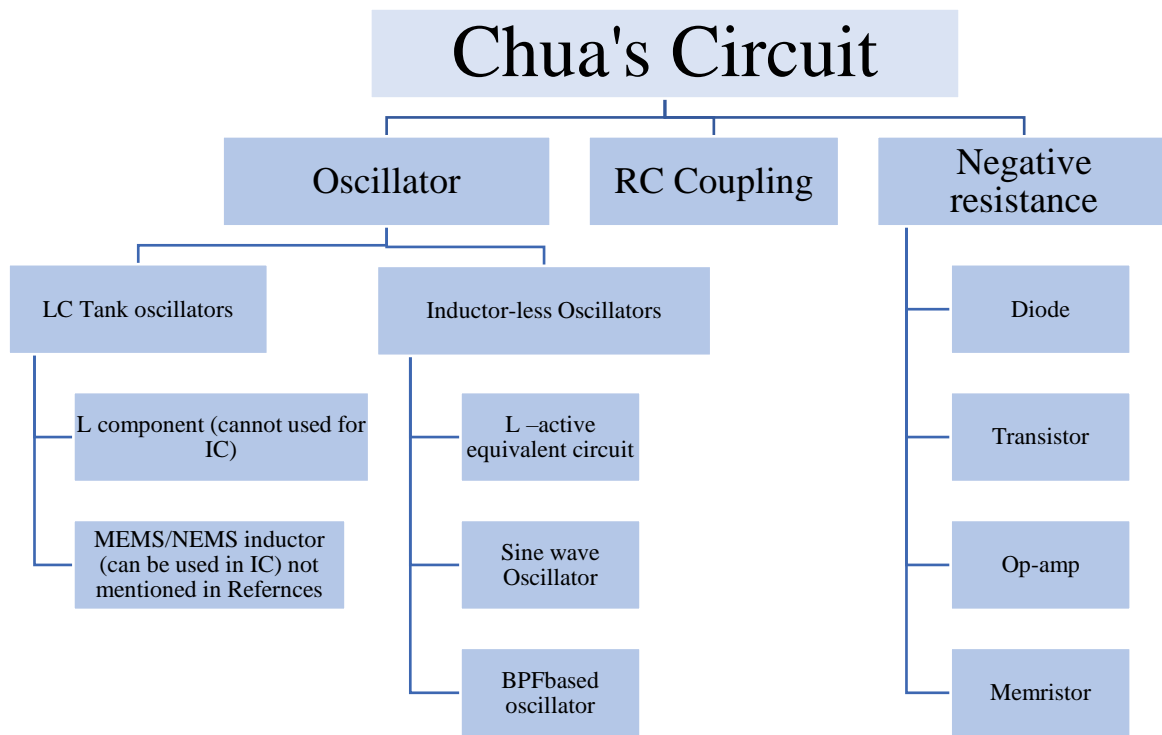
Figure 3-15 Chua circuit with different implementations concept

The design of the RC coupling circuit is very crucial to reach the bifurcation and randomness in the Chua circuit. It has to be mentioned that the capacitor presenting the parasitic capacitance from the NR section is mentioned in [157].

For the oscillator, two different implementations can be used. The first is to use the normal LC parallel circuit. The drawback for using this method is that L inductor was a very big problem

for PCB or IC design because of the magnetic effect and the size respectively. However, nowadays MEMS technology can be used to design inductor for IC design (MEMS/NEMS inductor is not used till now for Chua's circuit which makes it one of the hot points of research).

The second type can be divided generally into three categories: an active inductor, LC oscillator replacement, and active filter-based oscillator. The first category is just replacing the grounded inductor by its active op-amp circuit model or it is called synthetic inductor [160]. The second category is based on replacing the LC tank oscillator by sine wave oscillator [161]. The last one is based on the frequency response of the LC filter by designing active bandpass filter (BPF) shape and by moving one of the poles of the transfer function to the right side of the s-domain to oscillate the circuit [162].

In this report, the author uses the first category, because synthetic inductor mainly used opamp which is suitable for PCB design and the ease of implementing the NR by VOA or CFOA or OTA. For this reason, the research will examine the use of these topologies like NR and will focus only on VOA and CFOA implementation for the synthetic inductor.

It is observed from the state-space equation of Chua circuits, that Chua circuit has three outputs. The output terminals are the NR voltage, VC_1, and LC oscillator voltage or VC_2 and the current passing through the grounded inductor or i_L. The output signal can be taken from any of the three mentioned terminals. However, to reach the randomness the relation between these terminals needs to reach what is called a double scroll, as shown in Figure 3-16.

A double scroll graph shows that the system has two levels of voltages. Each voltage level has centre frequencies that can oscillate then at some chaotic point it travels to the voltage level then oscillates then gets back to the first voltage level and so on. However, the time to change its voltage level is random or in other words is chaotic. It is mentioned that when the Chua circuit reaches this behaviour this means the chaotic behaviour takes place and chaotic sequence can be obtained by one of the circuit's terminals. Figure 3-17 shows the output of each terminal when chaos occurs.
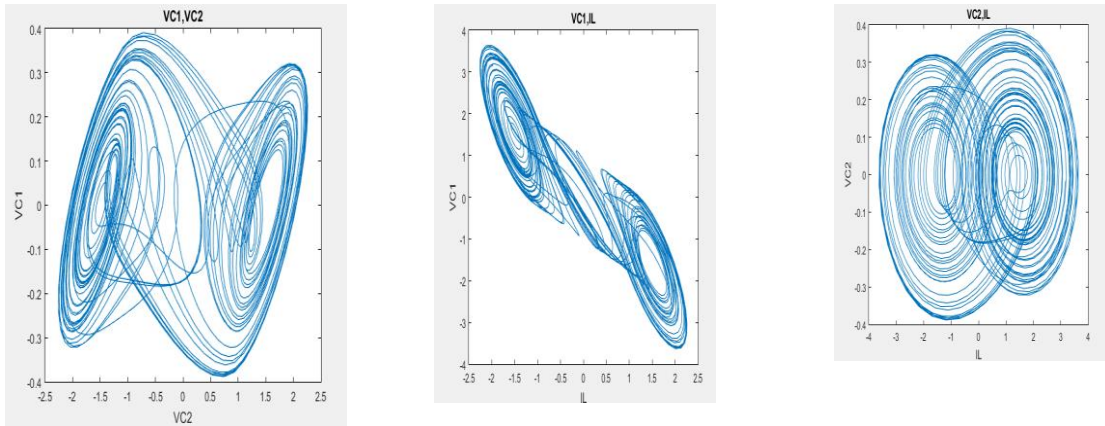
Figure 3-16 Chua circuit output terminals relations

VC1

VC2

IL
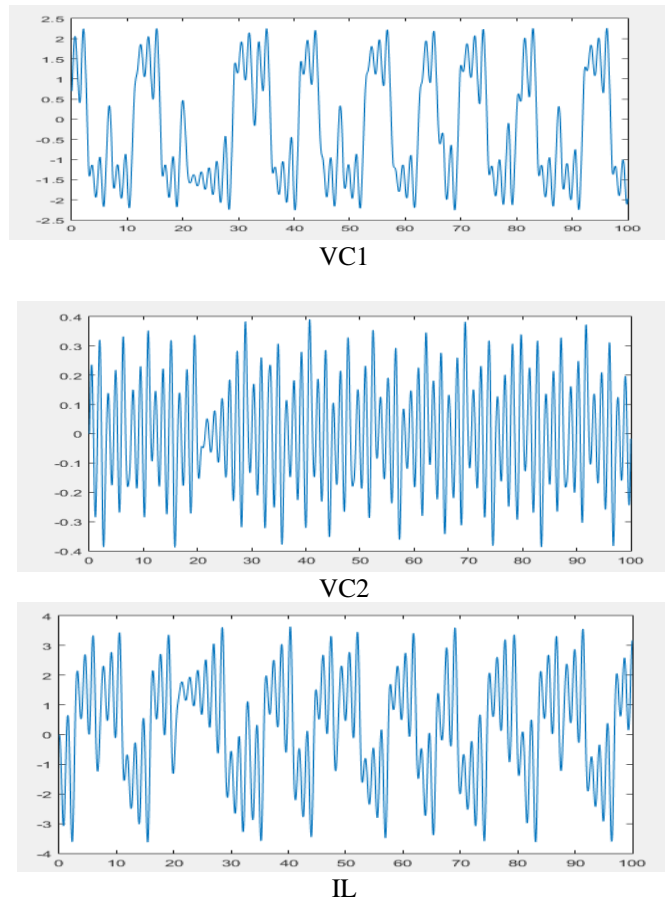
Figure 3-17 The output waveform VC1, VC2, and IL respectively

The key to reaching randomness or chaos behaviour (bifurcation) is the design of the RC coupling circuit. The variation of R by fixing C1 or variation of C1 by fixing R will cause the bifurcation. The difference between them is mentioned in [157]; the size of the double scroll attractor remains constant in the C1 variation because the equilibrium points are independent of

C1 which is not the same case for R (more details for the difference can be found in [163] and [157]).

Component value selection mainly depends on solving the state equation. Several solutions have been calculated to observe the chaotic attractor. Matsumoto et al. [164] mentioned three solutions for extracting the chaotic behaviour in the Chua circuit.

Choosing the component values mainly depends on one of these solutions. Besides, the actual components values may differ by small percent due to the tolerance and the standard values for the components. For example, several references design the RC coupling circuit by fixing the capacitor (C1) value and use the potentiometer for adjusting the R-value (bifurcation parameter).

3.8.   Conclusion

To conclude, this chapter presents first a brief overview of CS, AIC and analogue Chua circuit. It was shown that, while pre-processing section for AIC is analogue, the researchers use digital circuits to generate the random signal required for AIC. The researcher used digital PRNG for the AIC analogue frontend, as it is used also for the signal reconstruction part. However, it was reported that the signal reconstruction can be designed using analogue circuit design by means of the FPAA, has less power consumption in comparison to the digital implementations. These efforts did not focus on the power consumption and the security trade-offs. Also, some of these implementations used LFSR as a digital circuit to generate PRNG.

The power consumption and the security trade-offs for the AIC are presented. It was shown that digital presentation for the digital PRNG like LFSR uses a lot of resources in comparison to analogue chaotic oscillator like Chua circuit. A very brief introduction of Analogue Chua circuit is presented to replace the traditional digital PRNG by analogue.

There are three advantages for using analogue chaotic based PRNG in AIC framework:

1. No isolation required to reduce the crosstalk between analogue and digital circuit,

2. Chua circuit uses very few numbers of resources if it is compared with the digital chaotic oscillators shown before in the research, and

3. As one of the development steps for designing IoT device is to develop the analogue signal processing before using ADC to reduce the power consumption which is one of the main challenges of the IoT device design.

Chapter 4

Investigating the use of Analogue Chua Circuit for AIC Framework

4. INVESTIGATING THE USE OF ANALOGUE CHUA CIRCUIT FOR AIC FRAMEWORK

In the previous chapter, an overview was provided for the basics of the compressive sensing (CS) based analogue to digital converter (ADC), which is called analogue to information converter (AIC). AIC is presented to replace the traditional ADC found in the DAQ unit in the IoT based Manhole cover monitoring system. Because the heart of the AIC is the pseudorandom generator (PRNG), it motivated the researcher to use it to secure the data at the same time. While most of the AIC implementations are using a linear feedback shift register (LFSR) to generate PRNG, LFSR is lacking in security. This motivated several researchers to replace LFSR with more complicated digital PRNG for security.

These efforts have two drawbacks: power consumption and isolation required between the analogue part and the digital part found at the AIC analogue front end. Hence, analogue chaotic oscillators are presented to generate a low-power secured AIC analogue front end to replace the traditional digital PRNG.

Chua circuit was briefly introduced in the previous chapter as a first step to study the effect of replacing the traditional digital PRNG by the analogue chaotic oscillator. In this chapter, the performance of using analogue Chua circuit for the AIC framework is presented. The purpose of this chapter is to investigate the use of the analogue Chua circuit in the AIC framework with some common limitations that can be observed from the results.

To the knowledge of the researcher, implementing analogue Chua circuit in AIC framework has not been studied before while in the context of the compressive sensing, the use of chaotic sequence by means of the digital chaotic circuit has been studied and proven with good acceptable results. However, a hardware implementation for generating chaotic sequence from analogue circuits has not been addressed before in the AIC design.

This chapter presents the first step of studying generating chaotic sequence from an analogue circuit in the AIC framework. In this chapter, analogue Chua circuits are simulated, and the output of the circuit simulation is fed to AIC framework implemented in a Matlab toolbox software. The Matlab toolbox is based on random demodulator (RD) AIC technique.

As mentioned in chapter 3, an analogue Chua circuit has several implementations. Op-amp is one of the methods that are used to implement analogue Chua circuits. Voltage Operation

Amplifier (VOA) and Current Feedback Operation Amplifier (CFOA) are widely spread techniques used in references. Hence this chapter will study these two techniques to implement analogue Chua circuit in the AIC framework.

The simulation results for VOA and CFOA based Chua circuit implementations in the AIC framework show good performance in reconstructing the original signal in the absence/presence of noise. The several implementations of the Chua circuit have already been mentioned in several references based on off the shelf components. In this study, the researcher used the same designs with the lowest power supply recommended in the op amps datasheets to study these topologies in the lowest power consumption case. The results of this chapter show a motivation to use the analogue Chua circuit in the design of the ADC in the DAQ module for IoT based automated MC monitoring system.

The inductor for the LC oscillator section in the Chua circuit is also replaced by a synthetic grounded inductor. The synthetic grounded inductor is implemented in VOA and CFOA based circuits [158]. Hence the study will extend to simulate hybrid topologies by using a combination of CFOA and VOA for the analogue Chua circuit.

Before proceeding, some important points need to be taken into consideration:

1-   The components used to build the circuits in this research, can be easily implemented on PCB with low cost. This is needed because IoT is becoming more popular, thanks to low-cost open source hardware like Arduino. While these open source platforms are very low cost, they suffer from high power consumption as mentioned in Chapter 2. Hence, this study at this step can enhance the development of open source hardware by adding analogue modules that reduce the sampling rate of the ADC with the same concept of using commercial low-cost components. These platforms use typical commercial batteries of 5V which are also used in this study.

2-   Several types of research have been done to design very low-power consumption VOA and CFOA to be supplied with 1.1V or less which makes the power consumption a few mW and a fraction of mW. However, this research is considered to be state of art for using analogue Chua circuit in the AIC framework by means of off the shelf component and the scaling down of the power consumption can be done in the level of the IC circuit design.

This chapter is organized as follows: First, the several topologies to implement the analogue Chua circuit used in this study will be presented. Second, the RD based AIC framework

implemented in Matlab will be briefly shown. Then the results of the Multisim spice and the Matlab simulation will be presented with a discussion.

4.1. Chua Circuit topologies

Chua's circuits and equations consist of a three-dimensional autonomous system with a three-segment piecewise-linear function which gives rise to three equilibrium points. Chua circuit mainly consists of 3 subsections: LC oscillator, RC network, and negative resistance (NR). At least one of these subsections needs to be active. All NR implementations are designed by active elements like op amp. Based on the internal circuit design, op amp can be used as voltage operational amplifier (VOA), current feedback operational amplifier (CFOA), or operational transconductance amplifier (OTA). However, VOA and CFOA are the widest spread techniques used.

On the other hand, inductors have several disadvantages as shown in Chapter 3. Hence most of the oscillator section in analogue Chua circuits used synthetic grounded inductor which is mainly based on op amp as VOA or CFOA. Based on the brief introduction for the Chua circuit presented in the previous chapter, the NR implementation and the synthetic inductor are used in this study, presented as follows:

NR implementation

a) **Voltage operational Amplifier (VOA)**

Kennedy shows in [163] the ability to design NR using two op amps in parallel operating in their linear and nonlinear region with six resistors as shown in Figure 4-1. This design has been accepted to be the standard for discrete implementation as mentioned in [158]. The basic idea is that op amp has its negative resistance behaviour. However, it needs two op amps to reach the NR requirement as shown in Figure 4-1. Figure 4-1 also shows the simulated I-V characteristics for the NR using the Multisim software for Vcc=5V. The design of VOA based Chua circuit is chosen to make the inner slope of the Chua circuit to be G_a=-0.756 mA/V, while the outer slope is G_b=-0.409 mA/V with B_p=±1 V.

b) **Current Feedback Operational Amplifier (CFOA)**

El-Wakil and Kennedy published a CFOA based NR to overcome the bandwidth limitation for the VOA [158], [161], [165]. AD844 CFOA was used with only four

66

resistors. Here, the configuration CFOA operated as a nonlinear voltage controlled negative impedance converter (VNIC). Figure 4-2 shows the design with the simulated I-V characteristics. The design is chosen similar to the VOA design for the slopes and the breakpoints. Here the inner slope is G_a= -0.8 mA/V, while the outer slope is G_b= -0.5 mA/V with B_p= ±1V[158].
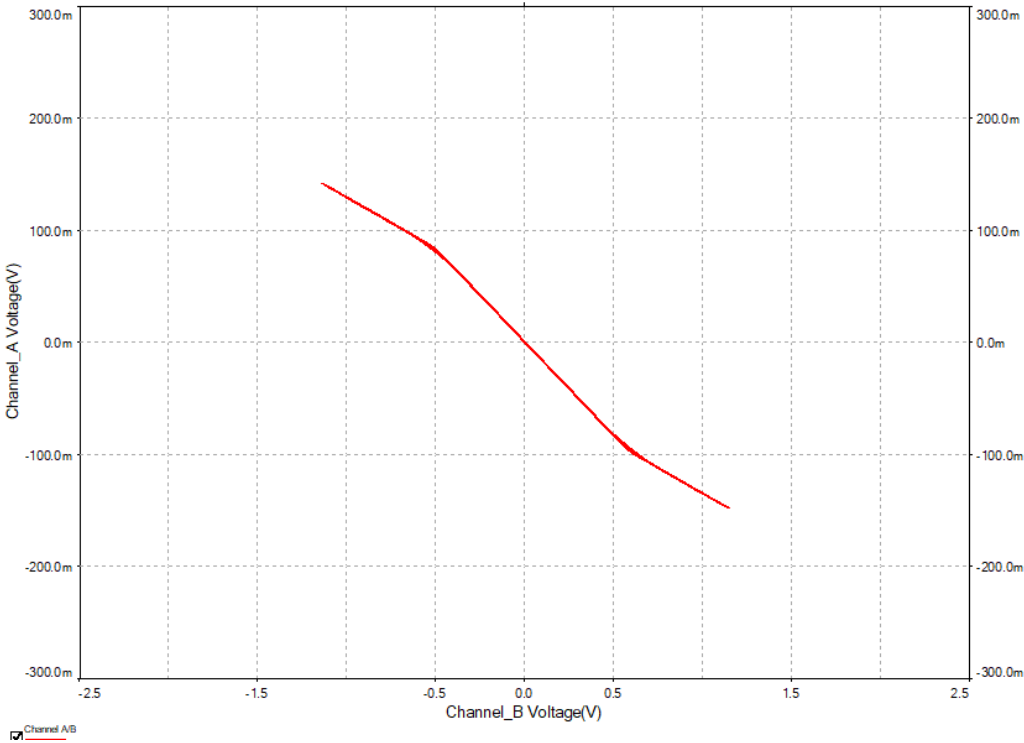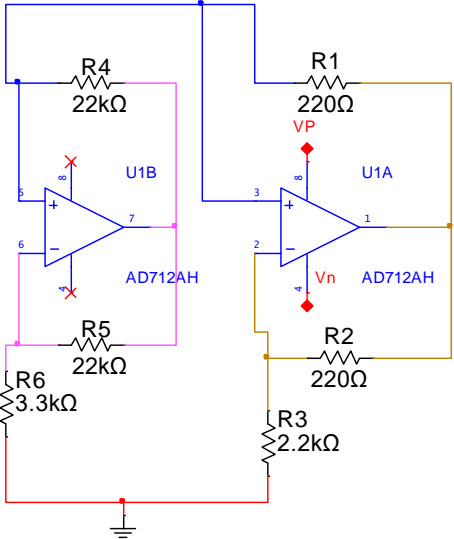

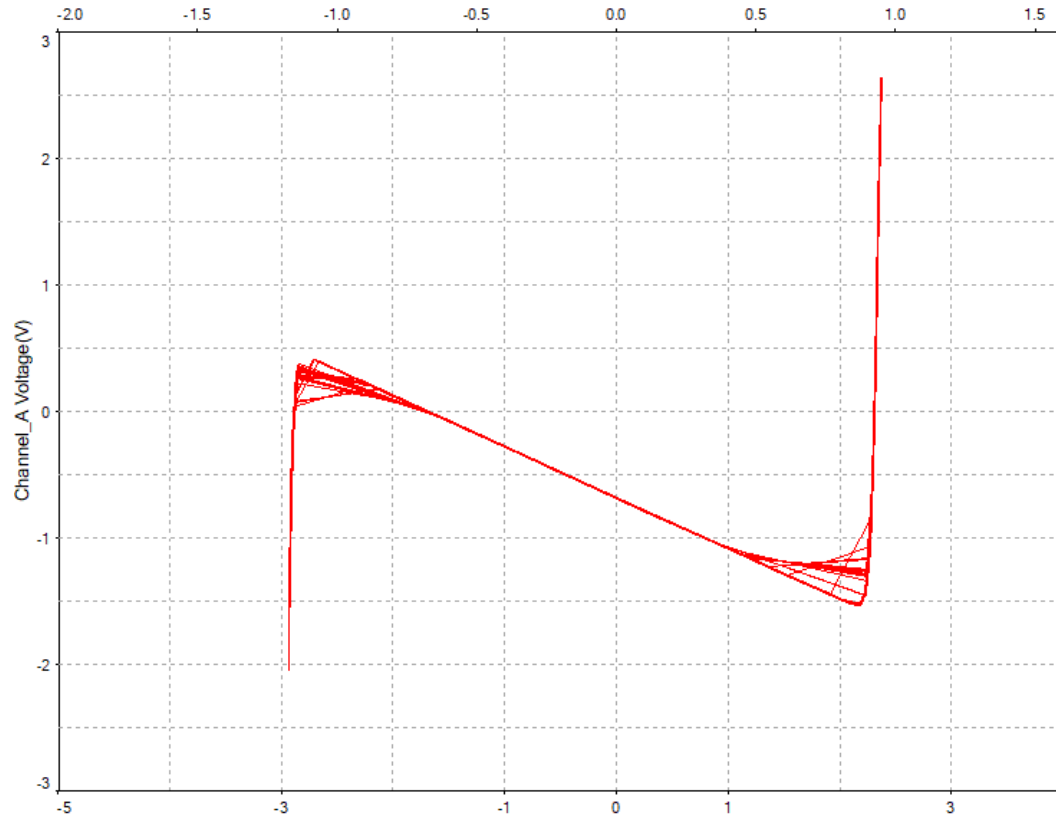
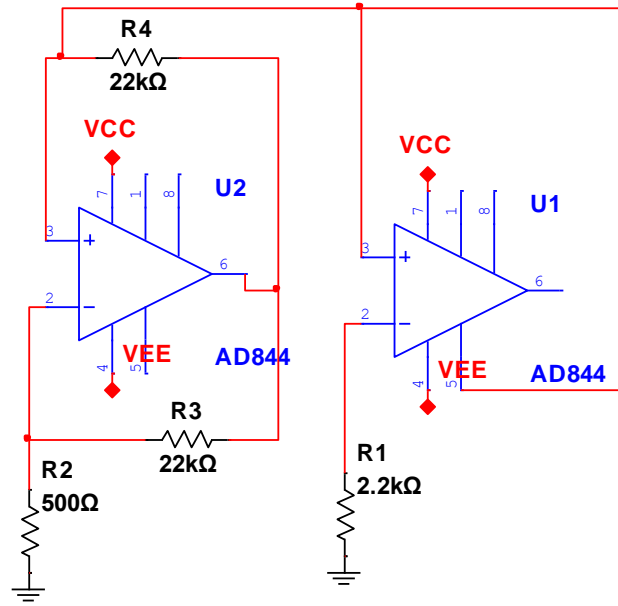Figure 4-1VOA based NR designed by Kennedy [88]

Figure 4-2 CFOA based designed by El-Wakil and Kennedy [83]

Synthetic inductor

Design synthetic inductor has several implementations. In this research and similar to NR design, VOA and CFOA based have been chosen to realize the LC oscillator.

a) *Voltage operational Amplifier (VOA)*

Researchers in [160] used one op amp to build synthetic inductor for the analogue Chua circuit shown in Figure 4-3. The equivalent inductor equation is presented in equation (4-1)
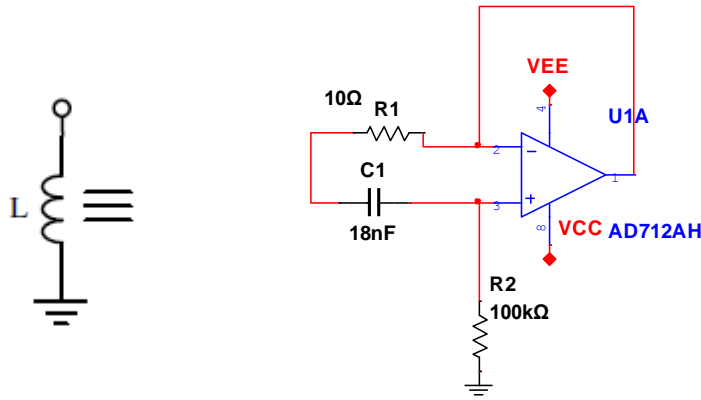

Figure 4-3 VOA based synthetic inductor

$$L_{eq} = CR_1R_2 \tag{4-1}$$

b) *Current Feedback Opamp (CFOA)*

Researcher in [165] used CFOA to build the synthetic inductor and used it for the Chua circuit as shown in Figure 4-4. The equivalent inductor equation is presented in equation (4-2)
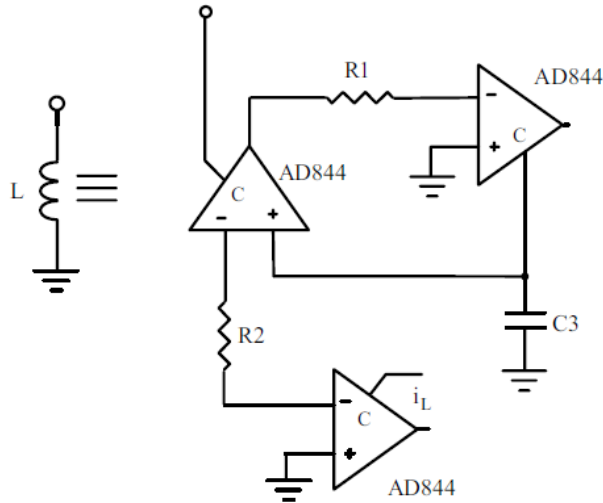
Figure 4-4 CFOA based synthetic inductor [165]

$$L_{eq} = C_3 R_1 R_2 \qquad (4\text{-}2)$$

4.2. Analogue Chua circuit design for the AIC framework:

The AIC Matlab framework toolbox used in this study is implemented by Michael Lexa et al. [166] based on Joel A. Troop et al. analysis [122]. The random demodulator (RD) toolbox is called Continuous-Time Spectrally-Sparse Sampling Toolbox (CTSS), and OMP algorithm is used for signal reconstruction. Also, this frame examines the signal reconstruction in the absence and the presence of the noise. On the other hand; the default settings are:

1- Generate multi-toned signal (which is similar to the multisensor system used for IoT based automated MC monitoring system) (option to add white Gaussian noise)
2- Assign the sampling rate N=1000;
3- Let M = 100
4- K=10
5- Integration using FIR filter.
6- Sampling (using Rand command followed by sign command to generate {-1,1} in a random sequence)
7- Recovery using OMP algorithm by means of all the data above
8- Display the signals in the time domain and frequency domain before and after recovery
9- Calculate the error between the original signal and the recovery

70

To apply the Chua circuit on the AIC framework, the frequency needs to be at least equal to or more than Nyquist rate. As the nature of the Chua circuit is to change the frequency from upper to lower frequency, the study will use the same design in the references for 3.75 kHz which satisfies the parameters in the Matlab toolbox. It has to be considered that in this stage of the research, the main focus is to check the ability of the Chua circuit to be implemented in AIC frontend. Hence, as mentioned before, more specification and the limitations will be addressed as future work.

Three different op amps are used for implementing VOA realization which are AD712AQ, LMC6482IN, and AD8605ACB; while for CFOA, IC AD844 is used as mentioned before.

4.3.   Results and Discussion

This section presents the results of applying the different realization for the analogue Chua circuit in the AIC framework. Table 4-2 shows the studies in this research which are: Circuit schematic, bifurcation figure; then the spectrum and the waveform of the original signal and the reconstructed signal after applying the AIC model. The figures used for AIC are only in the absence of the noise to be clear. On the other hand, Figures 4-5 and 4-6 show the average squared error for signal recovery in both the absence and presence of the noise respectively. In the same figures, the results are compared with the "rand" command using the Matlab toolbox. Figure 4-7 shows the ratio between the two cases, while Figure 4-8 shows the power consumption for each circuit used in this study.

As mentioned before, the RC_1 section is responsible for the bifurcation phenomenon. In this study, C_1 is fixed at the ratio of C_2/C_1= 10, which makes C_1 for all experiments equal to 10µF. While R is used as potentiometer varied till the circuit reaches bifurcation and generates the double scroll waveform. The values of the R that initiate the bifurcation are presented in Table 4-2

In the case of the absence of noise shown in Figure 4-5, most Chua circuit implementations show good performance than "rand" command, while in the noise presence, the output sequence of Chua circuit affected by the noise as the "rand" command as shown in Figure 4-6. Figure 4-7 shows the ratio of the average error of the signal reconstruction in the presence of noise to the absence of noise. It can be observed that some configurations show good performance than the
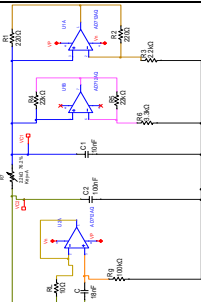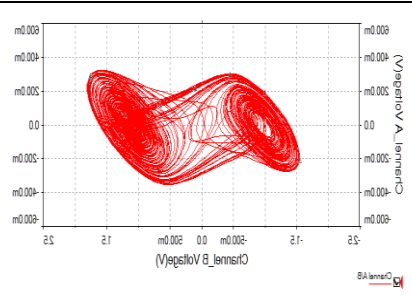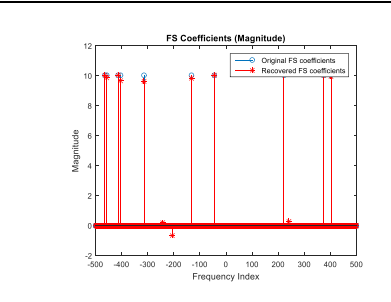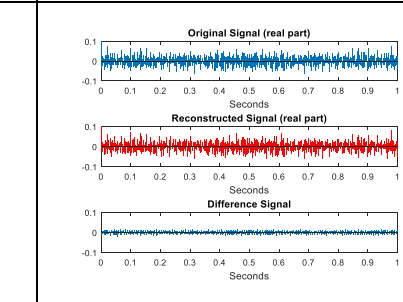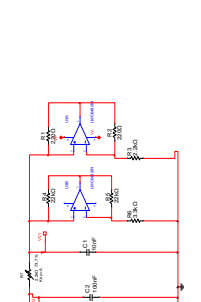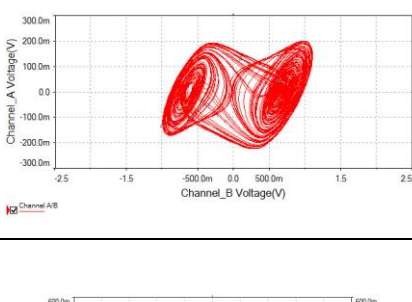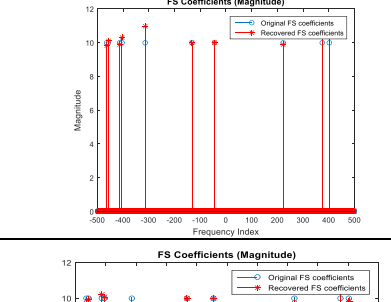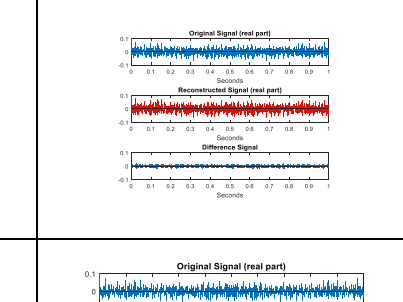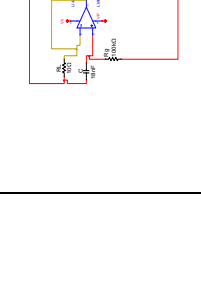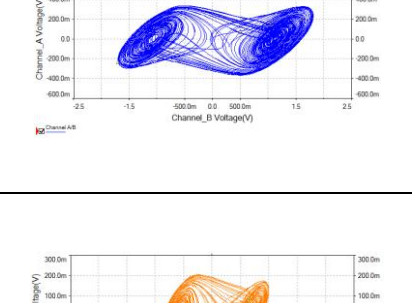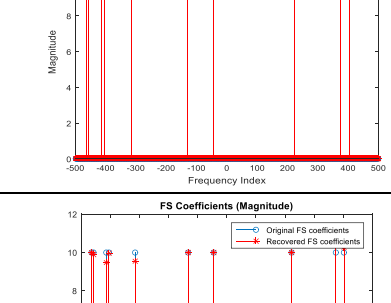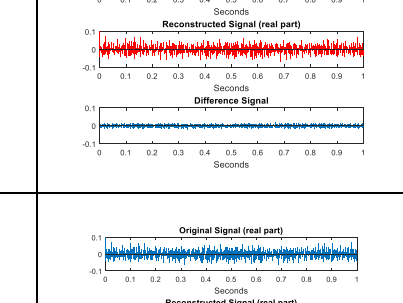
"rand" command. These configurations are all VOA based Chua circuit except forAD8605ACB, one case of hybrid1 (AD712AQ-AD844), and one case of hybrid2 (AD844-LMC6482IN).
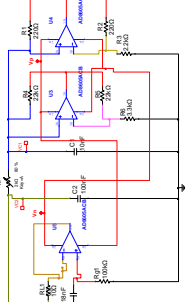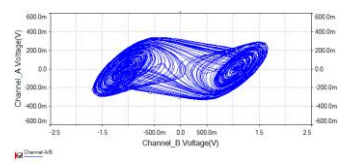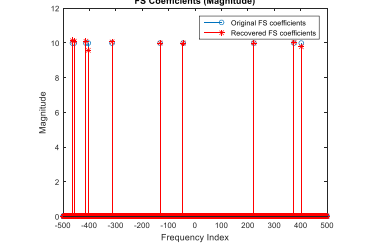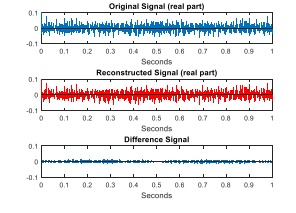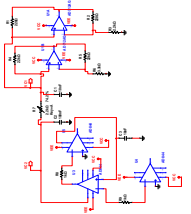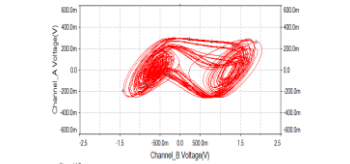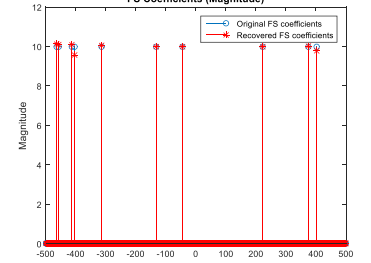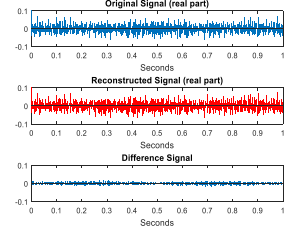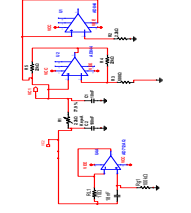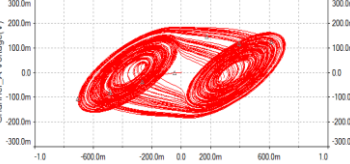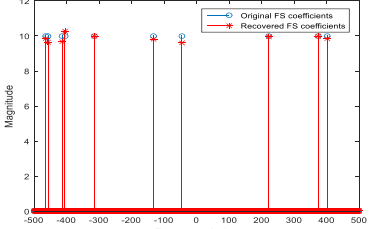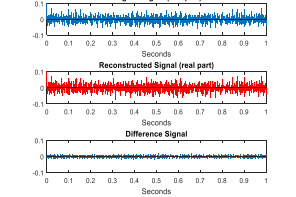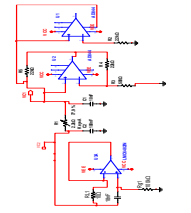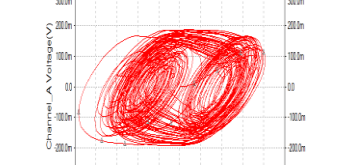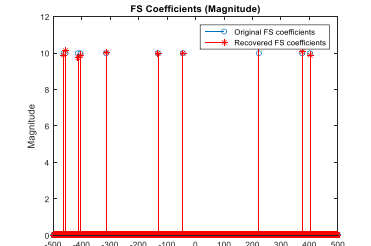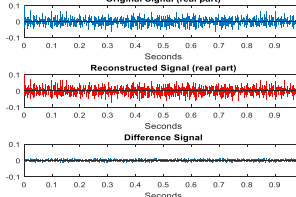
Without comparing with "rand" command, VOA, CFOA, Hybrid1 and Hybrid2 generate chaotic sequence which has a good performance for reconstructing the original signal. However, some points need to be taken into consideration: First, while CFOA is mainly used for its large bandwidth, it has less performance than VOA for reconstructing the signal. As the main section or unit for the Chua circuit is the oscillator section, choosing CFOA for implementing both the oscillator section and NR will affect the performance if it is required with large bandwidth. Hybrid2 configuration did not show any enhancing in this point. However, from a power consumption point of view, as shown in Figure 4-8, Hybrid2 configuration shows less than half of the power consumption for the CFOA.
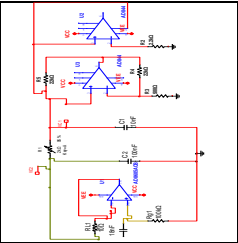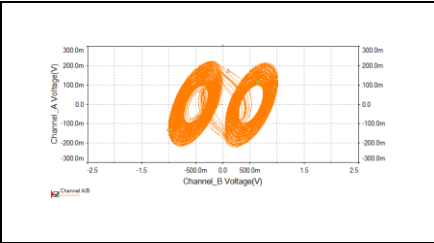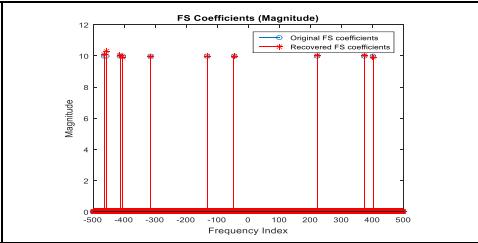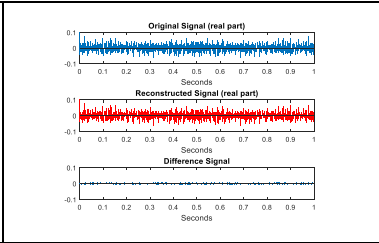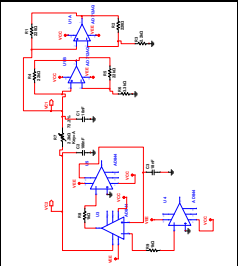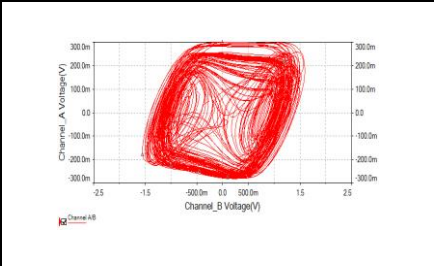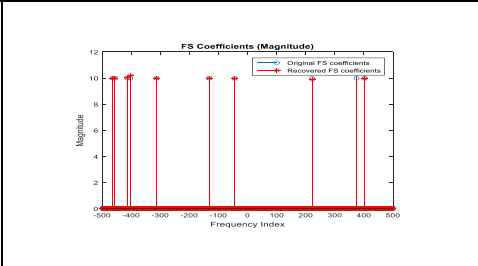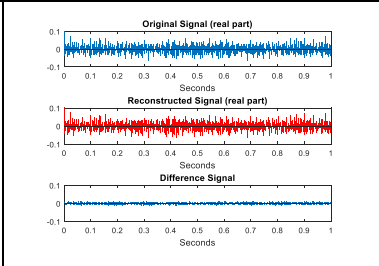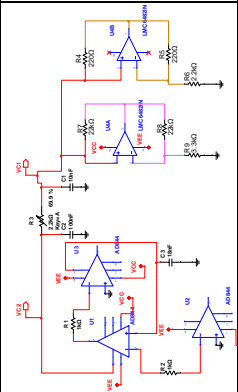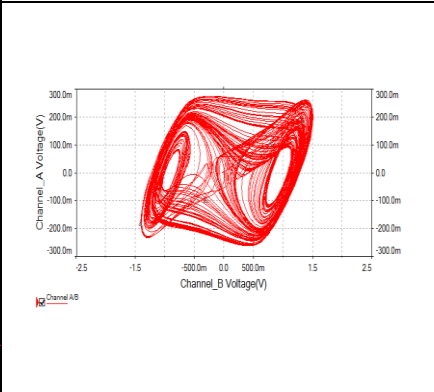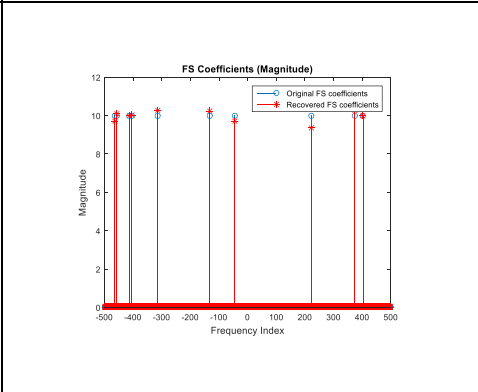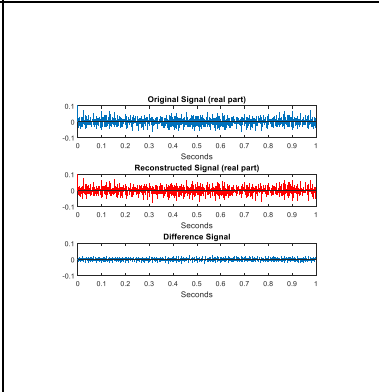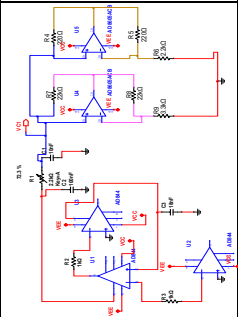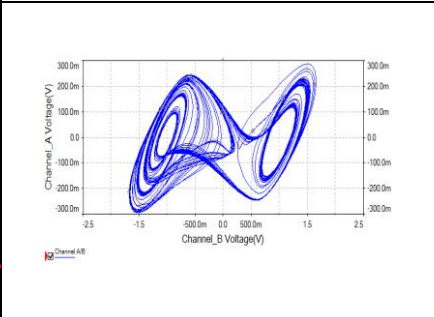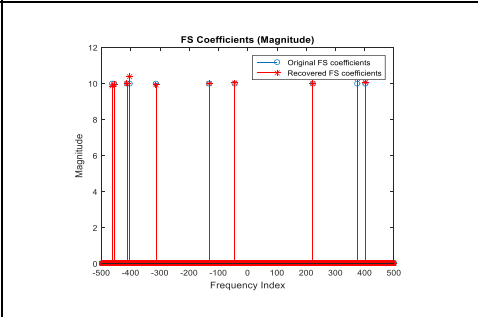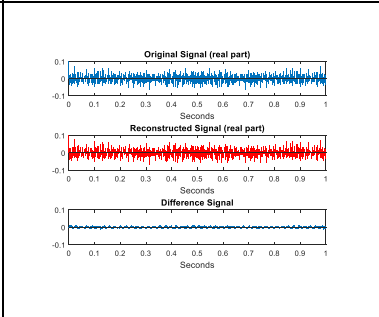
This point is very interesting because the difference in the signal reconstruction between both configurations can reach 0.001754614 in the worst case (Hybrid2 AD844-AD712AQ) in the presence of noise which can be suitable to use for low-power consumption applications as Hybrid2 consumes less power than CFOA by 270mW as shown in Figure 4-8.

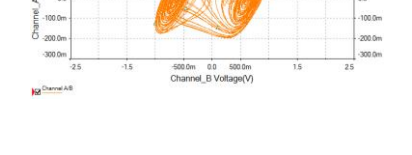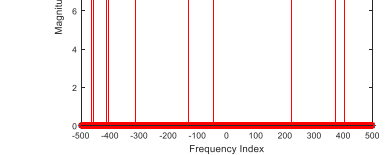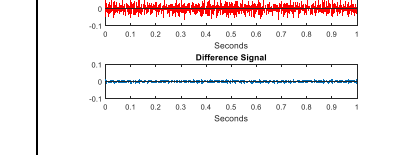Second, for the VOA and Hybrid1 implementations, it is shown from the same figures that Hyprid1 did not enhance signal reconstruction except for the case of AD712 which is based on FinFET technology. On the other side CMOS VOA shows good performance with low-power consumption, which makes VOA based analogue Chua circuit the most suitable for low-frequency applications. It has to be considered, that while the main target of the research is to reduce the power consumption of the ADC by using the AIC as a preprocessing circuit and to make this circuit only analogue to avoid any need of isolation required, analogue processing techniques need to be used also to reduce the power consumption for this analogue processing.

Table 4-1: Studies of using analogue Chua circuit in AIC framework

Study	Design	Schematic	Bifurcation	Spectrum	Waveform
VOA	AD712AQ				
	LM6482IN(3V)				
	LM6482IN(5V)				
	AD8605ACB(3V)				

73

	AD8605ACB (5)			
CFOA	AD844			
Hybrid1 (VOA_CFOA)	AD712AQ-AD844			
	LMC6482IN-AD844			

	AD8605ACB-AD844				
Hybrid 2	AD844-AD712AQ				
	AD844-LMC6482IN				
	AD844-AD8605ACB				

Figure 4-5 Average error of the signal reconstruction in the absence of the noise
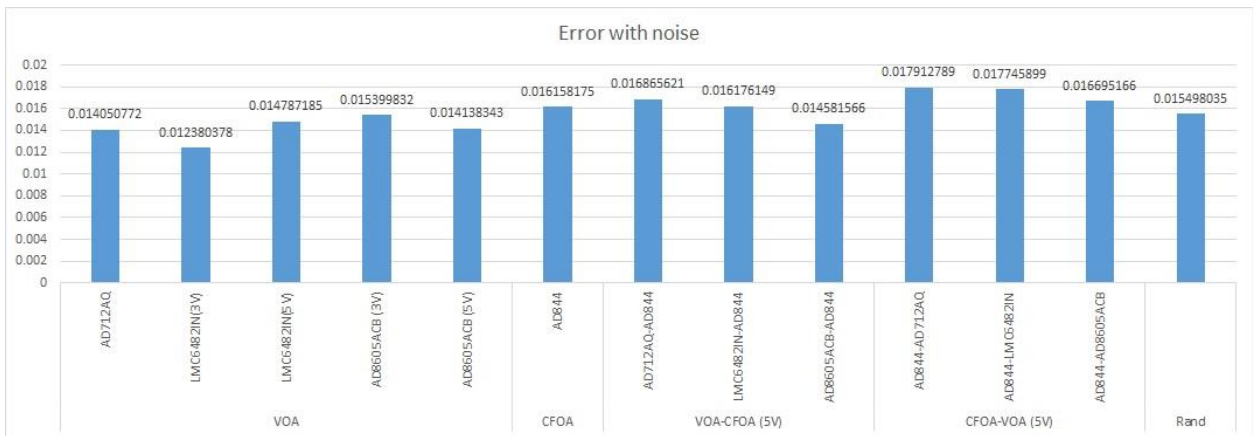
Figure 4-6 Average error of the signal reconstruction in the presence of the noise
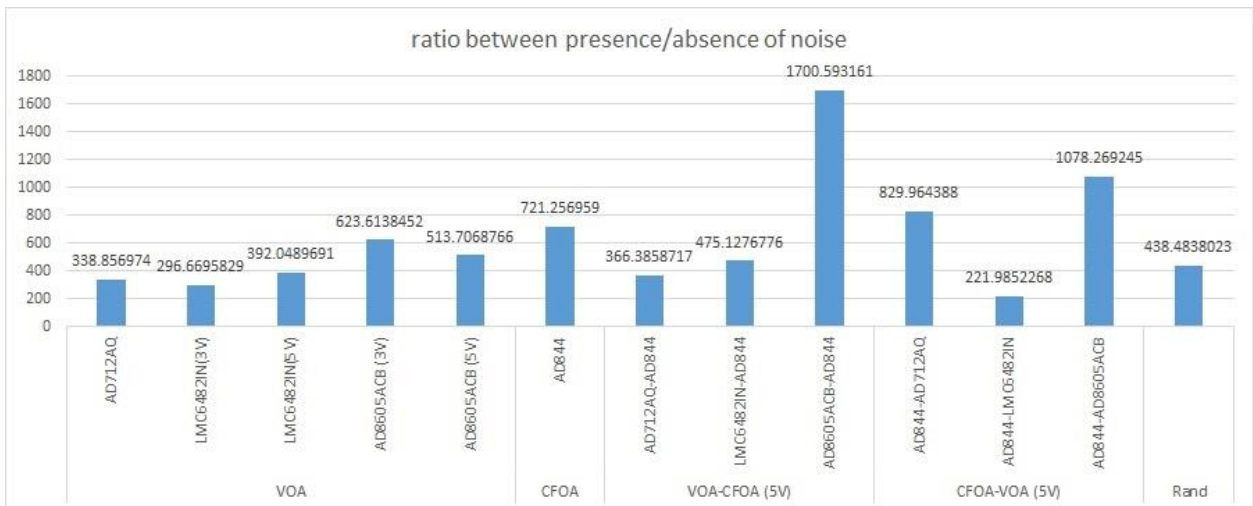
Figure 4-7 Ratio between the average error for signal reconstruction between the presence and the absence of the noise

76
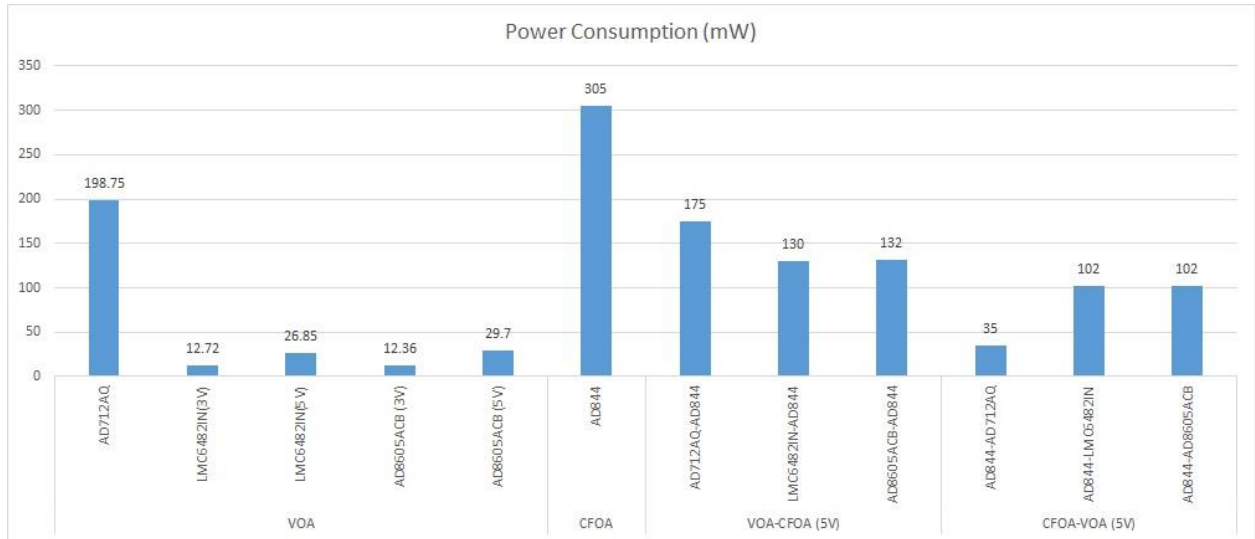
Figure 4-8 Power consumption for the analogue Chua circuit implementations simulated in this study

Table 4-2 Potentiometer values for the proposed system

Study	Design	R Values (kΩ)
VOA	AD712AQ	1.6764
	LM6482IN(3V)	1.6214
	LM6482IN(5V)	1.6214
	AD8605ACB(3V)	1.6
	AD8605ACB (5)	1.6
CFOA	AD844	2.625
Hybrid1 (VOA_CFOA)	AD712AQ-AD844	1.7138
	LMC6482IN-AD844	1.7138
	AD8605ACB-AD844	1.9
Hybrid 2	AD844-AD712AQ	1.5884
	AD844-LMC6482IN	1.5378
	AD844-AD8605ACB	1.5906

The tradeoffs between the bandwidth and the power consumption, especially for CFOA, is expected to be optimized more by redesigning the CFOA or changing the technology to be CMOS as in [167], [168]. AD844 is still the commercial CFOA till now and is used as a reference for several studies like [169], which makes it the dominant CFOA design used for most of the PCB circuit design which is one of the targets of this research. Based on the power consumption results, VOA will be addressed to be used for the proposed systems as will be shown later.

4.4. Conclusion

To conclude, this chapter shows by simulation the ability to use an analogue Chua circuit in AIC framework. As a Chua circuit is based mainly on three subcircuits named, LC oscillator, RC network, and negative resistance (NR), both LC oscillator and NR have been tested based on active circuit design using Voltage Operational Amplifier (VOA) and Current Feedback Operational Amplifier (CFOA).

The test extends to build the analogue Chua circuit based on hybrid (combination) between VOA and CFOA methods. The output of the circuit simulation fed to Random Demodulator (RD) based AIC framework by means of MATLAB software. The results show good performance when using analogue Chua circuit in the AIC framework in the absence and presence of noise with tradeoffs between these designs and the power consumptions.

All the simulation for the analogue Chua circuit was based on off the shelf components that are used in several references. Also, all the experiments use the minimum values of the power supply that are recommended from the op amps data sheets for less power consumption design.

As expected, based on the electronics circuits theory, CMOS technology based was less in power consumption in comparison to bipolar field effective transistor (BiFet) or bipolar junction transistor (BJT) technology. For this reason, the VOA based technique showed good performance over the CFOA or even the hybrid between them from the power consumption point of view. Thus, the rest of this research will focus only on VOA opamp.

Selecting the proper method to use for designing the required analogue Chua circuit depends also on the bandwidth. CFOA is originally designed to operate in large bandwidth in comparison with the VOA. Hybrid realization by using CFOA based synthetic inductor and VOA based NR show the optimum results for the signal reconstructing and the power consumption. However, the selection of the proper realization of the analogue Chua circuit is based on the application requirements and the tradeoffs.

Based on the results and analysis in this chapter, an analogue Chua circuit shows reasonable motivation to replace the digital PRNG circuits to make the analogue front end of AIC pure analogue to prevent any requirement for isolation of analogue part from the digital part that is found in most AIC framework implementation design. Also, by using proper circuit design and technology, power consumption can be reduced; besides the advantage of using Chua circuit in the hardware security, which are the main two requirements for developing smart cities applications and IoT devices.

However, a Chua circuit design using synthetic inductor needs three opamps to be implemented. Reduction of the active elements in the circuit will reduce the power consumption. This point will be the main point of the rest of this research. On the other hand, this chapter is the first step to investigate the use of the analogue chaotic oscillator circuit by means of an analogue Chua circuit in the AIC framework. As the main target of the research is to reduce the power consumption of the IoT based MC monitoring system, voltage opamp (VOA) will be used for the rest of the research to implement the proposed system as will be shown later.

Chapter 5
Astable Opamp Schmitt Trigger Modification Towards Chaotic Coupling Oscillators for AIC Framework

5. ASTABLE OPAMP SCHMITT TRIGGER MODIFICATION TOWARDS CHAOTIC COUPLING OSCILLATORS FOR AIC FRAMEWORK

In the previous chapter, the analogue Chua circuit was studied for the AIC framework as a first step to replace the traditional digital PRNG. The results showed a good performance for signal reconstruction. Thus, replacing digital PRNG by the analogue chaotic oscillator is not affecting the signal reconstruction, but it is sometimes more accurate than using digital PRNG. However, Chua circuit uses an inductor, and by replacing the inductor with its active circuit, the circuit uses at least 3 opamps. Increasing the number of the active elements in a circuit increases its power consumption. Thus this chapter studies the design of the analogue chaotic oscillator with less number of active elements.

By merging the analogue circuit design with other fields like neural network and neuroscience, new circuit design techniques start to give a new route for designing low-power systems. In this chapter, the coupling oscillator concept which is found in neuroscience is presented to generate a low-power chaotic oscillator.

The study in this chapter presents simple steps to design chaotic oscillators by means of the waveshaping technique and by the usage of opamp Schmitt trigger. The motivation for using the opamp Schmitt trigger is that it is one of the main blocks of the field programmable analogue array (FPAA). FPAA, as mentioned in Chapter 4, is used for CS signal reconstruction hardware implementation for the sake of reducing the power consumption.

The study in this chapter is the fundamental step for proposing two new analogue chaotic oscillators in the next chapter. This chapter is organized as follows: First, an introduction to show the motivation for the research to study the coupling oscillators is presented. Second, a very brief overview of coupling oscillator is presented. The waveshaping concept for the chaotic oscillator is given. Two new modifications of using astable opamp Schmitt trigger are explored in detail with mathematical analysis and simulations. Lastly, the conclusion for this chapter is presented.

5.1. Introduction

As shown in Chapter 3, compressive sensing (CS) is one of the promising techniques for reducing the power consumption in a way that the data size can be reduced at the same time. It was shown that the heart of the CS or analogue to information converter (AIC) is the pseudorandom number generator (PRNG), which makes it attractive to the researcher to use CS framework to secure the data at the same time reducing the power consumption of the ADC.

However, as mentioned in Chapters 2 and 3, the fundamental design for AIC uses the linear feedback shift register (LFSR) digital circuit to implement the (PRNG). While LFSR is very easy to be implemented and it is not consuming a lot of power, it lacked the security perspective. Hence, several researchers started to use complex circuits to replace the LFSR circuit to secure the data of the IoT device. Their efforts were very effective, but not dealing with the effect of the power consumption issue that can rise by replacing LFSR, especially when they replace LFSR with digital chaotic oscillators. Also, the isolation requirements between the analogue part and the digital part of the AIC front end were ignored.

In the previous chapter, the analogue Chua circuit was studied for the AIC framework as a first step to replace the traditional digital PRNG. Active VOA Chua circuit uses at least 3 opamps. Researchers proposed several designs with less number of active elements to generate chaotic oscillators like [168] which used 2 opamps only without inductors. The chaotic oscillator in [168] is based on what is called Jerk chaotic oscillators which are based on the third ordinary differential equations.

Most of the analogue chaotic oscillator designs start with differential equations that describe the dynamics of the oscillators then the hardware implementation. While differential equations can model the chaotic oscillators, they are sometimes very complicated. This sometimes leads to increasing the design to market time or even modelling to implementation time which is one of the disadvantages of the analogue circuit design.

This motivates the author to investigate and study other concepts to design analogue chaotic oscillators without the need of the differential equation modelling. Furthermore, this research investigates other fields to generate chaotic oscillators with less power consumption like neuroscience and biology [33]–[50], [52]–[62].

In the field of neuroscience, two coupled oscillators may generate chaotic behaviour based on the coupling mode[171]. From this point, this research starts to study the design of analogue chaotic oscillators based on the coupling oscillator theory. This research is not the first to study this point. However, most of the research and design done in this point started and developed the design based on differential equations which describe the dynamic systems of the oscillators and the coupling.

In the analogue circuit design of oscillators, the waveshaping technique has been used. The waveshaping design technique is well known for a long time as one of the concepts for designing relaxation oscillator circuits. However, the waveshaping technique is used in some researches for designing analogue chaotic oscillator but in shallow representation without using it as a tool to reach chaotic behaviour. The main target in this chapter is to find out the case of chaotic behaviour for coupling oscillator by means of waveshaping design technique without the need for using complex mathematical modelling based on differential equations.

In this chapter, the waveshaping design technique is investigated for designing an analogue chaotic oscillator based on coupling oscillators with less number of active elements for the sake of reducing the power consumption.

On the other hand, active elements like transistors or opamps are used to design normal or chaotic oscillators. In this research, the opamp Schmitt trigger will be used. The reasons for using opamp Schmitt trigger are:

1- From the neuroscience perspective, the coupled oscillators (or at some cases at least one of them) must be affected by the coupling to generate chaotic behaviour[171]. The opamp Schmitt trigger design shows the ability to design these types of oscillators by some modifications. This point has led to propose two modifications for the opamp Schmitt trigger, as will be shown in this chapter.
2- Opamp Schmitt trigger is one of the main blocks used to implement field programmable analogue array (FPAA)[172] which gives the systems the ability to be reconfigurable.
3- The simplicity of opamp Schmitt triggers design with the ease of adjustability for the frequency.

This chapter will propose two modifications for opamp Schmitt trigger and investigate the ability of these modifications to generate chaotic coupling oscillators that can be used under

the AIC framework by means of waveshaping design technique. As a starting point, a very brief overview for coupling oscillators is presented in the next section.

5.2. The Coupling Oscillator

The coupling oscillator has been observed by Christiaan Huygens in 1965 when he found that two pendulum clocks hanged side by side swing in perfect synchrony even if he interrupts this balance. He also observed that synchronising is not working if they hanged in the opposite side. These observations led to studying the coupled oscillator [171].

Coupled oscillators have been widely studied in almost every branch of science including chemistry, physics, neuroscience, quantum electronics, and more especially by merging some of these sciences together. Designing an analogue circuit based on neuroscience has become more promising for low-power consumption and is still in the early stages and started to show significant results in several applications [33]–[50], [52]–[62].

Scientists seek mathematical models to understand the behaviour of the coupling oscillators [173]. Coupling oscillators design can be modelled based on several approaches like the theory of the physics of dynamics, or based on the function, structure and effective connectivity.

Mathematical models present the system as differential equations. Some of these equations are unsolvable like Winfree equation. Another approach is to modify theses unsolvable equations to be solvable like Ariaratnam and Strogatz proposal. Besides the mathematical modelling, some researchers use what is called a phase response curve (PRC) diagram to analyse the coupling oscillators especially in neuroscience [169].

The effect of the coupling is based mainly on two points: structure and function. The structure covers the connection between the oscillators. Function covers the dynamic behaviour of the coupling and the oscillators. Studying and analysing the coupling functions lead to knowing more phenomena and characteristics like synchronising, network dynamics, amplitude death and more.

84

Based on [174], coupling oscillators are based on three functions:

a- Phase Coupling

It deals with the interacting oscillators through their phase dynamics. The phase coupling is susceptible to tiny perturbations. The phase dynamics is sufficient to treat certain effects of the interactions. Figure 5-1 [172] shows the effect of the phase coupling between two oscillators $x_1(t)$ and $x_2(t)$.
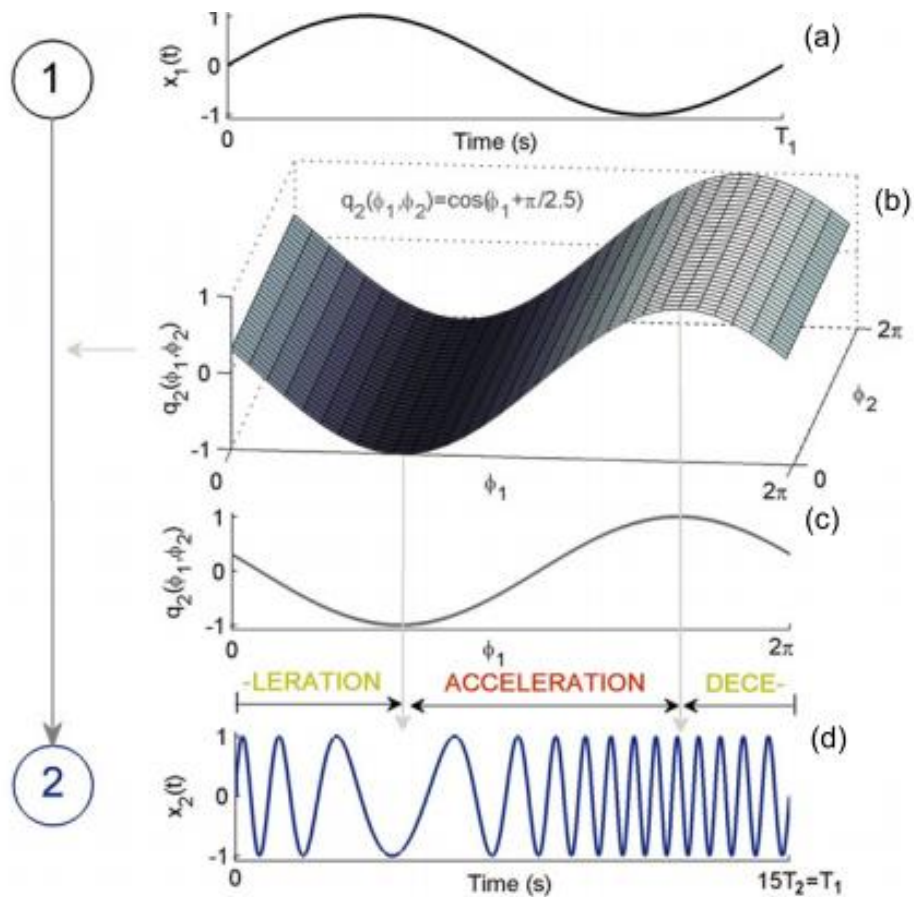
Figure 5-1 Phase Coupling function [172]

b- Amplitude Coupling

It deals with the amplitude dynamics of the systems as shown in Figure 5-2 [172]. Figure 5-2 shows the effect of the amplitude of the second signal because of the coupling function as shown in c and d. The model of the amplitude coupling function can often be a polynomial function or diffusive difference between the states.
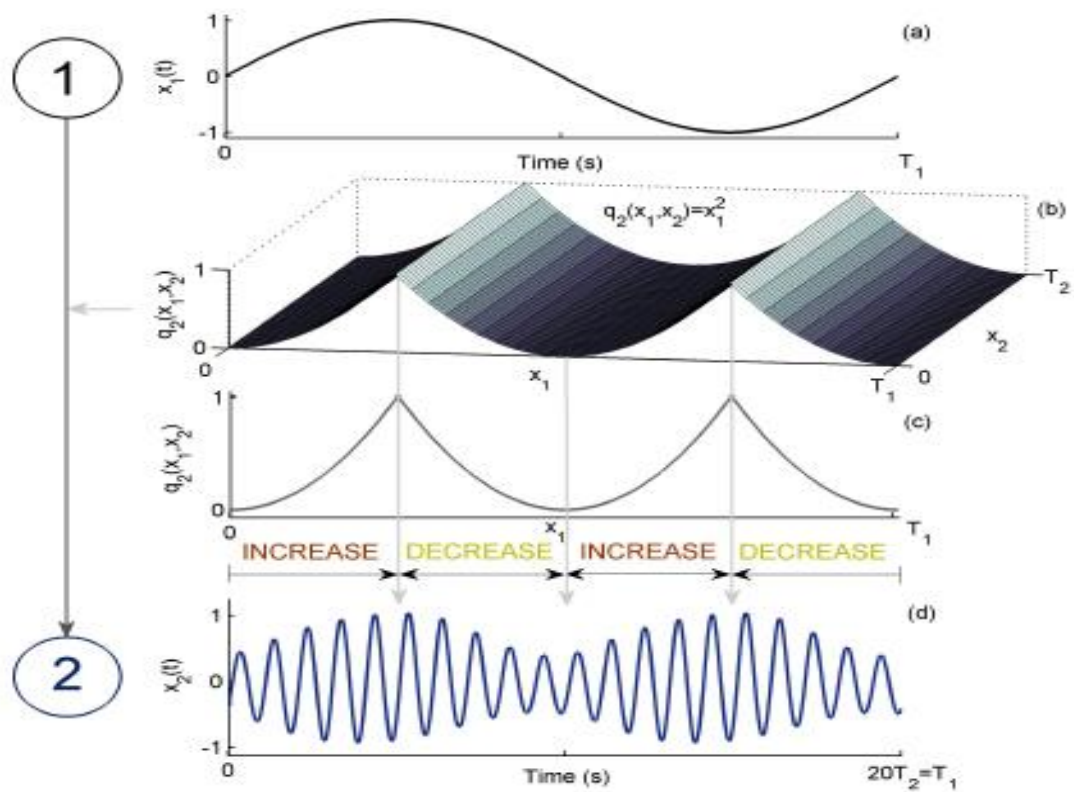
Figure 5-2 Amplitude Coupling function [172]

c- Multivariate

This function deals with coupling more than two oscillators as shown in Figure 5-3. In this case, each oscillator is influenced by the two other oscillators [174].

0.102379	0.076734	0.015955
0.083158	0.076308	0.074379
0.004978	0.003331	0.043222
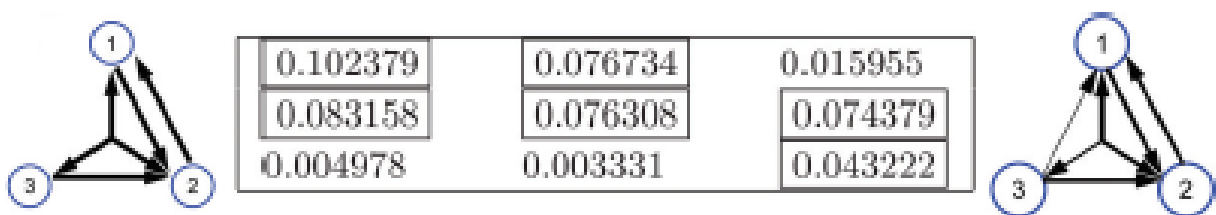
Figure 5-3 Multivariate Coupling [172].

All the previous functions can be formulated as differential equations. Differential equations have several challenges and obstacles to be implemented in digital circuits like the number of gates required, the high-power consumption resulting from such implementation and a variety of convergence problems [175]. The present research focuses on the analogue implementation of coupling oscillator.

However, differential equations that describe nonlinear dynamic systems like coupling oscillator may be difficult to understand or to solve which takes more time for the analogue designer to design such systems.

Another method of the analogue circuit design is presented in this research, which is easy to understand and implement, i.e. the waveshaping technique. In the next section, the waveshaping technique will be addressed which will be the basis of the proposed systems presented in the next chapter.

It can be observed from the results as will be shown later, in this chapter and the next chapter, that waveshaping technique based on capacitors charging and discharging affects the phase more than the amplitude. Hence, it is concluded that this method is one of the development methods for phase coupling function.

To conclude, this section gives a very brief introduction to coupling oscillators. Wave shaping technique will be presented in the next section to deliver an easy way to understand and design the coupling oscillator circuit.

5.3. Waveshaping circuit and chaotic oscillators

Using the waveshaping circuit design or relaxation oscillators design concepts to analyse the chaotic oscillators is not widely used. Few researchers highlighted the use of relaxation oscillators to generate chaotic oscillators like [174]- [175]. It can be observed from the literature in this field that the main reason for using differential equation as a starting point for hardware implementation is that most of the researchers prefer to be more generalised and give the opportunity for several researchers from other fields to cooperate.

However, it can take time and a lot of resources for analysis, especially if it is required to a couple more than two oscillators which is not the requirement of the application in this research.

In this section, we show some of the resources that use relaxation oscillators, which is one of the results of the waveshaping design technique for chaotic oscillators. After that, the research will investigate waveshaping design technique to design chaotic oscillator based on coupling oscillator method.

The research will focus on using the opamp as a discrete component, or in other words, the research will focus on the PCB hardware implementation more than IC. The research will use one of the main blocks for implementing relaxation oscillators which is opamp Schmitt trigger.

Transistor-based relaxation oscillators modified to chaotic oscillators were firstly proposed by Elwakeel and Kennedy [176], after that Lars Keuninckx, Guy Van der Sande, and Jan Danckaert [178] used transistor phase shift oscillators with multivibrator (Schmitt trigger circuit) as feedback to generate chaotic oscillators. While both designs were very impressive to use one or two transistors to generate chaotic oscillators with low-power consumption, using opamp based relaxation oscillators with fewer numbers of active elements has not been highlighted before to the knowledge of the author.

In [177], authors used the piecewise linear circuit design to redesign Chua circuits by the three types of relaxation oscillators (astable, monostable and bistable). The authors used 6 opamps for their design. In [175], Leonardo Acho presents the coupling of two opamps Schmitt trigger by another opamp for synchronization. However, Leonardo did not study the chaotic behaviour of this coupling.

The waveshaping design technique focuses on using energy storage elements to generate oscillation and the effect of connecting these energy storages with resistors or/and diodes. These energy storages are inductor or capacitor. As using an inductor is not preferable for low-frequency analogue circuit design, the research will focus on the capacitor. Energy storage elements in waveshaping circuits are connected to resistances, diodes or both. The proposed designs will focus only on resistance connection for simplicity.

The starting point for the proposed design is to study the effect of charging the capacitors from two different sources. This is because the chaotic oscillators are non-linear dynamic systems, and the charging and discharging of the capacitor rely on nonlinear relation (exponential).

For the sake of simplicity in this chapter, the study of charging the capacitor from two different sources will be presented in detail in Appendix II. The study covers the effect of charging the capacitor from two different sources with different frequencies and different waveshape (square and sinusoidal). The coupling is based on R-C-R (resistor-capacitor-resistor) coupling.

It is found from this result that the chaotic signal is not noticed or observed. The missing point is that the oscillators did not change their behaviour or the output in the presence of the coupling which is not the case in biological coupling oscillator. Hence, oscillators that are affected by the coupling must be used. At this point, the research proceeds to study the implementation of the two oscillators that can be affected by coupling to generate chaotic oscillator.

A new view of opamp Schmitt trigger design is presented in the next section. The motivation for this view is that it can mimic the real effect of coupling oscillators found in neuroscience which can reach chaotic behaviour under some conditions.

The modified opamp Schmitt trigger oscillators will be studied under the condition of coupling the modified Schmitt trigger with one of normal source. The study will be based on the waveshape design technique. The results of this study lead to designing two proposed systems of the chaotic oscillators that can be used to replace the digital PRNG found in AIC.

5.4. Modifications for Opamp Schmitt Trigger

Schmitt trigger is one of the main blocks of constructing the analogue and mixed circuit design like FPAA [170] which makes it easier to be implemented and reconfigured.

In this section, two modifications of opamp Schmitt trigger will be presented to be the basis of the proposed coupled oscillator systems found in the next chapter. Then the effect of these modifications in the design of coupling oscillators will be presented based on the waveshaping design technique not on the mathematical model.

5.4.1. Opamp Schmitt trigger design

Schmitt triggers circuit is based on using hysteresis of the positive feedback to an amplifier. Generally, opamp-based Schmitt trigger has two main topologies: an autonomous oscillator (Astable multivibrator or astable topology) or non-autonomous (converts any shape of AC signal to a square wave); the two topologies are shown in Figure 5-4. It should be noted that other modifications had been presented for opamp Schmitt trigger for several applications, like the monostable topology. Most of these modifications were targeting the two input terminals of the opamp to change the behaviour of the output. According to the same concept, the proposed modifications will target the input terminals to study the effect of changing the pulse width of the output pulse, which is the main target to reach chaotic oscillator.
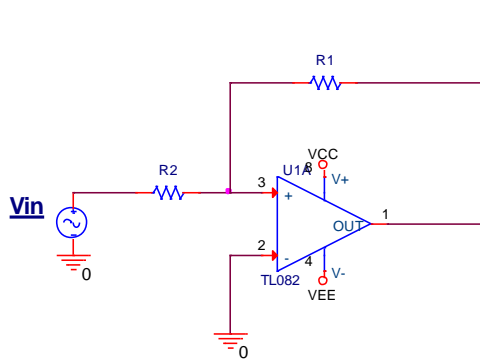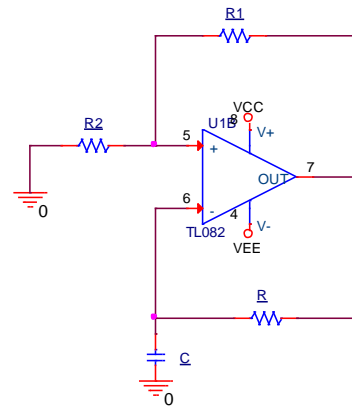
Figure 5-4 Opamp Schmitt trigger circuits topologies

Starting from the autonomous (Astable) opamp Schmitt trigger as shown in Figure 5-5, circuit analysis takes place as follows:
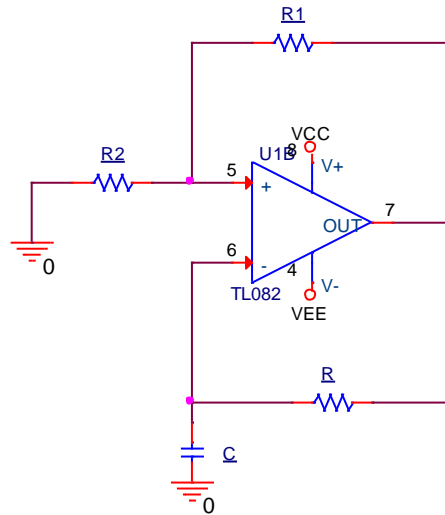
Figure 5-5 Autonomous Schmitt Trigger (Astable Multivibrator)

Because of the positive feedback, opamp acts as a comparator. Therefore, the output will be either positive or negative the voltage supply value (practically it is less than the power supply by few voltages) based on comparing the inverting and the non-inverting terminal of the opamp. Let us assume that the output is positive Vcc (Vcc is the value of the power supply); then the non-inverting terminal will be

$$V_p = V^+ = V_o \frac{R_1}{R_2 + R_1} \tag{5-1}$$

Where

$V_p = V^+$: is the non-inverting terminal

V_o : is the output voltage

And the output voltage will start to charge the capacitor based on the general charging capacitor formula:

90

$$V_c(t) = V^- = V_c(\infty) - [V_c(\infty) - V_c(0)]e^{\frac{-t}{RC}} \qquad (5\text{-}2)$$

When the capacitor voltage reaches the same value of the non-inverting terminal and starts to exceed it, the output voltage turns to –Vcc and the non-inverting terminal has the same value but in negative. Hence the new negative value of the output voltage will charge the capacitor to the negative value till it reaches the same value of the non-inverting terminal and when it exceeds the output, it gets back to the positive value and the function will repeat itself as shown in Figure 5-6. The output of Schmitt trigger is a square wave and the time for the one pulse is

$$T = RC\ln\left(\frac{1+\beta}{1-\beta}\right) \qquad (5\text{-}3)$$

Where

$$\beta = \frac{R_1}{R_2 + R_1}$$

Autonomous Schmitt trigger has a frequency based on the equation (5-3) which can be calculated as follows

$$f_{Autonomous\_Schmitt} = \frac{1}{2T} = \frac{1}{2RC\ln\left(\frac{1+\beta}{1-\beta}\right)} \qquad (5\text{-}4)$$
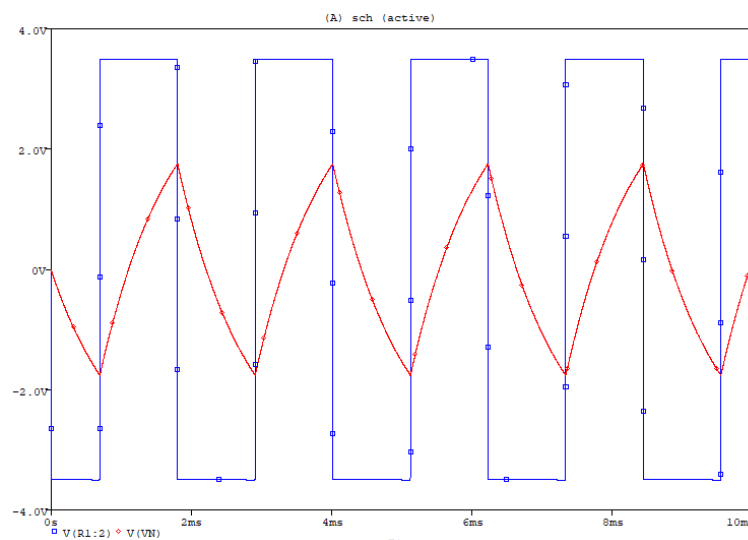
Figure 5-6 The output waveform (Blue) and the capacitor voltage (Red) waveform output of the autonomous opamp Schmitt trigger

The following proposed modifications for Schmitt trigger are targeting the two input terminals of the opamp. These modifications focus on the performance of the astable opamp

Schmitt trigger when it is fed by an external source. The proposed study will be based on mathematical and computer simulation results, followed by two general cases of the input wave shapes (sinusoidal and square). Using these shapes of wave covers the case of the input as it is instantaneously changed (sinewave case) and suddenly changed or DC (square wave case)

The two cases which expand to 18 experiments, as will be shown later, are analysed, simulated and implemented by using TL082, which is the most used opamp in the literature of the chaotic oscillators [170]. The intention of this study is to investigate using the astable opamp Schmitt trigger topology to generate chaotic oscillator based on coupling oscillator theory as will be shown in the next chapter.

5.4.2. First Modification

The first modified Schmitt trigger is shown in Figure 5-7; it involves the modification or the merging between the two topologies mentioned above and shown in Figure 5-4. The design is based on disconnecting the ground from R2 and connecting it to an external source. Hence the non-inverting terminal value will depend on both the input signal and the opamp output.
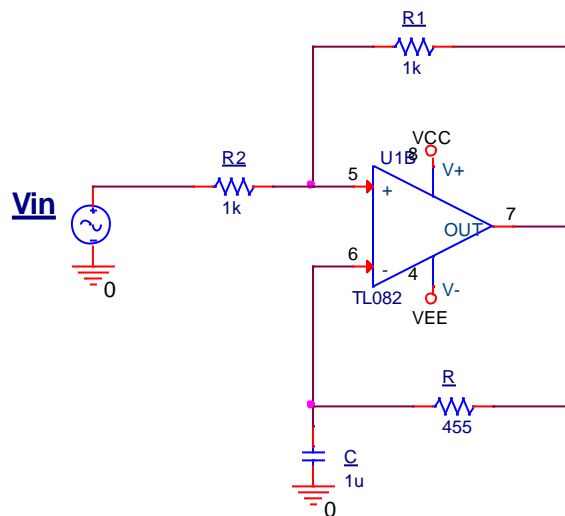
Figure 5-7 Modified Schmitt Trigger circuit: Non-Autonomous Schmitt Trigger with RC feedback

To analyse the first modified opamp Schmitt trigger, the governing equations of this design can be shown as follows:

Using superposition method at the non-inverting terminal voltage equation is

$$V^+ = V_{in} \frac{R_2}{R_1+R_2} + V_o \frac{R_1}{R_1+R_2} \ V \tag{5-5}$$

Then

$$V^+ = \frac{V_o+V_{in}}{2} \ V \tag{5-6}$$

And equation of charging the capacitor is still

$$V_c(t) = V_o - [V_o - V_c(0)]e^{\frac{-t}{RC}} \text{ V} \qquad (5\text{-}7)$$

Equation (5-5) shows that non-inverting terminal voltage is depending on both the input signal and the output of the opamp, controlled by the values of the resistors found in the positive feedback and the one connected to the non-inverting terminal. This will change the decision making by the comparator to set the output voltage to a positive or negative value.

To examine the effect of this design on the capacitor, first we adjust the frequency of the Schmitt Trigger circuit as all positive feedback resistance is 1 kΩ (Note that: the resistances ratio will be 1/β=2) and set the frequency to 1 kHz by putting the negative feedback capacitor is 1μF and the resistance is 455 Ω; and the output amplitude is nearly 3.5 /-3.5 V (power supply minus voltage drop).

It must be considered that there are three major points affecting the output of the modified opamp Schmitt trigger shown in the previous equations which are:

a- The waveshape of the input signal: this is because the input signal waveform shape may give different output if it is square or sinusoidal or another shape.
b- The frequency of the input signal compared to the frequency of the opamp Schmitt trigger.
c- The resistances ratio β.

Based on these points, studying the modified design will be based on the circuit simulator software and hardware with different scenarios to observe and analyse the output as follows:

a- Input signal wave shape will be the sinusoidal or square wave
b- The amplitude of the input signal will be less, equal or greater (not exceed the power supply value) than the output of the autonomous opamp Schmitt trigger
c- The frequency of the source examined also will be less, equal or greater than the frequency of the autonomous opamp Schmitt trigger
d- The resistance ratio will not change for fair judgment.

The cases of the study are shown in Table 5-1. The total number of cases is 18. However, in this chapter, the main cases which contribute in the context of the thesis will be analysed and the others will be presented without analysis in Appendix III as they did not show any modification for the output pulse width.

Table 5-1 Cases to study the modified Schmitt Trigger

Input Signal wave shape	Input frequency	Input signal Amplitude	Case #
Sinusoidal	100 Hz	1 V	a
		3.5 V	b
		5V	c
	1 kHz	1V	d
		3.5 V	e
		5V	f
	10 kHz	1V	g
		3.5 V	h
		5V	i
Square Wave	100Hz	1V	a
		3.5 V	b
		5 V	c
	1kHz	3.5V	d
		5 V	e
		1V	f
	10kHz	3.5V	g
		5 V	h
		1V	i

5.4.2.1.   Sinusoidal Cases:

Case "a":

Frequency: 100Hz

Amplitude: 1V

Figure 5-8 shows the waveforms of the input signal, output signal, non-inverting terminal and inverting terminal respectively for simulation and hardware results. As the input signal amplitude changes from low values to higher, the output pulses of the opamp start to be wide.
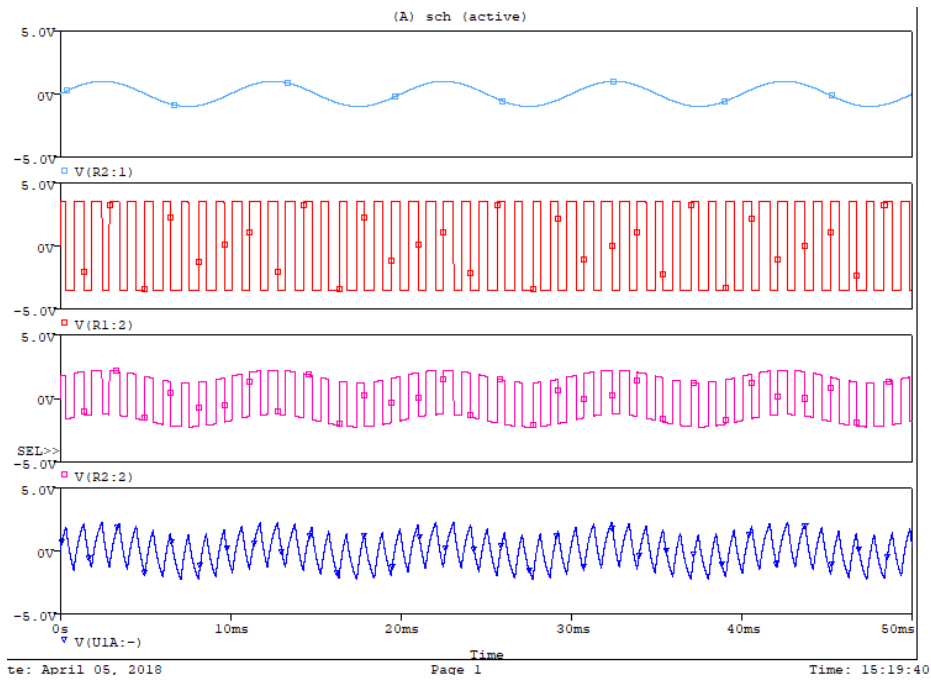
Simulation Results
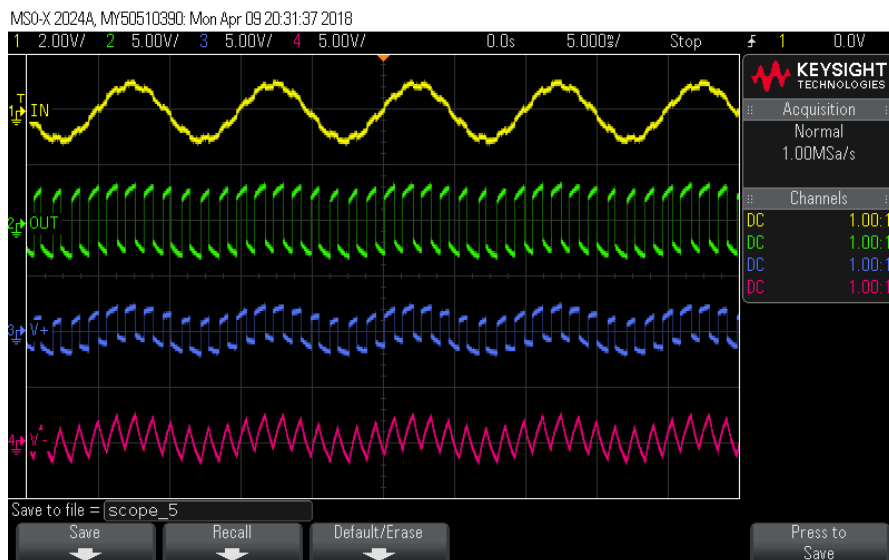
Hardware results

Figure 5-8 Case "a" Results

To understand this point, recall equation (5-6). The non-inverting terminal is equal to half of the sum of the opamp output and the input signals. The maximum and the minimum value of the non-inverting terminal is as follows:

$$V_{\max}^+ = \frac{3.5 + 1}{2} = 2.25 \text{ V} \tag{5-8}$$

$$V_{\min}^+ = \frac{-3.5 - 1}{2} = -2.25 \text{ V} \tag{5-9}$$

The capacitor in this modification is charged from the opamp output which is either +3.5V or -3.5V. The time constant for capacitance to charge (which is fixed for all experiments) is R×C = 455 Ω×1 μF= 455 μsec. Hence, the capacitor needs 2.275 msec to reach either 3.5 or -3.5V if its initial value is zero.

Assume the non-inverting point at the minimum value which is -2.25V, and the capacitor has no charge. Hence, the time required for the capacitor to reach to -2.25V to make the opamp output change from -3.5V to 3.5 can be calculated as follows

$$V_c(t) = V_o - [V_o - V_c(0)]e^{\frac{-t}{RC}} \ V$$

$$-2.25 = -3.5 - [-3.5 - 0]e^{\frac{-t_1}{455\mu}} \ V$$

$$1.25 = 3.5e^{\frac{-t_1}{455\mu}} \ V$$

$$t_1 = 455\mu \times \ln\left(\frac{3.5}{1.25}\right) \ \text{sec}$$

$$t_1 \cong 468.48 \ \mu\text{sec} \qquad\qquad (5\text{-}10)$$

Because the input signal is a sine wave with a frequency equal to 100Hz, the value of the input signal after 468.48μ sec starting from -1V will change to - 0.9999868 V. This slightly affects the non-inverting terminal value after this period. This slight change appears as squeezing of the pulse width of the opamp output as shown in Figure 5-9.

After this period, the opamp output will change from -3.5V to 3.5V; and the non-inverting terminal value will be approximately [3.5+(-0.9999868)]/2 V which is equal to 1.2500006 V. Also, this value will be slightly different after a period required for the capacitance voltage to reach the new value of the non-inverting terminal value as shown in Figure 5-10.

At the transition of the opamp output voltage, the capacitor voltage value is -2.2499934V, which is equal to the value of the non-inverting terminal exactly before the opamp output changes from -3.5 Vto 3.5V. As the input still increases, but with lower frequency, the time required for the capacitance to reach to +3.5 can be calculated as follows

$$1.2500006 = 3.5 - [3.5 - (-2.2499934)]e^{\frac{-t_2}{455\mu}} \ V$$

$$2.249994 = 5.7499934e^{\frac{-t_2}{455\mu}} \ V$$

$$t_2 = 455\mu \times \ln\left(\frac{5.7499934}{2.249994}\right) \ \text{sec}$$

$$t_2 \cong 426.9123 \ \mu\text{sec} \qquad\qquad (5\text{-}11)$$

By adding t_1 and t_2 it will be 895.3923 μsec which makes the input signal reach approximately -0.9999518 V, which makes the non-inverting terminal reach [3.5+(-0.9999518)]/2 Vwhich is equal to 1.2500241 V.

Therefore, the opamp output changes to -3.5 and the capacitor will have the same value of the non-inverting value just before converting and the process is then repeated. Because this variation is very slow, the output pulses widths are varied in a slow manner as shown in Figure 5-9.

Figure 5-10 shows the inverting and non-inverting terminal waveforms. The non-inverting terminal acts as an analogue signal affected by another high-frequency square as a crosstalk effect. Another observation, because of the big difference in the two frequencies (the input signal and the standalone opamp Schmitt trigger), the circuit acts as pulse density modulation (PDM) with weak performance.
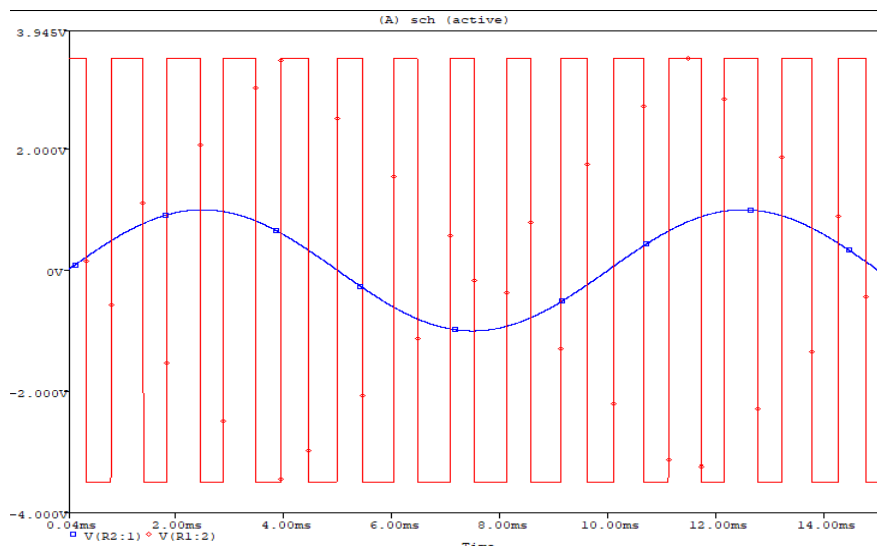
Figure 5-9 Input signal and output signal for Case "a"
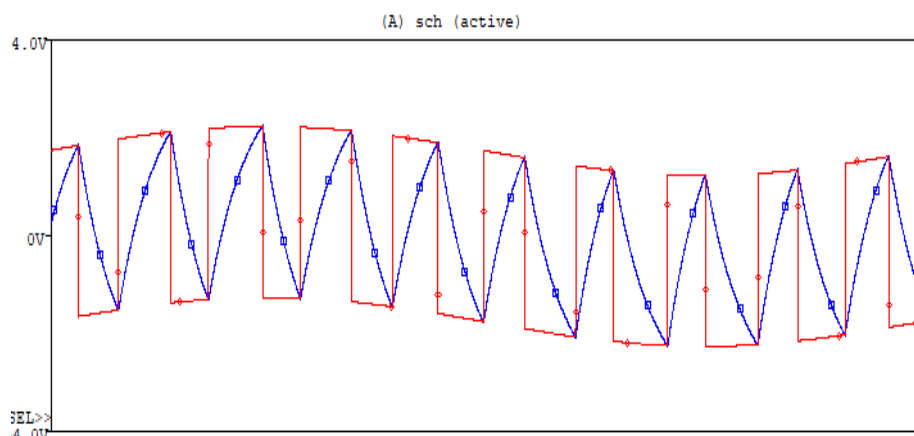
Figure 5-10 Inverting and non-inverting terminal for Case "a"

Case "b":

Frequency: 100Hz
Amplitude: 3.5V

Figure 5-11 shows the waveforms of the input signal, output signal, non-inverting terminal and inverting terminal respectively. While the frequency of the input signal is still less than the original opamp Schmitt trigger configuration, the increase of the input amplitude affects the output frequency of the opamp. As shown in Figure 5-11, by increasing the amplitude of the input signal, the maximum and minimum value of the noninverting value is greater than Case "a".

Simulation Results
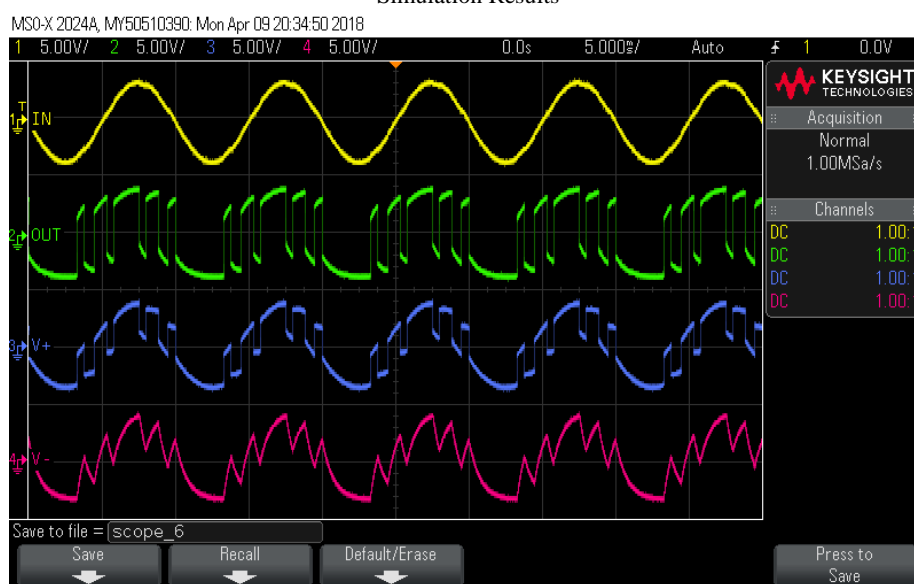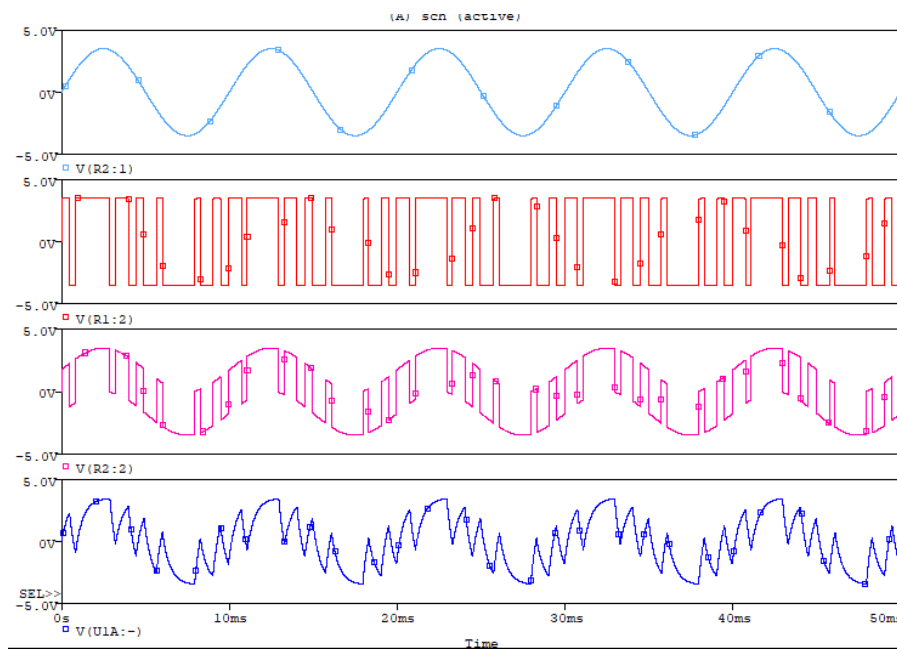
Hardware Results
Figure 5-11 Case "b" waveforms Results

In Figure 5-12, input and output voltage waveforms are shown together to check the effect of Case b configuration. The maximum and minimum value of the non-inverting terminal will be as follows and shown in Figure 5-13:

$$V_{max}^+ = \frac{3.5 + 3.5}{2} = 3.5 \text{ V} \tag{5-12}$$

$$V_{min}^+ = \frac{-3.5 - 3.5}{2} = -3.5 \text{ V} \tag{5-13}$$

Assume again the input signal starts at the minimum value (-3.5V) and the output of the opamp is at the minimum value (-3.5V) and the capacitor has no charge. As Case a, one cycle of the input signal is 10 msec, the capacitor voltage needs a 2.275 msec to reach to -3.5V.

Still the change of the input voltage increases slower than the charging of the capacitor; however, in this case, the value of the input signal after 2.275 V will be almost -2.95V which is greater than Case "a".
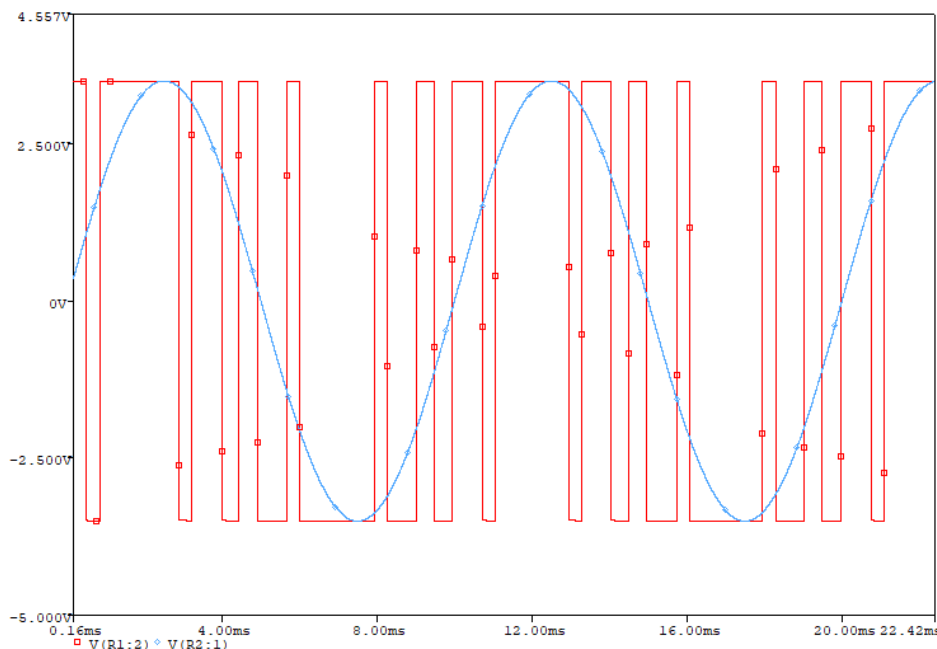
Figure 5-12 Input and output waveforms for Case "b"
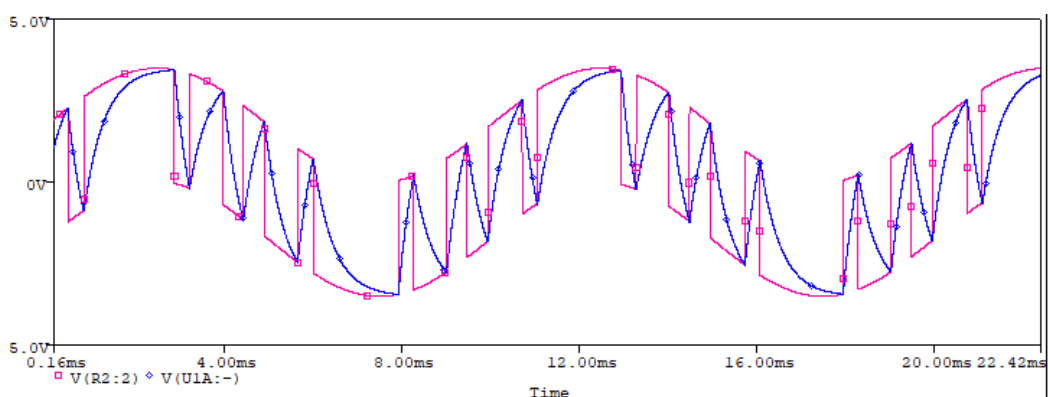
Figure 5-13 Waveforms for Inverting and Non-Inverting terminals for Case "b"

By the same method of analysis done in the previous case, it is found that the opamp output pulse width changes after each transition of the opamp output voltage. The output waveform shows that this case acts as a Delta-Sigma Modulation based on PDM (pulse-density modulation).

In this case, PDM behaviour is clearer than in Case a because of the input signal amplitude. This result is significant because it represents a low-power ADC without any sampling required.

Using astable Schmitt trigger with high frequency in comparison with the input signal and while the R-C circuit found at the negative feedback of the opamp acts as an LPF, gives the requirements for building SDM from high sampling rate (without the need of sampler circuit) and filtering.

The design of Case b can be used to generate a digital sequence by adding a diode to the opamp output or feed the output with a comparator with a ground reference to act as ADC. This design presents a low-power ADC. However, more study is required to investigate the boundary conditions and the performance [because it is a very special case] and the resolution, which is considered as one of the future research recommendations.

Case "c":

Frequency: 100 Hz

Amplitude: 5V

In this case, the amplitude of the signal is greater than the output of the opamp. The waveforms for Case c are shown in Figure 5-14. The non-inverting terminal voltage will exceed the voltage of the output at its maximum (and not exceed the value of the power supply) or it will be less than the absolute opamp output voltage as follows

$$V_{max}^+ = \frac{3.5+5}{2} = 4.25 \text{ V} \tag{5-14}$$

$$V_{min}^+ = \frac{-3.5-5}{2} = -4.25 \text{ V} \tag{5-15}$$

Based on these values, and while the capacitor is charged from the output voltage, the output opamp will be constant for a while as shown in Figure 5-14, because the input is increasing or decreasing beyond the opamp output voltage or in other words beyond the maximum or minimum capacitance voltage respectively.

Another observation, in this case, is the average value of the capacitance-voltage waveform. By comparing the capacitance-voltage waveforms in this case with the previous

100

cases (a and b), it can be noticed that the capacitance-voltage waveform is not swung or affected by the slow change of the frequency of the input signal. Figure 5-15 combines the input and output signals in one figure while Figure 5-16 combines the voltages waveform at the inverting and the non-inverting terminal in one figure.
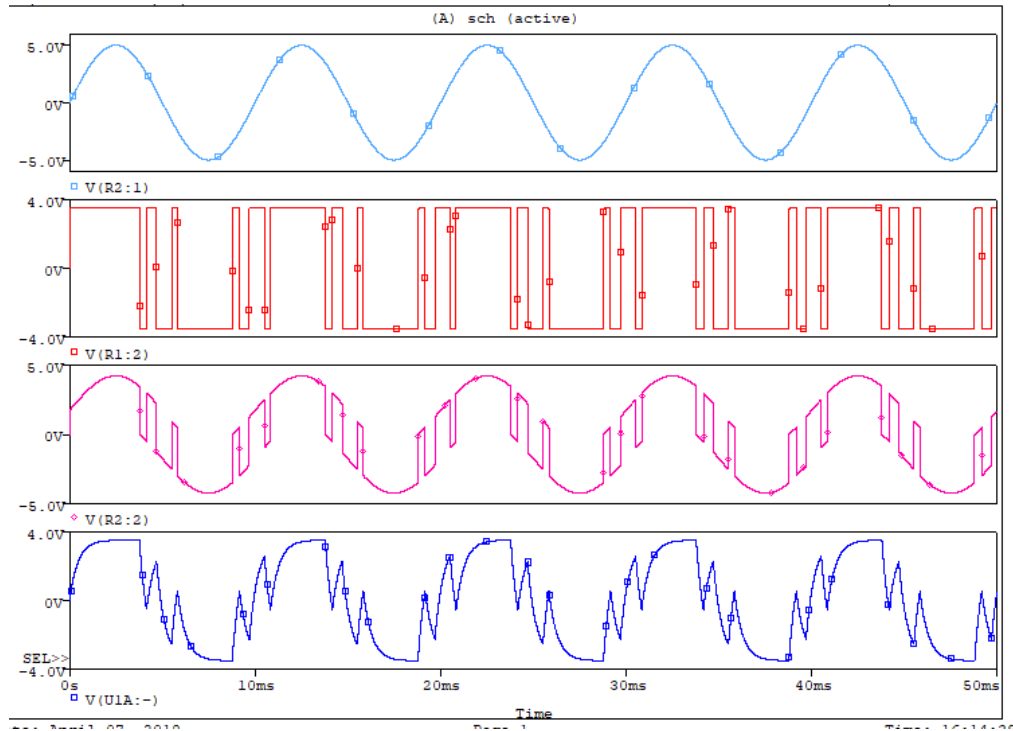
Simulation Results
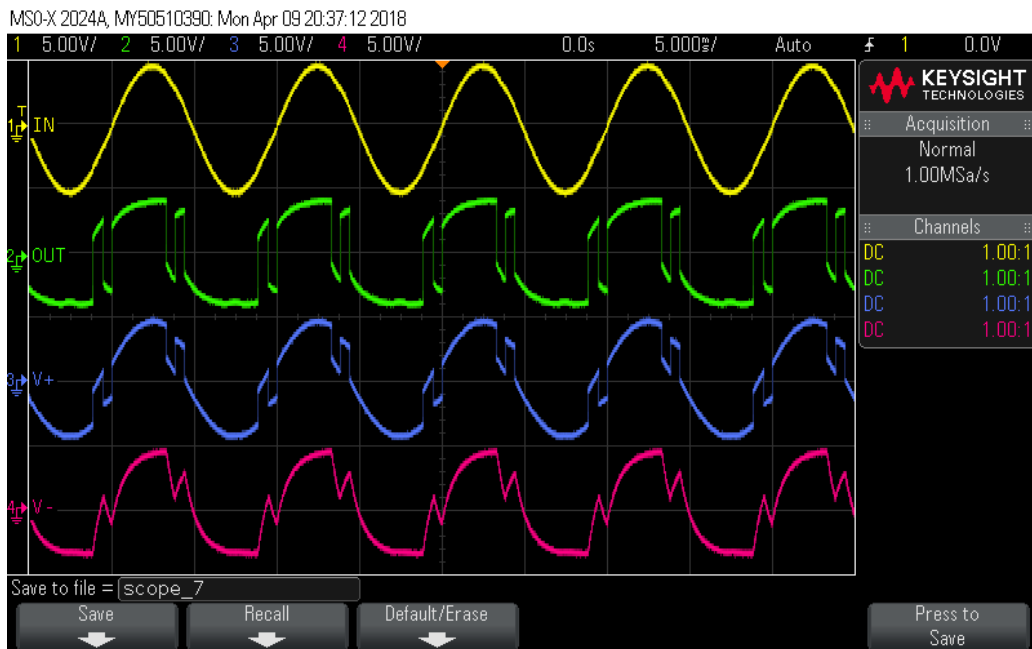
Hardware Results

Figure 5-14 Output results from Case "c"
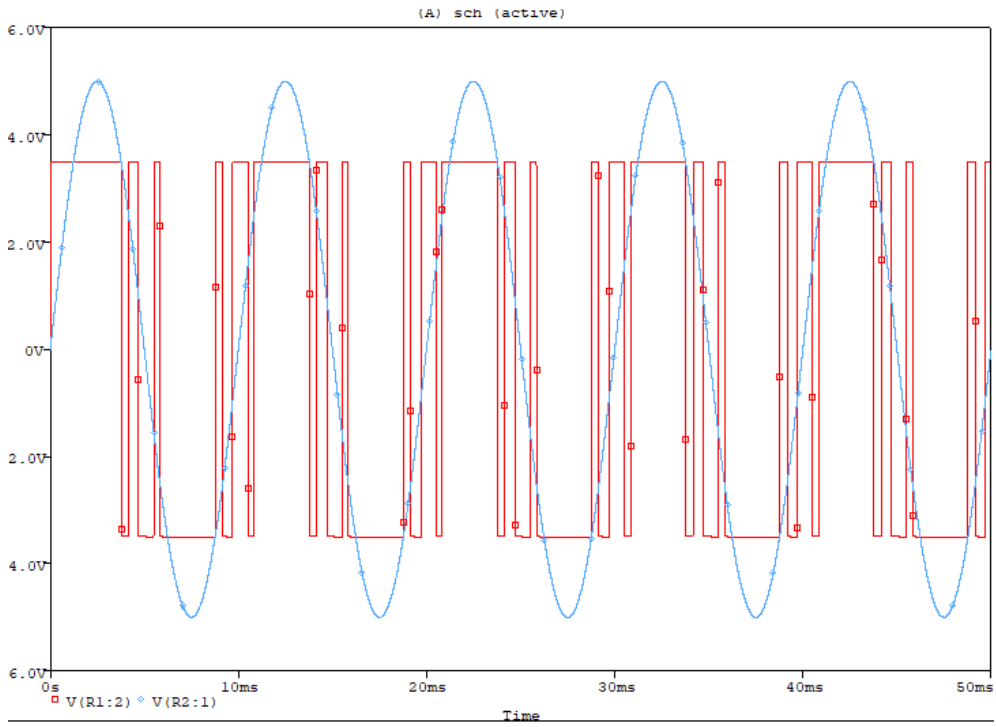
Figure 5-15 Input and output signal waveforms for Case "c"
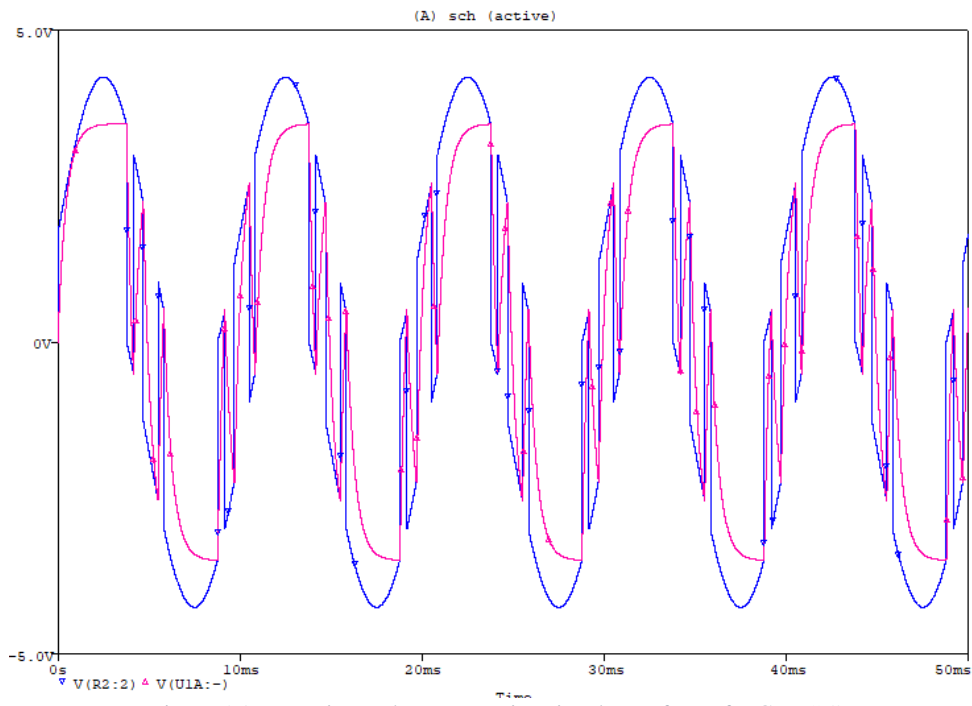
Figure 5-16 Inverting and Non-Inverting signal waveforms for Case "c"

Case "d":

Frequency: 1 kHz
Amplitude: 1V

By equating the input signal frequency to the astable opamp Schmitt trigger frequency, the behaviour of the output will change. Figure 5-17 shows the waveforms for Case "d". Figure 5-18 shows the opamp output and the input signal waveforms, which shows the same frequency with different amplitude. Figure 5-19 shows the inverting and non-inverting terminals waveforms. While the maximum and the minimum value of the non-inverting terminal is still the same as Case "a", the transition of the input signal is faster than the three previous cases. The mathematical analysis is not required because the chaotic effect is not observed.

Simulation Results
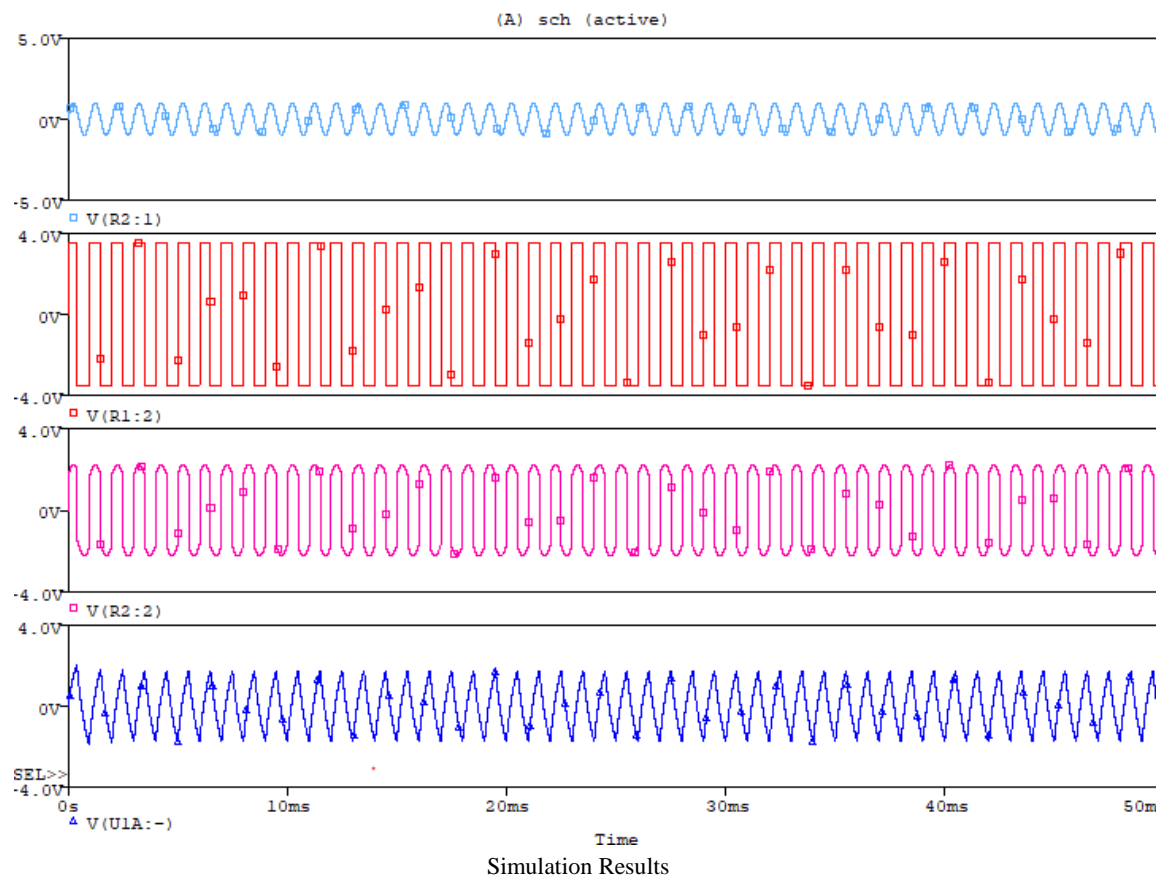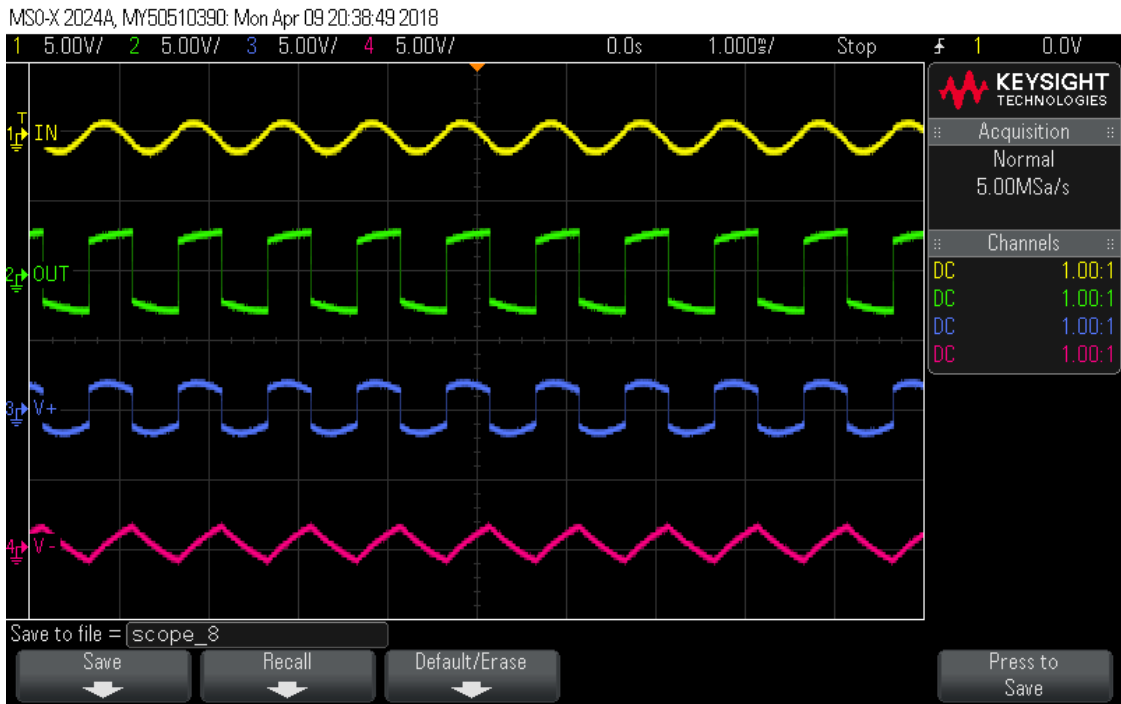
Hardware Results

Figure 5-17 Waveforms for Case "d"
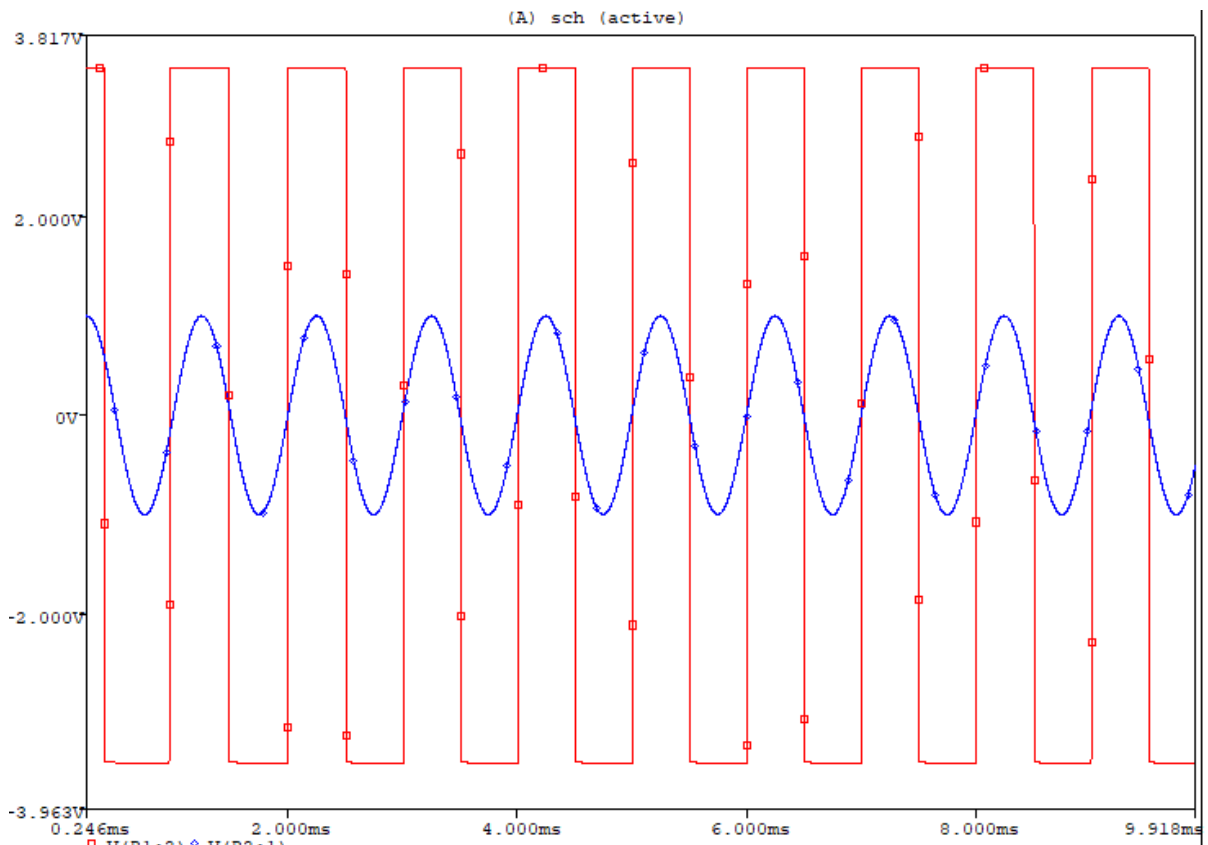
Figure 5-18 Input signal and opamp output for Case "d"
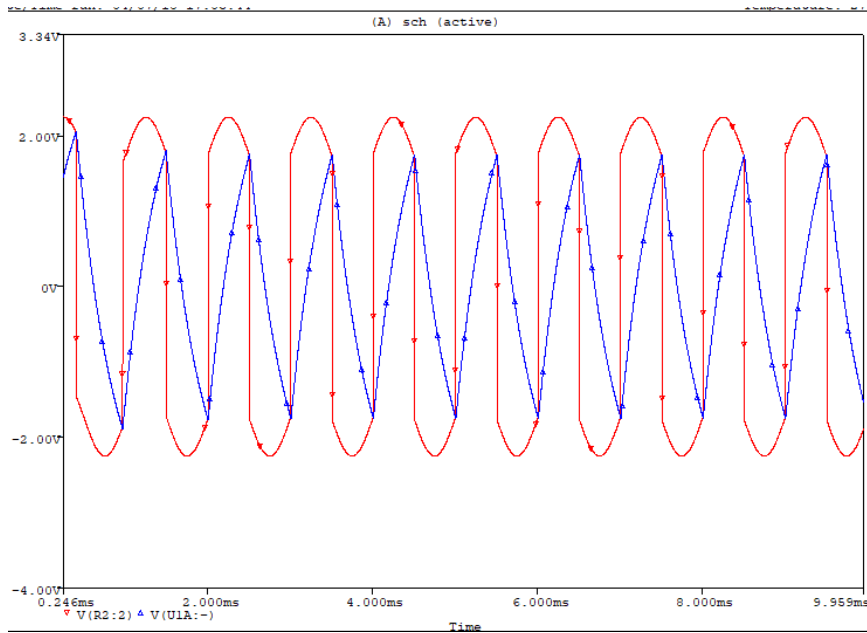
Figure 5-19 Inverting and Non-Inverting signal waveforms for Case "d"

Case "e":
Frequency: 1 kHz
Amplitude: 3.5V

By increasing the amplitude with the same frequency of the standalone astable opamp Schmitt trigger, the output pulses width will not change like Case "d" as shown in Figure 5-20. This observation in this case and the previous one can be explained as follows: when the two frequencies of the input and the standalone astable opamp Schmitt trigger are equal, the output will not be affected by the input. The rest of the cases found in Appendix III show this observation.

Simulation Results

105
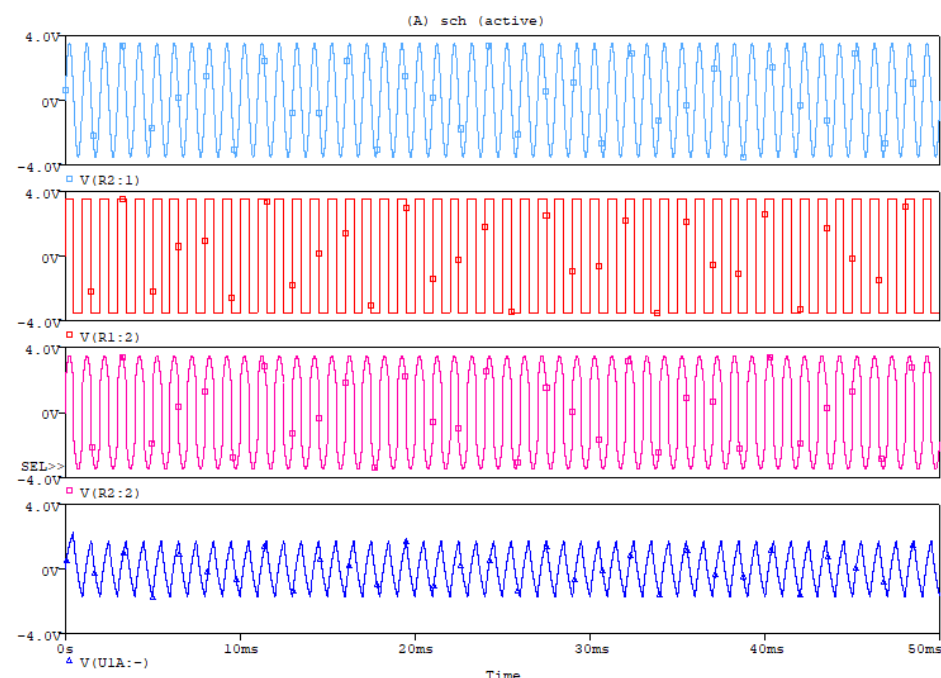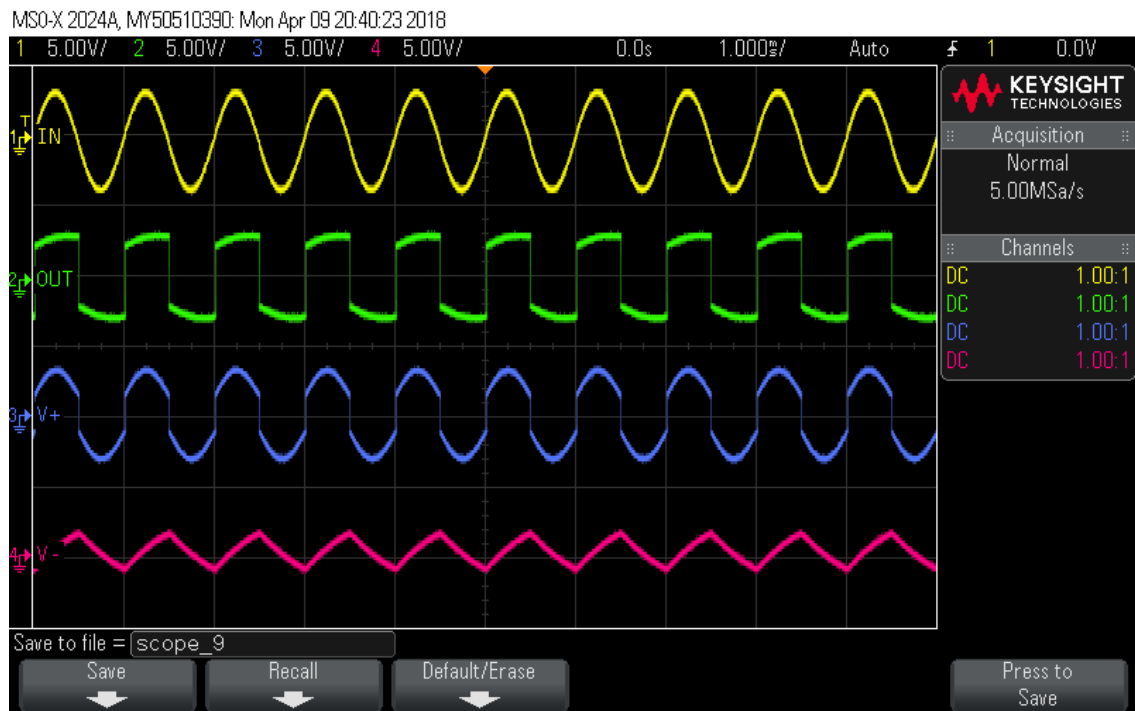
Hardware Results

Figure 5-20 Results of Case "e"

5.4.2.2. *Square wave Experiments*

Another shape of the input signal which will feed the first modification of the astable Schmitt trigger is the square wave. Using the square wave is based on the several studies of the coupling oscillators. Some of these studies focused on the effect of the pulse effect of the coupling oscillator. As mentioned in Table 5-1 the same 18 cases will be repeated. Only the cases with a variation of the pulse width will be presented in this chapter and the rest is found in Appendix III. Also, calculations will not be repeated, but only the shape of the output waveforms will be discussed, as the main target is to observe the change of the output pulse width.

Case "a":

Frequency: 100 Hz

Amplitude: 1V

Figure 5-21 shows the waveforms results of Case a by feeding small amplitude and frequency square wave to the first modification. Figure 5-22 shows the input and output waveforms only, followed by Figure 5-23 that shows only the two input terminals of the opamp. As Case "a" for sinusoidal input, the output pulses are slightly getting wide with the positive amplitude of the input while getting narrow with the negative amplitude of the input.

106
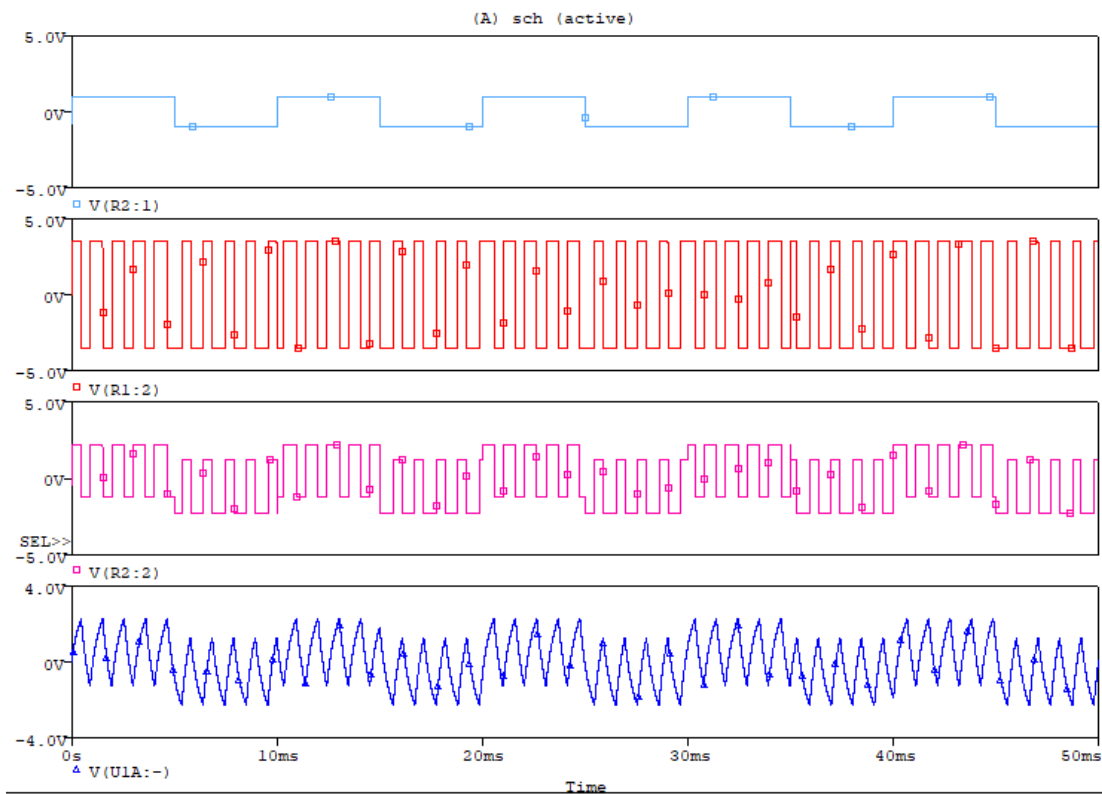
Simulation results

Hardware Results

Figure 5-21 Case "a" waveform results for square input

107
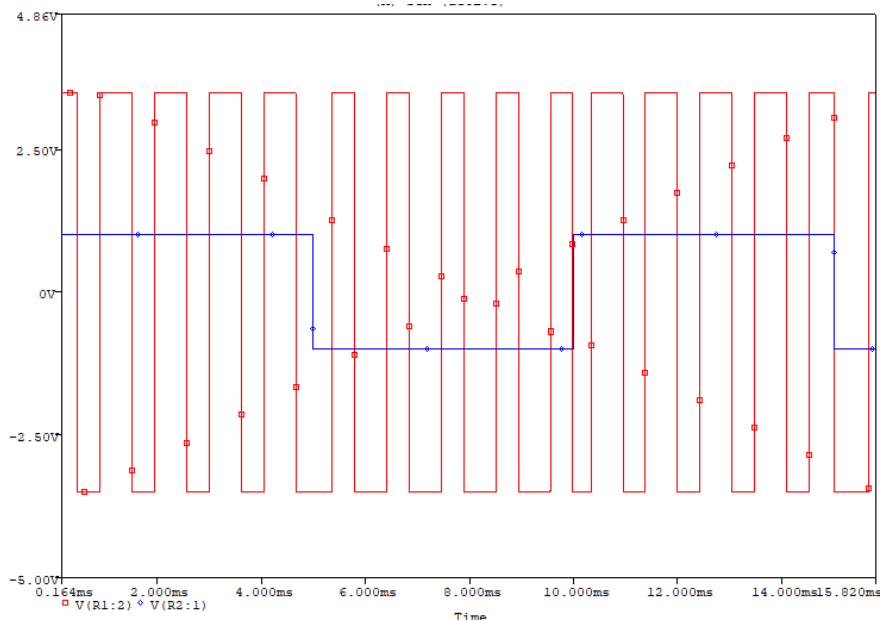
Figure 5-22 Input and Output signal waveforms for case "a"
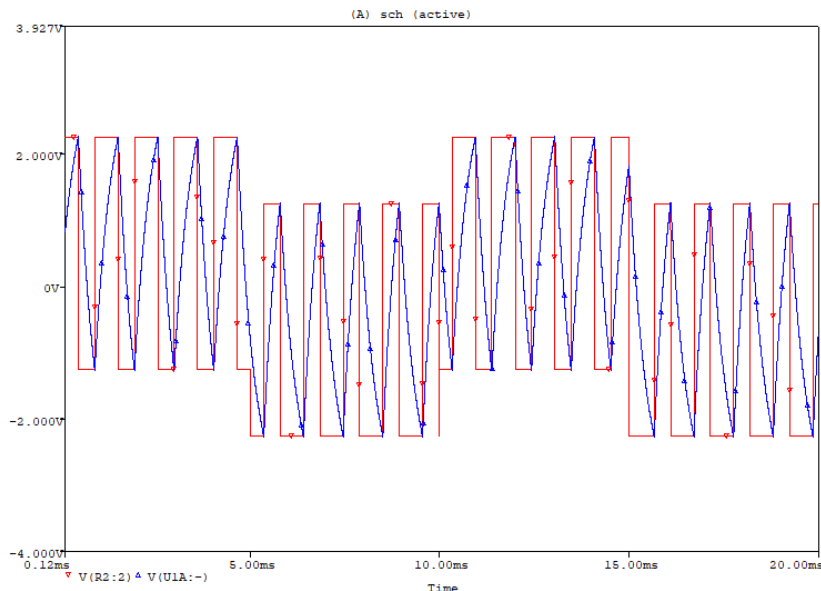
Figure 5-23 The inverting and the non-inverting terminal for case "a"

Case "b"

Frequency: 100 Hz

Amplitude: 3.5V

Figure 5-24 shows the waveforms results for Case "b". The difference between the simulation and the hardware is the high resolution required for simulation which was beyond the capability of the computer used. On the other hand, the output pulse width changes slightly for the positive input amplitude, which is the same result for a sinusoidal input. The main difference is that because of the sharp change in the square input signal, the number of pulses was reduced. Also, the frequency of the output changes to follow the

108

input frequency change. Input and output waveforms only are shown in Figure 5-25, while the inverting and non-inverting voltage waveforms are shown in Figure 5-26.
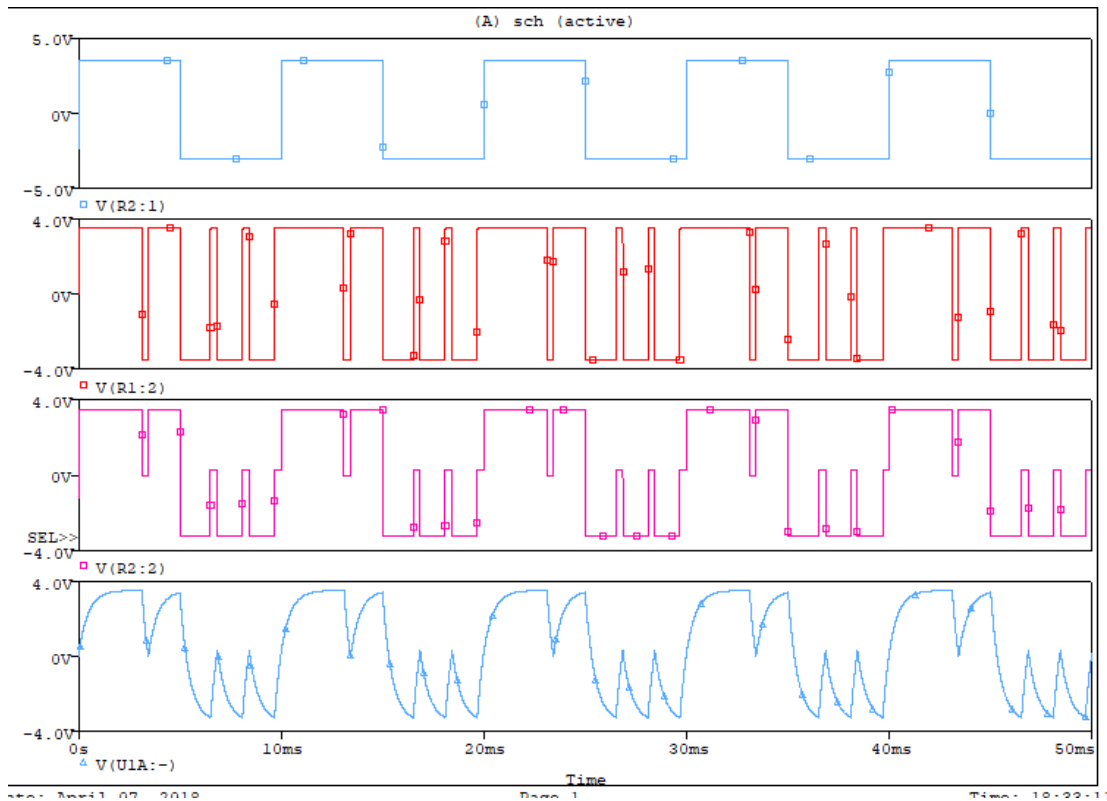
Simulation results

Hardware Results

Figure 5-24 Waveform Results for case "b"
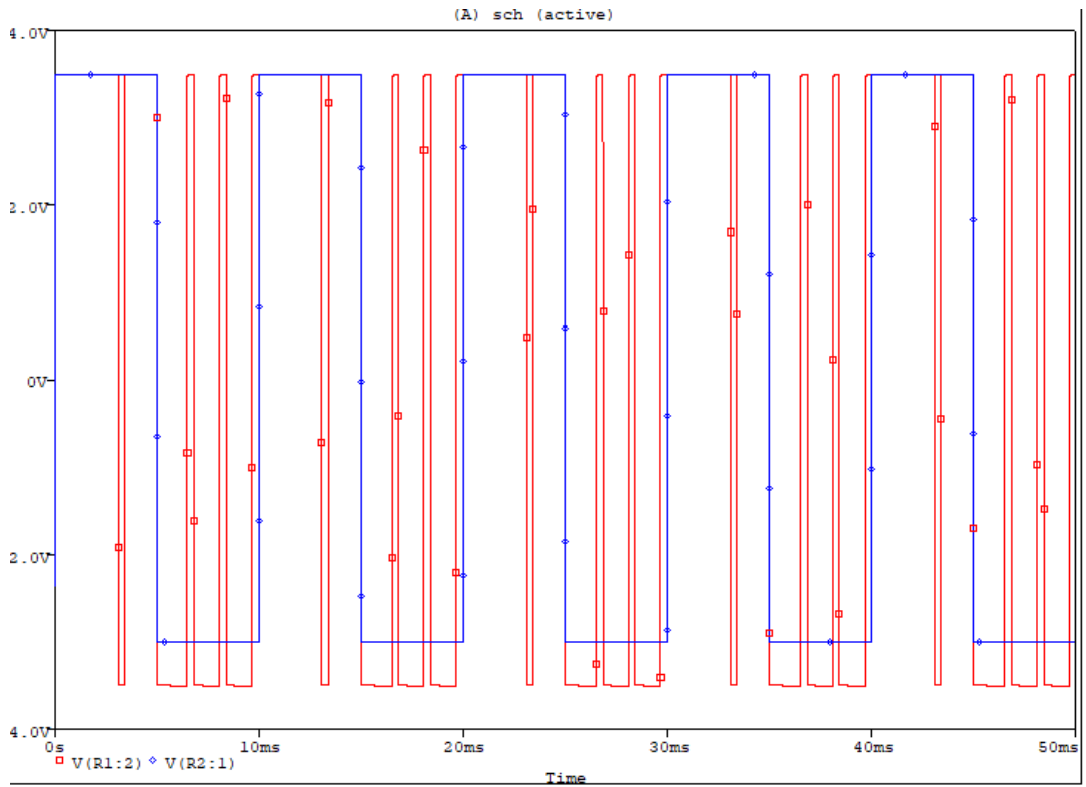
Figure 5-25 Input and Output waveforms for case "b"
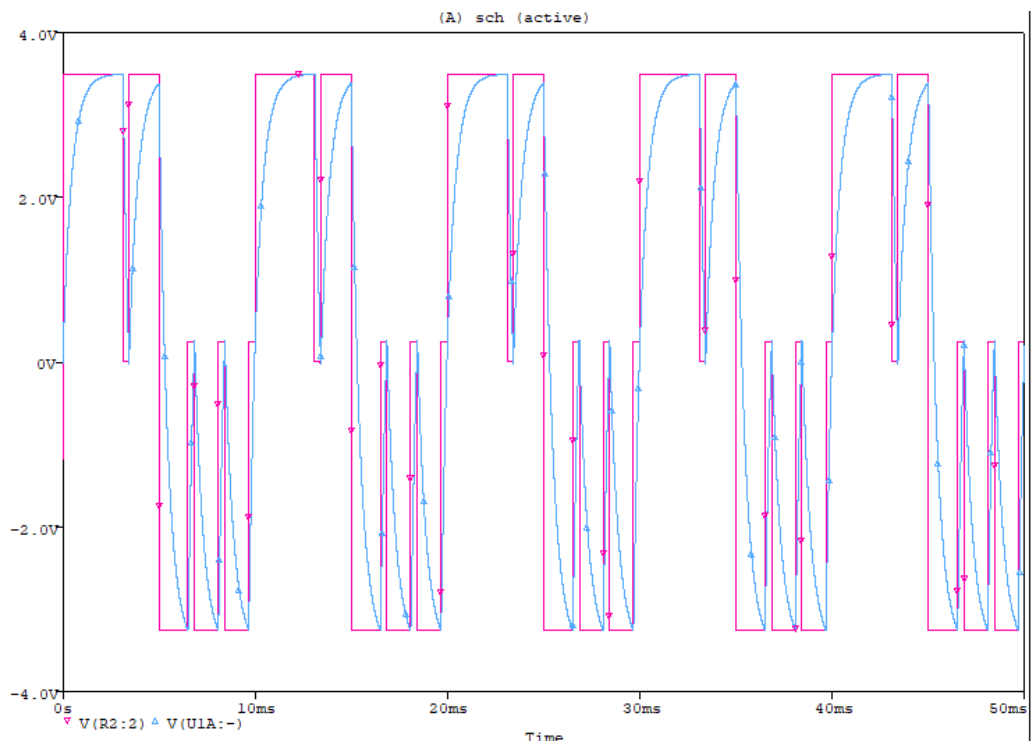
Figure 5-26 Inverting and Non-inverting terminals waveform for case "b"

110

As mentioned before, the rest of the cases are found at Appendix III, which does not show any effective change in the pulse width of the output. In this section, the first modification of Astable Schmitt trigger is presented. It is shown that in Cases "a", "b" and "c" for sinusoidal or square wave it acts as a pulse width modulation (PWM). Particularly, Case "b" for both sinusoidal and square acts as a very low-power Sigma Delta Modulation without the need of DAC circuit or oversampling circuit.

Case "b" requirements are: if the input signal has the same value of the maximum of the opamp output (or it can be slightly less) with low frequency compared to the standalone Schmitt trigger circuit, it generates pulse wave like ADC Sigma Delta modulation which follows the concept of DM as mentioned by Razavi [180]. However, this case can be considered as a special case because of its requirements.

It has been observed that as much as the input is changed smoothly from maximum to minimum, the output pulse will increase and change its width. It can be concluded that chaotic behaviour or changing of the pulse width of the output are observed when the input signal has less amplitude and frequency in comparison with the Schmitt trigger.

5.4.3. Second Modification

In this modification, the input signal will connect to the inverting terminal via resistance (R_{in}) as shown in Figure 5-27. In this case, the capacitor in the negative feedback will be charged from two different sources: the opamp output and the input signal. While the inverting terminal is the capacitor voltage, the non-inverting terminal voltage is only the voltage divider for the opamp output.
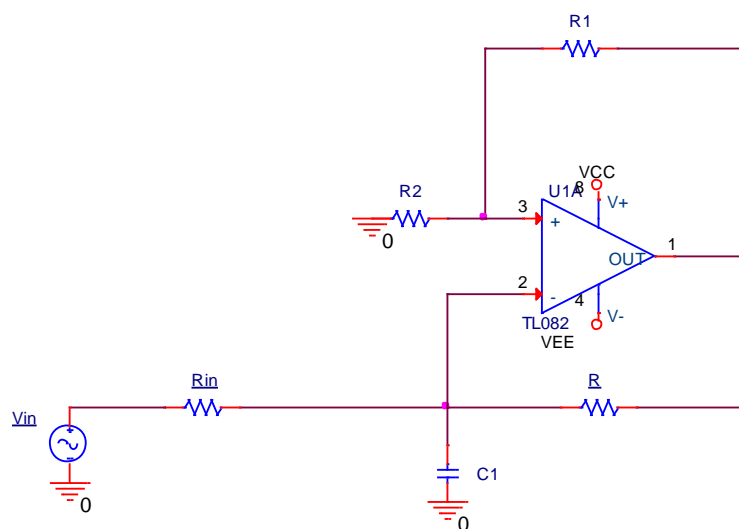
Figure 5-27 Modification 2 for opamp Schmitt trigger

Based on the analysis presented in Appendix II, rewriting governing equation of the capacitor voltage or the inverting terminal of the opamp is

$$V_c(t) = [V_{in} + V_o] - \{[V_{in} + V_o] - 2V_c(0)\}e^{\frac{-t}{\tau}} \text{ V} \qquad (5\text{-}16)$$

Where

$$\tau = R_{th}C \text{ sec}$$
$$R_{th} = R||R_{in} \text{ } \Omega$$

In [181], it is mentioned that the chaotic or semi-chaotic behaviour can be generated from a capacitor charged from several sources. Hence, if the coupling or the connection to the capacitor from the two sources affects its behaviour to be chaotic, the opamp output will be also chaotic.

Before applying the same cases as in modification 1, there is a new element added to the test, which is R_{in}. The effect of the input resistance is discussed in Appendix II, so, the experiments will be taken in under one condition which is R_{in} is greater than R. Hence, the R_{th} will be for all cases 312.71478 Ω and the time constant ʈ= 0.00031271478s=31.271478µsec.

Based on the results shown in modification 1, only Case a (this case shows promises to generate chaotic oscillators) will be shown. The remainder of the experiments will be shown in Appendix III.

5.4.4. Sinusoidal and Square Waves Experiments

As expected, and based on the analysis and the design shown in the first modification, using less amplitude and less frequency of the source shows the chaotic or semi-chaotic behaviour of the output is delivered. Figure 5-28 shows the input signal, output signal and capacitor waveforms respectively in the case of sinusoidal input (case "a"). The Figure shows the simulation and the hardware results. Also, Figure 5-29 shows the same case with square input. The output pulse width changes based on the slow change (less frequency) of the input amplitude.
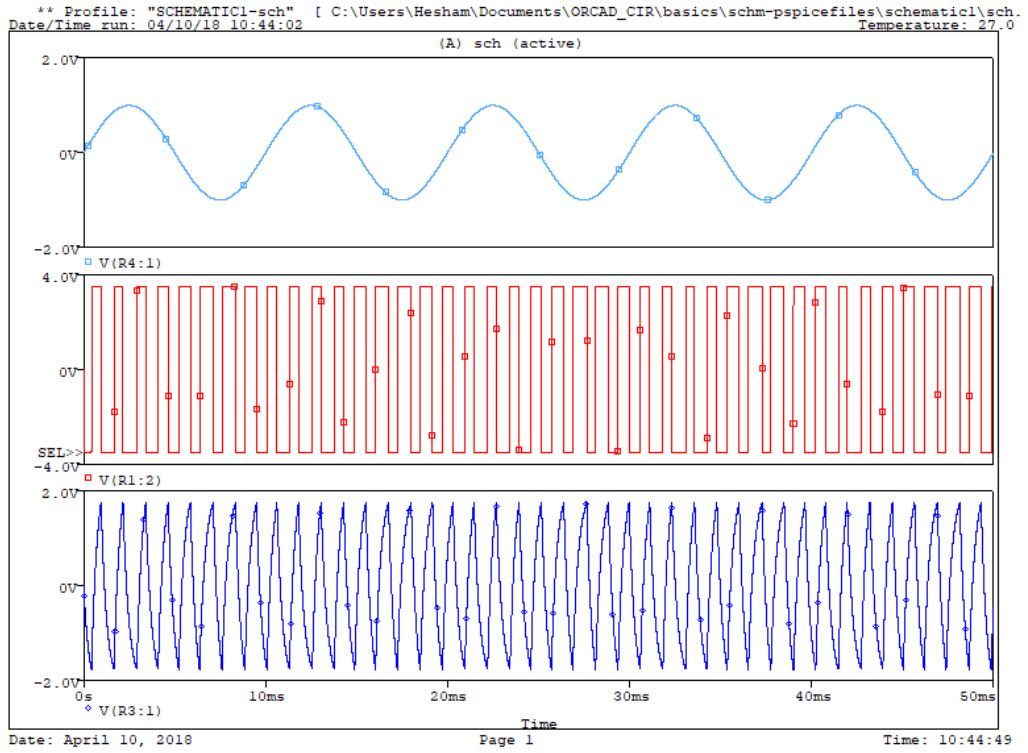
Simulation Results
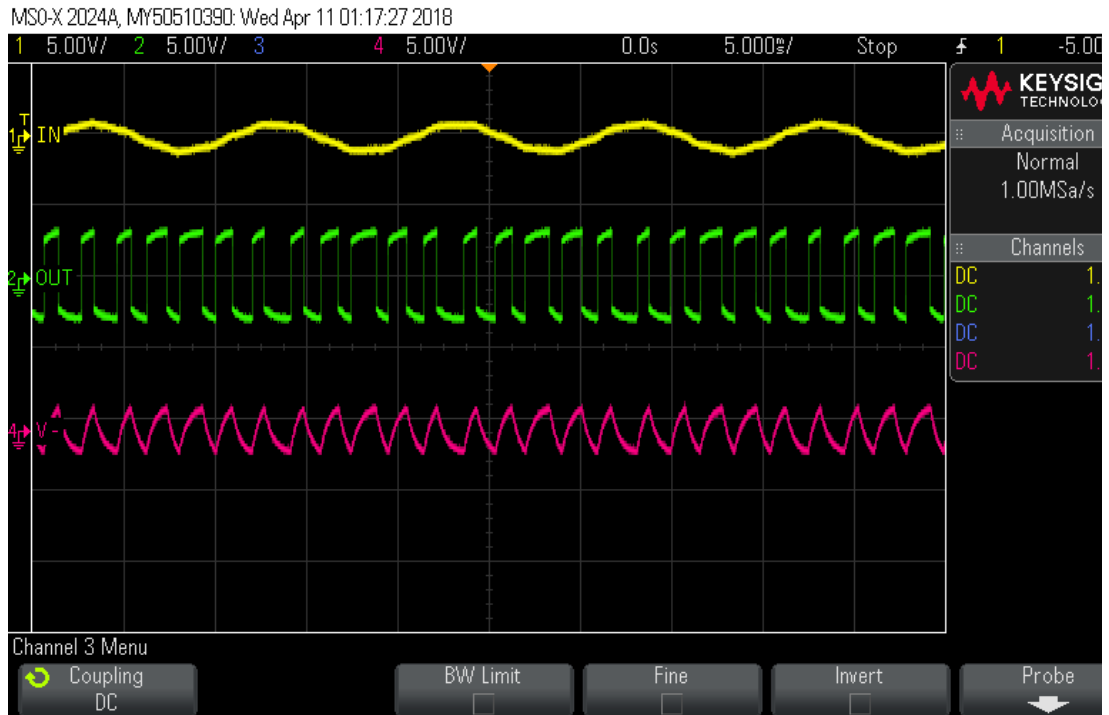
Hardware Results

Figure 5-28 Waveform Results for the second modification with sinusoidal input for case "a"
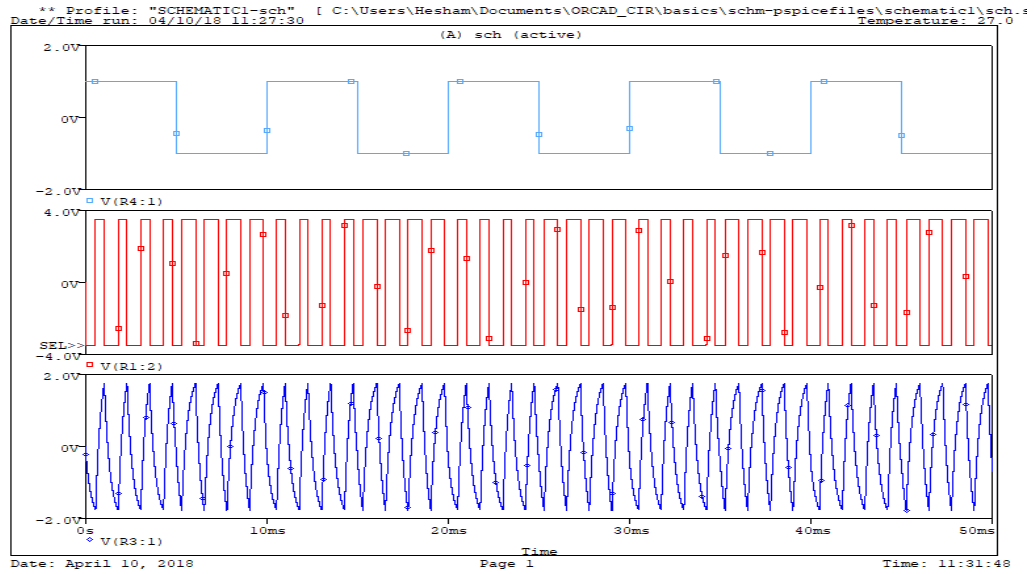
Simulation Results
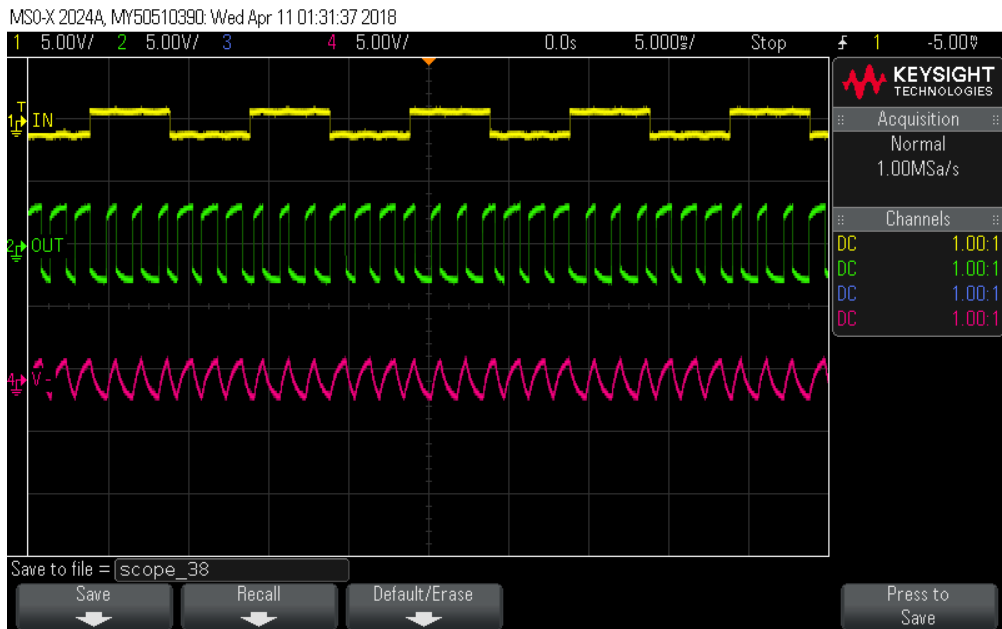
Hardware Results

Figure 5-29 Waveform Results for the second modification with square input for case "a"

Without using massive differential equation analysis or showing the results of the rest of the cases, it is observed and proved that for coupling two oscillators when one of them has less amplitude and less frequency, with R-C-R coupling leading to change in the output pulse width of the higher frequency oscillator.

However, this coupling should be governed by the condition that at least the output of one of these oscillators must be affected by the coupling to reach a semi-chaotic or irregular change in the pulse width of the output. While this condition is not enough to generate chaotic oscillator as will be seen in the next chapter, it gives the guide for the proposed systems in

Chapter 6. From this point, the next chapter will propose two analogue chaotic systems with more analysis and details especially the effect of this proposed system on AIC framework

5.5. Conclusion

After studying the use of analogue Chua circuit for AIC framework in Chapter 4, Chapter 5 studies the design of the analogue chaotic oscillator based on the coupling oscillators. The motivation for this study is to use less number of active elements in comparison to the Chua circuit to reduce the power consumption.

Neuroscience and biology and other fields show the ability to generate chaotic oscillators based on coupling oscillators. While most of the researches in the design of analogue chaotic oscillator start from differential equations, this chapter studies the use of waveshaping theory for the same purpose. This is because of the ease of the waveshaping theory. As the first step of this study, charging the capacitor from two different sources via resistors has been analysed as it is the main core of generating the chaotic behaviour.

After analysing the effect of charging the capacitor from several sources, this chapter continues to study the use of opamp Schmitt trigger to implement chaotic oscillator based on the coupling oscillators by means of the waveshaping oscillators.

Two new modifications for astable opamp Schmitt trigger were presented. This chapter also presents the new modifications of the opamp Schmitt trigger to address the conditions of changing the pulse width of the opamp output based on input signal. This has led to generating chaotic oscillations based on coupling oscillators.

The waveform techniques were used to analyse the modifications. It is concluded from the two modifications that the change of the output pulse width happened when the input signal has low frequency and low amplitude in comparison with a standalone astable opamp.

Several experiments based on simulation and hardware with analytical analysis were presented in this chapter and extended in Appendix III. The experiments were conducted by applying external source with different shape and frequency to the new modifications.

The experiments and analysis show that the width of the output pulse is varied under the condition of low amplitude and frequency for the input signal in comparison with the opamp Schmitt trigger design. This result is the main target of this chapter.

In the next chapter, these externally fixed oscillators will be replaced by the traditional astable opamp Schmitt trigger and the output applied to the AIC framework to evaluate the performance of the proposed design.

Chapter 6
Proposed Chaotic systems for AIC framework

6. PROPOSED CHAOTIC SYSTEMS FOR AIC FRAMEWORK

Chapter 5 studied the waveshaping design method to realize an analogue chaotic oscillator based on coupling oscillator. It used a fixed oscillator and a Schmitt trigger oscillator. In this chapter, the fixed oscillator is replaced by an astable Schmitt trigger. This replacement needs a good coupling to achieve chaotic behaviour. Two systems are proposed in this chapter. The two systems are based on (R-C-R) coupling and waveshaping technique as shown in Chapter 5. The two proposed systems are compared with the Jerk chaotic implementation. The validation results cover the power consumption and the thermal effect of the signal reconstruction for the two proposed systems, based on the range of the temperature found beneath the manhole cover.

6.1. Coupling function and the proposed systems

As shown in Appendix II, the R-C-R coupling function was studied. However, the study involved the coupling function in the presence of fixed oscillators, whose outputs will not affect the coupling despite the fact that it presented an intensive study of the capacitor voltage wave shaping affected by two different sources. In the literature on the chaotic oscillators, charging capacitance from several sources may lead to chaotic or semi-chaotic waveshaping signals. This fact is correct if and only if these oscillators are affected by the capacitance coupling.

From the study presented in Appendix III, it is shown that in the presence of the fixed oscillators, chaotic behaviour is not found. This can be explained as follows: while the capacitance is fed from the two sources, no current will be fed again to the sources which affect their output behaviour.

From the neuroscience point of view, the coupling type mode affects the behaviour of the coupled oscillators and may lead to chaotic behaviour. Hence, relaxation oscillators are used in this research. This type of oscillators is based on a threshold: if this threshold varies, the output will vary.

The only oscillators that will be used in this chapter for the proposed systems are the relaxation oscillators. Relaxation oscillators circuits are used for several reasons:

1- These types of oscillators generate a pulse shape waveform which is the main target of the research to generate PRNG as a square shape

2- Relaxation oscillators have mainly three types (astable, monostable, bistable) which can be classified as autonomous (astable) and non-autonomous (monostable and bistable). This classification gives the indication of the ability of these types to be modified to be affected by coupling.

3- Relaxation oscillator circuits can be designed by transistor or opamps, which gives the freedom to select the topology that suits the application.

4- From the chaotic oscillators point of view, coupling oscillators using relaxation oscillators are not widely studied; instead, modification of the relaxation oscillators design was studied more to generate chaotic oscillators. While this point may show the uselessness of studying coupling relaxation oscillators to generate chaotic oscillators from the power consumption point of view, the richness of the relaxation oscillators specification from one side and the need of studying the coupling oscillators in several applications and fields from the other, make it worth to study the use of coupling relaxation oscillators to generate chaotic oscillators, especially if the intention is to replace digital circuit systems that are based on differential equations that consume more power than analogue.

These reasons and more have motivated the author to study the design of coupling oscillators using relaxation oscillators to generate the chaotic sequence. The proposed systems will use the opamp Schmitt trigger and the modified opamp Schmitt trigger that was presented in the previous chapter for designing the two-coupling oscillators.

In addition, using a wave shaping analysis to design the well-known relaxation oscillators circuit, is not widely used for chaotic oscillators. Vector and dynamic mathematical analysis using the differential equation for linear and nonlinear systems is the most common[182]; it studies the behaviour of the trajectories of the signal. In this chapter, the author will continue to use the waveshaping like the previous chapter to present the proposed systems.

The chapter directly starts with proposing two new systems. The design of these proposed systems is based on the waveshaping technique as introduced in Chapter 5. The Schmitt trigger oscillator is the key circuit that will be used in this chapter, as also shown in Chapter 5. The performance of the proposed system relies on the ability of the output sequence to reconstruct the original signal from analogue to information converter algorithm (AIC). This is done like Chapter 4 by applying the output sequence on Matlab program to identify the performance of

the sequence to reconstruct the original signal with the ability to show the results in a graph (frequency domain and time domain) and by calculating the average square error.

6.2. Proposed System 1

In Chapter 5, it was shown that to reach chaotic or semi-chaotic oscillator, two oscillators can be used but with different frequencies. The design starts with the two astable Schmitt trigger oscillators, with one oscillator having a large frequency in comparison to the other. The two oscillators have frequencies of 100 Hz and 1 kHz respectively, as shown in Figure 6-1. The reason for these values is for the preparation of using the output of this study in Matlab, as it will be shown later. The output of the two oscillators and the corresponding capacitors are shown in Figure 6-2.
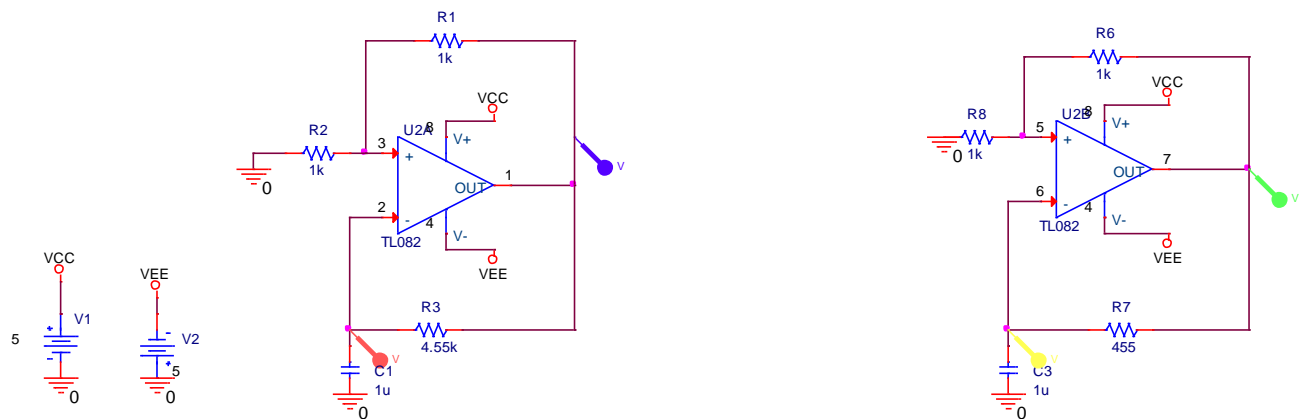
Figure 6-1 Two astable Schmitt trigger oscillators with one oscillator havingdouble the frequency of the other
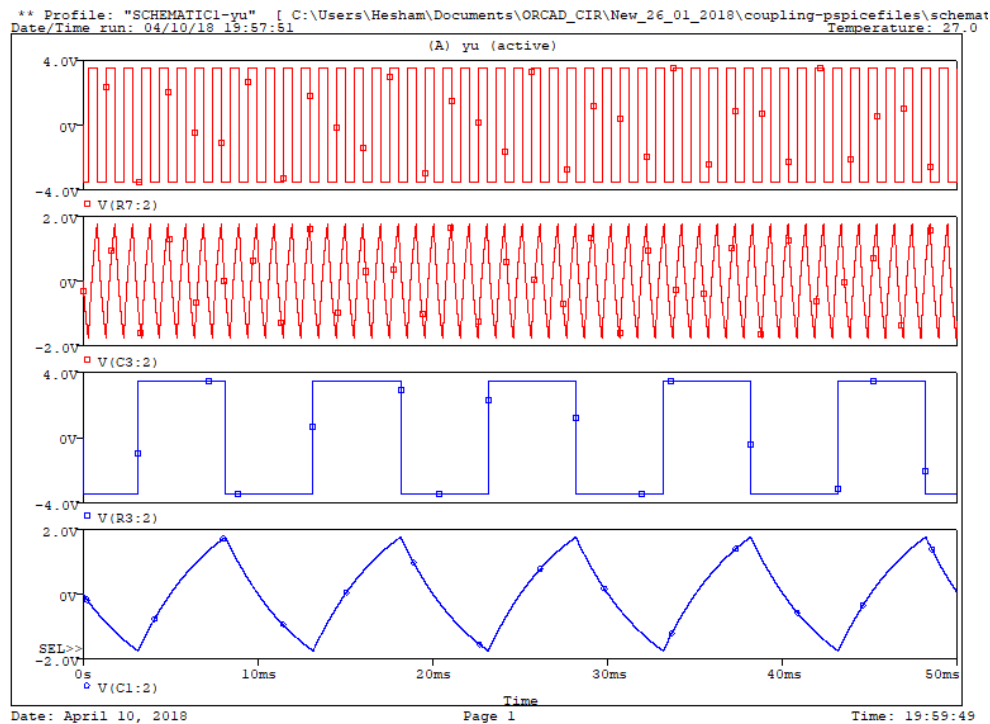
Figure 6-2 The output and the voltage of the two astable relaxation oscillators

119

Now, couple these two oscillators directly as shown in Figure 6-3. This coupling converts the second Schmitt trigger from autonomous to non-autonomous Schmitt trigger. The results of this direct coupling are found in Figure 6-4. This coupling affected the waveform of the non-autonomous Schmitt trigger. However, this direct coupling did not affect the phase but affected the amplitude only in a regular manner.
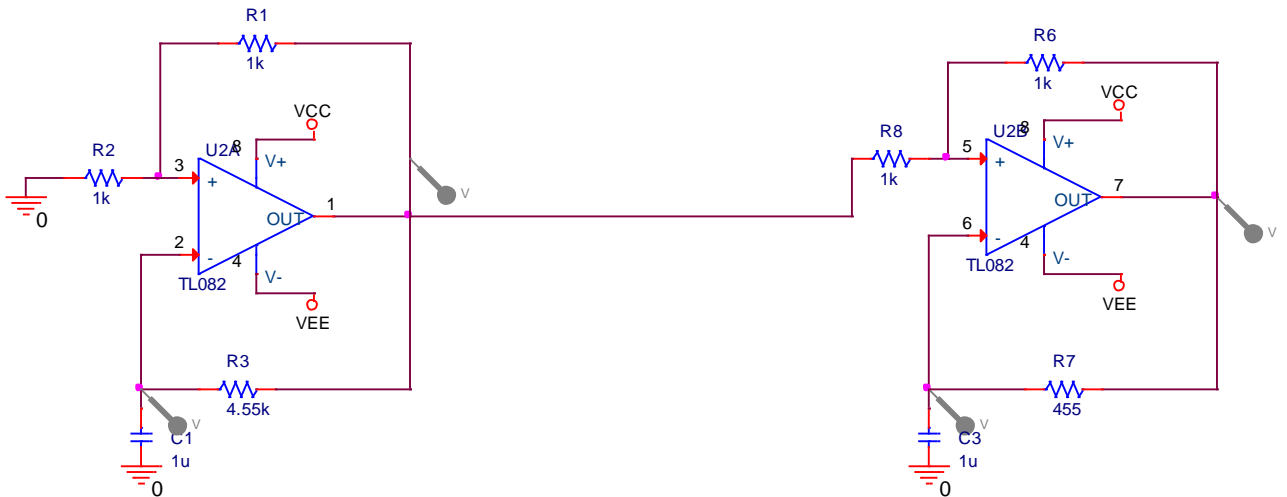
Figure 6-3 Direct coupling of the two astable Schmitt trigger
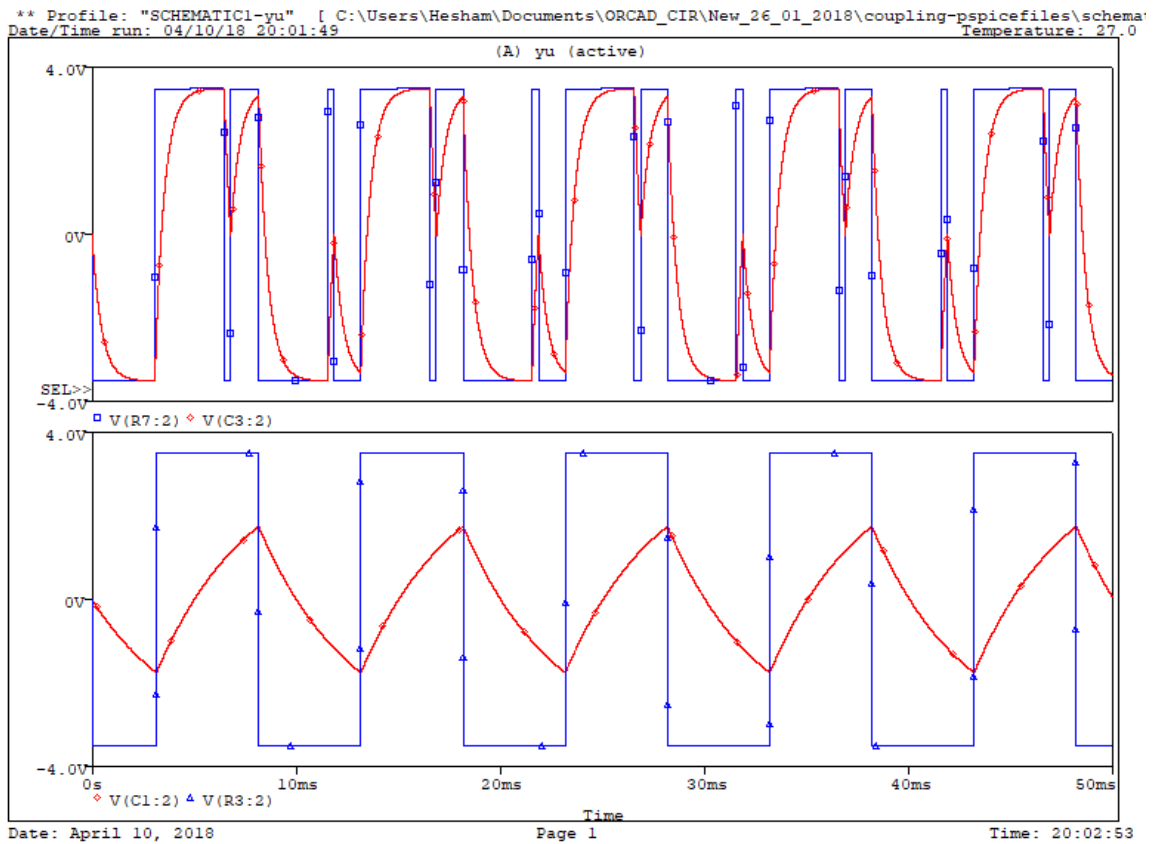
Figure 6-4 The output of the direct coupling Astable Schmitt trigger oscillators

120

By changing the coupling to resistive coupling as shown in Figure 6-5, the average voltage for the non-autonomous Schmitt trigger capacitor starts to change slightly. The output of the second Schmitt trigger gives a square wave with stripes as shown in Figure 6-6. Now, we have two frequencies; first is the large square wave and the frequency of the stripes which shows that it is six times more than the large square wave. It can be also described that there are two square waves, and one of them is affected by the other as a crosstalk effect. Hence, the noise effect starts to appear.
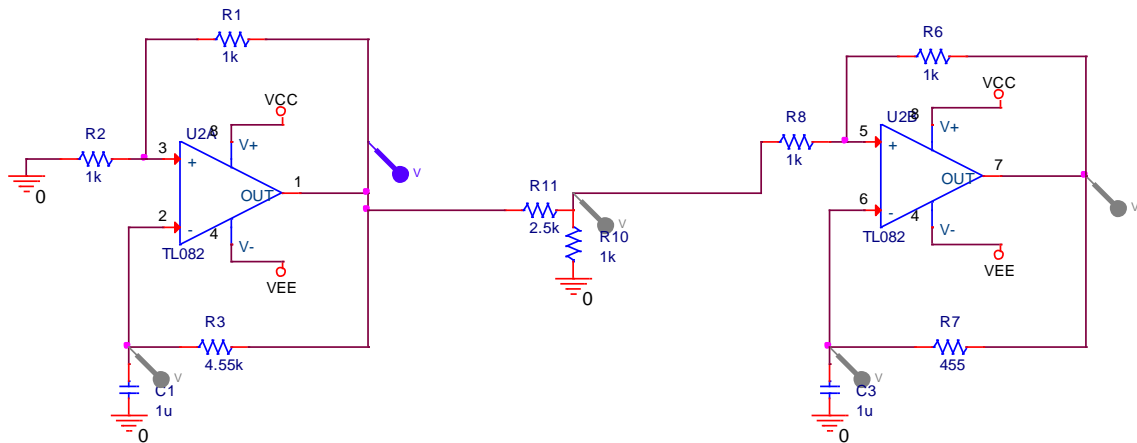
Figure 6-5 Resistive coupling of the two Schmitt trigger astable relaxation oscillators
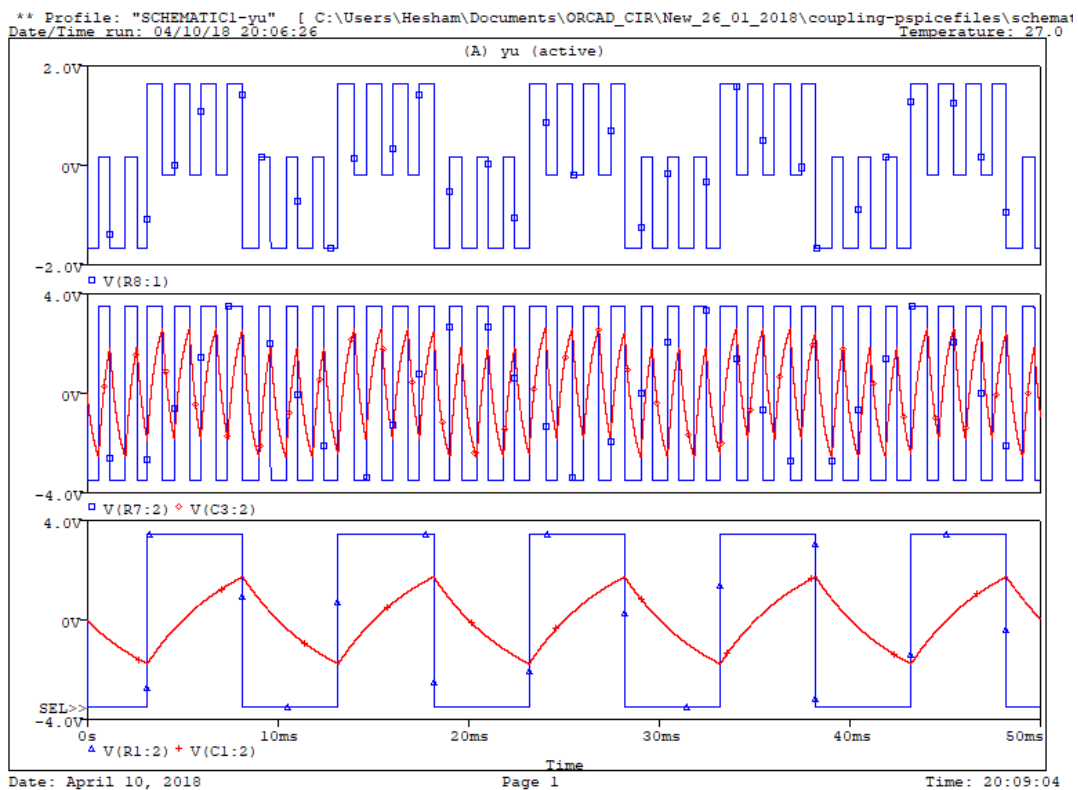
Figure 6-6 The output of resistive coupling and the waveform at the coupling resistor

121

Back to the basics of the implementation of chaotic oscillators, any chaotic circuits need at least three energy storage elements to generate chaotic oscillators. Based on this fact, and by observing the structure of the system, it can be easily seen there are only two energy storage elements, which are the two capacitors of the two Schmitt trigger.

Based on this observation, the coupling resistor has been replaced by a capacitor as shown in Figure 6-7. The output waveforms for this modification are shown in Figure 6-8. The output square wave starts to generate a square wave with a different width. However, this sequence is repeatable, which is not acceptable for our purposes.

By revising most of the analogue chaotic oscillators design, it has been observed that chaotic behaviour is achieved by changing the value of one resistor. Based on this observation again, all the capacitors values are fixed, and one resistor will change.
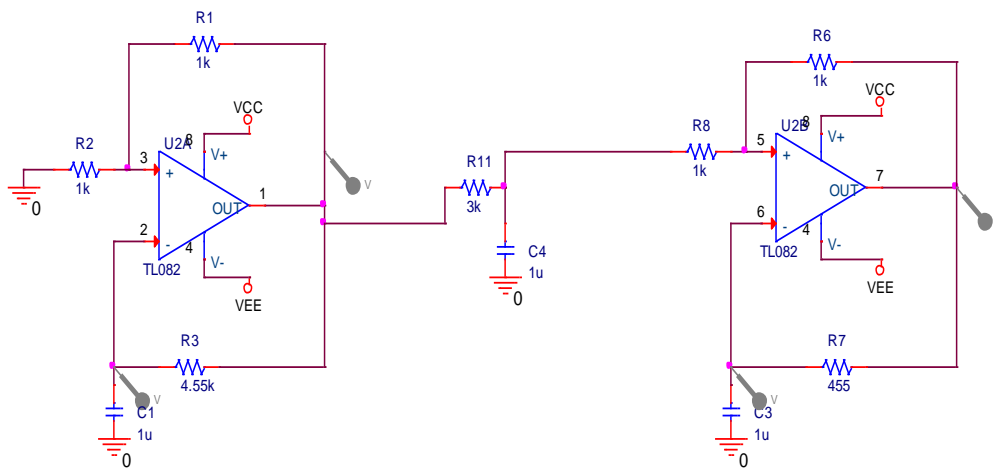
Figure 6-7 Replacing the coupling resistor by a capacitor
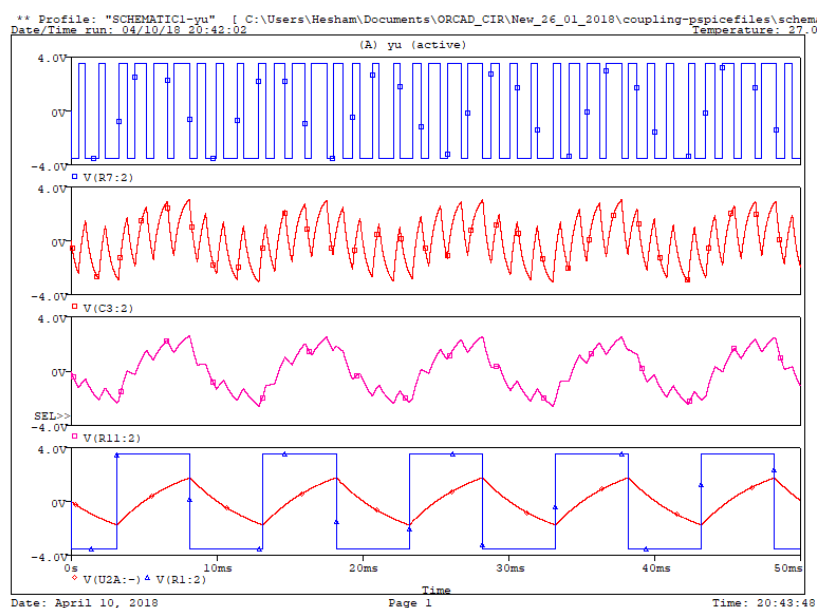
Figure 6-8 the output of replacing the coupling resistor with a capacitor

122

The question is: which of these resistors needs to be changed to reach the chaotic behaviour?

Neuroscience can answer this question. As mentioned in Chapter 5, in the neuroscience, most of the experiments of coupling the neuro oscillators did not change the oscillator itself but the coupling. Hence, the resistor that needs its value to be changed should not be one of the oscillators. Therefore, the series resistor connected to the output of the first oscillator or the astable Schmitt trigger will be the variable resistor that needs to be changed. Figure 6-9 shows the circuit by changing the series resistor to 3.8 k Ω. The chaotic behaviour starts to appear and is shown in Figures 6-10 to 6-13. These figures represent the relation of the capacitors' voltages. It has to be mentioned that we denote the first capacitor of the first Schmitt trigger as the input capacitor and output capacitor for the second oscillator capacitor.
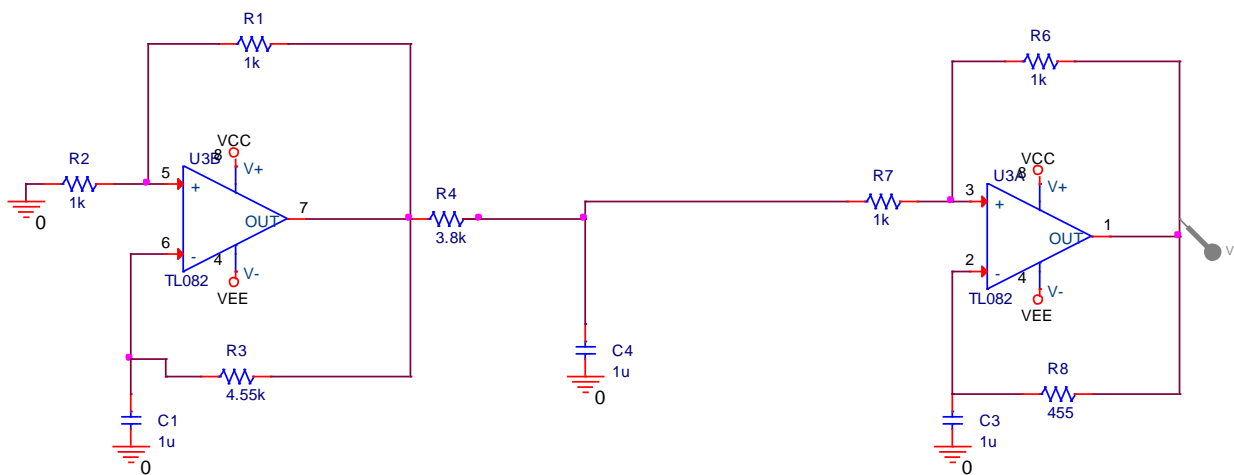
Figure 6-9 Changing the series resistor
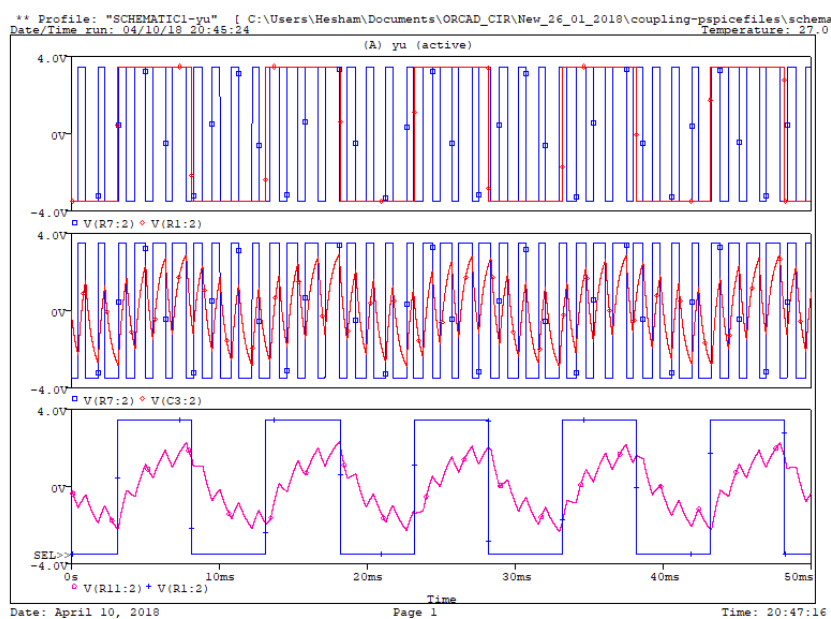
Figure 6-10 The output of changing the series resistor

123
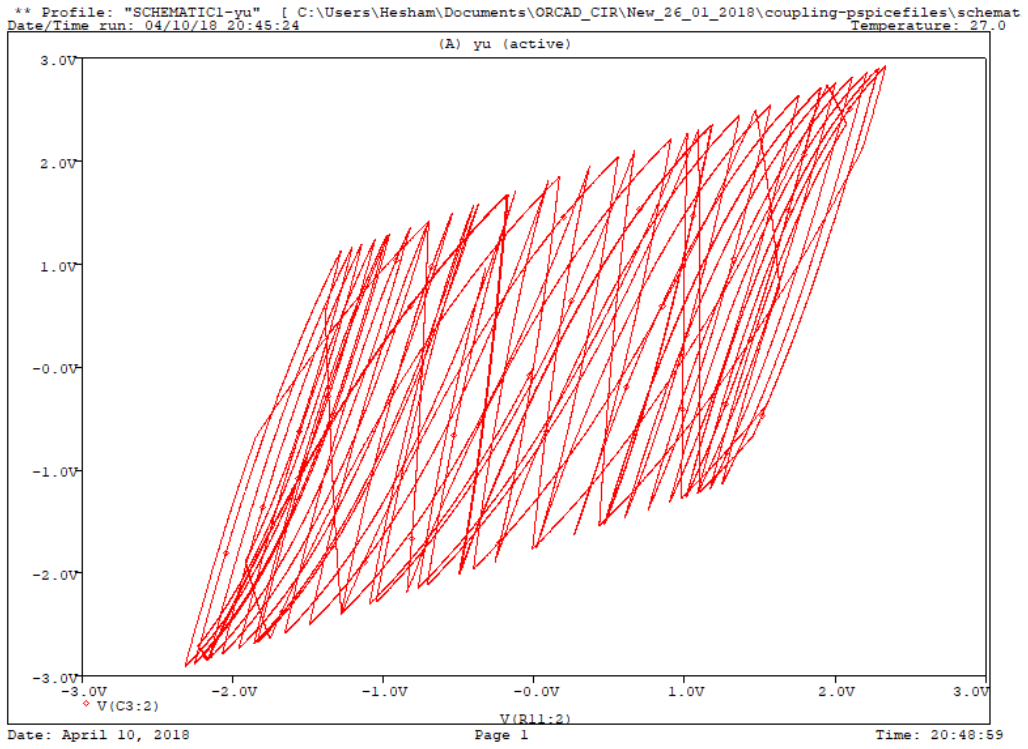
Figure 6-11 Output Capacitors Vs the mid Capacitors
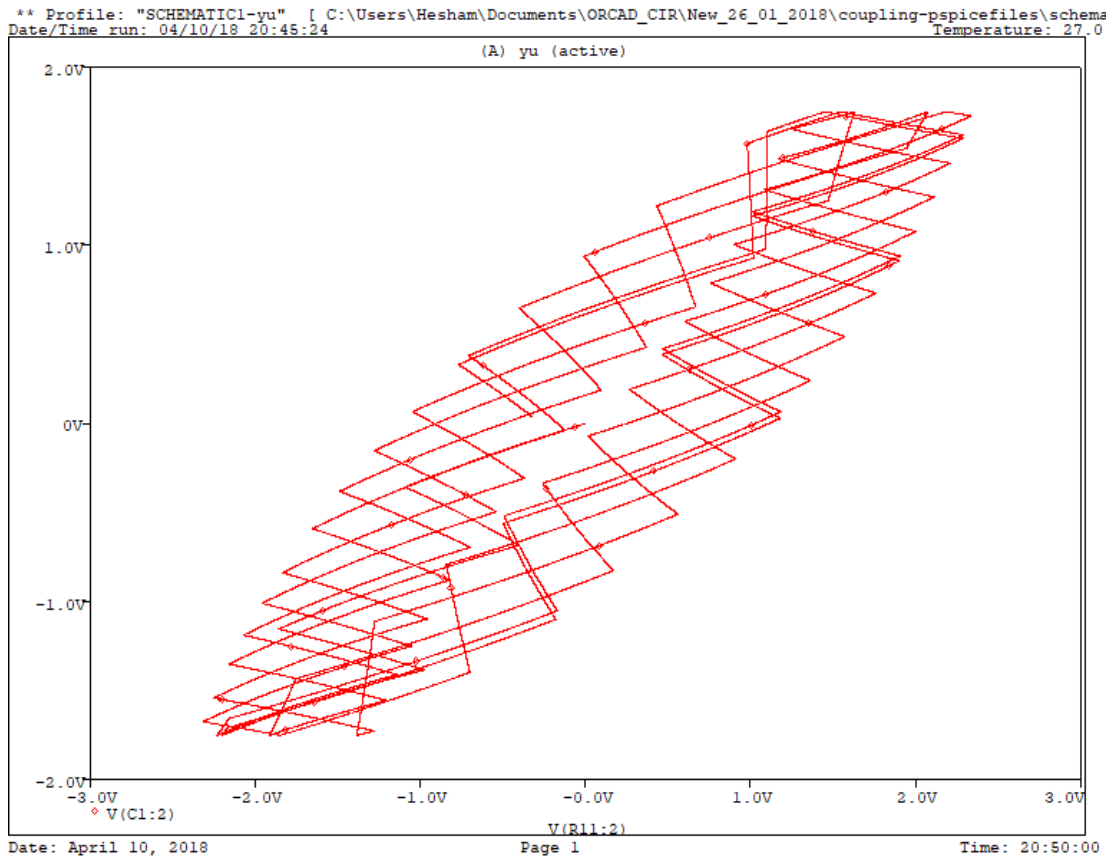
Figure 6-12 Input capacitor voltages Vs the mid-voltage capacitor
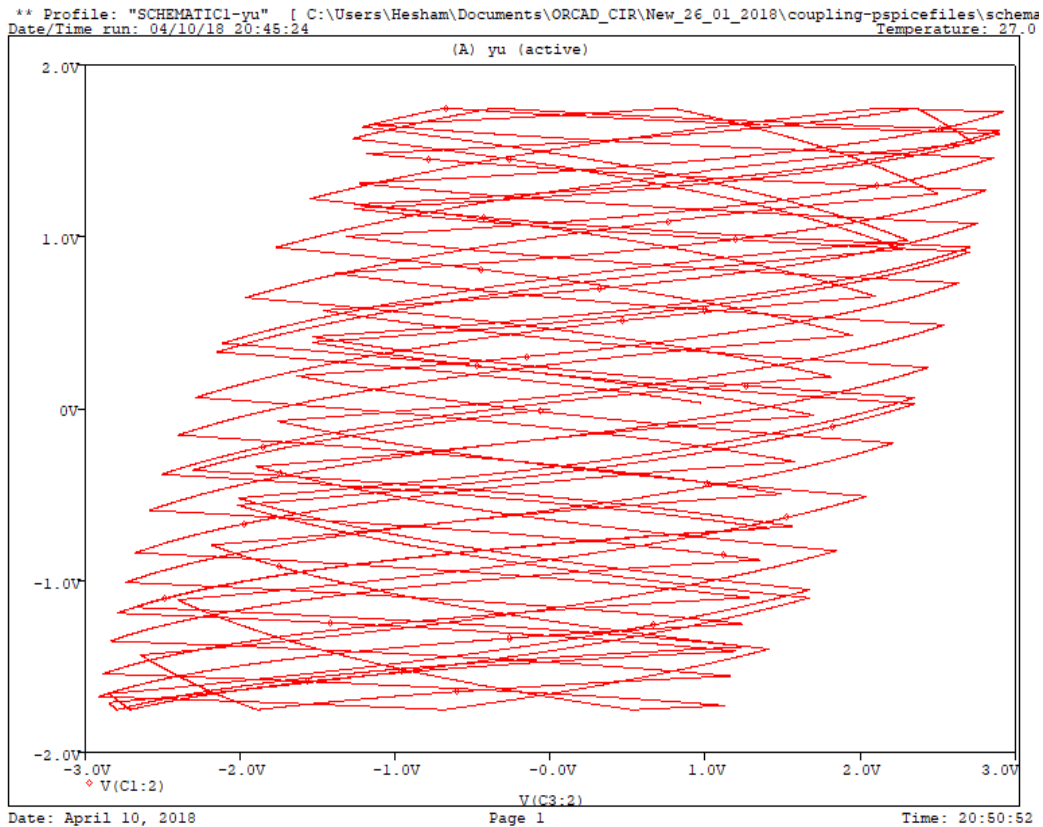
Figure 6-13 Input capacitor voltage Vs the output capacitor

As it is mentioned before, the results here rely on using the performance of the output sequence to reconstruct the original signal from the AIC algorithm made by Matlab program. The output sequence passed through this algorithm and the results are shown in Figure 6-14. The results show the failure to reconstruct the signal (Fourier spectrum only shown). Hence, the resistor value is changed again to 2.9 k Ω as shown in Figure 6-15. The sequence succeeds in reconstructing the original signal, as shown in Figures 6-16, 6-17 and 6-18. The average square error reaches 0.0000436833.
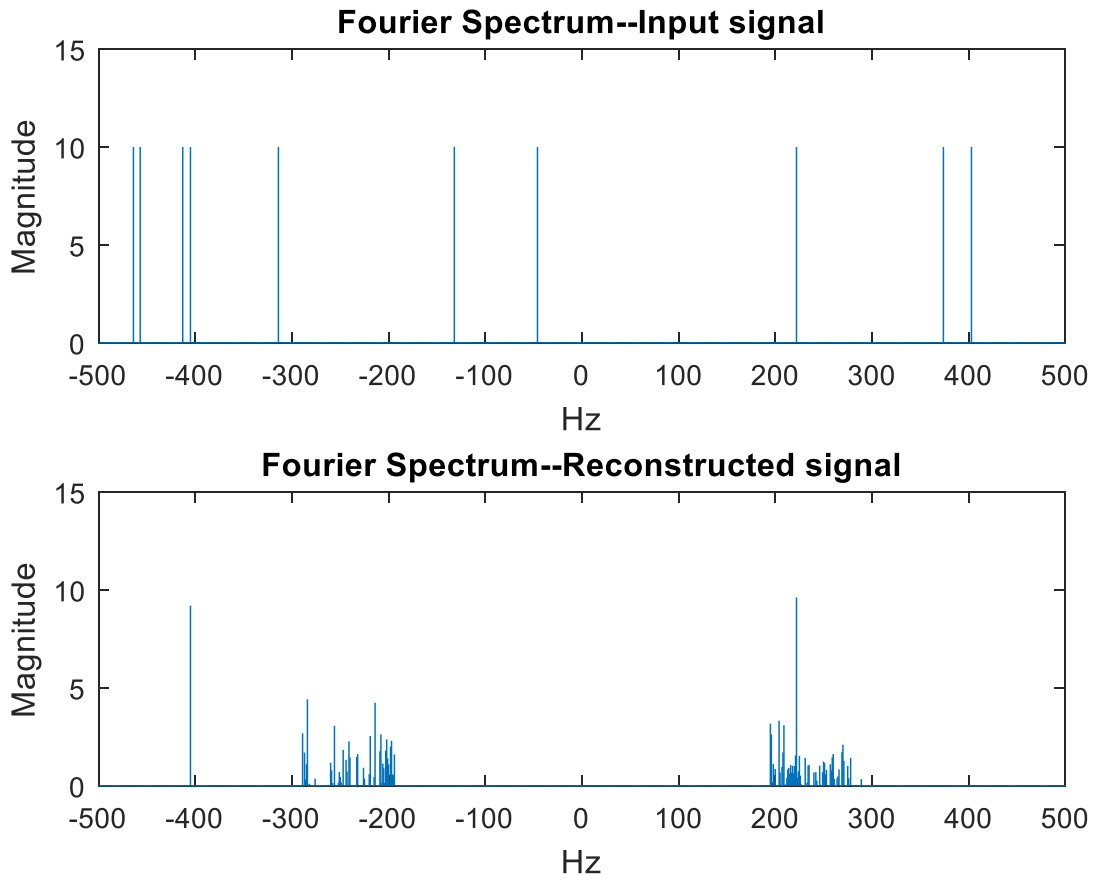
Figure 6-14 The results of the output sequence in the AIC framework (Fourier spectrum only)
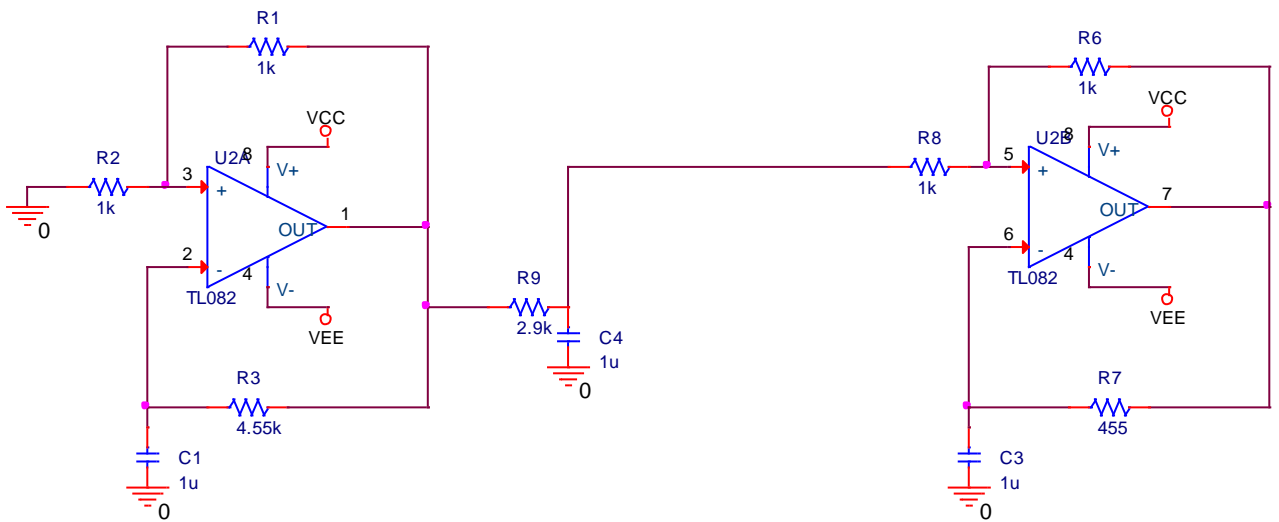
Figure 6-15 Changing the resistor value to 2.9 k Ω
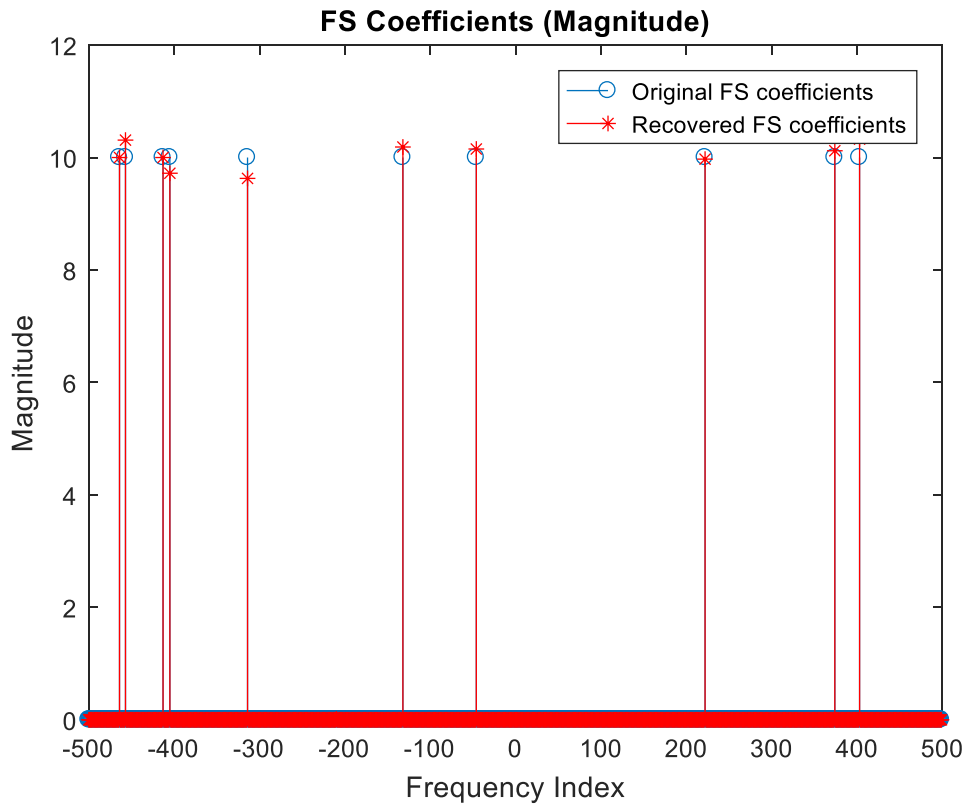
Figure 6-16 The Matlab output after changing the resistor value (FS coefficient)
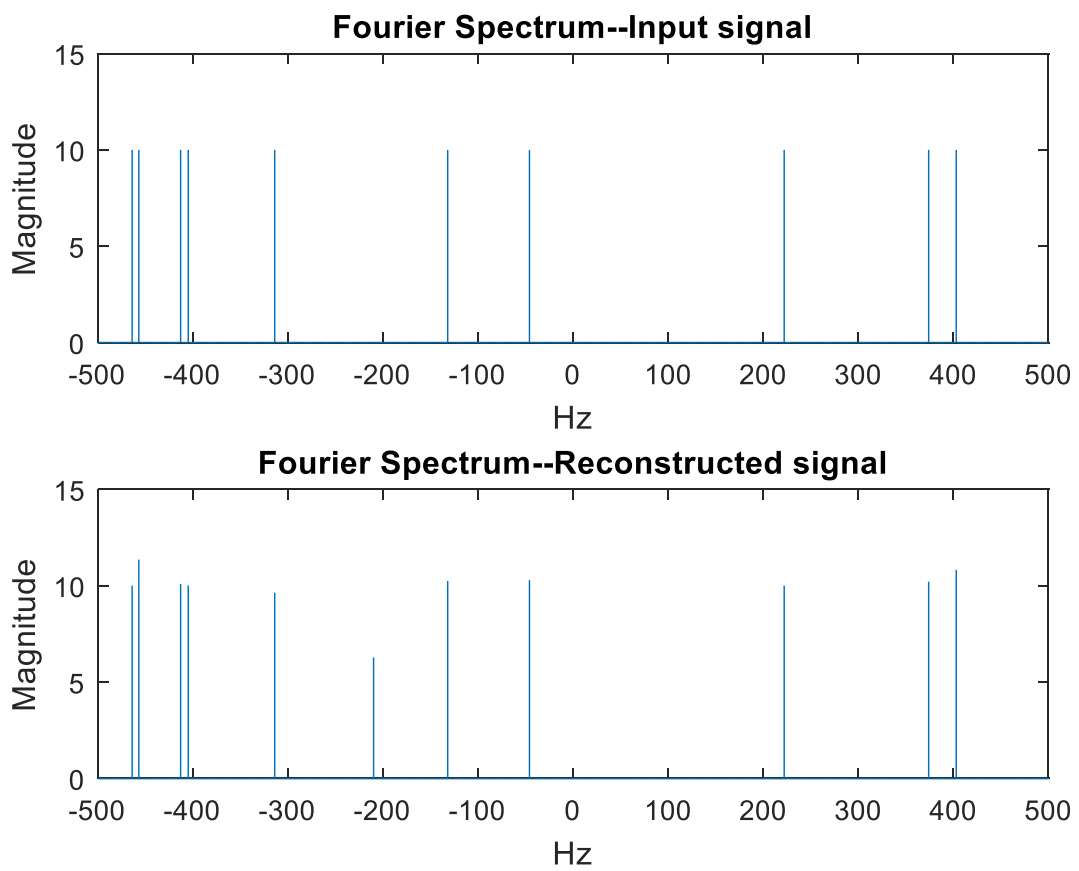
Figure 6-17 Matlab output after changing the resistor value (Fourier spectrum)
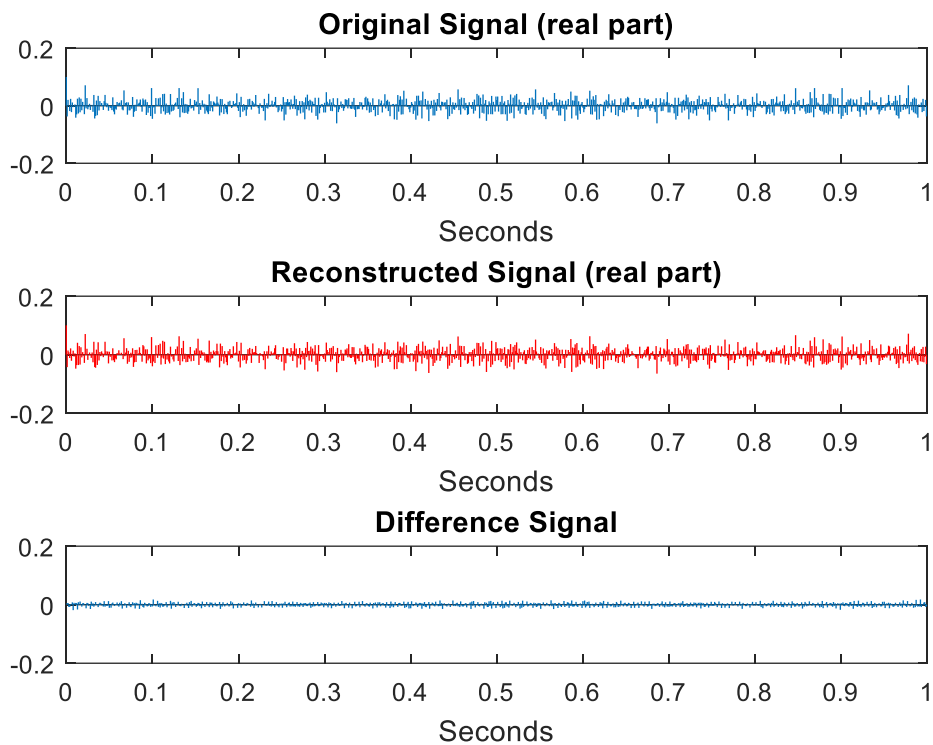
Figure 6-18 Matlab output after changing the resistor value (Time domain)

To realize the results, a Texas Instruments analogue kit was used, and the resistor values are changed to the standard values (R=455 Ω ➔470 Ω, R1=2.7 kΩ➔2.9 kΩ and 4.55 kΩ➔4.7 kΩ). The hardware results are shown in Figure 6-19. However, the output sequence after changing these values failed to reconstruct the signal as shown in Figure 6-20.
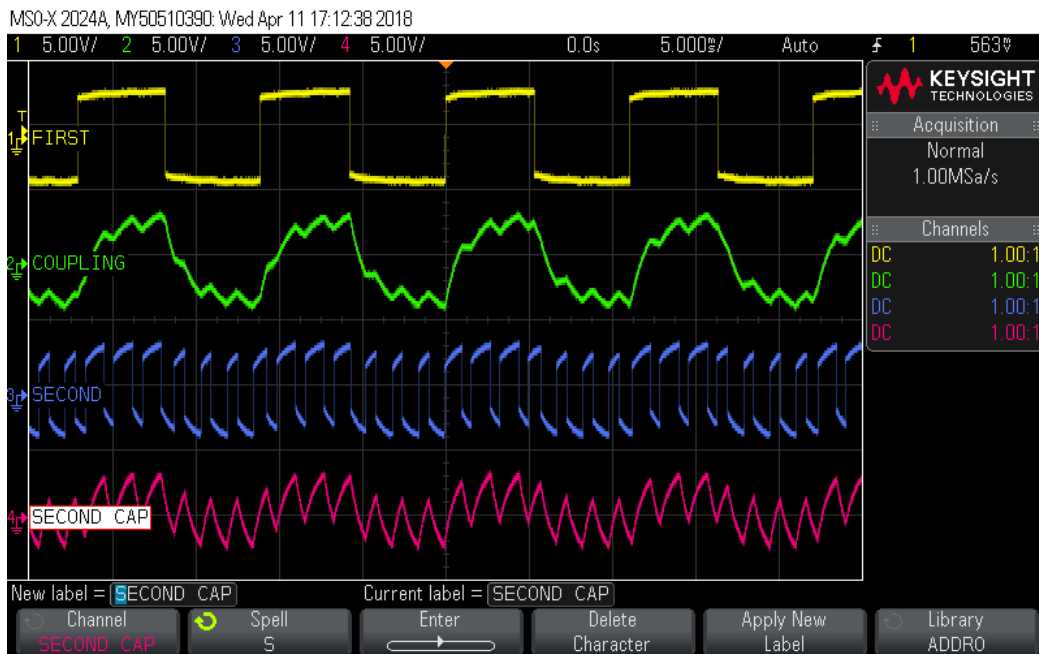
Figure 6-19 Hardware results after changing the resistor values to the standard
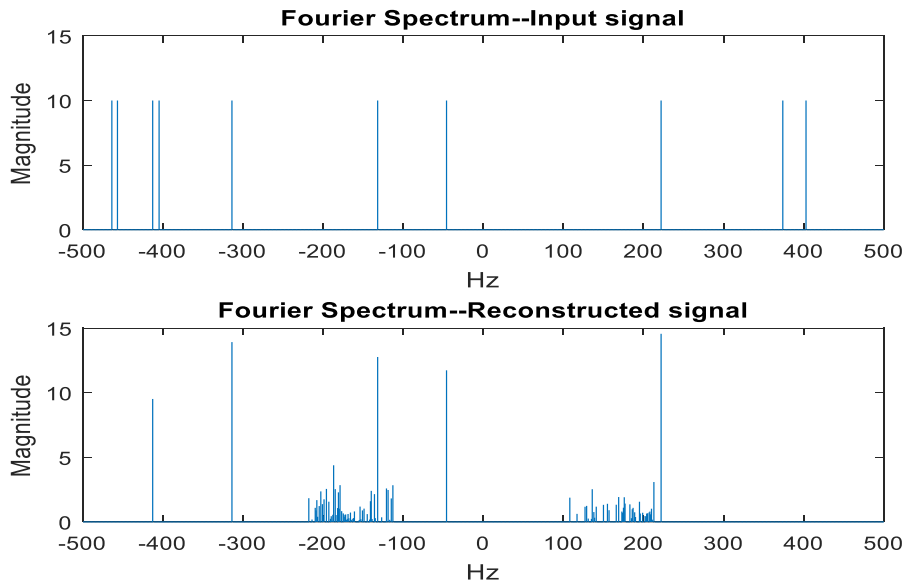
Figure 6-20 Hardware sequence results after passing the sequence to the AIC algorithm

Therefore, the series resistor changes to 3.6 kΩ in the hardware. The sequence is shown in Figure 6-21. The sequence passed the AIC algorithm, and the output is shown in Figures 6-22, 6-23 and 6-24 with average square error reaching of 0.0000150854. The difference may be due to the wiring which may add some noise that slightly affects the performance. On the other hand, the hardware results show the average voltage of the sequence is affected by the capacitor. This point can be avoided by adding another comparator as shown in Figure 6-25. However, this point is not essential because this does not affect the signal reconstruction.
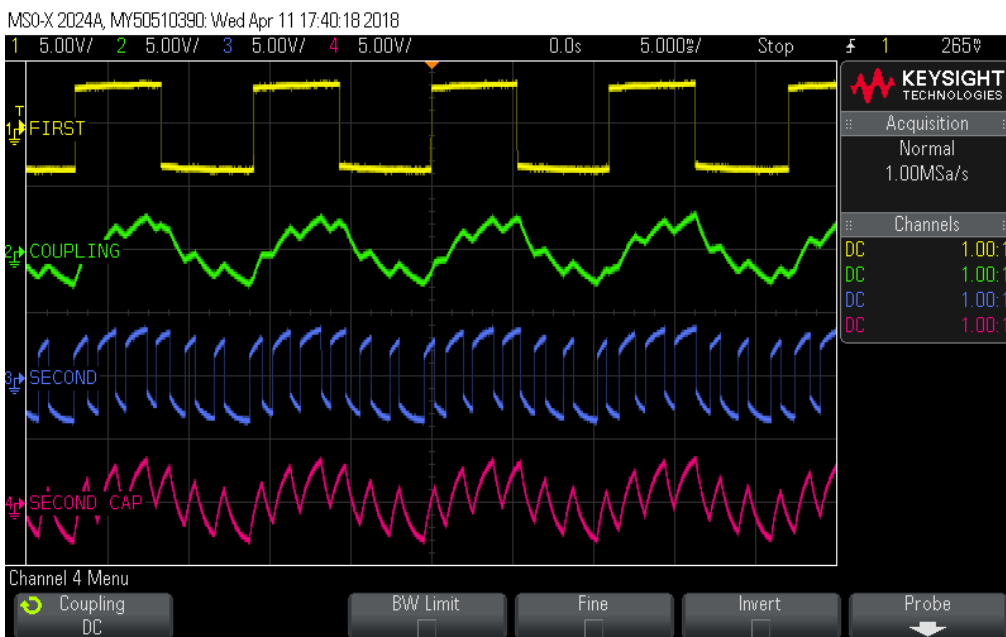
Figure 6-21 Hardware output after changing the series resistor
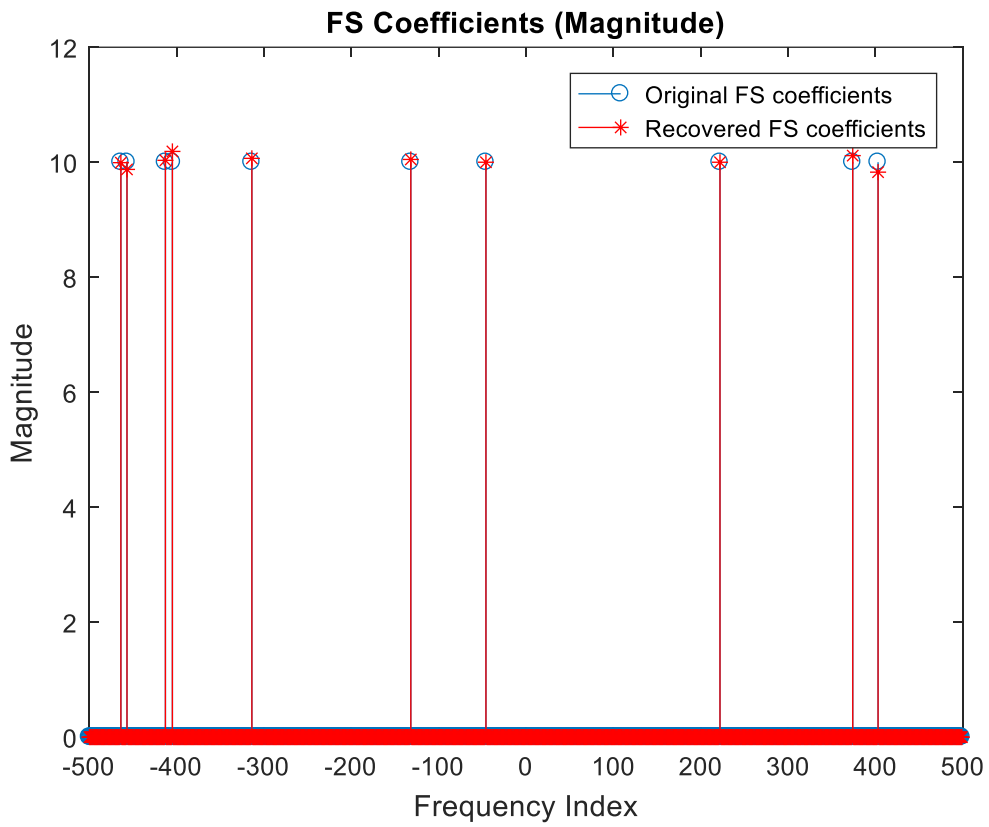
Figure 6-22 Hardware sequence results after passing the AIC Algorithm (FS Coefficient)
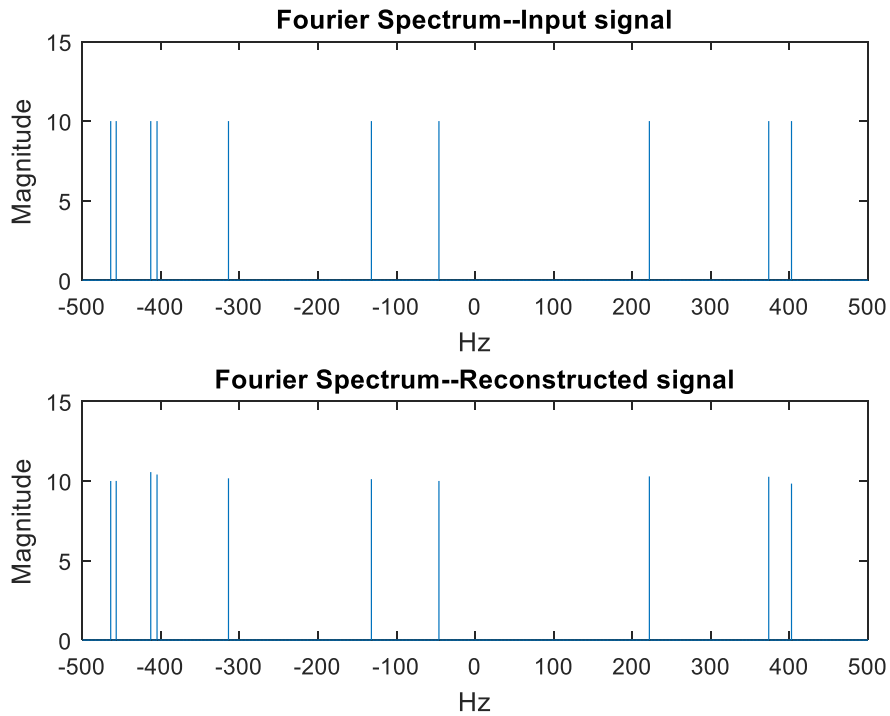
Figure 6-23 Hardware sequence results after passing the AIC Algorithm (Fourier spectrum)

Original Signal (real part)

Reconstructed Signal (real part)

Difference Signal
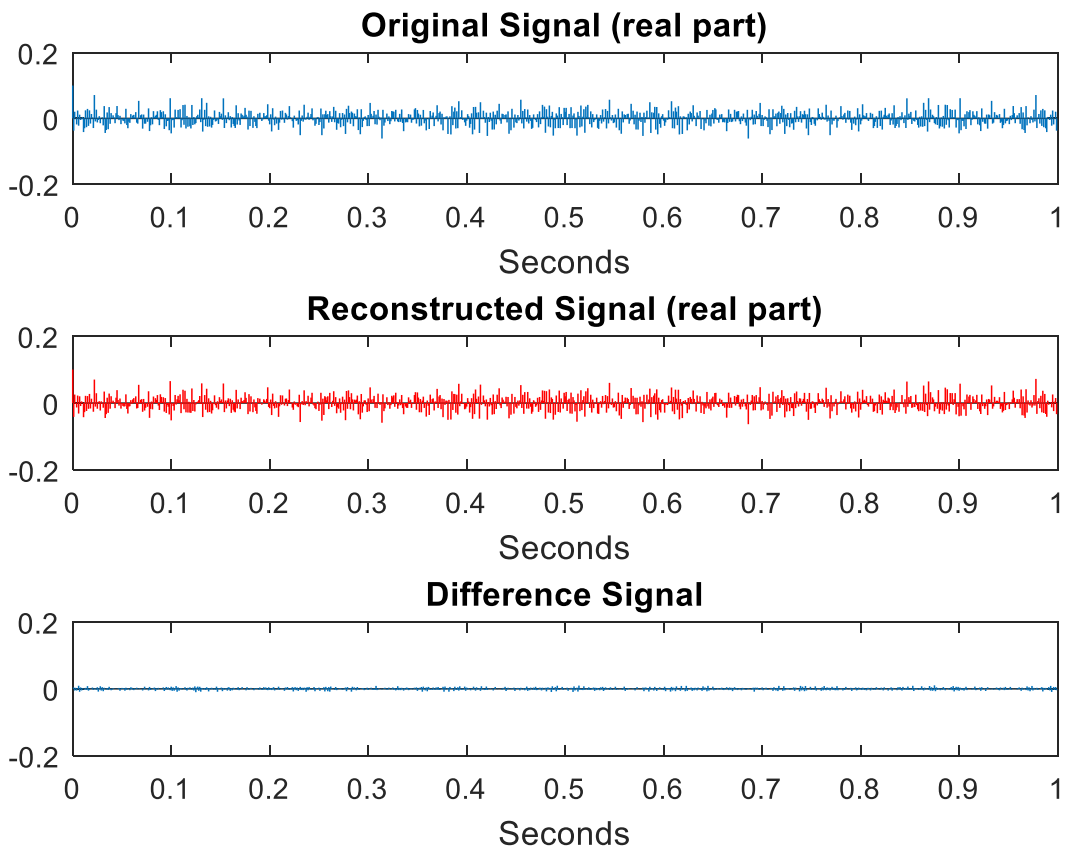
Figure 6-24 Hardware sequence results after passing the AIC Algorithm (time domain)
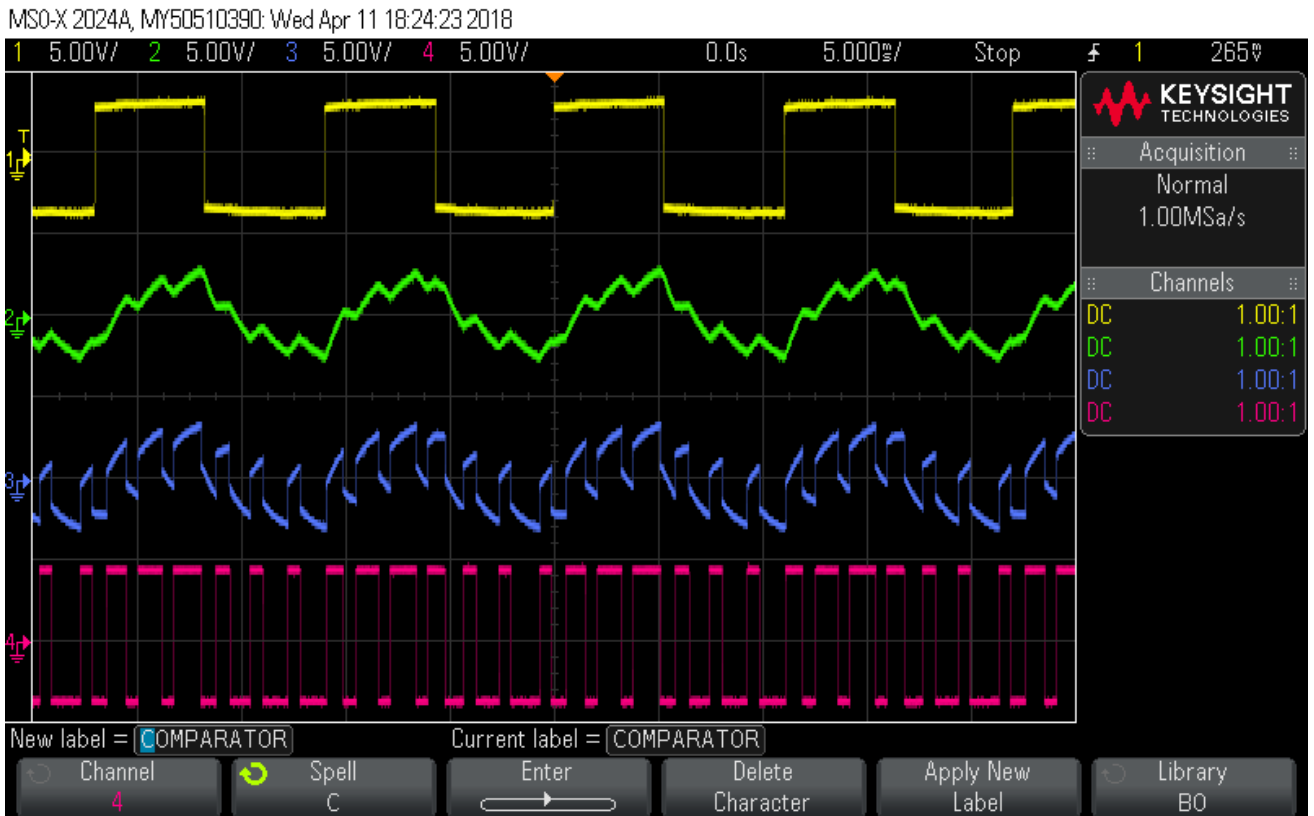
Figure 6-25 Hardware results after using Comparator

131

At the end of this section, it has been shown that based on the waveshaping technique and coupling oscillators, a simple method of constructing analogue chaotic oscillators is proposed and can be used for AIC. The heart of this proposed system is a Schmitt trigger and an RC coupling circuit. RC coupling acts as LPF that affects the sequence of the oscillators. In the next section, based on the second modification for the opamp Schmitt trigger presented in the previous chapter, another proposed system will be introduced along with its analysis.

6.3. Proposed System 2

In the previous section, the RC coupling capacitor was connected from the output of astable Schmitt trigger oscillator to the grounded resistor found in the positive feedback of the second Schmitt trigger oscillator. In this section, another connection will be introduced. This shows the richness of this design to have several chaotic oscillators from the same design with small variations.

Figure 6-26 shows the second proposed system. In this system, we use the presence of the capacitance of the oscillators and couple it with one T-shape RC circuit to generate the chaotic oscillator. By the same concept, all the capacitors have the same values and the T-shape R4 was fixed to 1 k Ohm and the R5 was changed till it reached the chaotic sequence as shown in Figure 6-27. Figures 6-28, 6-29 and 6-30 show the transfer characteristics between the capacitors voltages found in the design. It has to be mentioned that this design starts with standard values of the resistors to avoid any changes in the hardware. The frequency of the first oscillator is almost 96 Hz while the second is 968 Hz. The ratio of the resistors found in the negative feedback of the two oscillators is the same of the first proposed system which is 1/10.

While the output in Figure 6-27 shows poor irregular sequence, bifurcation appeared in Figure 6-30. This shows the good performance of this design. However, this study relies on the performance of the design to reconstruct the original signal from the AIC framework. The sequence is fed to the Matlab AIC framework; it succeeds in reconstructing the original signal as shown in Figures 6-31, 6-32 and 6-33 with an average squared error of 0.0000071490. This value is very low compared to the first proposed system. This may refer of the bifurcation found in this system.
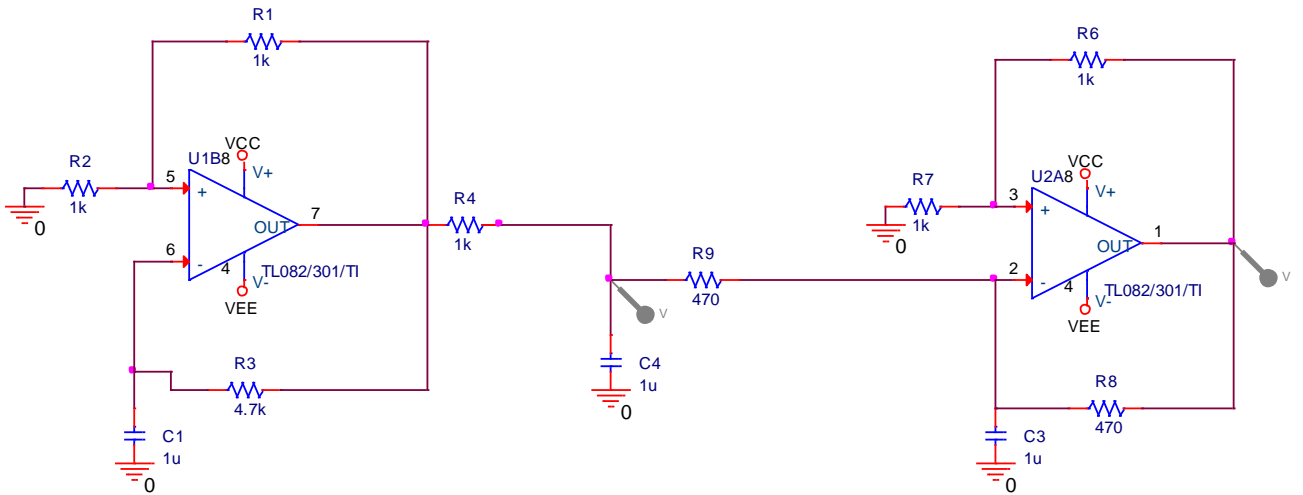
Figure 6-26 Proposed System 2

(A) secc (active)

□ V(R6:2) ◇ V(R4:2)

Time

Date: July 16, 2018   Page 1   Time: 00:48:41
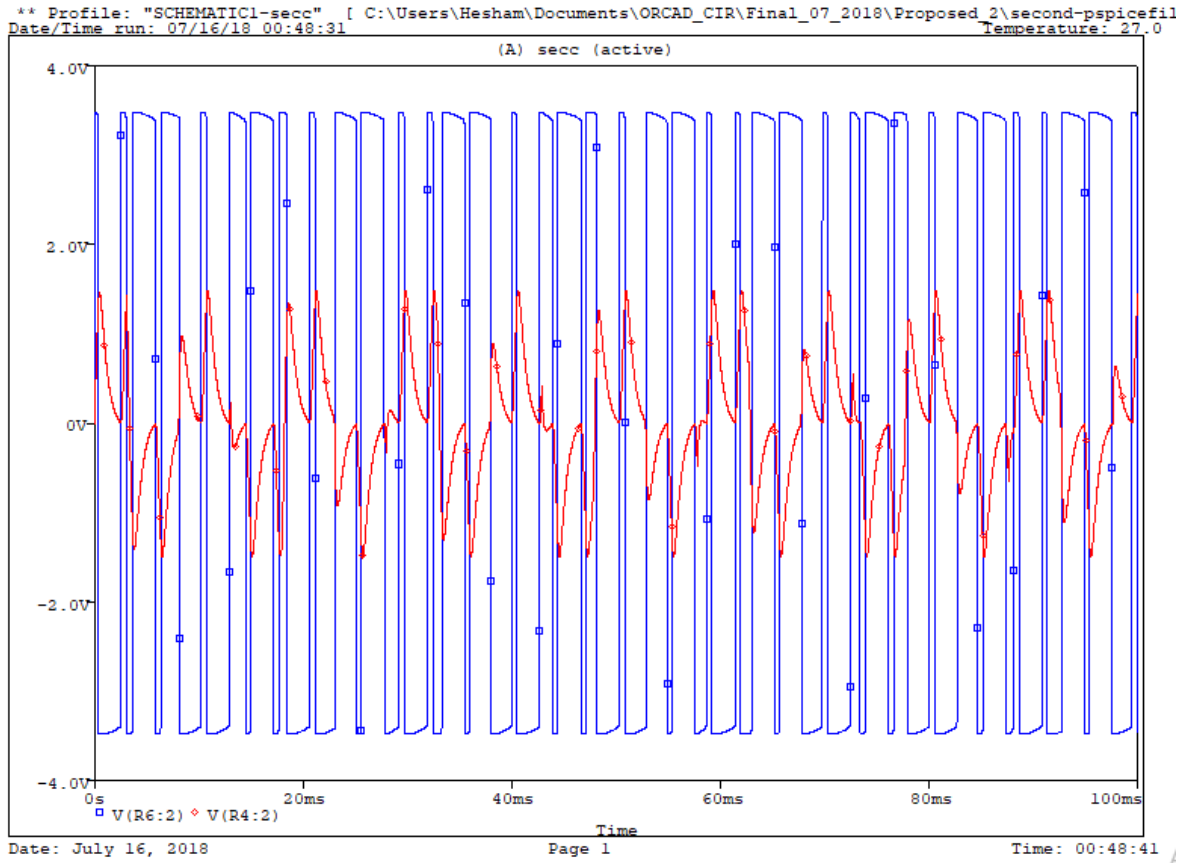
Figure 6-27 The oscillator and the voltage capacitor waveform

133

(A) secc (active)
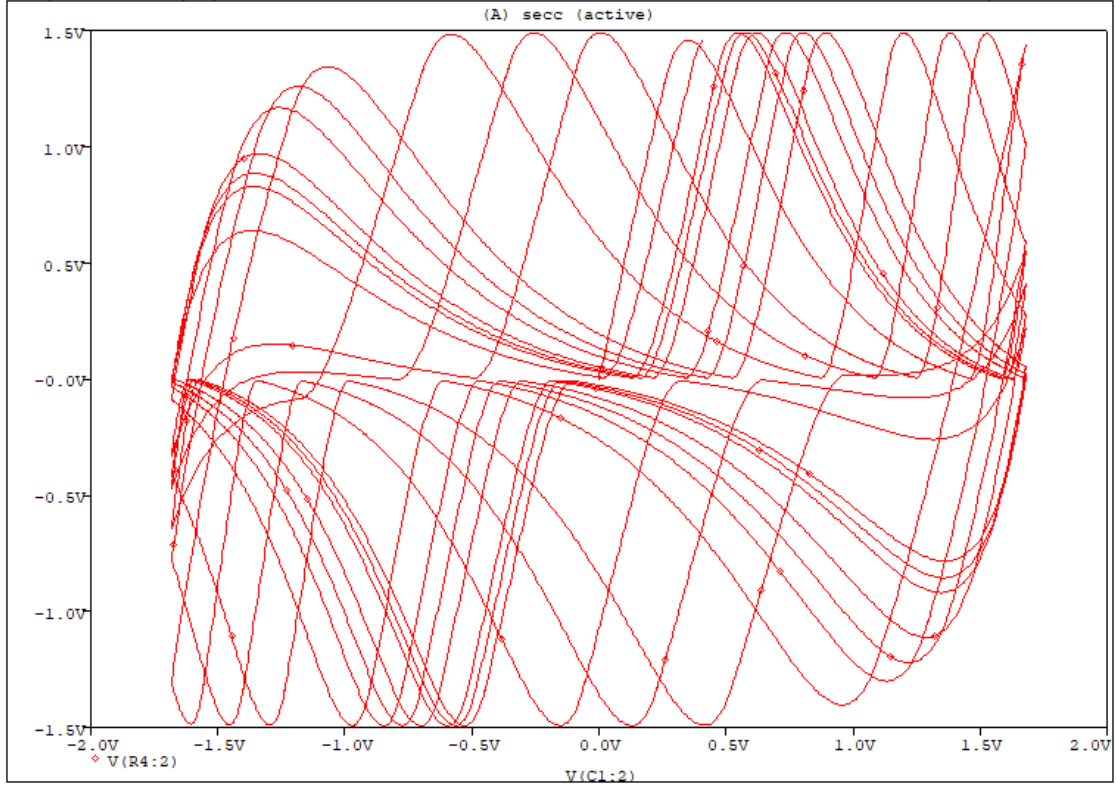
Figure 6-28 The transfer characteristics between the first oscillator capacitor and the coupled capacitor

(A) secc (active)
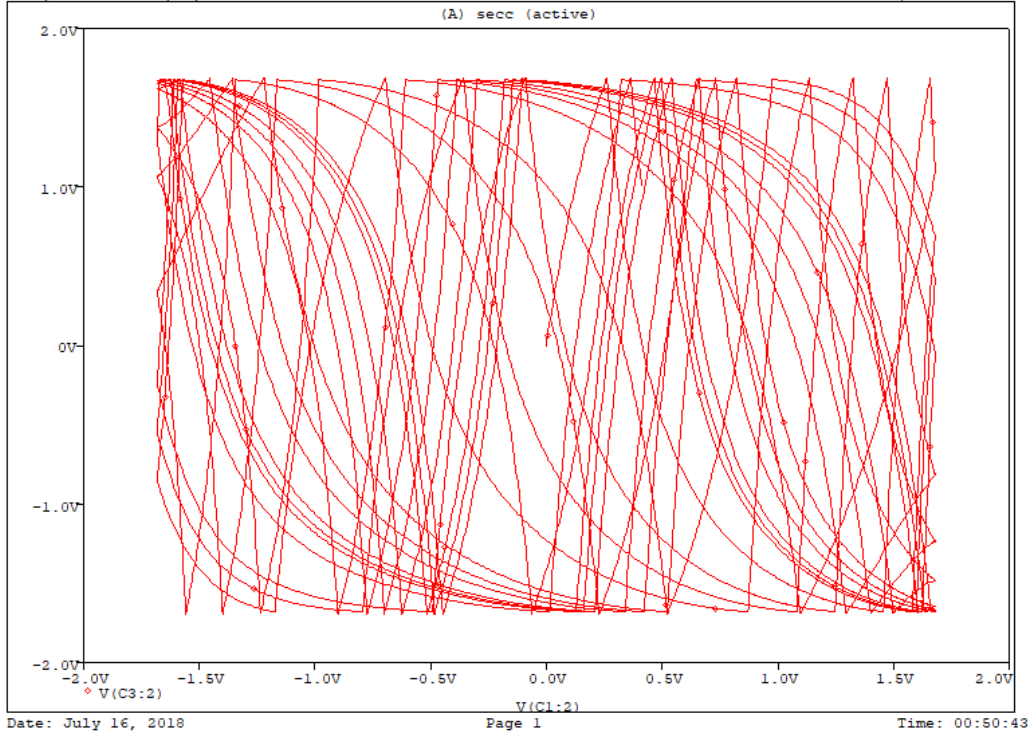
Figure 6-29 The transfer characteristics between the input and the output capacitors

134
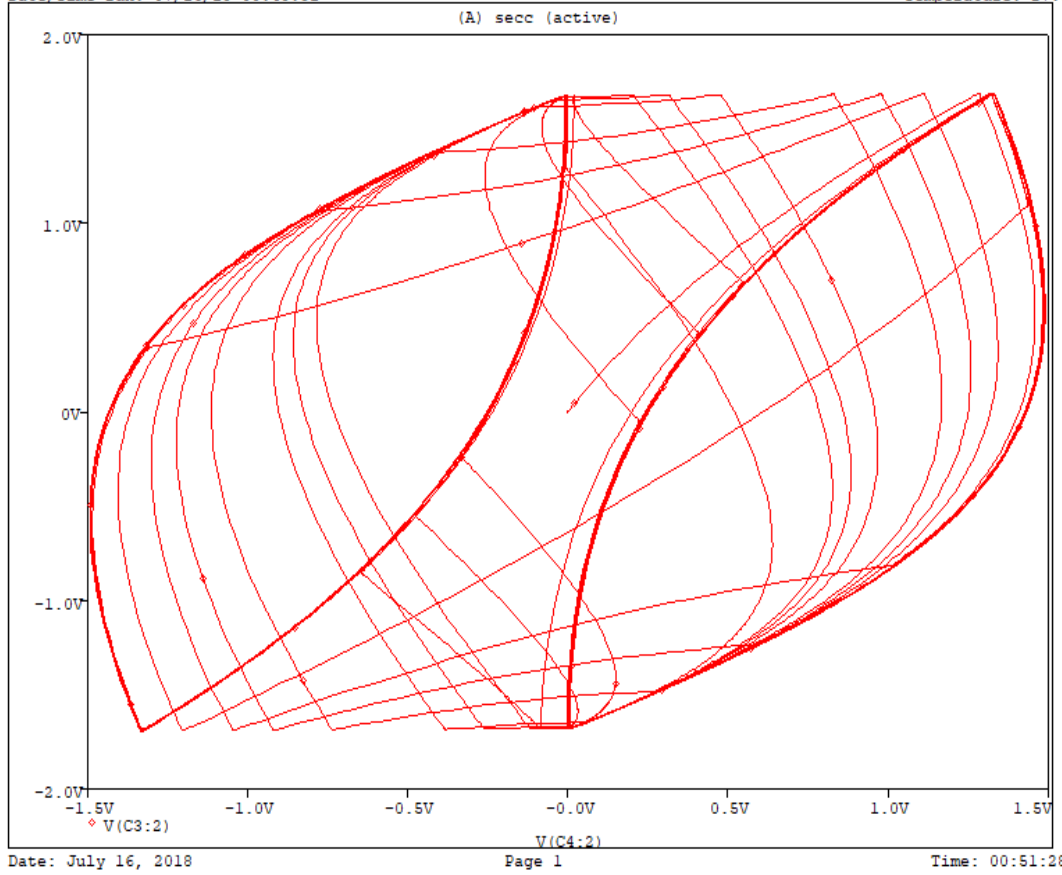
Figure 6-30 The transfer characteristics between the coupled capacitor and the output oscillator
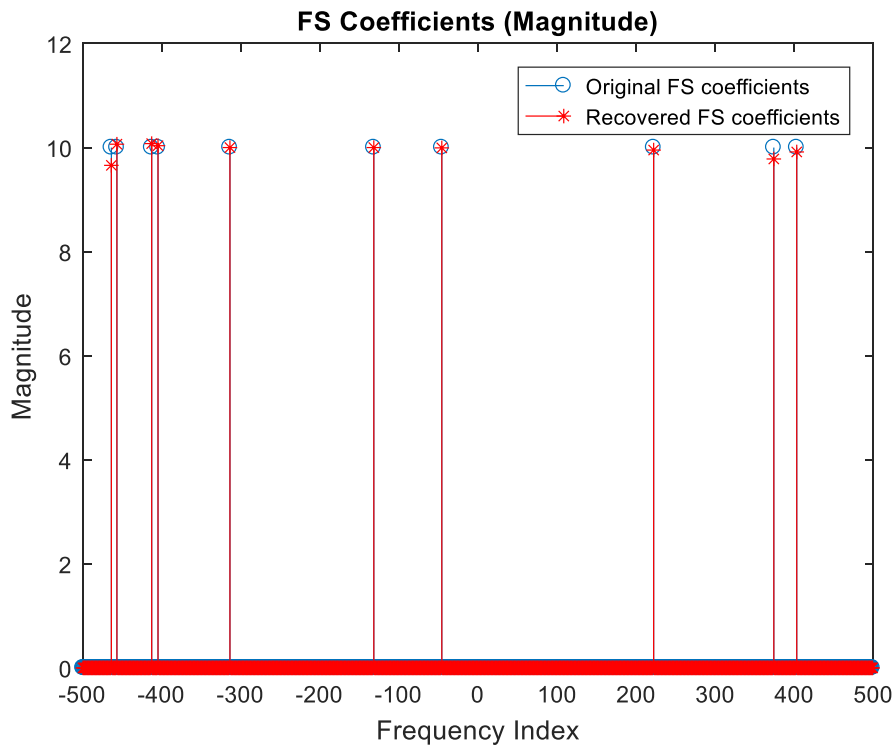
Figure 6-31 Matlab Results for the second proposed system (FS Coefficient)
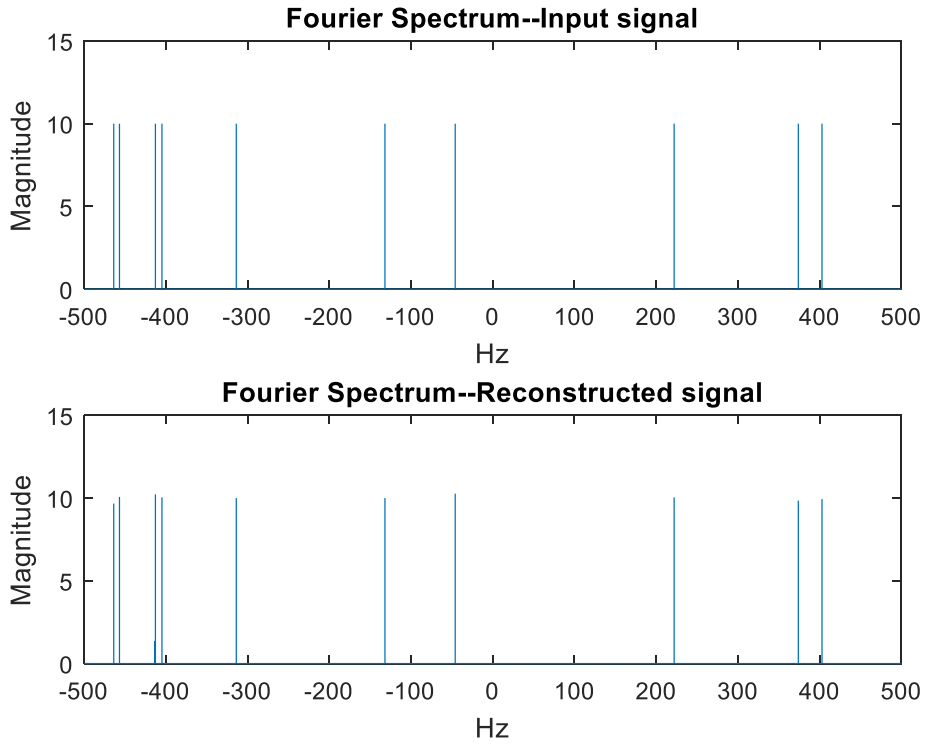
Figure 6-32 Matlab Results for the second proposed system (Fourier spectrum)
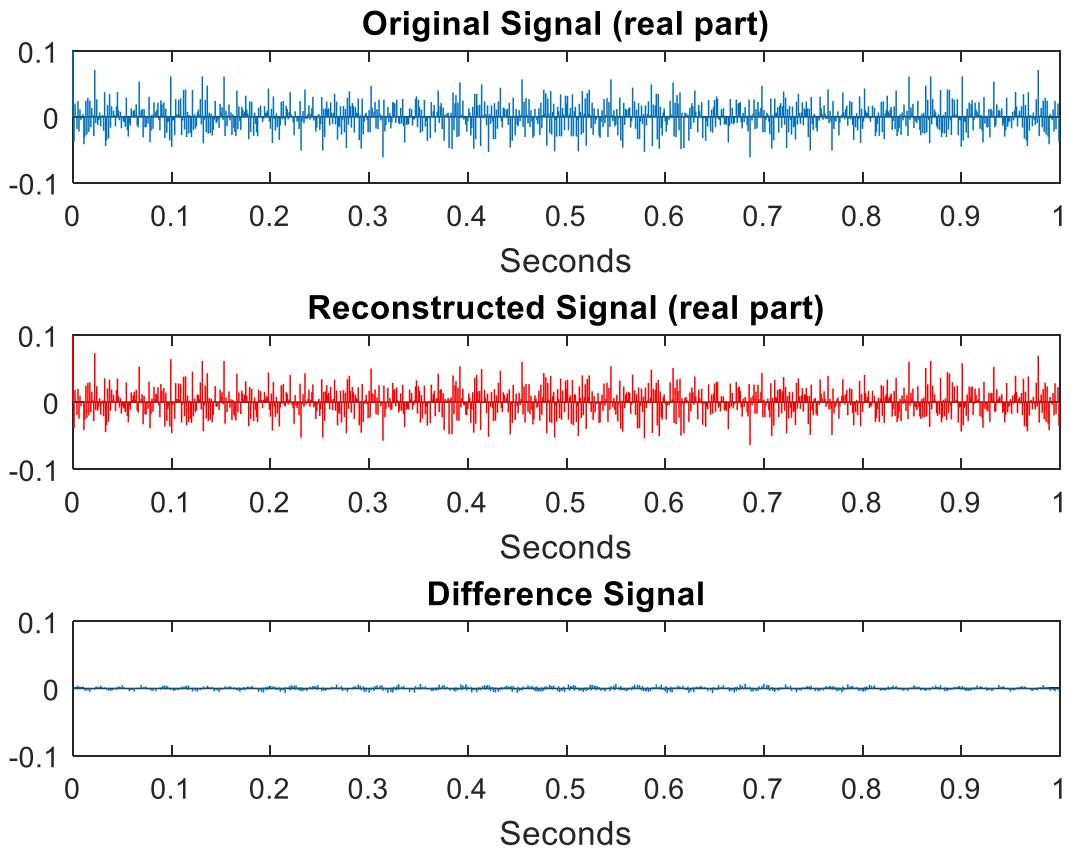
Figure 6-33 Matlab Results for the second proposed system (time domain)

By replacing the simulated component values to standard values and as in the first proposed system, R1 changed to 1.8 kΩ to avoid the wires effect as shown in Figure 6-34. The output waveforms of the hardware are shown in Figure 6-35. The hardware output sequence is fed to the Matlab AIC framework, and the results are shown in Figures 6-36, 6-37 and 6-38. The hardware output sequence succeeds in reconstructing the original signal with average squared error equal to 0.0000256813 which shows more improvement than the simulation.

Another point needs to be highlighted. As the coupling was connected to the capacitor at the negative feedback of the second oscillator, the average voltage of the output of the second oscillator is not affected by the coupling and is still zero. This gives more improvement of this design that does not need to add any comparator to generate a chaotic sequence with a perfect square waveshape.
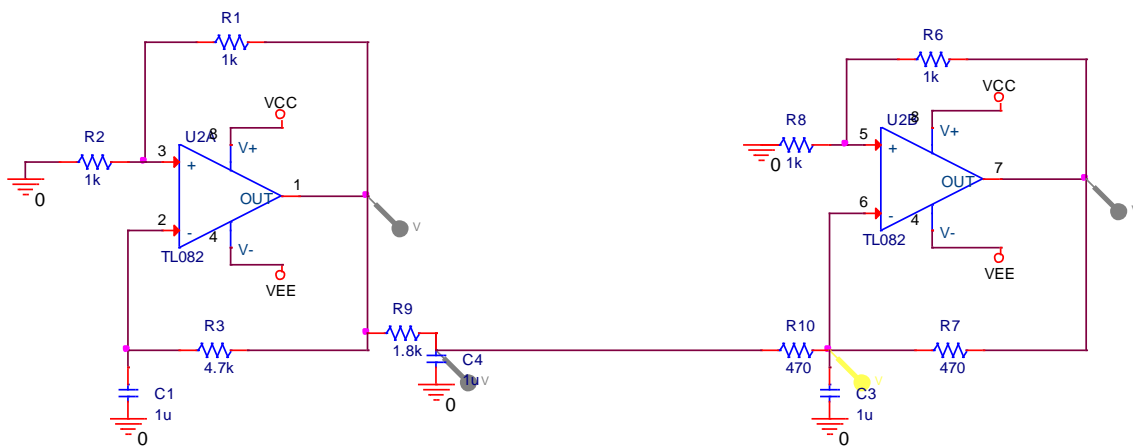
Figure 6-34 Hardware values for the secondly proposed systems
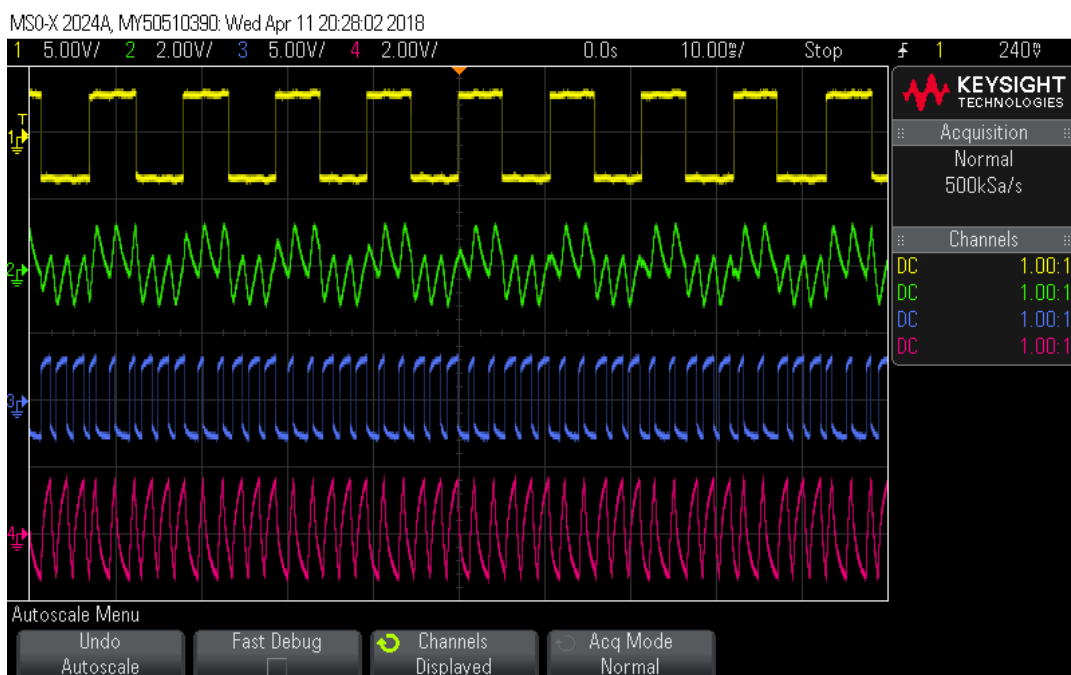
Figure 6-35 Output waveforms of the hardware sequence

137
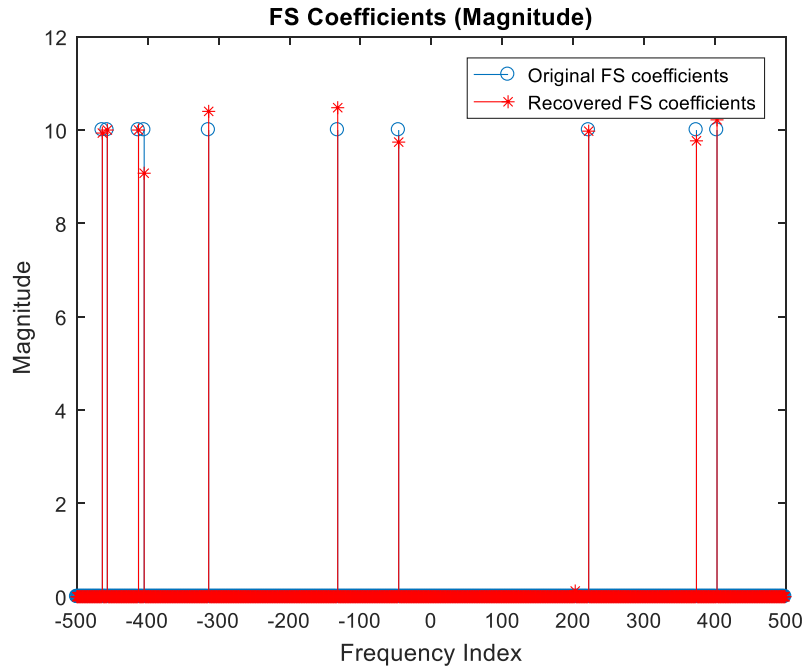
Figure 6-36 Matlab results for the hardware results (FS Coefficient)
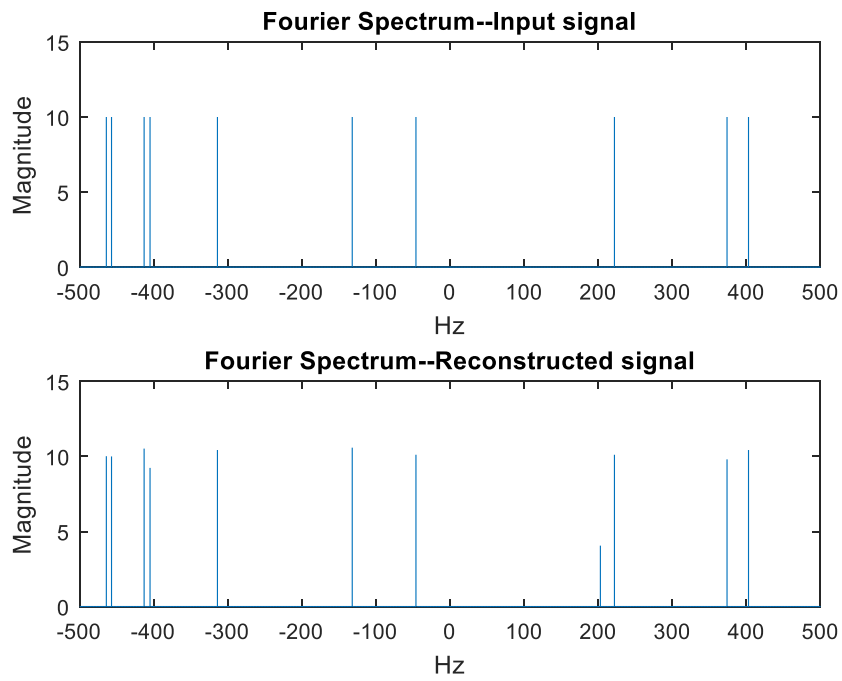
Figure 6-37 Matlab results for the hardware results (Fourier spectrum)
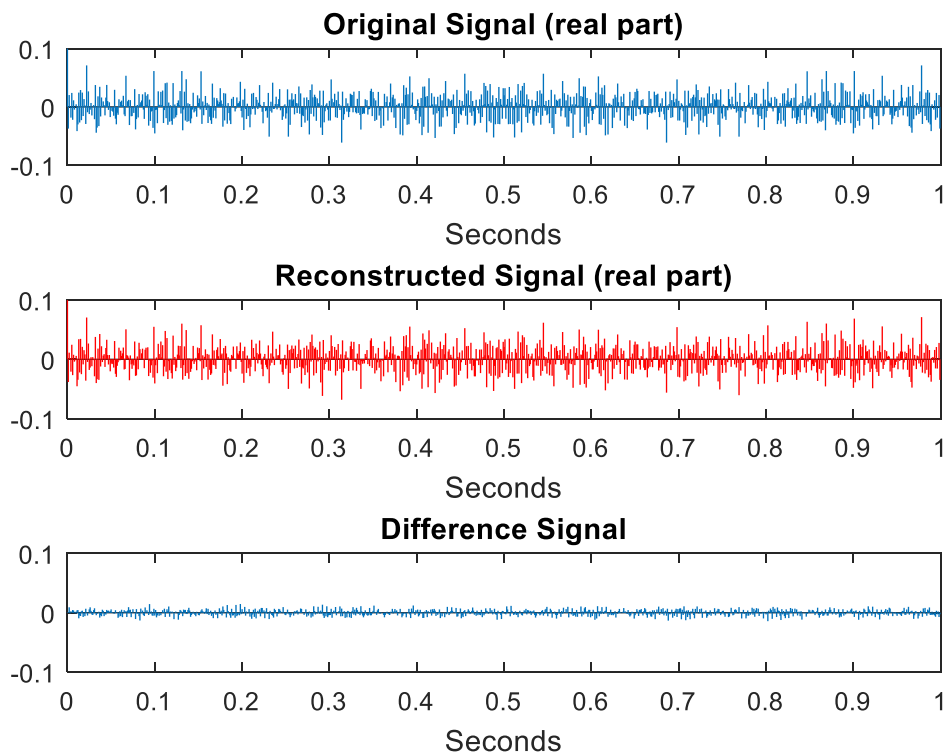
Figure 6-38 Matlab results for the hardware results (time domain)

At the end of this section, the second proposed system is like the first one, except for the choice of the terminal to be connected to the coupling circuit. This proposed system improves the signal reconstruction for AIC framework in comparison with the first proposed system. Both proposed systems can be used by one FPAA that can change the connection easily by using the switched capacitor technique that is used in FPAA design. However, these systems need to be validated as will be shown later in this chapter.

6.4. The Proposed Systems from the Security point of view

The main aim of this research is to replace the traditional digital PRNG with analogue circuit design to improve the circuit design of the IoT device with low-power consumption. However, as mentioned before, the IoT device circuit designer needs to take all the IoT device design challenges into considerations. One of these challenges is the security issue. To achieve the security point of the proposed systems for AIC framework, two points need to be highlighted: randomness and the system's ability to reconstruct the original signal. Both points have been shown earlier in this chapter and the key point is the selection of the component values, as can be illustrated as follows:

6.4.1. Randomness

In the context of CS theory [37], [53]– [66] ,[183], only the random signal can be used in CS. The random signal has to be independent and identically distributed (i.i.d) and obeys the restricted isometry property (RIP) condition of perfect recovery [183]. The Matlab code used in this research [166] covered this point.

The chaotic sequence from the proposed systems has successfully passed this test. If the sequence is not random with the CS conditions, the original signal cannot be reconstructed. This point was very clear when adjusting the component values. The output chaotic sequence from the proposed systems could pass the simulation only at certain values of the components. This means at certain values, the chaotic sequence from the proposed system is following the CS conditions.

6.4.2. The ability of the Signal reconstruction

Most of the researchers in the communication security use the ability of the system to reconstruct the original signal with the identical chaotic sequence to test the security like [184]– [190]. We can consider the AIC analogue frontend as a transmitter and the signal reconstruction algorithm is a receiver as shown in Figure 6-39.
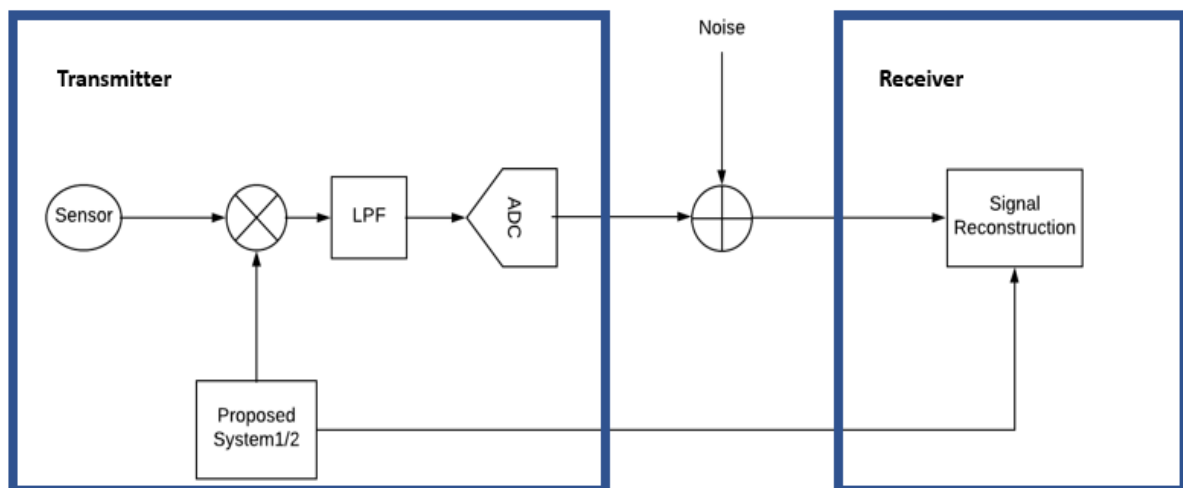
Figure 6-39 AIC analogue front end and the signal reconstruction act as transmitter and receiver

Two points proved the security of the system:

1- If the proposed chaotic systems, which act as noise, affect the ability of the receiver to reconstruct the original signal, then the proposed systems will fail.

140

2- The first point is valid only at certain values of the components. Any changing of the values leads to unsuccessfully reconstructing the original signal. This point proved the hardware security concept for the design.

Based on all the information mentioned in this section, it can be concluded that the proposed systems are considered as hardware secured systems with low-power consumption, which can be used to design and develop an IoT device to be used for several Smart City's applications

6.5. Validation

As mentioned before, a digital representation of the chaotic system is more complex and needs more size, this leads to more power consumption. Thus, validation or comparison will not be obtained with digital circuit but with analogue chaotic circuits.

The comparison will focus on some main parameters:

1- Number of the active elements (opamp)
2- Power consumption.
3- The accuracy of signal reconstruction in ambient temperature
4- The accuracy of signal reconstruction in a harsh environment

The fourth point is to show the ability of the design to reconstruct the circuit under the variation of the temperature found beneath the Manhole cover.

Memristor-based circuits like Chua circuit or Jerk based chaotic oscillator like Jessica and Sprott [168] can be used to validate the proposed system. However, Chua circuit required at least three opamps in the case of replacing inductor with its circuit model. Therefore, the concept of using fewer components to reduce the power consumption will not be valid. For this purpose, Jessica and Sprott design will be used for comparison.

Manhole cover temperature can vary from place to another and from one utility to another. According to the investigation done by the researcher, the temperature can vary from -30º C to 60ºC. For the following experiments, the maximum temperature coefficient will be used based on its value mentioned in the datasheet. TL082 opamp is used in this research and is the same opamp used by Jessica and Sprott's implementation.

Symbol	Parameter	Conditions	TL082C			Units
			Min	Typ	Max	
V_{OS}	Input Offset Voltage	$R_S = 10\ k\Omega,\ T_A = 25°C$		5	15	mV
		Over Temperature			20	mV
$\Delta V_{OS}/\Delta T$	Average TC of Input Offset Voltage	$R_S = 10\ k\Omega$		10		μV/°C

Figure 6-40 Tl082 Input offset voltage Temperature Coefficient (Datasheet)

TL082 has a typical value of $\pm 10 \mu V/^o C$ from the datasheet as shown in Figure 6-40. This can be translated into the variation of the offset voltage based on the following equation

$$V_{offset}/_{Temperature} = (T_{amb} - T_{ref}) \times \frac{\Delta V_{os}}{\Delta T} \text{ V} \qquad (6-1)$$

Where T_{amp} is the ambient temperature and T_{ref} is the reference temperature (27°C) and $\frac{\Delta V_{os}}{\Delta T}$ is the temperature coefficient of the input offset voltage. Hence at -30 °C

$$V_{offset @ -30^o} = (-30 - 27) \times \pm 10\mu = \pm 570 \mu V \qquad (6-2)$$

And at 60 °C

$$V_{offset @ 60^o} = (60 - 27) \times \pm 10\mu = \pm 330 \mu V \qquad (6-3)$$

As the two opamps are in the same IC Tl082, it will be assumed that both are affected similarly. All of this will be added to the maximum offset voltage, which is 15 mV for reference voltage and we will neglect the maximum over temperature offset.

Therefore, each experiment will be tested by calculating Offset Voltage ± the temperature coefficient of the input offset voltage (offset is added because it was not found in the PSpice model of TL082). Offset voltage will be assumed always positive for simplicity. Table 6-1 summarizes the initial setup of the experiments and the results will be shown in the next section.

Table 6-1 Validation initial setup cases

Cases	Implementation	Temp (°C)	OFFSET (mV)
A	Jessica and Sprott [168]	-30	15.57
B			14.43
C		27	15
D		60	15.33
E			14.67
F	Proposed 1	-30	15.57
G			14.43
H		27	15
I		60	15.33
J			14.67
K	Proposed 2	-30	15.57
L			14.43
M		27	15
N		60	15.33
O			14.67

6.5.1. Validation Experiments

The validation experiments will compare between the proposed system and Jerk chaotic oscillator, which uses 2 opamps similar to the proposed system. The reason for selecting this implementation is that Jessica and Sprott's implementation used only two opamps and few RC circuits, which is similar to the proposed system from the component selections point of view only, while the concept of the design differs. This makes the comparison clearer regarding power consumption and signal reconstruction between two different concepts for designing analogue chaotic oscillator.

All opamps are TL082 powered by the 5V power supply. The selection of low-power opamps can extend to select another opamp with less power supply. However, for the fair judgement to Jessica and Sprott design, the level of power supply will be the same as mentioned in [168]. The comparison will be based on two categories: Power consumption and Signal reconstruction.

All experiments will be simulated by using ORCAD Cadence PSpice Lite version only (ORCAD Cadence Lite version deals only with few nodes which satisfy the requirements for this comparison). The Power consumption will be calculated based on the power consumed from the supply, i.e. $P_{consumption}=V_{supply}*I_{supply}$ and shown using the watt probe used in the software. The signal reconstruction will be similar to what was done before for the proposed systems. The output sequence of each circuit will be fed to the MATLAB AIC framework to test the performance of the signal reconstruction as mentioned in Chapter 4.

However, this comparison will examine the power consumption and signal reconstruction at three different temperatures (-30°C, 27°C and 60°C). These temperatures cover the minimum, normal and maximum temperature respectively, which can be found beneath the manhole cover.

The simulation of the power consumption and the signal reconstruction will be done for each circuit followed by a comparison of the results of each simulation. Signal reconstruction performance test via Matlab program like the one in Chapter 4 runs as follows:

Jessica and Sprott Implementation
The circuit is prepared as shown in Figure 6-41. Power consumption with a variation of temperature is shown in Table 6-2. For Jessica and Sprott design, signal reconstruction output figures and the average squared error based on Matlab simulation are shown in Tables 6-3 to 6-7.

143
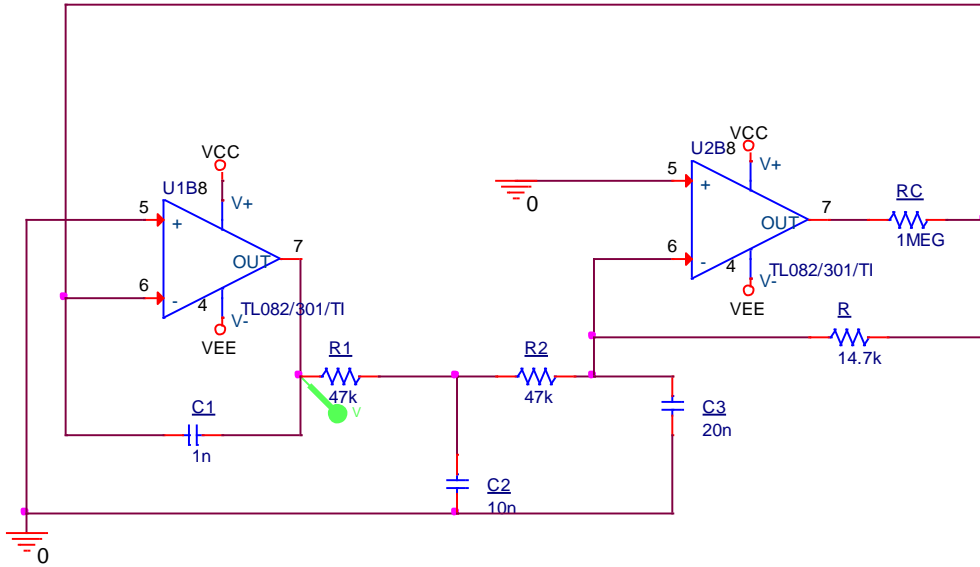
Figure 6-41 Jessica and Sprott Implementation [168]

Table 6-2 Power consumption for Jessica and Sprott design with the variation of temperature

Temperature (Celsius)	-30	27	60
Power Consumption (mWatt)	48.456	48.617	48.618

Case "A"

Table 6-3 Case "A" Signal Reconstruction Matlab Results

Original and reconstructed signal in Frequency domain	Original, Reconstructed and difference signal waveforms	Average squared error
		3.52151E-05

144

Case "B"

Table 6-4 Case "B" Signal Reconstruction Matlab Results

Original and reconstructed signal in Frequency domain	Original, Reconstructed and difference signal waveforms	Average squared error
		2.29676E-05

Case "C"

Table 6-5 Case "C" Signal Reconstruction Matlab Results

Original and reconstructed signal in Frequency domain	Original, Reconstructed and difference signal waveforms	Average squared error
		2.27975E-05

Case "D"

Table 6-6 Case "D" Signal Reconstruction Matlab Results

Original and reconstructed signal in Frequency domain	Original, Reconstructed and difference signal waveforms	Average squared error
		1.29838E-05

145

Case "E"

Table 6-7 Case "E" Signal Reconstruction Matlab Results

Original and reconstructed signal in Frequency domain	Original, Reconstructed and difference signal waveforms	Average squared error
		2.96774E-05

Proposed system 1

As in Jessica and Sprott implementation, the proposed system number one is prepared for thermal analysis as shown in Figure 6-42. Power consumption for the system under the selected temperature is shown in Table 6-8. The results for cases "F", "G", "H", "I" and "J" are shown in Table 6-9 to Table 6-13.
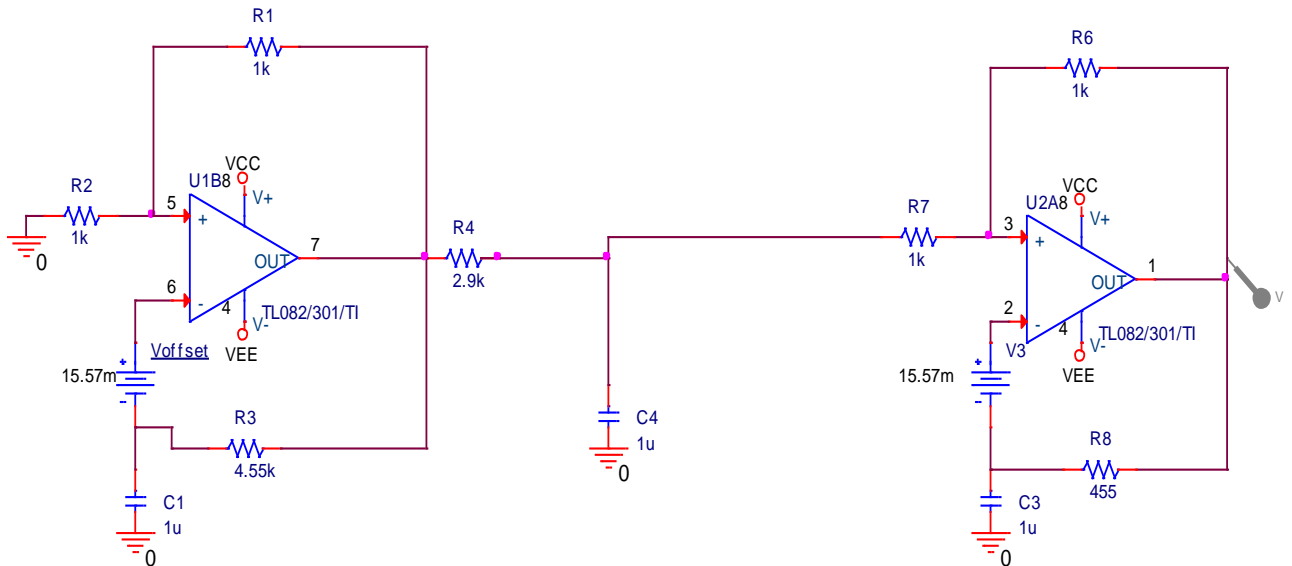
Figure 6-42 Proposed Circuit for system 1

Table 6-8 Power consumption for the Proposed system 1 design with the variation of temperature

Temperature (Celsius)	-30	27	60
Power Consumption (mWatt)	46.725	46.726	46.718

Case "F"

Table 6-9 Case "F" Signal Reconstruction Matlab Results

Original and reconstructed signal in Frequency domain	Original, Reconstructed and difference signal waveforms	Average squared error
		2.96774E-05

Case "G"

Table 6-10 Case "G" Signal Reconstruction Matlab Results

Original and reconstructed signal in Frequency domain	Original, Reconstructed and difference signal waveforms	Average squared error
		1.98607E-05

147

Case "H"

Table 6-11 Case "H" Signal Reconstruction Matlab Results

Original and reconstructed signal in Frequency domain	Original, Reconstructed and difference signal waveforms	Average squared error
		4.36833E-05

Case "I"

Table 6-12 Case "I" Signal Reconstruction Matlab Results

Original and reconstructed signal in Frequency domain	Original, Reconstructed and difference signal waveforms	Average squared error
		3.89123E-05

Case "J"

Table 6-13 Case "J" Signal Reconstruction Matlab Results

Original and reconstructed signal in Frequency domain	Original, Reconstructed and difference signal waveforms	Average squared error
		5.37207E-05

Proposed system 2

Figure 6-43 shows the proposed circuit two prepared for thermal analysis. The power consumption for this design is shown in Table 6-14. The results of the signal reconstruction for cases "K", "L", "M", "N" and "O"are shown in Table 6-15 through to Table 6-19.
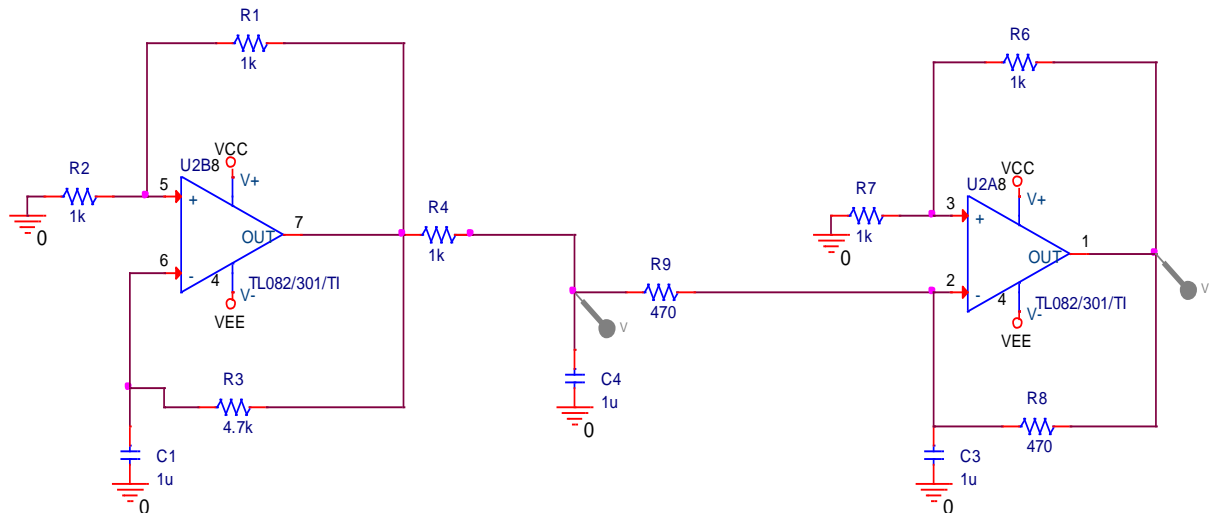
Figure 6-43 Proposed circuit for system 2

Table 6-14 Power consumption for Proposed system 2 with the variation of temperature

Temperature (Celsius)	-30	27	60
Power Consumption (mWatt)	-46.752	-46.740	46.750
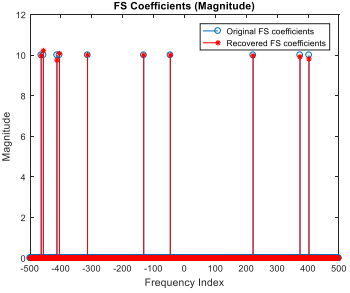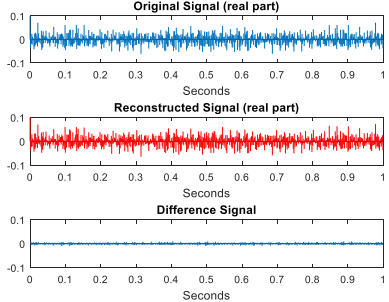
Case "K"

Table 6-15 Case "K" Signal Reconstruction Matlab Results

Original and reconstructed signal in Frequency domain	Original, Reconstructed and difference signal waveforms	Average squared error
		2.96774E-05

149
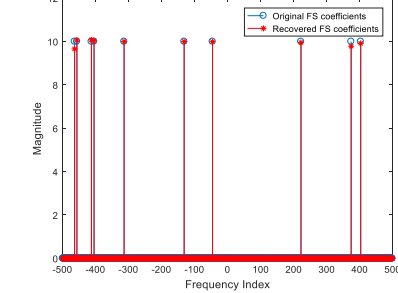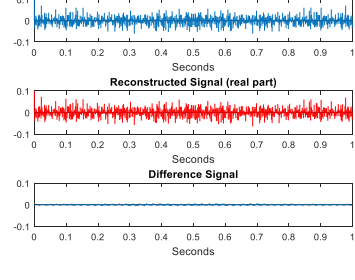
Case "L"

Table 6-16 Case "L" Signal Reconstruction Matlab Results

Original and reconstructed signal in Frequency domain	Original, Reconstructed and difference signal waveforms	Average squared error
		1.22878E-05
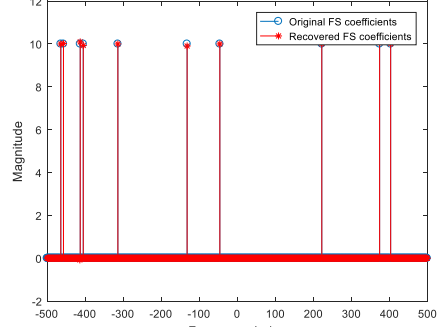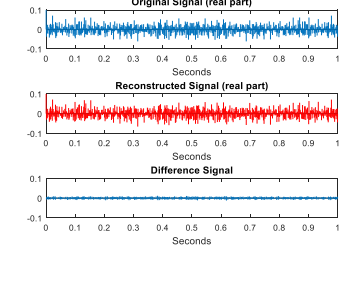
Case "M"

Table 6-17 Case "M" Signal Reconstruction Matlab Results

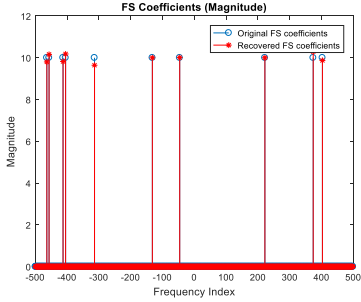| Original and reconstructed signal in Frequency domain	Original, Reconstructed and difference signal waveforms	Average squared error
		0.000007149
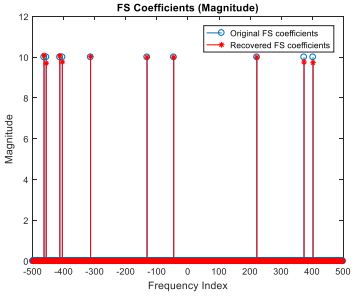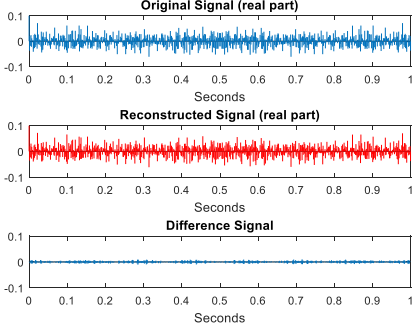
Case "N"

Table 6-18 Case "N" Signal Reconstruction Matlab Results

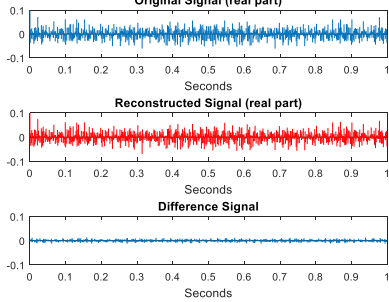| Original and reconstructed signal in Frequency domain	Original, Reconstructed and difference signal waveforms	Average squared error
		2.24216E-05

Case "O"

Table 6-19 Case "O" Signal Reconstruction Matlab Results

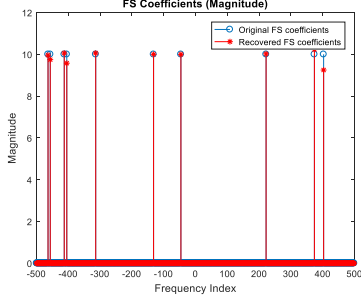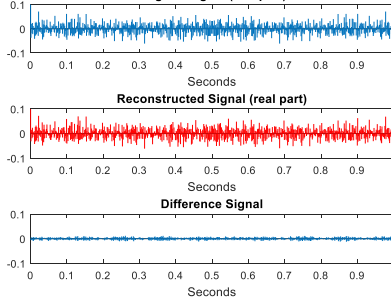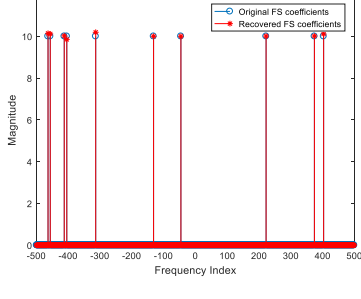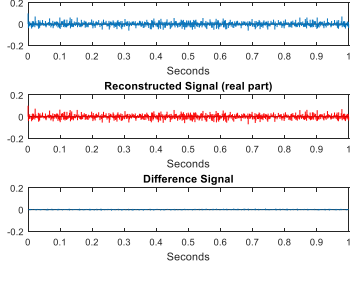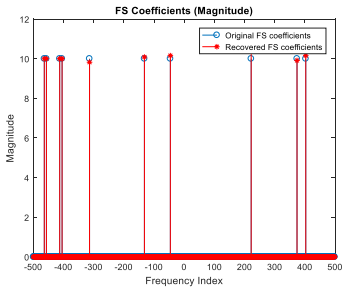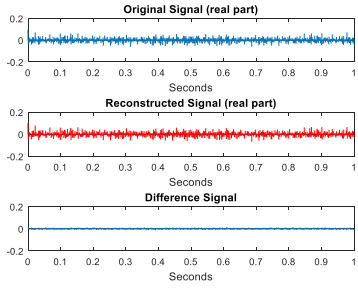| Original and reconstructed signal in Frequency domain	Original, Reconstructed and difference signal waveforms	Average squared error
		1.34669E-05

6.5.2. Analysis of the Results and discussion

Power Consumption

Figure 6-44 shows the power consumption of the three circuits. The proposed systems consume less power than Jessica and Sprott implementation by about 2 mW as shown in Figure 6-44. The difference in power consumption between Jessica and Sprott from one side and the proposed system on the other side is shown in Figure 6-45.

While it seems too small as a difference, in applications like in monitoring manhole cover which lifetime is about 25 years, this difference extends the lifetime to about one year as shown in Figure 6-46. Figure 6-46 shows estimated 5V Lithium-Ion battery lifetime, which is recommended in several references to use in underground monitoring systems.

The difference in Figure 6-46 shows about the one-year difference between Jessica et al's implementation and the proposed systems, which is very effective from the economic point of view for such applications. The calculations of Lithium-Ion battery lifetime estimations are done by using the results of the experiments and the parameters of the battery data sheet, and fed to DIGIKEY online battery lifetime calculator [191].

It must be considered that most of the power consumption for the three circuits is based on the selection of the opamps and the complexity and the values of the RC circuit. The results can be enhanced from the circuit design point of view by using ultra low opamp design, which is out of the scope of this thesis. However, as the three circuits are using the same opamp IC, the proposed systems enhance the power consumption and battery lifetime of the system.
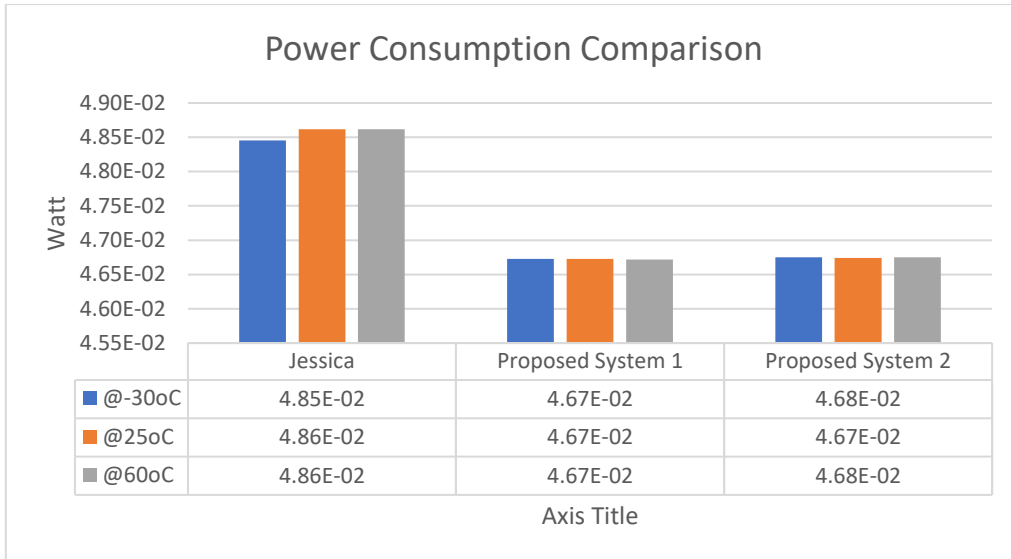
Figure 6-44 Power Consumption Comparison
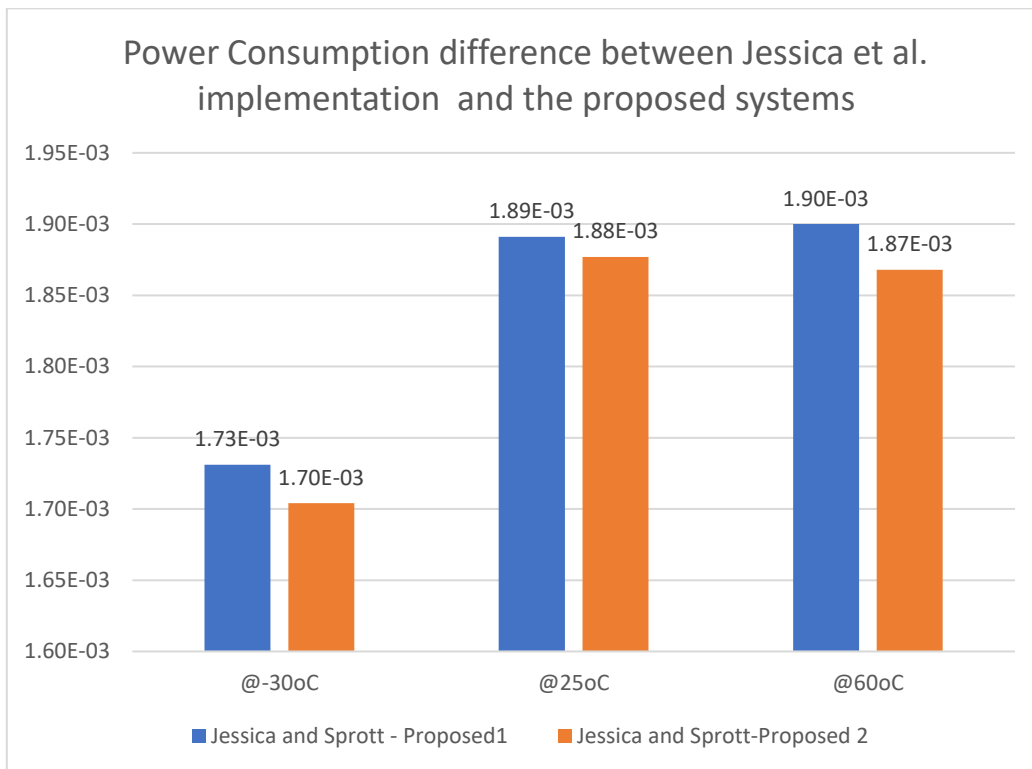
Figure 6-45 Power Consumption difference between Jessica et al. implementation and the proposed systems
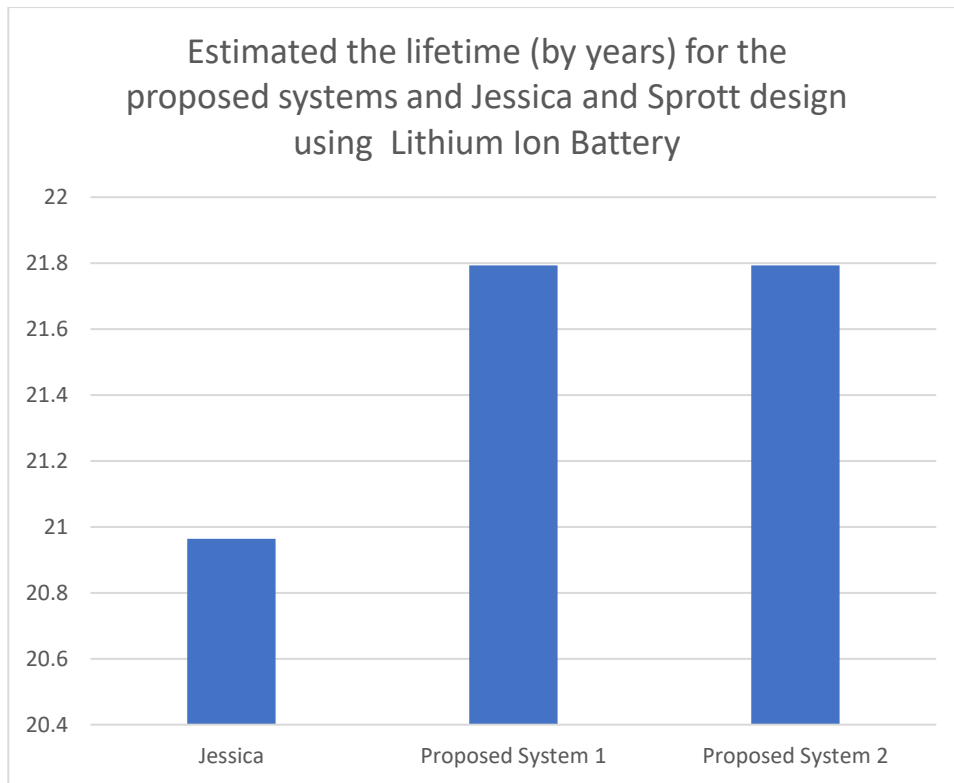
Figure 6-46 Estimated lifetime for the proposed systems and Jessica and Sprott design Lithium-Ion Battery

Signal Reconstruction

Figure 6-47 shows all the average square error for each case. The proposed system 1 shows less performance in reconstructing the original signal in comparison to the other two circuits at room temperature (27°C) and high temperature. However, at low temperature, it has good performance more than Jessica et al's implementation.

The second proposed system has good performance in all temperature variations in comparison with the other circuits. This can be understood because the coupling directly affects the capacitance of the second oscillator which is the main element to vary the output because of charging and discharging.

Figure 6-48 shows all the average square error for each case in the presence of the noise. The figure shows that the proposed system 2 can reconstruct the signal in the presence of noise more than the other systems. The proposed system 1 has acceptable results but less performance from the other two systems. Jessica and Sprott's design had good performance in only one case. Still, the proposed system 2 shows good performance in the absence and the presence of noise.

On the other hand, if the chaotic sequence generated from analogue chaotic oscillators used in this test is compared to the PRNG sequence generated from a software algorithm used by the Matlab AIC framework, it is found that the analogue chaotic oscillators show good performance of reconstructing the original signal in the presence of noise as shown in Figure

153

6-49. It is shown from Figure 6-49, that the proposed system 1 improves the signal reconstruction by 6.94% while the second proposed system improves the signal reconstruction by 17.831%. This point is very important from the security point of view.

To conclude, this section validates the proposed system by making a comparison between the proposed systems and one of the Jerk analogue chaotic oscillators from the power consumption and the signal reconstruction point of view. The proposed systems and the Jerk chaotic oscillators are tested using off the shelf components and the results fed to Matlab for AIC framework. The results show the improvement done by using the proposed systems in both power consumption and signal reconstruction. Because the test used the off-shelf components to mimic biological oscillators, it is expected to develop for the open source hardware based on neuroscience [192], [193] to overcome the power consumption issue.
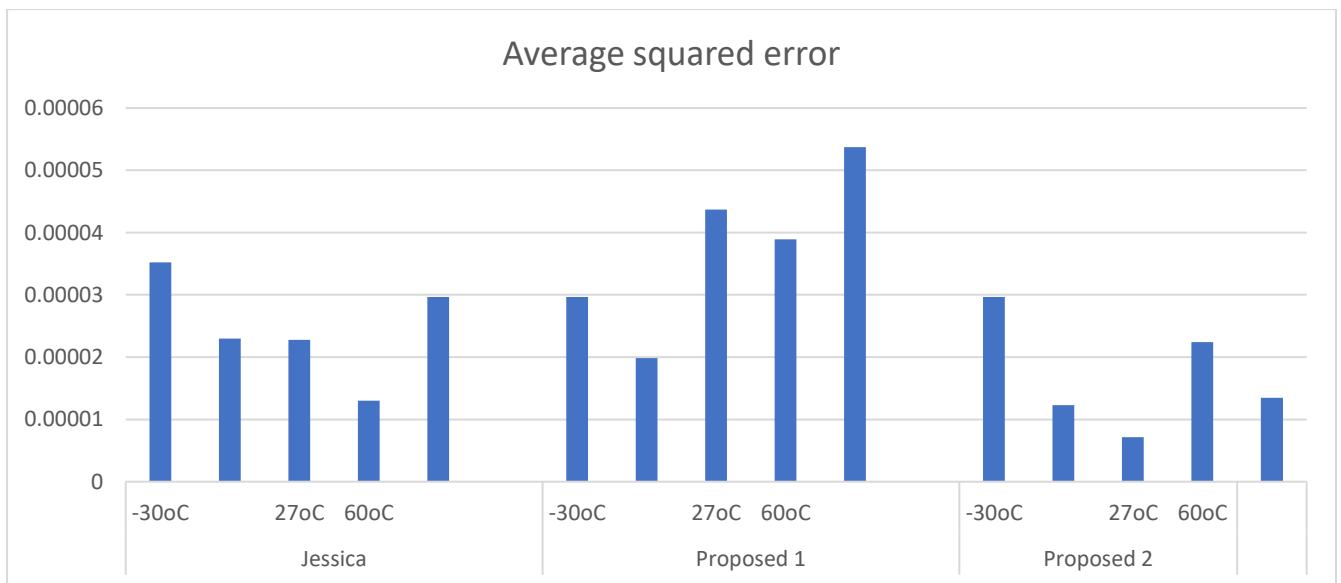
Figure 6-47 Average square error for all the cases mentioned in Table 6-1
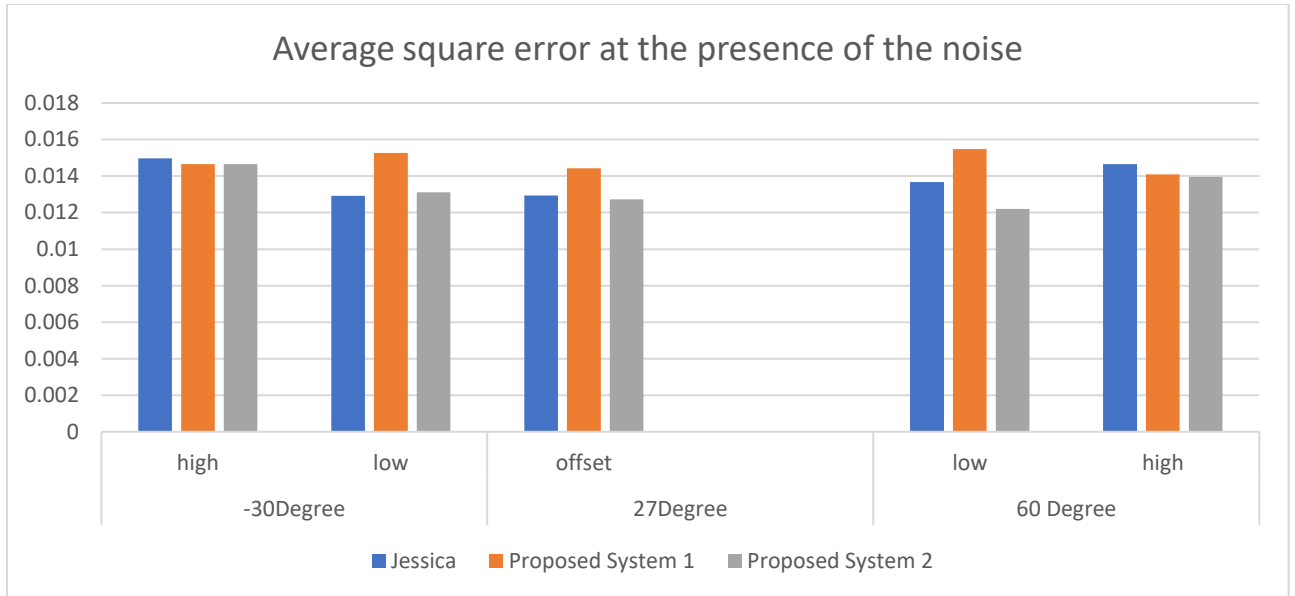
Figure 6-48 Average square error for all the cases mentioned in Table 6-1 in the presence of the noise
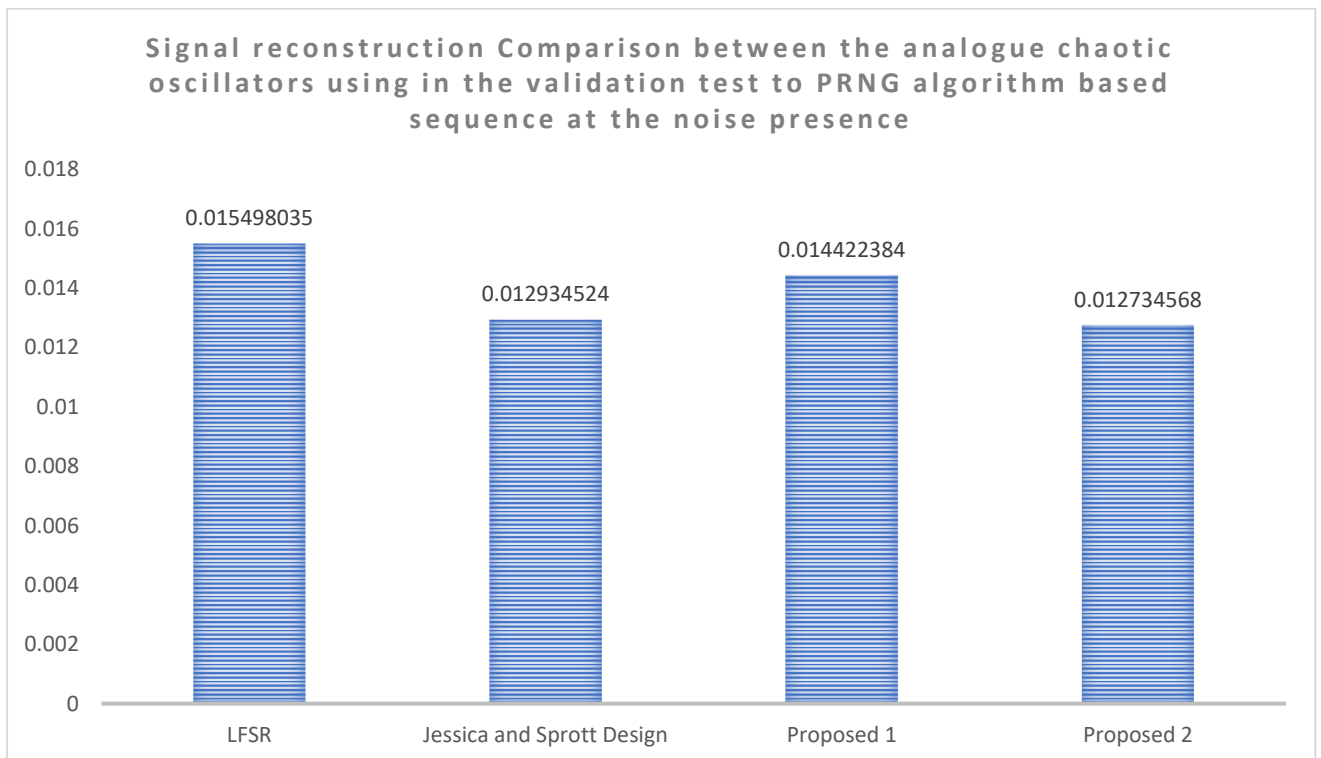
Figure 6-49 Signal reconstruction Comparison between the analogue chaotic oscillators using in the validation test to PRNG algorithm-based sequence in the presence of noise.

6.6. Conclusion

In this chapter, two low-power, secured systems have been proposed and presented based on coupling oscillator. The heart of the proposed systems are the modifications of the astable opamp Schmitt trigger oscillator presented in Chapter 5.

155

The proposed systems are designed based on the waveshaping technique presented in Chapter 5. Both systems show good performance from the power consumption and the signal reconstruction perspective in the absence and the presence of noise.

In comparing the proposed systems to the similar Jerk chaotic oscillators using two opamps based chaotic oscillator, the proposed systems have less power consumption, which makes their lifetime extend almost one year for long lifetime applications like monitoring manhole cover. The validation test takes place based on the range of temperatures found beneath the manhole cover.

Moreover, the proposed systems, (especially the proposed system 2) have a good performance of signal reconstruction in the presence of noise. In comparison to the PRNG output sequence from a software algorithm, the first proposed system improves the signal reconstruction by 6.094 % while the second system improves the signal reconstruction by 17.83%.

On the other hand, as the Schmitt trigger is one of the main blocks of FPAA, the proposed systems can be programmed which gives the advantage of the design to generate several chaotic sequences that can enhance the security of IoT devices.

Several advantages are found in the proposed systems:

1- Low-power consumption in comparison with another concept of designing analogue chaotic oscillator.

2- The ease of the design without the need of using intensive mathematical calculations.

3- The two proposed systems can be found together at the same time in one monitoring system with only two opamps and without any need to extend the size of PCB. This advantage is very important from several points of view:

    a. Circuit design: any size extension for PCB is not preferable for the IoT device design that may add more cost to the product.

    b. Security: Using two different analogue chaotic systems in the same system results in two different sequences of the bits, which adds more security to the data. Both systems show the improvement of signal reconstruction in the presence of the noise.

    c. FPAA design: As an FPAA design is based on the switched capacitor concept, this means that by using one electronic switch and changing the frequency of some switched capacitor, which can be easily programmed by FPAA, two chaotic oscillators can be designed.

d. Open source hardware: Because the proposed systems use the off the shelf components, it is expected to open a new route to design the open source hardware which suffers from high power consumption. This point is very attractive as open source hardware based on neuromorphic engineering is still in its early stage.

Based on the study in this chapter and the previous chapter, coupling oscillators can be designed using two oscillators with three main conditions:

1- One of these oscillators needs to have less amplitude and less frequency in comparison to the other oscillator

2- The output of the second oscillator (with higher amplitude and higher frequency) needs to be affected by the coupling. This means that the output of the second oscillator is relying on its input behaviour.

3- Based on the chaotic oscillators design, at least three energy storage elements have to be found in the design.

Finally, the design used simulation and hardware by means of OrCAD PSpice and Texas instrument analogue toolkit respectively. The PSpice helps to simulate the design in a normal situation and in harsh thermal effect. The hardware toolkit helps to set up the hardware in short time to design a benchmark.

Chapter 7
Conclusion and Future work

7. CONCLUSIONS AND FUTURE WORK

7.1. Conclusions

The main aim in this research is to investigate and design a low-power IoT -based manhole cover (MC) monitoring system to be used for smart city applications taking into consideration the IoT device design requirements and challenges. To reach this aim and based on investigation done by this research, compressive sensing was studied as it was proved from other applications its ability to reduce the power consumption for IoT device by reducing the sampling rate of the used ADC.

As a first step in this research, MC types and issues have been investigated deeply. Based on this investigation, a new detailed classification of manhole cover issues with the current monitoring systems is proposed. This classification presents good guidance for the modern governments to identify the main requirements to improve the safety and the security for their societies. Also, this classification gives a new vision for the researchers who work in the smart city's underground and road monitoring applications. It was concluded from this classification and investigation that analogue to digital converter (ADC) found in DAQ module is the main source for consuming power for the MC automated monitoring system. In this research, a low power automated MC monitoring system with IoT device design requirements was the target to be suitable for Smart City's application.

Compressive sensing framework proved in several applications its ability to reduce the power consumption for monitoring systems by using low sampling rate ADC. The CS based ADC is named analogue to information converter (AIC). The AIC has become more attractive to the IoT device designers because the heart of the AIC is a pseudorandom number generator (PRNG) which can be used for the data security.

However, most of the current PRNG circuit found in the AIC circuit design is implemented by digital circuit which has drawbacks which are: a) power consumption, b) using the digital PRNG at AIC analogue frontend mainly required isolation between the analogue part and the digital part by using separate power supplies and separate grounds. The present research focused on using an analogue PRNG to overcome the digital PRNG issues for AIC.

In this research, two analogue chaotic oscillators are proposed by using one of the main blocks of the FPAA (FPAA proved its ability to implement CS signal reconstruction algorithms with low-power consumption) which is the opamp Schmitt trigger. The heart of the two

proposed systems is two new modifications of the opamp Schmitt trigger to mimic biological oscillators.

The proposed systems are based on coupling oscillators, which are inspired by the neuroscience field. While this research is not the first research which studies the coupling oscillator, but it is the first that introduces the waveshaping technique to design coupling chaotic oscillator without the need of using differential equations for modelling. This point opens a new route for designing chaotic oscillators based on relaxation oscillators.

Furthermore, the proposed systems can both be implemented on the same PCB using only 2 opamps with switches to act as selectors for the RC coupling network and the connected nodes. This point is very attractive which gives the proposed system the richness to design secured DAQ module with two or more different chaotic sequence with low-power consumption. Furthermore, this type of connection is very suitable for the FPAA design, which is based on a switching capacitor design concept.

The two proposed systems have been introduced and studied from the power consumption and signal recovery points of view at the range of the temperatures found beneath the manhole cover (-30°, 25°C 60°). The two proposed systems show a good performance from a power consumption point of view as they can be used for at least 21.8 years using the Li-Ion battery. This achievement is suitable for monitoring manhole cover structure that has a lifetime which can reach up to 25 years, while the current automated MC monitoring systems have a lifetime of maximum 3-5 years.

From the signal reconstruction point of view, the proposed systems show good performance of the signal recovery which can reach 0.00000179 average square error in the absence of noise. In the presence of noise and by comparing the proposed systems to PRNG sequence generated from the algorithm and fitted to the AIC, the proposed system 1 improves the signal reconstruction by 6.094 % and the proposed system 2 improves the signal reconstruction by 17.831%. This achievement is very significant from a security point of view, as it is shown before that signal reconstructing in the presence of noise is used to assess communication system security.

Finally, the research used off the shelf components which is very interesting in the IoT device design based on open source hardware which mainly suffers from the high-power consumption issue. The merging between the open source hardware and the neuroscience is still in the early steps, which makes this research helpful in the development in such applications. It is expected that this research develops several smart city's applications like underground and road monitoring.

7.2. Future work

1- Full implementation of the system and attaching it to manhole cover with testing is one of the main future work targets.

2- The effect of the opamps internal circuit with different technologies and design on the proposed systems opens a new route for more improvement of the system, especially from the power consumption point of view.

3- Studying the same design concept in radio frequency (RF) range to reduce the power consumption of the communication module for the IoT device design.

4- Using diodes in the coupling of the proposed systems will be studied to investigate their effects on the performance of the proposed systems.

8. REFERENCES

[1]   G. Hancke, B. Silva, and J. G. Hancke, "The Role of Advanced Sensing in Smart Cities,"
        Sensors, vol. 13, no. 1, pp. 393–425, 2012.

[2]   H. H. Aly, Abdel Hamid Soliman, and Mansour Mouniri. "Towards a fully automated
        monitoring system for Manhole Cover: Smart cities and IOT applications." 2015 IEEE First
        International Smart Cities Conference (ISC2). IEEE, 2015.

[3]   J. B. Hughes, *Manhole Inspection and Rehabilitation*. American Society of Civil Engineers,
        2009.

[4]   B. Rumberg, "Sensor Interface Analog Processing Improves Battery Life and Sensor
        Intelligence In the IoT Quick Links Home Browse by Topic Twitter Feed Find It Fix It
        Forum," 2016. [Online]. Available: http://www.sensorsmag.com/sensor-interface/analog-
        processing-improves-battery-life-and-sensor-21294

[5]   Becker, Stephen R. Practical compressed sensing: modern data acquisition and signal
        processing. Diss. California Institute of Technology, 2011.

[6]   Šalamon, Matej. "Chaotic electronic circuits in cryptography." Applied cryptography and
        network security. IntechOpen, 2012.

[7]   MotorcycleActionGroup, "Fill It In Manhole Cover," 2012. [Online]. Available: http://fill-it-
        in.mag-uk.org/fill_it_in_manhole_cover_.html.

[8]   Department of Traffic. (2013,Nov), Reported Road Casualties in Great Britain: Quarterly
        Provisional Estimates Q2 2013, Government of United Kingdom. Available:
        https://assets.publishing.service.gov.uk/government/uploads/system/uploads/attachment_data/f
        ile/255125/road-accidents-and-safety-quarterly-estimates-q2-2013.pdf

[9]   University College London, "Metal Theft- Crime Over View," 2010. [Online]. Available:
        http://www.ucl.ac.uk/jdibrief/crime/metal-theft. [Accessed: 05-Jan-2013]

[10]   W. NEWS, "Manhole covers a problem, says report," Water Industry Contractor, vol. 19, no. 2,
        p. 16, Feb-2013

[11]   P.Saint-G. P. U. Thompson, "From price to cost - LocalGov," 2011. [Online]. Available:
        http://www.localgov.co.uk/From-price-to-cost/24942. [Accessed: 01-Jan-2014].

[12]   G. Quist and D. Drake, "Development and Deployment of a Real-Time Remote Continuous
        Monitoring System for Manholes," *Proc. Water Environ. Fed.*, pp. 3090–3102, 2006

[13]   J. Pasquet, T. Desert, O. Bartoli, M. Chaumont, and C. Delenne, "Detection of manhole covers

in high-resolution aerial images of urban areas by combining two methods," no. 2, pp. 2–5, 2015.

[14]   United States Environmental Protection Agency, "Manhole Intrsuion Sensors," 2005. [Online].
        Available: www.epa.gov/cgi-bin/epaprintonly.cgi. [Accessed: 01-Feb-2013]

[15]   Chang, Allen Y., et al. "Search, identification and positioning of the underground manhole with
        RFID ground tag." 2009 Fifth International Joint Conference on INC, IMS and IDC. IEEE, 2009.

[16]   Eriksson, Jakob, et al. "The pothole patrol: using a mobile sensor network for road surface
        monitoring." Proceedings of the 6th international conference on Mobile systems, applications,
        and services. ACM, 2008.

[17]   Shunping, Ji, Shi Yun, and Shi Zhongchao. "Manhole cover detection using vehicle-based multi-
        sensor data." International Archives of the Photogrammetry, Remote Sensing and Spatial
        Information Sciences 39 (2012): B3.

[18]   Katz, Allen, Fadi Karaa, and Edip Niver. Innovative and effective techniques for locating
        underground conduits. No. FHWA-NJ-2011-001. New Jersey Institute of Technology, 2011.

[19]   Y. Yu, H. Guan, and Z. Ji, "Automated Detection of Urban Road Manhole Covers Using Mobile
        Laser Scanning Data," IEEE Transactions on Intelligent Transportation Systems, vol. 16, no. 6,
        pp. 3258–3269, 2015.

[20]   ConEdison, "Secondary System Analysis - 2005 Stray Voltage Detection and Electric Facility
        Inspection Report," 2005. [Online]. Available: http://www.coned.com/publicissues/PDF/2008
        Testing and Inspection Programs Final.pdf. [Accessed: 01-Feb-2014]

[21]   IEEE Working Group on Voltages at Publicly and Privately Accessible Locations, "Working
        Definitions," pp. 1–2, 2013.

[22]   Siemens Power Transmission & Distribution, (2005, Dec.) Independent Assessment of
        Dislodged   Manhole   Covers   [Online].   Available:
        https://core.ac.uk/download/pdf/146674107.pdf

[23]   U.S. Environmental Protection Agency (EPA), (2012,May)CSO Post Construction Comliance
        Monitoring Guidance, [Online]. Available: https://www.epa.gov/sites/production/files/2015-
        10/documents/final_cso_pccm_guidance.pdf .

[24]   M. Purton, News Shopper (2011,April,10th), "Noisy manhole cover making woman's life 'a
        living   hell'   (From)," 2011.   [Online].   Available:
        http://www.newsshopper.co.uk/news/8965486.Noisy_manhole_cover_making_woman_s_life_
        _a_living_hell_/. [Accessed: 01-Jan-2014].

[25]   Trip Advisor, "Hesperia Bristol Playa Photo : manhole cover broken," [Online]. Available:

https://www.tripadvisor.com/LocationPhotoDirectLink-g580322-d577754-i35874205-Hesperia_Bristol_Playa-Corralejo_La_Oliva_Fuerteventura_Canary_Islands.html.

[26] D. Gaster, "Odor control," 2011. [Online]. Available: http://www.ncrwa.com/External/WCPages/WCWebContent/WebContentPage.aspx?ContentID=105.

[27] Hasan, Basim O. "Effect of salt content on the corrosion rate of steel pipe in turbulently flowing solutions." Al-Nahrain Journal for Engineering Sciences 13.1 (2010): 66-73..

[28] J. B. Hughes, Manhole Inspection and Rehabilitation. American Society of Civil Engineers, 2009.

[29] National Association of Sewer Service Companies (NASSCO), Specification for Sewer Manhole Sealing. Maryland:, 2012. [Online]. Available: https://www.nassco.org/sites/default/files/manhole-avanti.pdf.

[30] Metje, Nicole, et al. "Real time condition monitoring of buried water pipes." Tunnelling and Underground Space Technology 28 (2012): 315-320.

[31] Jung, Deokwoo, Thiago Teixeira, and Andreas Savvides. "Sensor node lifetime analysis: Models and tools." ACM Transactions on Sensor Networks (TOSN) 5.1 (2009): 3.

[32] Alippi, C., et al. "An Adaptive Sampling Algorithm for Effective Energy Management in Wireless Sensor Networks With Energy-Hungry Sensors." IEEE Transactions on Instrumentation and Measurement, vol. 59, no. 2, 2010, pp. 335–344., doi:10.1109/tim.2009.2023818..

[33] H. Kori, I. Z. Kiss, S. Jain, and J. L. Hudson, "Partial synchronization of relaxation oscillators with repulsive coupling in autocatalytic integrate-and-fire model and electrochemical experiments," Chaos: An Interdisciplinary Journal of Nonlinear Science, vol. 28, no. 4, p. 045111, 2018..

[34] L. S. Memory, H. An, M. S. Al-mamun, M. K. Orlowski, and Y. Yi, "Learning Accuracy Analysis of Memristor-based Nonlinear Computing Module on Long Short-term Memory.," Proc. Int. Conf. Neuromorphic Syst. ACM, 2018.

[35] V. Calayir, M. Darwish, J. Weldon, and L. Pileggi, "Analog Neuromorphic Computing Enabled by Multi-Gate Programmable Resistive Devices," Design, Automation & Test in Europe Conference & Exhibition (DATE), 2015, 2015.

[36] E. Murphy, "Implications of Travelling Weakly Coupled Oscillators for the Cortical Language Circuit" University College London (UCL) ,2017, [Online]. Available:

https://www.ucl.ac.uk/pals/sites/pals/files/murphy_2017_implications_of_travellin_weakly_coupled_oscillators_for_the_cortical_language_circuit.pdf

[37] A. N. Pisarchik, R. Jaimes-Reátegui, and M. A. García-Vellisca, "Asymmetry in electrical coupling between neurons alters multistable firing behavior," Chaos: An Interdisciplinary Journal of Nonlinear Science, vol. 28, no. 3, p. 033605, 2018.

[38] W. Brickner and M. S. Ullah, "Use of a Hysteresis Loop Activation Function to Enable an Analog Perceptron to Gain Memory," Sci. J. Circuits, Syst. Signal Process., vol. 7, no. 2, pp. 68–73, 2018.

[39] S. Olmi, A. Politi, and A. Torcini, "Chimera states and collective chaos in pulse-coupled neural networks," BMC Neuroscience, vol. 12, no. S1, 2011.

[40] D. Vodenicarevic, N. Locatelli, F. A. Araujo, J. Grollier, and D. Querlioz, "A Nanotechnology-Ready Computing Scheme based on a Weakly Coupled Oscillator Network," Scientific Reports, vol. 7, no. 1, 2017.

[41] B. K. Bera, S. Majhi, and D. Ghosh, "Chimera states : Effects of different coupling topologies," vol. 118, no. April, pp. 1–7, 2017.

[42] M. A. Glover, "An Analogue VLSI Implementation of an Integrate-and-Fire Neural Network for Real-Time Auditory Data Processing," The University of Edinburgh, 1999.

[43] K. Xu, J. P. Maidana, S. Castro, and P. Orio, "Synchronization transition in neuronal networks composed of chaotic or non-chaotic oscillators," Scientific Reports, vol. 8, no. 1, 2018.

[44] A. N. Pisarchik and F. Pozo-guerrero, "Bistability in hindmarsh-rose neural oscillators induced by asymmetric electrical coupling," Cybernetics and Physics, vol. 6, no. 3, 2017.

[45] J. Ma, P. Zhou, B. Ahmad, G. Ren, and C. Wang, "Chaos and multi-scroll attractors in RCL-shunted junction coupled Jerk circuit connected by memristor," Plos One, vol. 13, no. 1, 2018..

[46] R. Miru and R. M. George, Structural plasticity in neuromorphic systems Structural Plasticity in Neuromorphic Systems. Disser. Universität Zürich, 2018.

[47] C. D. Schuman et al., "A Survey of Neuromorphic Computing and Neural Networks in Hardware," arXiv:1705.06963v1, pp. 1–88, 2018.

[48] S. A. Gerasimova, A. N. Mikhaylov, A. I. Belov, D. S. Korolev, O. N. Gorshkov, and V. B. Kazantsev, "Simulation of Synaptic Coupling of Neuron-Like Generators via a Memristive Device," vol. 62, no. 8, pp. 1259–1265, 2017.

[49] N. Rakesh and J. S. John, "A Amenable Neuromorphic Integrated Circuit Tolerates Device

Mismatch Was Implemented in Cadence 45 nm Technology," Int. J. Adv. Res. Electron. Commun. Eng., vol. 6, no. 8, pp. 891–900, 2017.

[50]   O. Kavehei, Memristive Devices and Circuits for Computing , Memory , and Neuromorphic Applications. Diss. University of Adelaide, 2011.

[51]   D. P. Bueno, Coupled oscillators : chaotic synchronization , high-dimensional chaos and wavefronts in bistable media. Diss. University of Santiago de Compostela, Spain, 2003.

[52]   O. Krestinskaya, S. Member, A. James, S. Member, and L. O. Chua, "Neuro-memristive Circuits for Edge Computing : A Review," arXiv:1807.00962v2., pp. 1–20, 2018.

[53]   A. Basu, J. Acharya, and T. Karnik, "Low-Power , Adaptive Neuromorphic Systems : Recent Progress and Future Directions," IEEE J. Emerg. Sel. Top. Circuits Syst., vol. 8, no. 1, pp. 6–27, 2018.

[54]   W. Singer, "Neuronal oscillations: Unavoidable and useful?," Eur. J. Neurosci., no. October 47(8), pp. 0–2, 2018.

[55]   G. Andreas, B. Andreas, "Neuromorphic Computing", Physics Institute Heidelberg, Universität Heidelberg   2017.   [Online].   Available: https://www.physi.uni-heidelberg.de/Einrichtungen/FP/anleitungen/F09.pdf

[56]   M. A. Edelman, E. E. N. Macau, and Sanjuán Miguel A. F., Chaotic, fractional, and complex dynamics: new insights and perspectives. Cham: Springer, 2018..

[57]   F. D. Broccard, S. Joshi, J. Wang, and G. Cauwenberghs, "Neuromorphic neural interfaces : from neurophysiological inspiration to biohybrid coupling with nervous systems," J. Neural Eng., vol. 2, no. 14, 2017.

[58]   V. Saxena, X. Wu, I. Srivastava, and K. Zhu, "Towards Neuromorphic Learning Machines using Emerging Memory Devices with Brain-like Energy Efficiency," J. Low Power Electron. Appl., no. July, pp. 1–17, 2018.

[59]   A. Panchuk, D. P. Rosin, P. Hövel, and E. Schöll, "Synchronization Of Coupled Neural Oscillators With Heterogeneous Delays," International Journal of Bifurcation and Chaos, vol. 23, no. 12, p. 1330039, 2013.

[60]   C. V. D. Malsburg and J. Buhmann, "Sensory segmentation with coupled neural oscillators," Biological Cybernetics, vol. 67, no. 3, pp. 233–242, 1992.

[61]   V. Saxena, X. Wu, I. Srivastava, and K. Zhu, "Towards Neuromorphic Learning Machines using Emerging Memory Devices with Brain-like Energy Efficiency," 2018

[62] D. Vodenicarevic, N. Locatelli, and D. Querlioz, "A neural network based on synchronized pairs of nano-oscillators," 2017 IEEE 17th International Conference on Nanotechnology (IEEE-NANO), 2017.

[63] T. S. Mak, K. Lam, H. Ng, G. Rachmuth, and C.-S. Poon, "A Current-Mode Analog Circuit for Reinforcement Learning Problems," 2007 IEEE International Symposium on Circuits and Systems, 2007.

[64] B. Moradi and A. Mirzaei, "A New Automated Design Method Based on Machine Learning for CMOS Analog Circuits," Int. J. Electron., vol. 103, no. 11, pp. 1868–1881, 2016.

[65] S. Yoon, Wireless Signal Networks: A Proof of Concept for Subsurface Characterization and A System Design with Reconfigurable Radio. Diss. Lehigh University. 2013.

[66] Guoliang Ye, Jize Yan, Zi Jing Wong, K. Soga and A. Seshia, "Optimisation of a piezoelectric system for energy harvesting from traffic vibrations," 2009 IEEE International Ultrasonics Symposium, Rome, 2009, pp. 759-762..

[67] R. G. Baraniuk, "Compressive Sensing [Lecture Notes]," in IEEE Signal Processing Magazine, vol. 24, no. 4, pp. 118-121, July 2007..

[68] A. Sadeghioon, N. Metje, D. Chapman, and C. Anthony, "SmartPipes: Smart Wireless Sensor Networks for Leak Detection in Water Pipelines," J. Sens. Actuator Networks, vol. 3, no. 1, pp. 64–78, 2014.

[69] M. Noureddine and R. Bashroush, "A provisioning model towards OAuth 2.0 performance optimization," 2011 IEEE 10th International Conference on Cybernetic Intelligent Systems (CIS), 2011.

[70] R. Fisher, L. Ledwaba, G. Hancke, and C. Kruger, "Open Hardware: A Role to Play in Wireless Sensor Networks?," Sensors, vol. 15, no. 3, pp. 6818–6844, 2015.

[71] C. Amarawardhana, K. S. Dayananada, H. Porawagama, and C. Gamage, "Case study of WSN as a replacement for SCADA," ICIIS 2009 - 4th Int. Conf. Ind. Inf. Syst. 2009, Conf. Proc., no. December, pp. 49–54, 2009.

[72] A. Nechibvute and C. Mudzingwa, "Wireless Sensor Networks for SCADA and Industrial Control Systems," vol. 3, no. 12, 2013.

[73] U. S. Patil, "Study of Wireless Sensor Network in SCADA System for Power Plant," Ad Hoc Networks, vol. 9738, no. 2248, pp. 41–44, 2011.

[74] D. E. Ott, "IoT Security through the Lens of Energy Efficiency: Energy as a First-Order Security Consideration," Proc. - 2016 Cybersecurity Symp. CYBERSEC 2016, pp. 20–25, 2017.

[75]   S. Ray, T. Hoque, A. Basak, and S. Bhunia, "The power play: Security-energy trade-offs in the IoT regime," 2016 IEEE 34th International Conference on Computer Design (ICCD), 2016.

[76]   C. Profentzas, "Verified Boot in IoT Devices with Low Power Consumption." Proceedings of the IDEA League Doctoral School on Transiently Powered Computing, p. 14-15 .2017. [Online]. Available: http://publications.lib.chalmers.se/records/fulltext/254585/local_254585.pdf

[77]   M. Suárez-Albela, T. M. Fernández-Caramés, P. Fraga-Lamas, and L. Castedo, "A practical evaluation of a high-security energy-efficient gateway for IoT fog computing applications," Sensors (Switzerland), vol. 17, no. 9, pp. 1–39, 2017.

[78]   C.-W. Hung and W.-T. Hsu, "Power Consumption and Calculation Requirement Analysis of AES for WSN IoT," Sensors, vol. 18, no. 6, p. 1675, 2018.

[79]   J. Yuan, J. Lin, Q. Alasad, and S. Taheri, "Ultra-Low-Power Design and Hardware Security Using Emerging Technologies for Internet of Things," Electronics, vol. 6, no. 3, p. 67, 2017.

[80]   M. H. Padgavankar and S. R. Gupta, "Big Data Storage and Challenges," vol. 5, no. 2, pp. 2218–2223, 2014.

[81]   Montestruque, Luis, M. Lemmon, and L. L. C. EmNet. "Csonet: a metropolitan scale wireless sensor-actuator network." International Workshop on Mobile Device and Urban Sensing (MODUS). 2008..

[82]   Quist, Gregory & A Drake, David & H Hobbs, Justin. (2010). Knowledge is Power -Using Remote Monitoring to Optimize Operations. Proceedings of the Water Environment Federation. 2010..

[83]   S. W. Monitoring and A. T. Wireless, "SeWatch: Wastewater and Sewage Wireless Monitoring and Control System," 2002. [Online]. Available: www.tlmw.com.

[84]   L. Montestruque, M. D. Lemmon, and L. EmNet, "Csonet: a metropolitan scale wireless sensor-actuator network," in International Workshop on Mobile Device and Urban Sensing (MODUS), 2008.

[85]   H. Le, Design and implementation of a reconfigurable data acquisition integrated circuit. Diss. University of Australia. 2005.

[86]   B. Rumberg, "Analog Processing Improves Battery Life and Sensor Intelligence In the IoT _ Sensors," 2016. [Online]. Available: http://www.sensorsmag.com/sensor-interface/analog-processing-improves-battery-life-and-sensor-21294. [Accessed: 11-Feb-2016].

[87]   H. F. Zhou, L. Huang, and J. Li, "Compressive sampling for spectrally sparse signal recovery

via one-bit random demodulator," Digit. Signal Process. A Rev. J., vol. 81, pp. 1–7, 2018.

[88]   D. Donoho, A. Maleki, and A. Montanari, "How to design message passing algorithms for compressed sensing," Department of Electrical Engineering, Stanford University 2010. [Online]. Available: https://www.ece.rice.edu/~mam15/bpist.pdf

[89]   Y. Kabashima and T. Wadayama, "A signal recovery algorithm for sparse matrix based compressed sensing," arXiv1102.3220, pp. 0–4, 2011.

[90]   Y. Eldar, "Compressed Sensing of Analog Signals in Shift-Invariant Spaces," IEEE Transactions on Signal Processing, vol. 57, no. 8, pp. 2986–2997, 2009..

[91]   Y. C. Eldar and G. Kutyniok, Eds., Compressed Sensing: Theory and Applications. Cambridge: Cambridge University Press, 2012.

[92]   E. J. Candes and M. B. Wakin, "An Introduction To Compressive Sampling," in IEEE Signal Processing Magazine, vol. 25, no. 2, pp. 21-30, March 2008.

[93]   M. Trakimas, R. D'Angelo, S. Aeron, T. Hancock, and S. Sonkusale, "A compressed sensing analog-to-information converter with edge-triggered SAR ADC core," IEEE Trans. Circuits Syst. I Regul. Pap., vol. 60, no. 5, pp. 1135–1148, 2013.

[94]   S. Qaisar, R. M. Bilal, W. Iqbal, M. Naureen, and S. Lee, "Compressive sensing: From theory to applications, a survey," J. Commun. Networks, vol. 15, no. 5, pp. 443–456, 2013.

[95]   Z. Dong and Y. Zhang, "An integral sampler for analog-to-information converter," Proceedings of 2012 IEEE-EMBS International Conference on Biomedical and Health Informatics, 2012.

[96]   J. A. Tropp, J. N. Laska, S. Member, M. F. Duarte, J. K. Romberg, and R. G. Baraniuk, "Beyond Nyquis: Efficient Sampling of Sparse Bandlimited Signals," IEEE Trans. Inf. Theory, vol. 56, no. 1, pp. 520–544, 2010.

[97]   Romberg, Justin, and Michael Wakin. "Compressed sensing: A tutorial." IEEE Statistical Signal processing workshop. 2007.

[98]   D. L. Donoho, A. Maleki, and A. Montanari, "Message-passing algorithms for compressed sensing.," Proc. Natl. Acad. Sci. U. S. A., vol. 106, no. 45, pp. 18914–9, Nov. 2009.

[99]   D. L. Donoho, "Compressed sensing," IEEE Trans. Inf. Theory, vol. 52, no. 4, pp. 1289–1306, Apr. 2004.

[100]   E. J. Candès, Y. C. Eldar, D. Needell, and P. Randall, "Compressed sensing with coherent and redundant dictionaries," Applied and Computational Harmonic Analysis, vol. 31, no. 1, pp. 59–73, 2011.

[101]   D. Sharma, A. Khalid, and S. Parashar, "Cryptographically Secure Linear feedback shift Register," vol. 3, no. 10, pp. 3504–3507, 2014.

[102]   M. K. Stojčev, M. R. Kosanović and L. R. Golubović, "Power management and energy harvesting techniques for wireless sensor nodes," 2009 9th International Conference on Telecommunication in Modern Satellite, Cable, and Broadcasting Services, Nis, 2009, pp. 65-72.

[103]   S. T. Andrew Dawson, Michael Flaherty, "Stray voltage". Bsc. project. Worchester Polytechnic Institute, 2012. [Online]. Available: https://web.wpi.edu/Pubs/E-project/Available/E-project-042512-133226/unrestricted/SVD_MQP_FINAL_PDF.pdf

[104]   M. Angel and T. Arredondo, Acoustic Emission Testing and Acousto-Ultrasonics for Structural Health Monitoring. Msc. Thesis. Universität Siegen. 2013

[105]   C. Delebarre, T. Pujolle, G. Cousin, A. Domon, J. Froux, and J. Jourdan, "Wireless Low Cost CO2 Monitoring System Design and Evaluation Using Non Dispersive Infrared Sensor," Wireless Sensor Network, vol. 10, no. 06, pp. 119–130, 2018.

[106]   Shawcity, "Infra-Red Sensors _ Shawcity LTD." [Online]. Available: http://www.shawcity.co.uk/infra-red-sensors. [Accessed: 01-Jan-2013].

[107]   R. Valenti, I. Dryanovski, and J. Xiao, "Keeping a Good Attitude: A Quaternion-Based Orientation Filter for IMUs and MARGs," Sensors, vol. 15, no. 8, pp. 19302–19330, 2015.

[108]   T. Vidal-Calleja, D. Su, F. De Bruijn and J. V. Miro, "Learning spatial correlations for Bayesian fusion in pipe thickness mapping," 2014 IEEE International Conference on Robotics and Automation (ICRA), Hong Kong, 2014, pp. 683-690.

[109]   L. V Voronkova, "Ultrasonic Testing Possibilities of Cast Iron Ingots," In the 9th European Conference on NDT , 2006, pp. 1–13.

[110]   N. Yadav and C. Bleakley, "Accurate orientation estimation using AHRS under conditions of magnetic distortion," Sensors (Switzerland), vol. 14, no. 11, pp. 20008–20024, 2014.

[111]   K. Yoo, C. Lee, and J. Kim, "A digital accelerometer using a microscale liquid-metal droplet in photosensitive glass channel," TRANSDUCERS 2009 - 2009 International Solid-State Sensors, Actuators and Microsystems Conference, 2009.

[112]   D. Balageas, "Introduction to Structural Health Monitoring," Structural Health Monitoring, pp. 13–43,2006.

[113]   E. Bergamini, G. Ligorio, A. Summa, G. Vannozzi, A. Cappozzo, and A. Sabatini, "Estimating

Orientation Using Magnetic and Inertial Sensors and Different Sensor Fusion Approaches: Accuracy Assessment in Manual and Locomotion Tasks," Sensors, vol. 14, no. 10, pp. 18625–18649, 2014

[114]   Analog Devices, "± 250 ° / sec Yaw Rate Gyroscope," ADXRS612 Datasheet, 2007 [Revised Nov. 2013].

[115]   V. Giurgiutiu, "Embedded Non-destructive Evaluation for Structural Health Monitoring, Damage Detection, and Failure Prevention," Shock Vib. Dig., vol. 37, no. 2, pp. 83–105, 2005.

[116]   Honeywell, "3-Axis Magnetoresistive Sensor," HMC2003 Datasheet, 2003[Revised Dec. 2014].

[117]   B. Lin and V. Giurgiutiu, "Modeling of power and energy transduction of embedded piezoelectric wafer active sensors for structural health monitoring," Sensors and Smart Structures Technologies for Civil, Mechanical, and Aerospace Systems 2010, 2010.

[118]   S. O. H. Madgwick, A. J. L. Harrison, and R. Vaidyanathan, "Estimation of IMU and MARG orientation using a gradient descent algorithm," 2011 IEEE International Conference on Rehabilitation Robotics, 2011.

[119]   E Kiziroglou, Michail & E Boyle, David & Wright, S & Yeatman, Eric. (2015). Acoustic energy transmission in cast iron pipelines. Journal of Physics: Conference Series..

[120]   P. Poshala, "Why oversample when undersampling can do the job?,"Texas Instrument, Application Report no. July, p. 12, 2013.

[121]   J. A. Tropp, J. N. Laska, M. F. Duarte, J. K. Romberg and R. G. Baraniuk, "Beyond Nyquist: Efficient Sampling of Sparse Bandlimited Signals," in IEEE Transactions on Information Theory, vol. 56, no. 1, pp. 520-544, Jan. 2010.

[122]   T. Okazawa and I. Akita, "A Time-Domain Analog Spatial Compressed Sensing Encoder for Multi-Channel Neural Recording," Sensors, vol. 18, no. 2, p. 184, 2018.

[123]   S. Shapero, C. Rozell, and P. Hasler, "Configurable hardware integrate and fire neurons for sparse approximation," Neural Networks, vol. 45, pp. 134–143, 2013.

[124]   C. R. Schlottmann, S. Member, P. E. Hasler, and S. Member, "A Highly Dense , Low Power , Programmable Analog Vector-Matrix Multiplier : The FPAA Implementation," IEEE J. Emerg. Sel. Top. Circuits Syst., vol. 1, no. 3, pp. 403–411, 2011.

[125]   S. Shapero, A. S. Charles, C. J. Rozell, and P. Hasler, "Low Power Sparse Approximation on Reconfigurable Analog Hardware," IEEE Journal on Emerging and Selected Topics in Circuits and Systems, vol. 2, no. 3, pp. 530–541, 2012.

[126] C. J. Rozell and P. Garrigues, "Analog sparse approximation for compressed sensing recovery," 2010 Conference Record of the Forty Fourth Asilomar Conference on Signals, Systems and Computers, arXiv:1111.4118, 2010.

[127] . Kirolos, J. Laska, M. Wakin, M. Duarte, D. Baron, T. Ragheb, Y. Massoud, and R. Baraniuk, "Analog-to-Information Conversion via Random Demodulation," 2006 IEEE Dallas/CAS Workshop on Design, Applications, Integration and Software, 2006.

[128] Analog Devices, "Printed Circuit Board (Pcb) Design Issues," 2008. [Online]. Available: https://www.analog.com/media/en/training-seminars/design-handbooks/Basic-Linear-Design/Chapter12.pdf. [Accessed July 2, 2016]

[129] V. Kafedziski and T. Stojanovski, "Compressive sampling with chaotic dynamical systems," 2011 19thTelecommunications Forum (TELFOR) Proceedings of Papers, 2011.

[130] M. Mishali, S. Member, Y. C. Eldar, and S. Member, "From Theory to Practice : Sub-Nyquist Sampling of Sparse Wideband Analog Signals," vol. 4, no. 2, pp. 375–391, 2010.

[131] J. Li, J. Sheng Li, Y. Yang Pan, and R. Li, "Compressive optical image encryption," Sci. Rep., vol. 5, pp. 1–10, 2015.

[132] H. Liu, D. Xiao, Y. Liu, and Y. Zhang, "Securely compressive sensing using double random phase encoding," Optik (Stuttg)., vol. 126, no. 20, pp. 2663–2670, 2015.

[133] Y. Zhang, L. Y. Zhang, J. Zhou, L. Liu, F. Chen, and X. He, "A Review of Compressive Sensing in Information Security Field," IEEE Access, vol. 4, pp. 2507–2519, 2016.

[134] S. H. Hsieh, T. H. Hung, C. S. Lu, Y. C. Chen, and S. C. Pei, "A Secure Compressive Sensing-Based Data Gathering System via Cloud Assistance," IEEE Access, vol. 6, pp. 31840–31853, 2018.

[135] M. R. Mayiami, B. Seyfe, and H. G. Bafghi, "Perfect secrecy via compressed sensing," 2013 Iran Workshop on Communication and Information Theory, 2013..

[136] A. Orsdemir, H. O. Altun, G. Sharma, and M. F. Bocko, "On the security and robustness of encryption via compressed sensing," MILCOM 2008 - 2008 IEEE Military Communications Conference, 2008.

[137] L. Vinet and A. Zhedanov, "Kryptein: A Compressive-Sensing-Based Encryption Scheme for the Internet of Things," J. Phys. A Math. Theor., vol. 44, no. 8, p. 085201, 2011.

[138] J. Sheng, C. Yang, and M. C. Herbordt, "Hardware-efficient compressed sensing encoder designs for WBSNs," 2015 IEEE High Performance Extreme Computing Conference (HPEC),

2015.

[139] Anne Canteaut, "The, LFSR-based Stream Ciphers", in Error-Correcting Codes and their Applications to Symmetric Cryptography, pp 43-77, 2017.

[140] E. Zenner, On cryptographic properties of LFSR-based pseudorandom generators", Dess. Universit¨at Mannheim, 2004.

[141] A. Pande and J. Zambreno, "Design and hardware implementation of a chaotic encryption scheme for real-time embedded systems," 2010 International Conference on Signal Processing and Communications (SPCOM), Bangalore, 2010, pp. 1-5.

[142] X. Liu, W. Mei, and H. Du, "Optical image encryption based on compressive sensing and chaos in the fractional Fourier domain," J. Mod. Opt., vol. 61, no. 19, pp. 1570–1577, 2014.

[143] A. Pande and J. Zambreno, "A chaotic encryption scheme for real-time embedded systems: Design and implementation," Telecommun. Syst., vol. 52, no. 2, pp. 551–561, 2013.

[144] V. Pudi, A. Chattopadhyay, and K. Y. Lam, "Secure and Lightweight Compressive Sensing Using Stream Cipher," IEEE Trans. Circuits Syst. II Express Briefs, vol. 65, no. 3, pp. 371–375, 2018.

[145] D. B. Thomas and W. Luk, "The LUT-SR family of uniform random number generators for FPGA architectures," IEEE Trans. Very Large Scale Integr. Syst., vol. 21, no. 4, pp. 761–770, 2013.

[146] M. Bakiri, "Hardware Implementation of Pseudo Random Number Generator Based on Chaotic Iterations", Dess. Université de Bourgogne Franche-Comté, 2018.

[147] S. Jiao, Z. Zhuang, C. Zhou, W. Zou, and X. Li, "Security enhancement of double random phase encryption with a hidden key against ciphertext only attack," Opt. Commun., vol. 418, no. February, pp. 106–114, 2018.

[148] J. Choi, "Secure Transmissions via Compressive Sensing in Multicarrier Systems," in IEEE Signal Processing Letters, vol. 23, no. 10, pp. 1315-1319, Oct. 2016.

[149] D. E. Bellasi, L. Bettini, C. Benkeser, T. Burger, Q. Huang, and C. Studer, "VLSI design of a monolithic compressive-sensing wideband analog-to-information converter," IEEE J. Emerg. Sel. Top. Circuits Syst., vol. 3, no. 4, pp. 552–565, 2013.

[150] K. M. C. Alan V. Oppenheim, "Chaotic Signals and Signal Processing," in Digital Sigmal Processing Handbook, 1999.

[151] C. Svensson and J. J. Wikner, "Power consumption of analog circuits: A tutorial," Analog Integr.

Circuits Signal Process., vol. 65, no. 2, pp. 171–184, 2010.

[152] A. J. Michaels, "Quantitative comparisons of digital chaotic circuits for use in communications," Proceedings of the Joint INDS'11 & ISTET'11, Klagenfurt, 2011, pp. 1-8.

[153] I. Koyuncu, A. T. Ozcerit, and I. Pehlivan, "Implementation of FPGA-based real time novel chaotic oscillator," Nonlinear Dynamics, vol. 77, no. 1-2, pp. 49–59, 2014.

[154] Z. Liu, S. Y. Chen, and F. Xi, "Chaotic analogue-to-information conversion with chaotic state modulation," IET Signal Process., vol. 8, no. August 2013, pp. 373–380, 2014.

[155] L. Chua, M. Komuro and T. Matsumoto, "The double scroll family," in IEEE Transactions on Circuits and Systems, vol. 33, no. 11, pp. 1072-1118, November 1986.

[156] R. Kilic, A Practical Guide for Studing Chuas Cicuits. World Scientific, 2010.

[157] F. Yuan, G.-Y. Wang, and X.-Y. Wang, "Dynamical characteristics of an HP memristor based on an equivalent circuit model in a chaotic oscillator," Chinese Phys. B, vol. 24, no. 6, p. 060506, 2015.

[158] Muthuswamy, Bharathwaj, Tamara Blain, and Kyle Sundqvist. "A Synthetic inductor implementation of Chua's circuit". Technical Report No. UCB/EECS-2009-20, Electrical Engineering and Computer Sciences, University of California at Berkeley, 2009.

[159] A. S. Elwakil and M. P. Kennedy, "Improved implementation of Chua's chaotic oscillator using current feedback op amp," IEEE Trans. Circuits Syst. I Fundam. Theory Appl., vol. 47, no. 1, pp. 76–79, 2000.

[160] T. Banerjee, "Single amplifier biquad based inductor-free Chua's circuit," Nonlinear Dynamics, vol. 68, no. 4, pp. 565–573, 2011.

[161] M. P. Kennedy, Robust OP AMP realization of Chuas circuit. Berkeley: Electronics Research Laboratory, College of Engineering, University of California, 1992.

[162] T. Matsumoto, A chaotic attractor from Chuas circuit. Berkeley: Electronics Research Laboratory, College of Engineering, University of California, 1984.

[163] R. Kiliç, "A comparative study on realization of Chua's circuit: hybrid realizations of Chua's circuit combining the circuit topologies proposed for Chua's diode and inductor elements," Int. J. Bifurc. Chaos Appl. Sci. Eng, vol. 13, no. 6, pp. 1475–1493, 2003.

[164] Lexa, Michael, Mike Davies, and John Thompson. "Sampling sparse multitone signals with a random demodulator." University of Edinburgh, Institute of Digital Communications, Tech. Rep. (2010).

[165] R. K. Nagaria, M. G. Krishna, and C. Engineering, "Comparative Performance of Low Voltage CMOS - CFOA Suitable for Analog VLSI," vol. 5, no. 6, pp. 226–231, 2008.

[166] H. Jassim, "A New Design Technique of CMOS Current Feed Back Operational Amplifier (CFOA)," vol. 2013, no. January, pp. 11–15, 2013.

[167] H. Çiçekli and A. Gökçen, "Realization of Tuneable MOS-C Quadrature Sinusoidal Oscillator Using Composite Current Conveyor," In Proceedings. 19th International Conference on Circuits, Systems, Communications and Computers, 2015, pp. 1–4.

[168] J. R. Piper and J. C. Sprott, "Simple autonomous chaotic circuits," IEEE Trans. Circuits Syst. II Express Briefs, vol. 57, no. 9, pp. 730–734, 2010.

[169] A. Granada, R. M. Hennig, B. Ronacher, A. Kramer, and H. Herzel, "Chapter 1 Phase Response Curves" in Elucidating the Dynamics of Coupled Oscillators, 1st ed., vol. 454, no. C. Elesvier Inc., 2009.

[170] S. F. Al-sarawi, Design Techniques for Low Power Mixed Analog-Digital Circuits with Application to Smart Wireless System. Diss. Alexandria University. 2003.

[171] Hua Luo A VLSI Design for Phase Synchronization of Two Globally Coupled Oscillators. Diss. University of Maryland. 2017

[172] T. Stankovski, T. Pereira, P. V. E. Mcclintock, and A. Stefanovska, "Coupling functions: Universal insights into dynamical interaction mechanisms," pp. 1–53, 2017.

[173] G. Edward and R. Cowan, "A VLSI Analog Computer / Math Co-processor for a Digital Computer," 2005.

[174] A. S. Elwakil and M. P. Kennedy, "Low-voltage, low-power, chaotic oscillator, derived from a relaxation oscillator," Microelectronics J., vol. 31, no. 6, pp. 459–468, 2000.

[175] L. Acho, "Modeling and Synchronization of Multivibrator Oscillator", Cybernetic and Physics. vol. 2, no. 1, pp. 5–9, 2013.

[176] L. Keuninckx, G. Van Der Sande, and J. Danckaert, "Simple Two-Transistor Single-Supply Resistor-Capacitor Chaotic Oscillator," IEEE Trans. Circuits Syst. II Express Briefs, vol. 62, no. 9, pp. 891–895, 2015.

[177] Campos-Cantón, Eric, et al. "A multivibrator circuit based on chaos generation."in International Journal of Bifurcation and Chaos, vol. 22, Issue 01, January 2012.

[178] B. Razavi, "The Delta-Sigma Modulator [A Circuit for All Seasons]," in IEEE Solid-State Circuits Magazine, vol. 8, no. 2, pp. 10-15, Spring 2016.

[179] J. C. Sprott, Elegant chaos: algebraically simple chaotic flows. Hackensack, NJ: World Scientific, 2010.

[182] Ing. Jiří Petržela. Analysis and modelling of the non-linear dynamical systems. Dess. Brno University of Technology. 2012.

[183] M. Rani, S. B. Dhok, and R. B. Deshmukh, "A Systematic Review of Compressive Sensing: Concepts, Implementations and Applications," IEEE Access, vol. 6, pp. 4875–4894, 2018.

[184] A. Durdu, A. T. Özcerit, and Y. Uyaroğlu, "A novel chaotic system for secure communication applications," Inf. Technol. Control, vol. 44, no. 3, pp. 271–278, 2015.

[185] Khaled El Hadad, "A New Technique for Secure Image Communication via Chaotic Circuit," IJCST vol. 9, Issue 1, Jan - March 2018

[186] X. Li, Y. J. Lu, Y. F. Zhang, X. G. Zhang, and P. Gupta, "Design and hardware implementation of a new chaotic secure communication technique," PLoS One, vol. 11, no. 8, pp. 1–19, 2016.

[187] R. Rizwana and I. Raja Mohamed, "Applicability of strange nonchaotic Wien-bridge oscillators for secure communication," Pramana, vol. 91, no. 1, p. 10, 2018.

[188] U. E. Kocamaz, S. Çiçek, and Y. Uyaroğlu, "Secure Communication with Chaos and Electronic Circuit Design Using Passivity-Based Synchronization," J. Circuits, Syst. Comput., vol. 27, no. 04, p. 1850057, 2018.

[189] Z. Li, K. Li, C. Wen, and Y. C. Soh, "A new chaotic secure communication system," IEEE Trans. Commun., vol. 51, no. 8, pp. 1306–1312, 2003.

[190] M. Zapateiro, Y. Vidal, and L. Acho, "A chaotic secure communication scheme based on duffing oscillators and frequency estimation," IFAC Proc. Vol., vol. 9, no. PART 1, pp. 749–754, 2013.

[191] Digi-Key, "Battery Life Calculator," 2017. [Online]. Available: https://www.digikey.co.uk/en/resources/conversion-calculators/conversion-calculator-battery-life. [Accessed 21,June 2017].

[192] Pierre Boulet, Philippe Devienne, Pierre Falez, Guillermo Polito, Mahyar Shahsavari, et al.. "N2S3,an Open-Source Scalable Spiking Neuromorphic Hardware Simulator". [Research report] Université de Lille 1, Sciences et Technologies; CRIStAL UMR 9189. 2017.

[193] S. Friedmann, J. Schemmel, A. Grübl, A. Hartel, M. Hock and K. Meier, "Demonstrating Hybrid Learning in a Flexible Neuromorphic Hardware System," in IEEE Transactions on Biomedical Circuits and Systems, vol. 11, no. 1, pp. 128-142, Feb. 2017.

[194] M. K. Stojčev, M. R. Kosanović and L. R. Golubović, "Power management and energy

harvesting techniques for wireless sensor nodes," 2009 9th International Conference on Telecommunication in Modern Satellite, Cable, and Broadcasting Services, Nis, 2009, pp. 65-72.

[195] olakowski, P. "Structural health monitoring-A review with the emphasis on low-frequency methods". Engineering Transactions, vol.55,2007, pp239-275.

[196] H. Guo, G. Xiao, N. Mrad, and J. Yao, "Fiber optic sensors for structural health monitoring of air platforms.," Sensors (Basel)., vol. 11, no. 4, pp. 3687–705, Jan. 2011.

[197] M. Angel and T. Arredondo, "Acoustic Emission Testing and Acousto-Ultrasonics for Structural Health Monitoring." [Online]. Available: http://www.mb.uni-siegen.de/imr3/forschung/abgeschlossene_projekte/strukturdiagnose/copy_of_arredondo.html. en?lang=en. [Accessed: 01-Mar-2013].

[198] M. Safety, "Electrified Cover Safeguard." [Online]. Available: http://manholesafety.com/. [Accessed: 01-Dec-2013].

Appendices

9. APPENDIX I: SENSOR TYPE SELECTION FOR IoT BASED MANHOLE COVER MONITORING SYSTEM

As mentioned at the end of Chapter 2, an intensive study has been performed to identify the types of sensors needed to be used for an IoT based automated MC monitoring system. Generally, sensor types are divided into two main parts: passive and active sensors. A passive sensor detects and responds to some type of input or variations from the physical environment. While the active sensors need an external power supply to operate. It is obvious that passive sensors are less power consuming than active ones; however, active sensors are more controllable and used widely because of the good accuracy and wider applications where they can be used.

Stojvec, et al in [194] has classified sensors used based on power consumption as shown in Table I-1. Ultra high-power sensors are considered more power hungry than communication module. On the other hand, due to the big development in sensor design and fabrications like MEMS (microelectromechanical systems) sensor, the cost of sensors is becoming very low with very high accuracy.

The study of sensor types includes investigation in other fields to identify the most suitable sensing techniques. As the target of this research is to monitor the MC which is a metallic structure, and by considering only the physical phenomena that need to be addressed, the study extends to investigate the sensors used in several fields like aerospace and civil engineering. Besides those fields, another type of study is included which is based on monitoring the source of the issue instead of monitoring the effect of this source on the MC as will be shown later.

Table I- 1 STOJVEC'S sensor classification based on the power consumption [195]

Sensor type	Sensor	Power consumption (mw)
Micro Power		
SFH 5711	Light Sensor	0.09
DSW98A	Smoke Alarm	0.108
SFH 7741	Proximity	0.21
SFH 7740	Optical Switch	0.21
ISL 29011	Light Sensor	0.27
STCN75	Temperature	0.4
Low -power		
TSL 2550	Light Sensor	1.155
ADXL202JE	Accelerometer	2.4

SHT 11	Humidity/temperature	2.75
MS55ER	Barometric Pressure	3
QST108KT6	Touch	7
SG-Link(1000Ω)	Strain gauge	9
Medium-power		
SG-LINK (350Ω)	Strain gauge	24
iMEMS	Accelerometer	30
Ov7649	CCD	44
2200-600	Pressure	50
	High-power	
T150	Humidity	90
DDT-651	Motion Detector	150
EM-005	Proximity	180
BES 516-371-S49	Proximity	180
EZ/EV-18M	Proximity	195
GPS-9546	GPS	198
LUC-M10	Level sensor	300
CP18,VL18,GM60	Proximity	350
TDA0160	Proximity	420
Ultra high -power		
FCS-GL1/2A4-AP8X-H1141	Flow Control	1250
FCBEX11D	CCD	1900/2800
XC56BB	CCD	2200

Physical Phenomenon for the Upperground/Common issues

Orientation

The first physical phenomenon which needs to be addressed is the orientation of MC. Based on Chapter 2, three MC result issues are related to the orientation of the MC: security, tilting and shattering. These issues result in the movement of the MC structure. As shown in Chapter 2, several automated techniques are used for security issues including tilting.

The movement of MC structure can differ if it is for security or based on soil movement or because of high traffic. The difference between these issues is the angle and direction of the MC structure movement. While the mentioned techniques in Chapter 2 can be used, other sensor types can be proposed, and used in several applications

In the aerospace field, planes orientation needs to be known as shown in Figure I-1. The sensor type widely used for this application is the inertial measurement unit (IMU). Also, in robotics design, IMU is used to make the robotics "feel" to avoid "falling" as shown in Figure I-2.
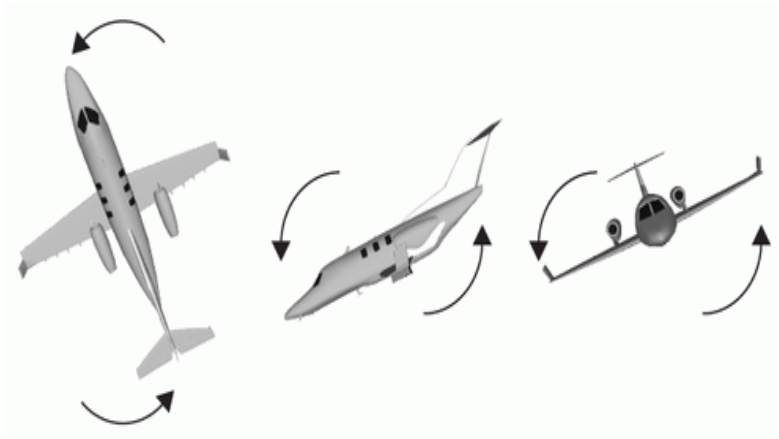
Figure I- 1 Planes Orientations
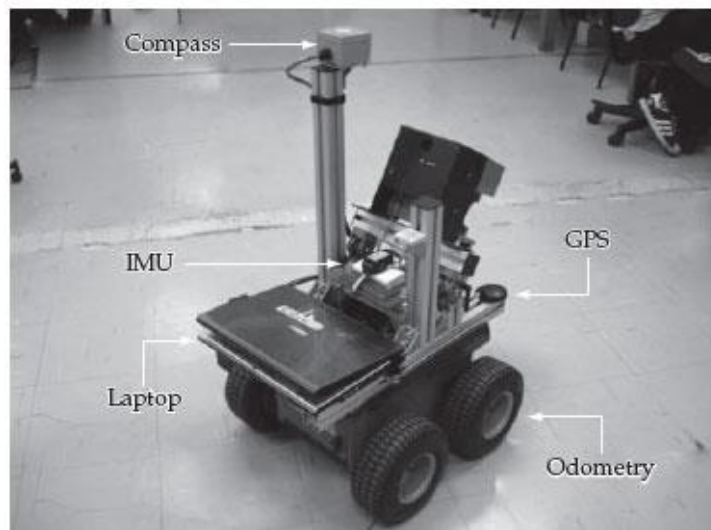
Figure I- 2 IMU for Robotics

IMU consists of two sensors: accelerometer and gyroscope and sometimes magnetometer and named MIMU [114]. In some references and for more accuracy, another sensor can be used with IMU, i.e. MARG sensor (magnetic, Angular Rate, and gravity sensors) [108]. However, at this point, the IMU sensor will be considered for orientation, and it will need more study to check if MARG is needed or not, which is not in the scope of this research.

The accelerometer is used to measure the speed of the plane, but it can also be used to measure misalignment in XYZ coordinates while the gyroscope measures the rotation movement as shown in Figure I-3. By using IMU, it is easy to monitor any movement in the MC. On the other hand, some references value or thresholds need to be identified to distinguish between the source of movement and this is mainly done by specific sensor fusion technique which is out of the scope of this study. Besides that, IMU now is used for several applications and well known at very low cost.
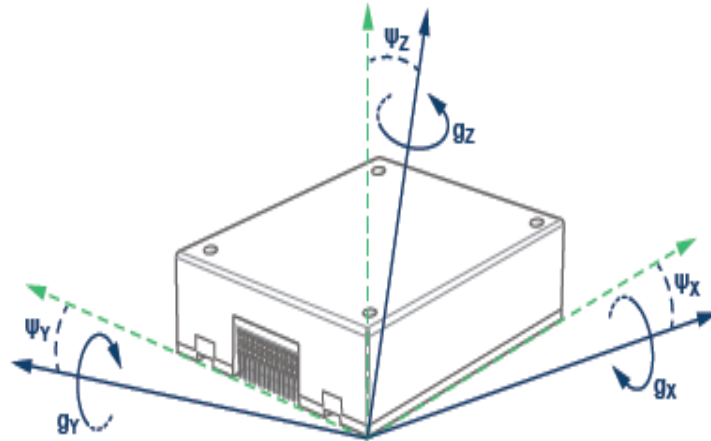
Figure I- 3 Inertial Measurement Unit (IMU)

The other parameter which needs to be specified is the bandwidth. For the accelerometer, it can start from very low frequency to 3200 Hz as mentioned in [112], while the gyroscope can reach up to 2.5 kHz while its resonance frequency (maximum frequency) is 17 kHz as mentioned in [115]. And for the magnetometer sensor, the bandwidth can reach 75 Hz as mentioned in [117], which means that for the IMU sensor, the maximum bandwidth is 17 kHz.

Structure degradation

While the movement has been reported to be monitored automatically, structure degradation which includes corrosion and structure deformation has no automated system for MC. For this reason, it needs more study and investigation to reach the suitable sensor type. To be more specific, in this section corrosion, crack, and skid resistance need to be addressed in the context of monitoring the cast iron structure.

In the civil engineering area, structure health monitoring (SHM) is emerging as a vital tool to help engineers in monitoring structure every moment during its life [113]. SHM is concerned about monitoring the structure performance regarding several parameters. The investigation takes place to study how to measure metallic structure based on SHM.

Testing and evaluation for monitoring structures are mainly based on two techniques: non-destructive and destructive. For monitoring MC, non-destructive techniques are more suitable. SHM uses vibration technique for Non-Destructive Testing and Evaluation (NDT/E) monitoring by means of active sensors like acoustic, ultrasound, eddy current, magnetic particle, etc. According to [195], Table I-2 shows the different NDT/E from the SHM point of view:

Table I- 2 Several NDT/E sensing Techniques in SHM [195]

Method	Advantage	Disadvantage
Ultrasound	• The possibility of detecting both volume and planar defects, • Safe operation conditions for the staff • Relatively low cost of testing.	• No detection of discontinuities positioned along the ultrasonic beam • Difficulty in examining rough surfaces or irregular shapes, • The necessity of using the coupling medium for piezoelectric probes
Radiographic testing	• The possibility of testing objects of various, complicated shapes, • Good detectability of volume defects and planar defects along the radiation beam, • No necessity of contact between the object and equipment.	• Harmful operation conditions for the staff • Poor detection of discontinuities positioned perpendicular to the radiation beam, • The relatively high cost of testing and bulky equipment.
Acoustic Emission	• No necessity of exciting the object or structure (service load is sufficient), • The ability to differentiate between stable and growing defects.	• Difficulties in quantifying defects (commercial AE systems can only estimate qualitatively) • The extension of damage in the material and can tell approximately how long the components will last • Weak signals, therefore high sensitivity to environmental noise.
Magnetic particle inspection	• Possibility of detecting planar (even narrow or shallow) discontinuities on/underneath the surface, • Low cost of equipment.	• Harmful operation conditions for the staff (toxic powder components), • Limited applicability to ferromagnetic materials.
Eddy current	• The possibility of detecting planar discontinuities on/underneath the surface, • Applicability to coated (e.g. painted) surfaces.	• The necessity of having extensive knowledge and experience by the operator, • Difficulties in the interpretation of the signal affected by electric conductivity, magnetic penetrability and operating frequency.
Penetrate Method	• The possibility of detecting planar discontinuities on/underneath the surface,	• Harmful operation conditions for the staff (toxic components),

	• The possibility of detecting discontinuities in locations of rapid changes of the cross-section (hardly possible by any other method),	• No applicability to coated (e.g. painted) surfaces, • Tedious (many stages) process of testing
Fibre optics [196]	• High sensitivity • Accurate • Can be used in a harsh environment	Expensive

NDT/E techniques for cast iron are mainly visual, magnetic particle or radiographic inspection. These methods are not suitable for monitoring MC automatically, so other techniques have to be taken into consideration. Fibre optics and piezoelectric sensors are very attractive but have their disadvantages. Fibre is very expensive, and using it in such application which requires a huge number of nodes will be extortionate.

The PZT sensor is used in many SHM applications as active sensors while some techniques can use PZT as passive sensors. While active sensors have their drawbacks regarding power consumption, selecting the technique for monitoring structure using PZT can optimize this issue based on the frequency required from the PZT sensor. On the other hand, the PZT sensor proved to be suitable in many types of research in the efficiency and the cost and is very suitable for MC monitoring application.

As the PZT sensor has been suggested to be used, there are several techniques of the PZT sensor used in SHM. However, this study will focus on the studies published to monitor cast iron material which is the most used type of MC. These techniques are [195]:

1. Ultrasonic (US) Sensor: Using US for testing metallic structure is very wide in SHM. One of the US sensors is piezoelectric wave acoustic surface PWAS. Figure I-4 shows two methods for using PWAS. The first one is to use two probes as transmitter and receiver to detect the damaged region (named "pitch-catch method"). The other method is to use one sensor to be both transmitter and receiver, to identify the damage or the crack of the material. Generally, the US sensor for cast iron can reach from few kHz [118] to 5 MHz [110] This means that 5 MHz will be taken as the maximum bandwidth for the US which can be used.
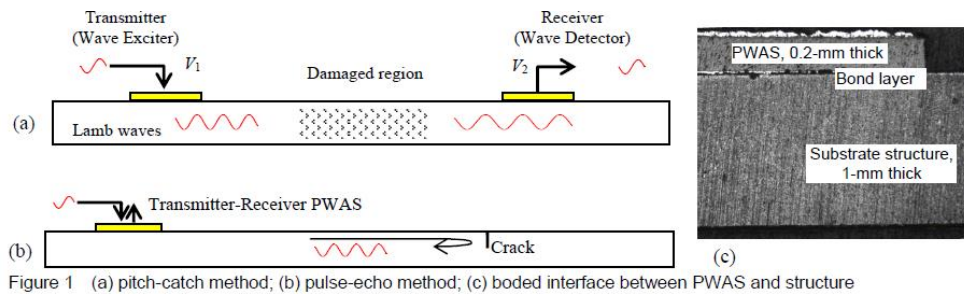
Figure I- 4 piezoelectric wave acoustic surface PWAS [113]

2.   Acoustic Emission (AE): this is defined as the class of phenomena in which transient elastic waves are generated by the rapid release of energy from a localized source or sources within a material (ASTM E1316) [120]. An AE wave is an elastic wave, having a wide frequency up to 100 kHz [120] while it is based on passive technique.

3.   Acoustic-Ultrasonic: (AU) is defined as a non-destructive method that uses stress waves to detect and evaluate diffuse defects, damage, and variations in the mechanical properties of materials. However, AU is based on active sensing techniques. Both AE and AU are shown in Figure I-5[197]
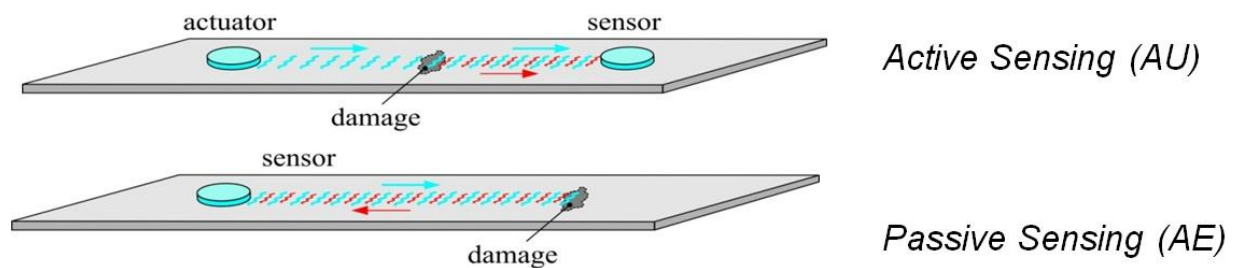
Figure I- 5 AE and AU[198]

The wide range of using PZT for monitoring the structure degradation like MC structure can be seen. Moreover, it is expected to use the PZT sensor to measure the skid resistance which can contribute in both MC and underground metallic structure monitoring and also in SHM field.

The bandwidth of the PZT sensor for this research may vary from a few Hz to MHz; to be specific in this review it can reach 5 MHz. Combining several methods like AE and AU also improves the monitoring systems like in [105] while in the same reference very high sampling rate (50 MHz) was used to avoid the effect of the noise; and as mentioned in [109] the sampling for US sensor reaches 125 MHz. However, this research will consider only the sensors bandwidth and the sampling rate required, which will be based on Nyquist-Shannon theory as mentioned before.

Physical Phenomenon for the Underground Utility type

Electrification

As mentioned in Chapter 2, only one reference mentioned the invention of an automated stray/contact voltage sensor [198]. No theoretical background has been mentioned except that this device is activated when the metal structure has been electrified.

From this point, this study searches a new or a different sensing technique to be used. Several methods are mentioned in [104] which use a handheld device to monitor the stray voltage. For the MC and from the study done in Chapter 2, the source of the electrification most of the time is not from the upper environment but from the cables beneath the MC. In [104], a simple circuit has been proposed with the same concept to detect the stray voltage as shown in Figure I-6. The system proposed in [104] is based on the manual (non-contact) concept, while in this study it is used for the automated system. The system detects 60 Hz signal.
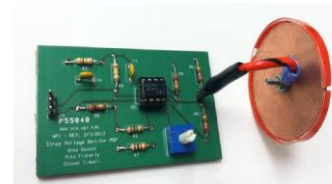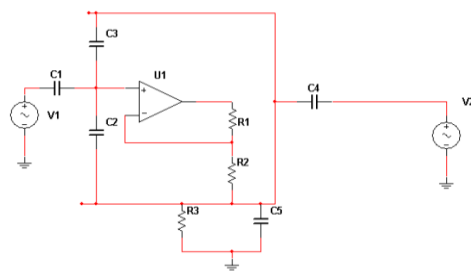
Figure I- 6 Stray voltage detector [106]

Explosion

It is mentioned in Chapter 2 that explosion can be caused by fire from electric cables or from the gas leak. From the conducted literature study, automated explosion monitoring techniques based on electrical cables has been used, while for gas leak this is not the case. Generally, the simple gas detector can monitor the gas leak. Hence, the event-driven method can be used and does not consume much power. Although this issue is very important, the sensing technique can be only a switch to indicate if there is any danger or not. However, if it is required to measure any gas for some level, the sensing technique will be different. Several techniques can be used for gas detection. The more suitable for MC monitoring is IR gas sensor because it can be used to determine several gases which makes monitoring more accurate. IR

gas sensor bandwidth depends on the type of gas [106]. From the off shelf market datasheet, the sampling rate required can reach 1 kHz or less [106].

To conclude, this Appendix presents sensor types selection study for an IoT based automated MC monitoring system. It has been shown that not all the issues need to be monitored because few of them are based on the type of underground utility. However, it is also shown that the highest sensor bandwidth is for detecting the common MC issues. Hence, the DAQ module for an IoT based automated MC monitoring system needs to be designed based on low power consumption design consideration.

Table I-3 shows the summary of the sensor types needed for an IoT based automated MC monitoring system. The target in this Appendix is to identify the sensor types needed, then identify the bandwidth of these types to determine the ADC sampling rate required for the IoT based automated MC monitoring system.

It is also shown that some of these sensor types need more investigation. Although this is an important part of the design the IoT based automated MC monitoring system, it is out of the scope of this research. However, it opens a good opportunity to develop in not just monitoring MC but also in several fields.

Table I- 3 Sensors type suggested to be used for an IoT based automated MC monitoring system

Sensor	MC Issues				Frequency
Inertial Measurement Unit (IMU) (Accelerometer-Gyroscope)	Security	tilting	Shattered (Structure Degradation)	Collapsed (Structure Degradation)	350 Hz-17kHz
Piezoelectric sensor (PZT)	Crack (Structure Degradation)	Corrosion	Skid resistance (expected)		Few hundreds of Hz-MHz (≈5MHz)
Voltage sensor (Electrical/Telecommunication utilities only)	Stray/contact (expected)				≈60Hz
Smoke/fire sensor(Electrical/Telecommunication utilities only)	Explosion				ON/OFF switch or IR gas

10. APPENDIX II: WAVE SHAPING CIRCUIT ANALYSIS

This appendix presents the governing equations of charging the capacitors and the effect of charging capacitors from two different sources. The study in this appendix uses sinusoidal and square wave sources. The study will extend to investigate the effect of changing the resistors values on the waveshaping of the capacitor.
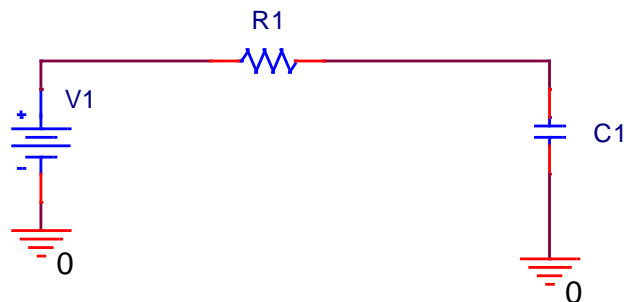
Figure II- 1 Charging capacitor circuit

The governing equation for charging and discharging the capacitor for the circuit shown in Figure II-1 is:

$$V_c(t) = V_c(\infty) - [V_c(\infty) - V_c(0)]e^{\frac{-t}{\tau}} \text{ V}$$

In which

$V_c(t)$: Voltage of the capacitor

$V_c(\infty)$: The maximum voltage that capacitor voltage can reach (in other words it is the amplitude of the AC input or the value of the DC input)

$V_c(0)$= the initial voltage of the capacitor

T = time

the τ= time constant (R*C)

If the input signal is a DC, the input and the output waveforms are shown in Figure II-2. The capacitor voltage will reach full charge after 5 times its time constant or 5τ. Based on the values shown in Figure II-8, the capacitor needs at least 5 ms to be fully charged.
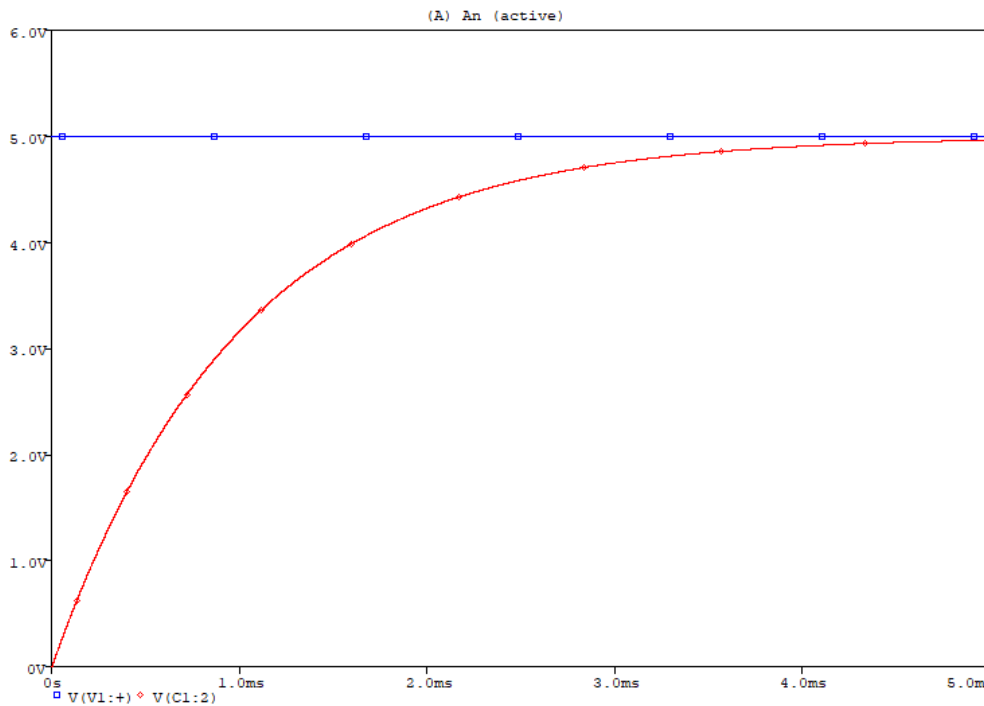
Figure II- 2 Charging capacitor waveform.

If we change the input to a square wave with frequency 1 kHz for example (one cycle period=1 msec), the input and output or the capacitors voltage waveforms of the capacitor will be as shown in Figure II-3. For each half period of the square wave, the capacitor looks at the input source as a DC source. Based on the time of the half period which is less than 5c (half cycle period is 0.5ms), the shaped waveform of the capacitor becomes nearly linear and like the triangle wave shape.
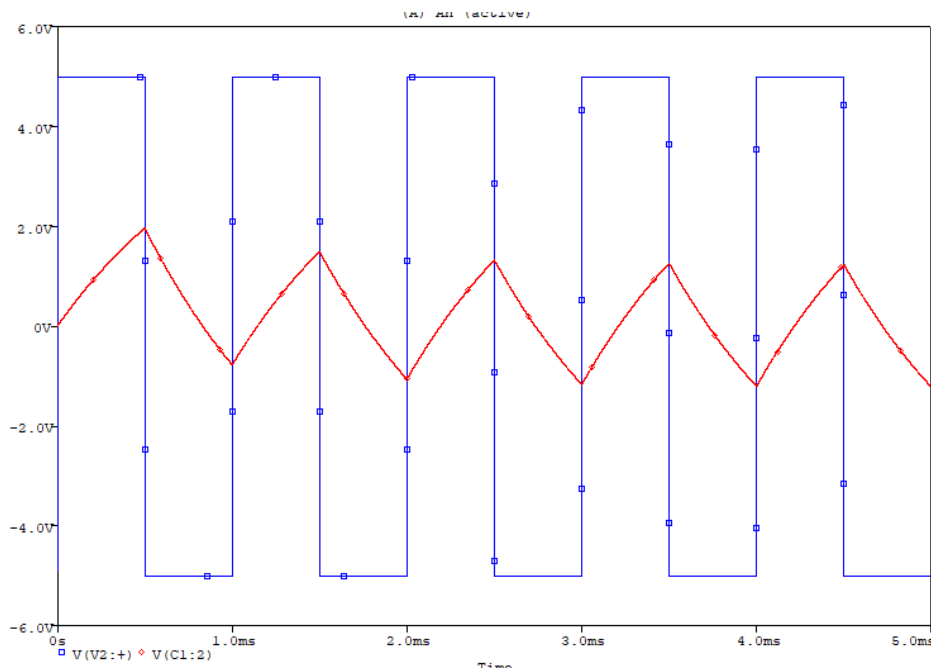
Figure II- 3 Input (blue) and capacitor voltage (red) waveform

189

Charging the Capacitor from two different sources
This section studies charging the capacitor from two different sources. The study will examine the effect of the shape, frequency and resistance effects on the capacitance charging. Figure II-4 shows the case of using two different sources to charge a capacitor. It can be considered as R-C-R coupling function.
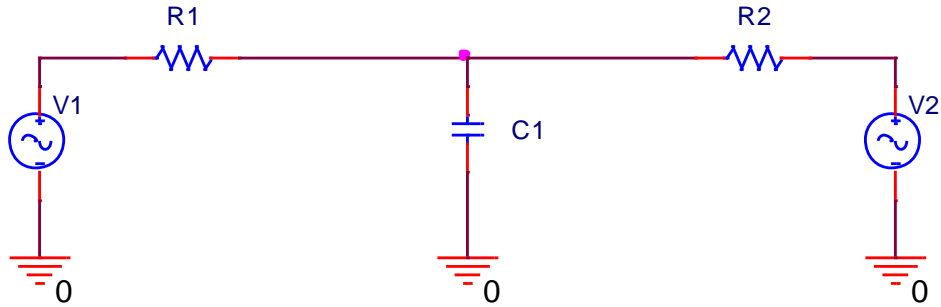
Figure II- 4 Charging capacitor from two different sources

To analyse the circuit above, first, apply the superposition method. Let V2 be grounded as shown in Figure II-5. Hence apply Thevenin theorem to get the Vth and Rth as follows

$$V_{th1} = V_1 \frac{R_2}{R_1+R_2} \text{ V}$$

And by grounding the V1 and making the capacitor an open circuit

$$R_{th1} = R_1 \parallel R_2 = \frac{R_1 \times R_2}{R_1+R_2} \Omega$$
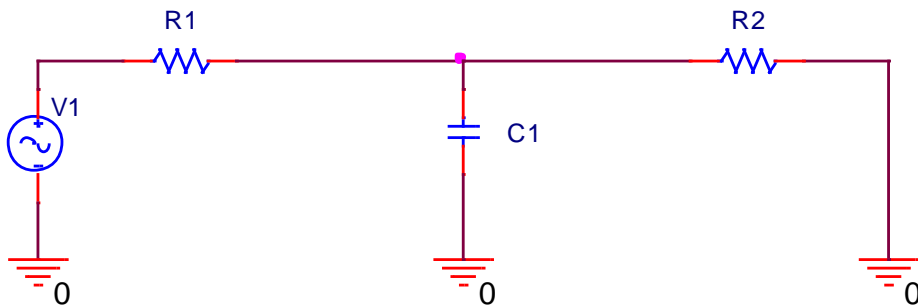
Figure II- 5 V2 is grounded

The final circuit will be as shown in Figure II-6
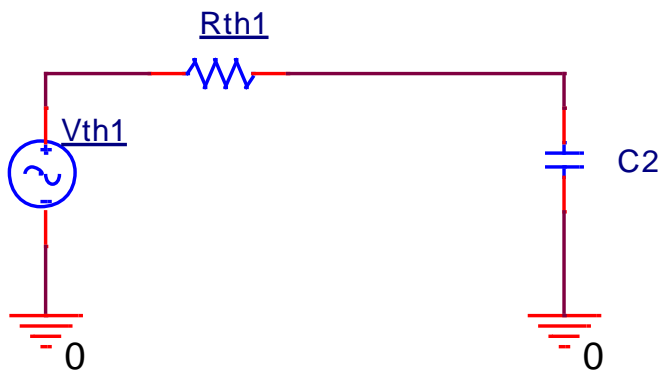
Figure II- 6 The final circuit using Thevenin theory

190

Recalling the charging capacitor presented in the section above, then

$$V_{c1}(t) = V_{th1}(\infty) - [V_{th1}(\infty) - V_c(0)]e^{\frac{-t}{\tau_1 C}} \text{ V}$$

Where

$$\tau_1 = R_{th1}C \text{ sec}$$

Similarly, when grounding the first source and applying the Thevenin theorem, we found:

$$V_{th2} = V_2\frac{R_1}{R_1+R_2} \text{ V}$$

$$R_{th2} = R_1 \parallel R_2 = \frac{R_1 \times R_2}{R_1+R_2} \Omega$$

$$V_{c2}(t) = V_{C2}(\infty) - [V_{C2}(\infty) - V_c(0)]e^{\frac{-t}{\tau_2}} \text{ V}$$

Where

$$\tau_2 = R_{th2}C \text{ sec}$$

Hence the final expression for the capacitor will be

$$V_c(t) = V_{c1}(t) + V_{c2}(t)$$

$$V_c(t) = V_{C1}(\infty) - [V_{C1}(\infty) - V_c(0)]e^{\frac{-t}{\tau_1}} + V_{C2}(\infty) - [V_{C2}(\infty) - V_c(0)]e^{\frac{-t}{\tau_2}}$$

And as observed that the two-time constants are equal

$$\tau = \tau_1 = \tau_2 \text{ sec}$$

Then we can rewrite the final expression as follows

$$V_c(t) = [V_{C1}(\infty) + V_{C2}(\infty)] - \{[V_{C1}(\infty) + V_{C2}(\infty)] - 2V_c(0)\}e^{\frac{-t}{\tau}} \text{ V}$$

Based on the last equations, charging capacitors relies on the time of charging besides the two sources waveforms. However, in this section, the only simulation based will be presented due to the large number of experiments which cannot allow analysing each case.

Hence, the study in this section will focus first on changing the sources waveforms by changing the shape, frequency and amplitude. Later, the effect of changing the resistors values will be discussed.

Case 1:

The two sources are identical with the same resistance value

a- A square wave with f=1 kHz and amplitude 5 V

The input signals and the capacitor waveform are shown in Figure II-7. The capacitor waveform is like a uniform sawtooth. Hence, the effect of both sources was the same on the capacitor which cannot lead to chaotic behaviour. The effect shows non-uniform integration.
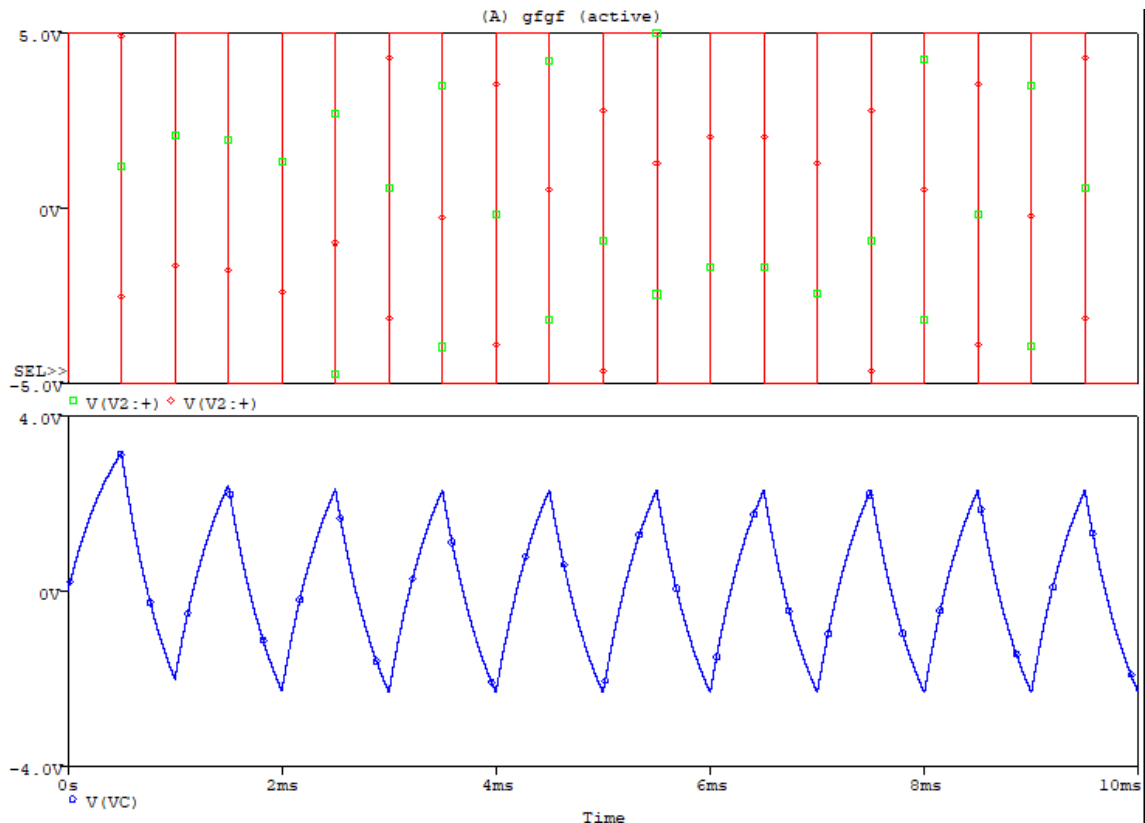
Figure II- 7 Two identical square wave sources case 1

b- 2 sources are sinewave with f=1 kHz and amplitude 5V. The same concept for integration effect is shown in Figure II-8 like in case a.
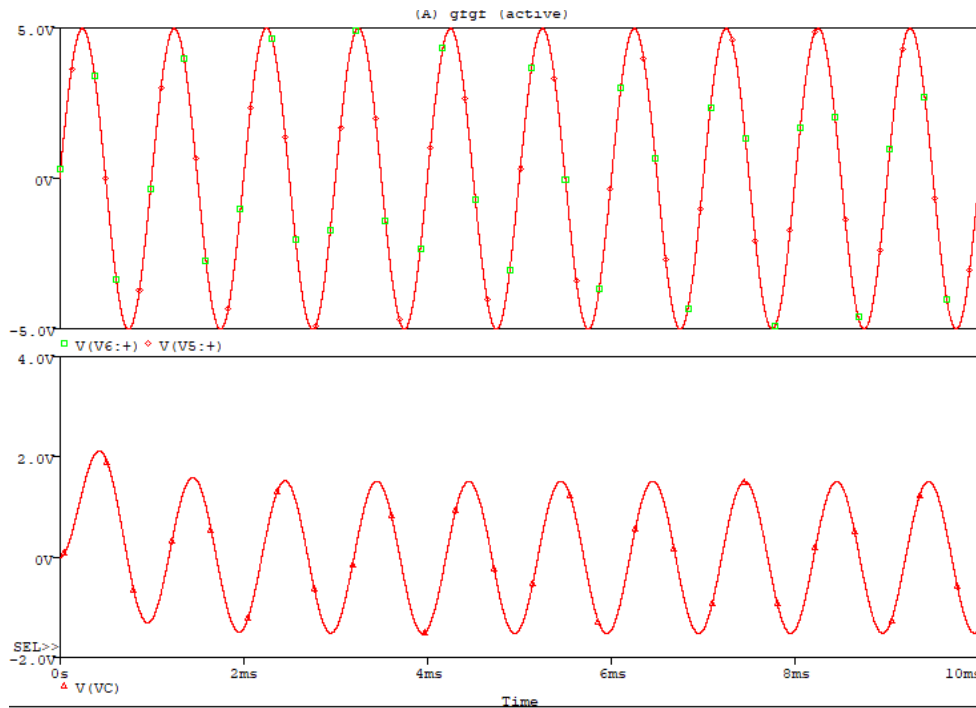
Figure II- 8 Two identical sinusoidal sources case 1

Case 2:

The same wave shape signal with the same frequency with a different amplitude

c- A square wave with frequency 1 kHz and amplitudes 5 V and 1 V respectively. The effect is still the same as case 1. The integration is the main theme of the capacitor waveform as shown in Figure II-9.
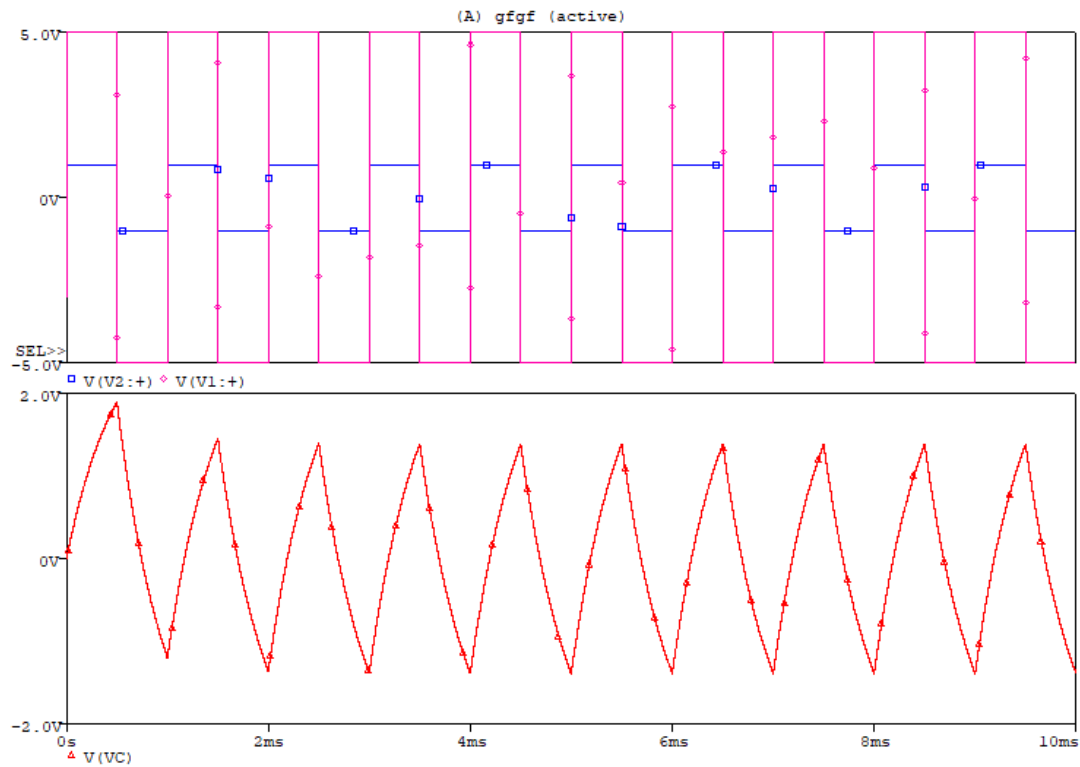
Figure II- 9 Different square wave amplitude case 2

Changing the input waveform to sine wave also leads to the same results. Non-uniform integration is still found, as shown in Figure II-10.
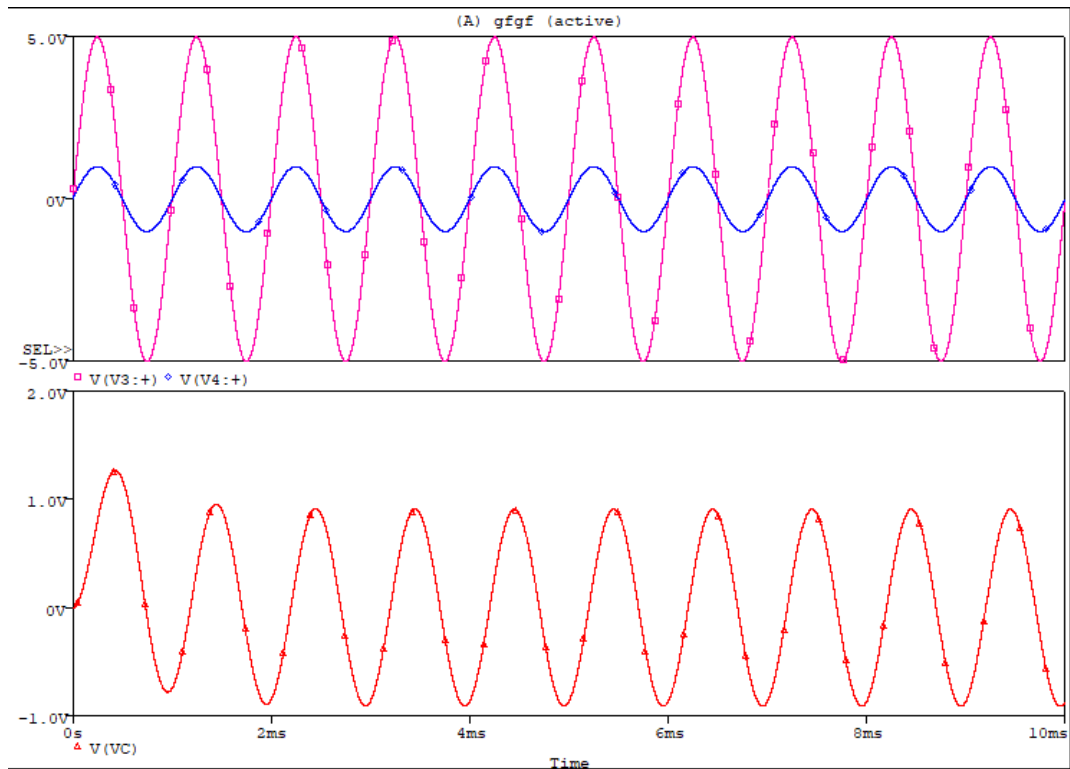
Figure II- 10 Different amplitude sinusoidal case 2

Case 3

Different waveshaping sources, the input signals are sinusoidal and square wave respectively with the same amplitude and same frequency. The capacitor waveform acts as combining both cases 1 and 2 without irregular effect on the shape as shown in Figure II-11.
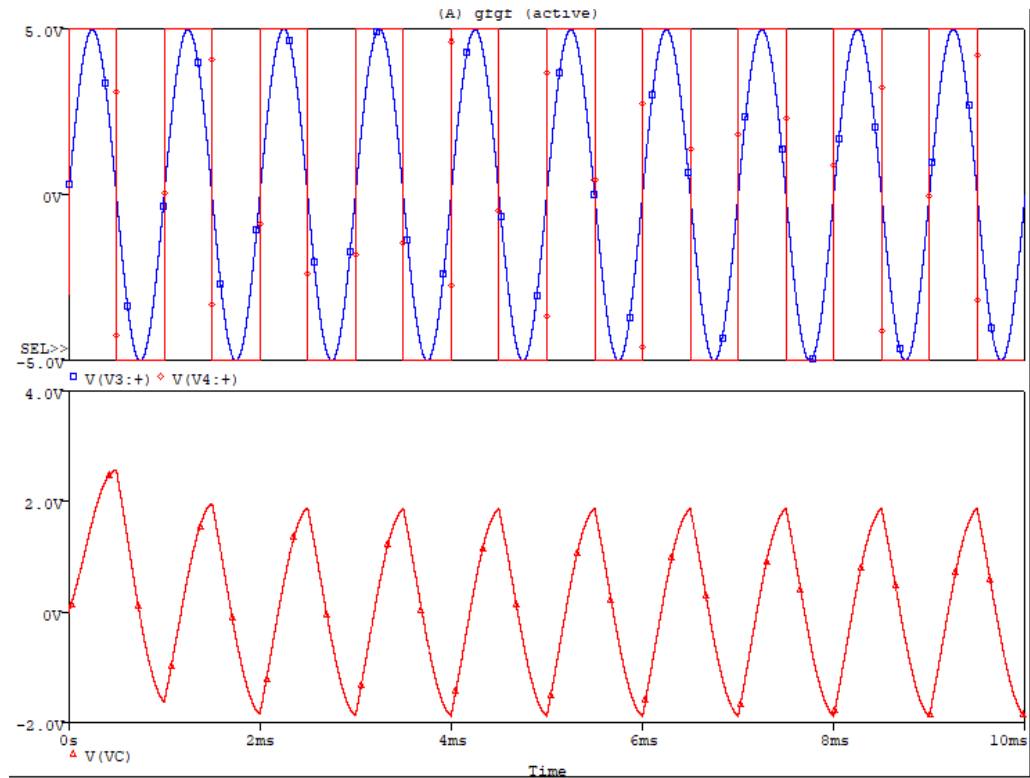
Figure II- 11 Square waves, Sinusoidal sources and capacitor waveforms case 3

Case 4

By changing the amplitudes of the two sources used in case 3, the capacitor waveform shows the integration effect but with different response based on the higher input waveshape signal. This can be observed from the two Figures II-12 and II-13, where the shape takes a semi-triangle or sawtooth shape with higher amplitude of the square wave and sinusoidal shape when sinewave was with higher amplitude. An irregular or chaotic shape is not found in this case.
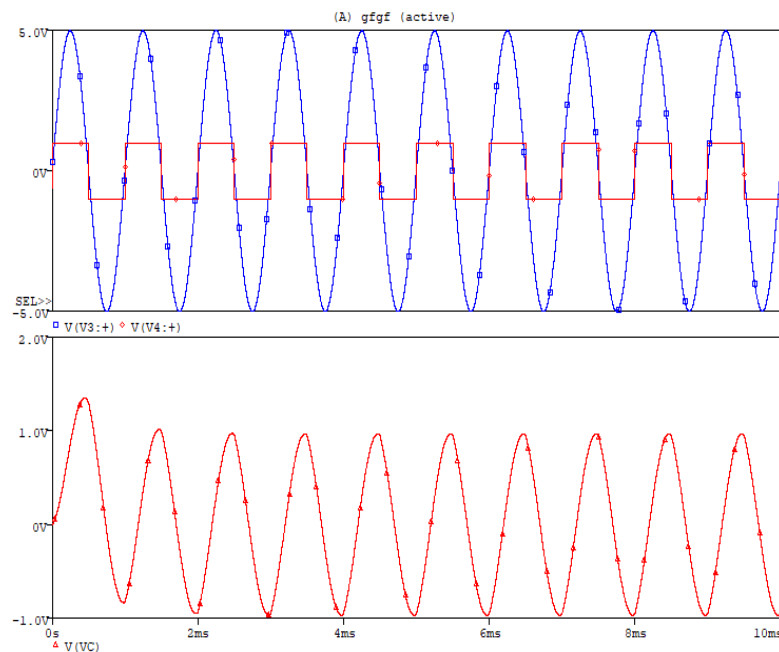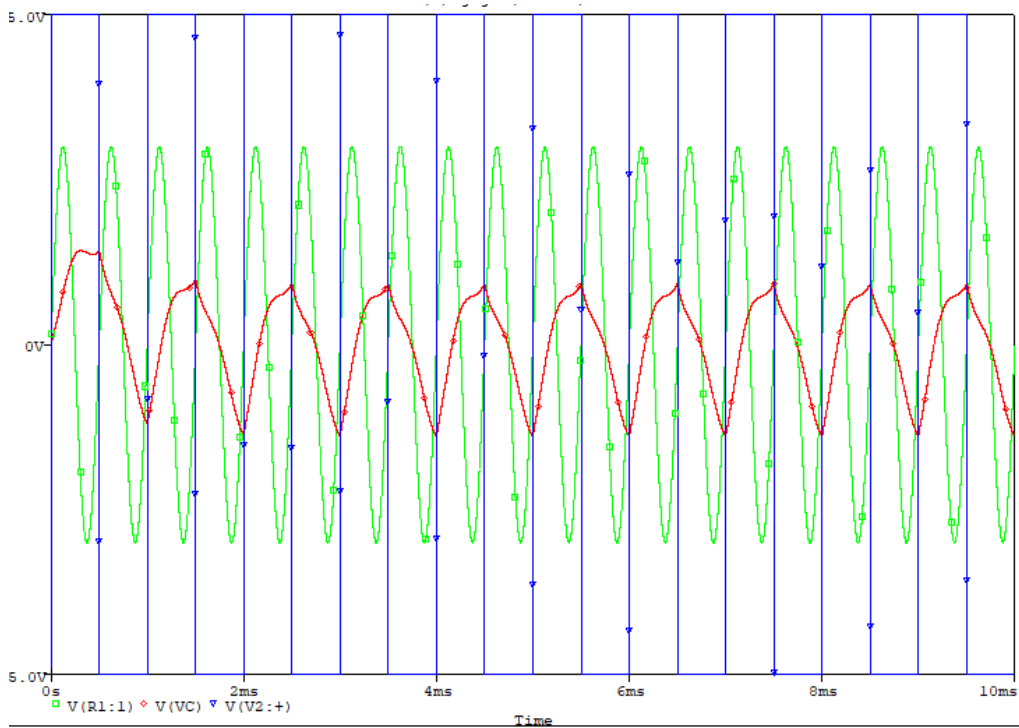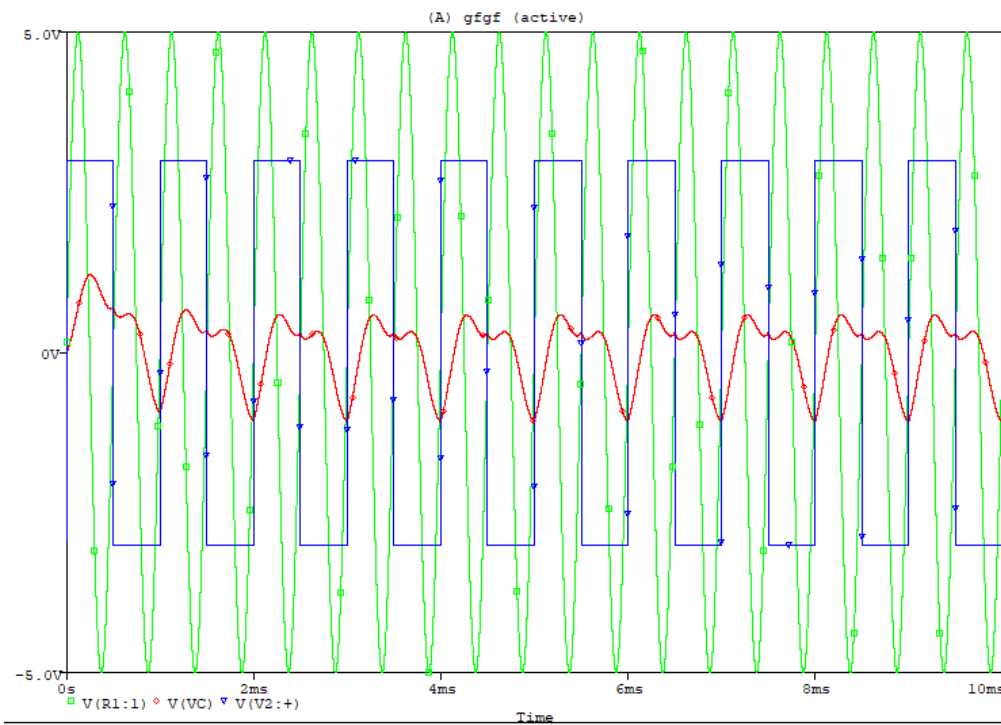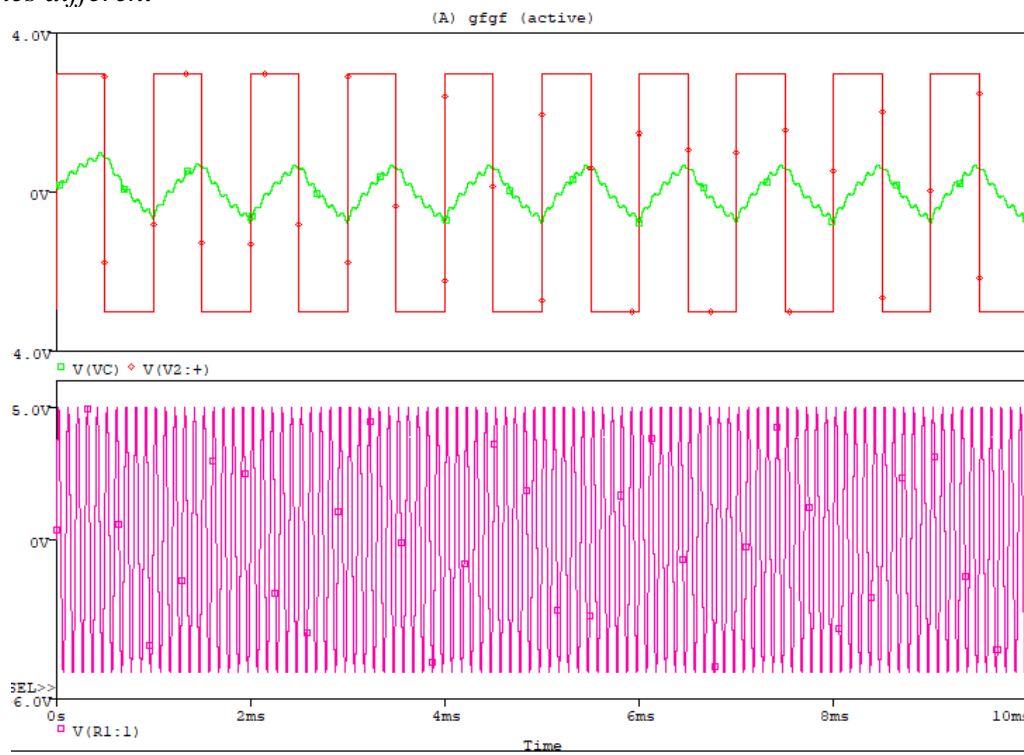

Figure II- 12 Square waves (low amplitude), Sinusoidal sources and capacitor waveforms case 4
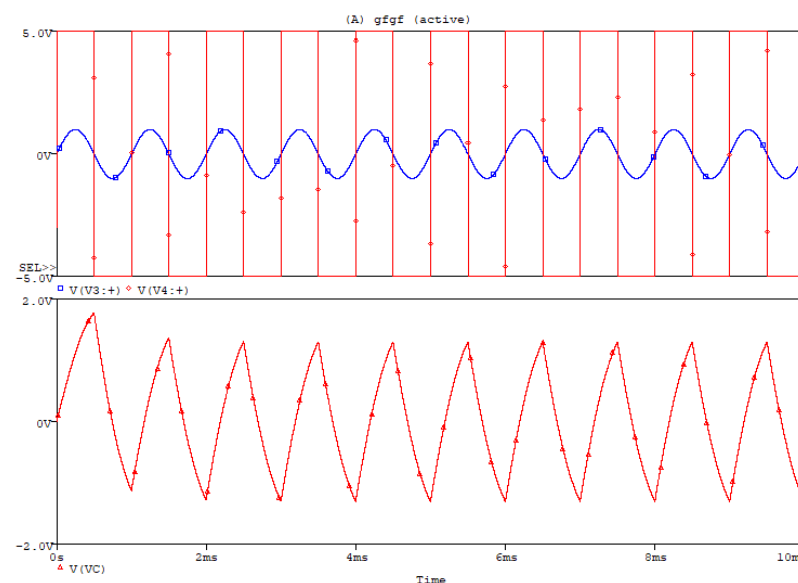
Figure II- 13 Square waves (high amplitude), Sinusoidal sources and capacitor waveforms case 4

197

Case 5

By changing the frequency for the same waveform sources as shown in Figure II-14, the capacitor waveform shows some of the irregular waveform. This can be easily expected as the voltage that charges the capacitor changes with time. Hence humps shape is found for the capacitor voltage as in Figure II-15 for the double time difference (square wave input sources case) between the two input sources. The change in the frequency was also tested for ten times difference between the two input sources. The experiments are done for the square wave and the sine wave inputs respectively as following and the input waves and the corresponding output waveforms are shown in Figure II-15, Figure II-17, Figure II-18 and Figure II-19.

a- 2 square waves
Double time different
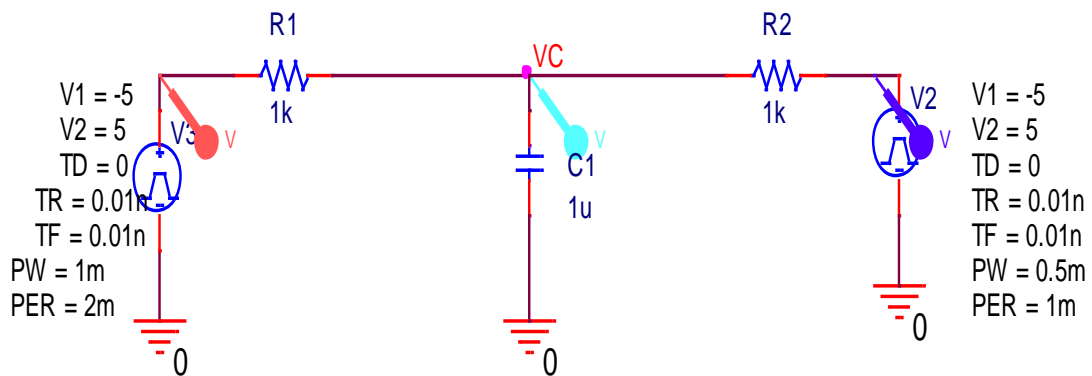
Figure II- 14 Two square wave input with the same amplitude and a different frequency is charging a capacitor
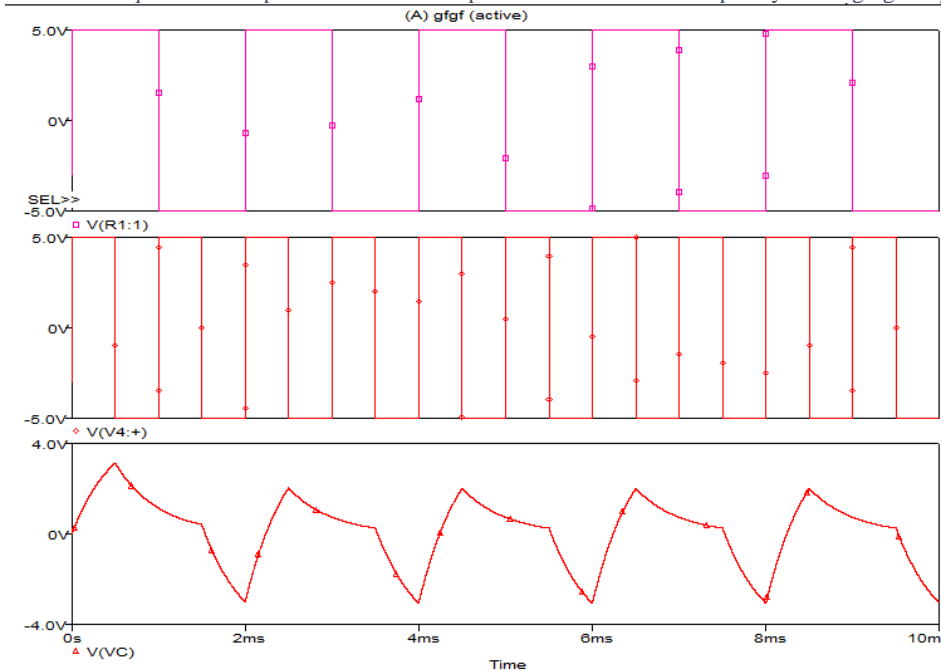
Figure II- 15 Input and capacitor waveforms based on the circuit shown in Figure II-14

10 times different

R1
VC
R2

V1 = -5
V2 = 5
TD = 0
TR = 0.01n
TF = 0.01n
PW = 0.5m
PER = 1m

V3
V

1k

C1
1u

1k

V2
V

V1 = -5
V2 = 5
TD = 0
TR = 0.01n
TF = 0.01n
PW = 0.05m
PER = 0.1m

0

0

0
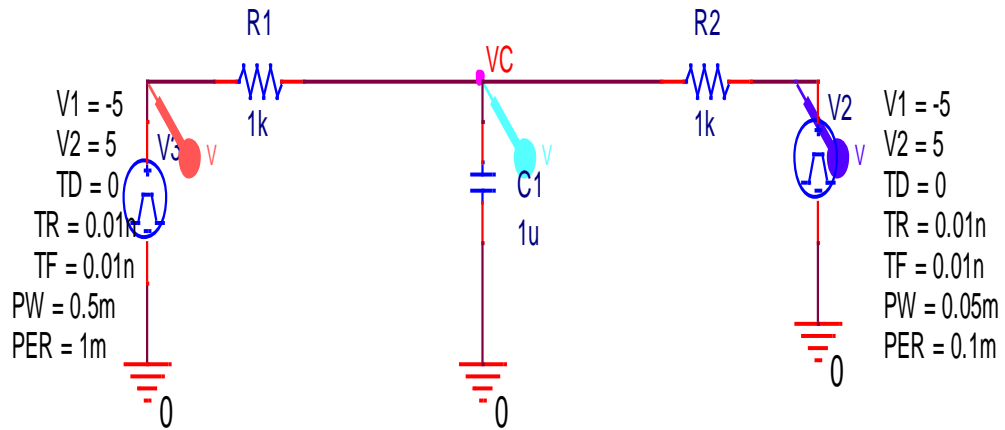
Figure II- 16 Two square wave input 10 times different in frequency and the same amplitude
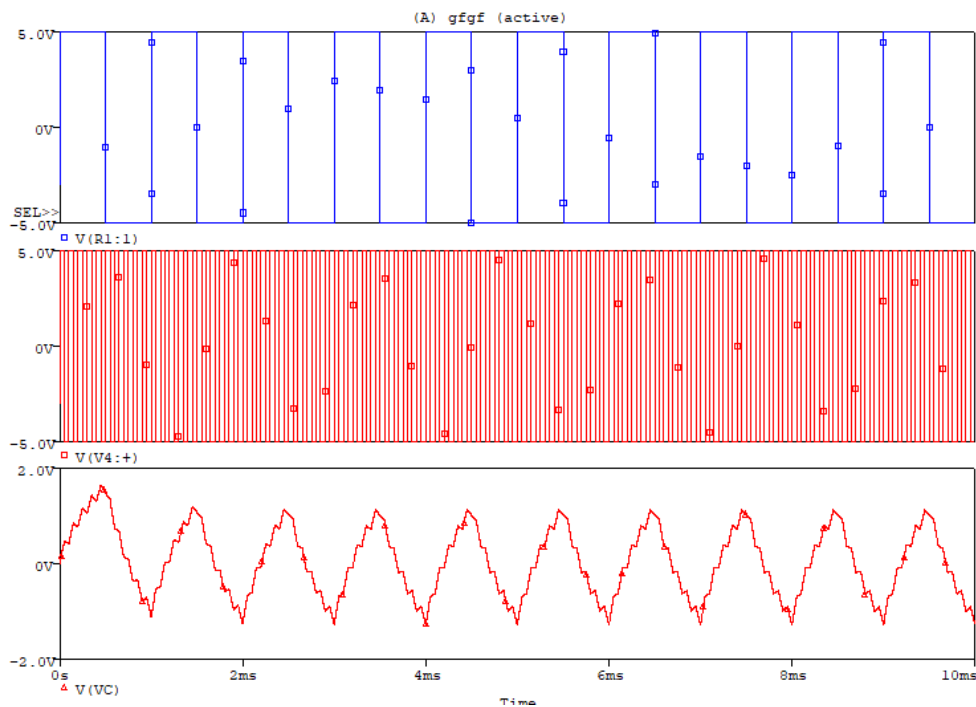
Figure II- 17 Input and capacitor voltage waveforms

b- 2 Sine waves

Double time different

c-
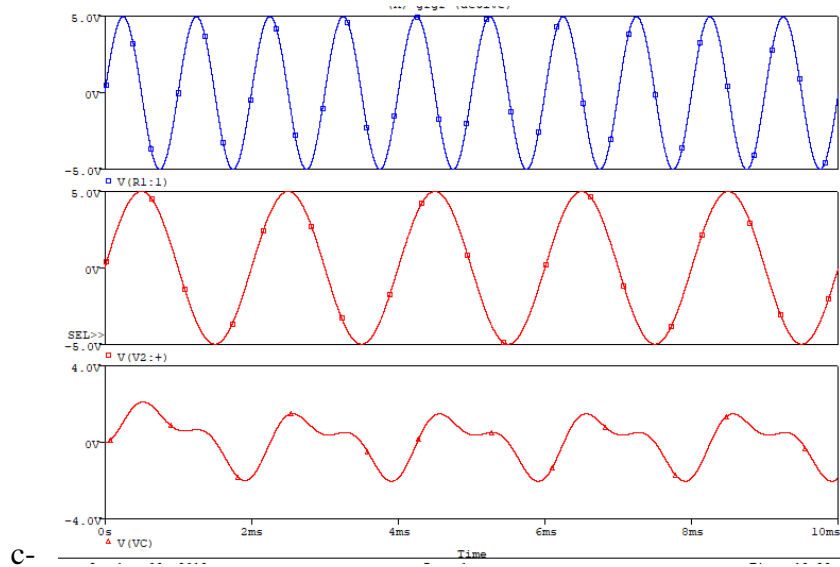
Figure II- 18 Input and capacitor voltage waveforms by using two sinusoidal sources with double frequency difference and the same amplitude

10 times difference
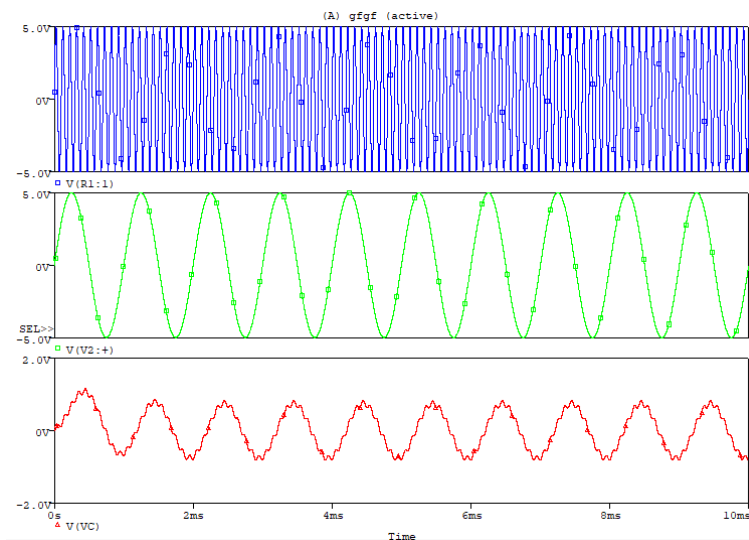
Figure II- 19 Input and capacitors voltage waveforms for using two sinusoidal sources with 10-time difference in Frequency and same amplitude

Case 6

Repeating the experiments as case 5 but with different waveshape sources, the same effect with different shape of the humps has been found as shown in Figures II-20, II-21

Double time different
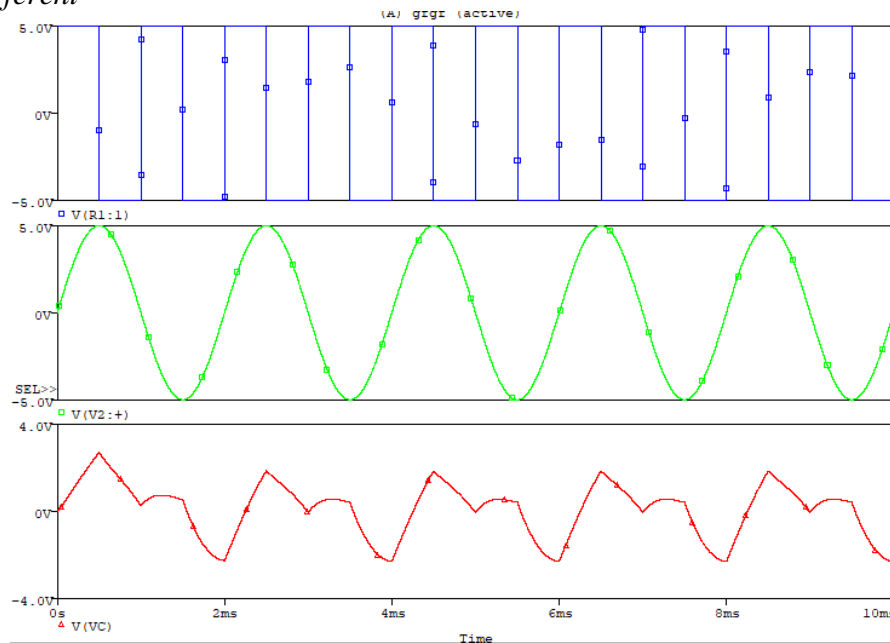
Figure II- 20 Two different wave shape source with double different in the frequency and same amplitude charging a capacitor

10 times different
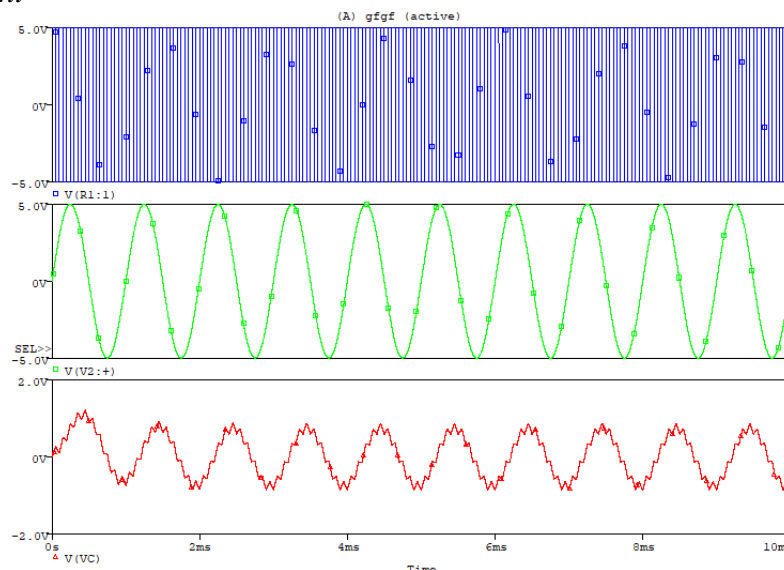
Figure II- 21 The input and the capacitor voltage waveforms for using different sources waveshape with 10 times difference in the frequency with the same amplitude.

Case 7

Repeat the previous case with different amplitudes for the circuit shown in Figure II-22 and the output at Figures II-20, II-22, and II-23.
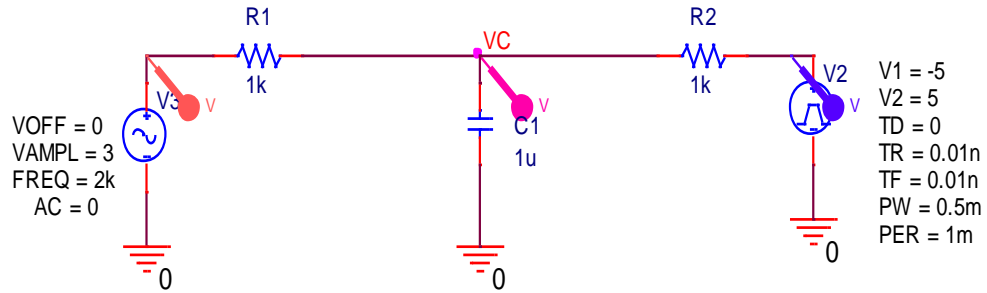
Figure II- 22 Case 7 configuration

Double time different

Figure II- 23 Square waves (high amplitude), Sinusoidal sources and capacitor waveforms case 7

Figure II- 24 Square waves (low amplitude), Sinusoidal sources and capacitor waveforms case 7

10 times different

Figure II- 25 Square waves (low amplitude), Sinusoidal (higher frequency) sources and capacitor waveforms case 7
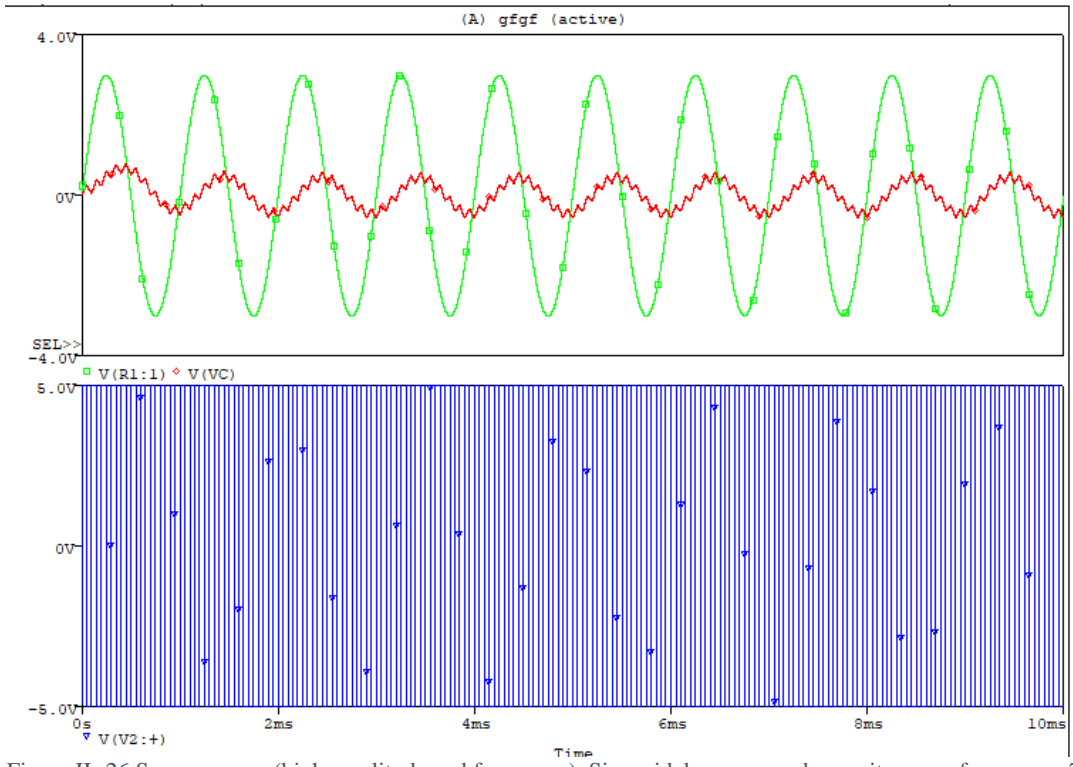
Figure II- 26 Square waves (high amplitude and frequency), Sinusoidal sources and capacitor waveforms case 7

Section Discussion

In this section, two sources charge a capacitor with different cases have been presented. By changing the frequency, shape and amplitude of the sources, several results have been found. Generally, the irregular shapes for capacitor voltage wave shape resulted were found in the cases of different frequencies between the two sources, especially if the difference was big. However, these irregular shapes are not chaotic. This result leads to two choices to study the chaotic generation.

The first one is that all the previous cases used the same resistance. From neuroscience and physics point of view, this can be expected. If we apply force law of physics, we can mimic the sources as forces affect the body (capacitor). Hence, the change of the forces leads to instability of the body. From the same point of view, the two sources do not affect or have any feedback effect from the coupling. Therefore, using normal oscillators is not suitable for the study. Instead, relaxation oscillator is preferred. This is because relaxation oscillators are based on voltage threshold which is capacitor voltage.

From a chaotic oscillators design point of view, chaotic behaviour cannot be expected from these experiments. This is because the chaotic oscillator design needs at least three energy storage elements to generate chaotically. Hence, the main effective result from the previous experiments is that irregularity of capacitor voltage waveforms happened only with a different frequency from the sources. This point can be used as a start point for designing chaotic oscillator based on coupling capacitors. However, the effect of resistors values needs to be studied which is more like the effect of the coupling oscillators in the neuroscience field.

Resistance Effect

As mentioned before, it is expected from these experiments that no chaotic oscillations will take place without three energy storage elements. However, these experiments give us some indications and guidance to convert their output oscillation to chaotic oscillation. Hence, by studying the effect on the capacitor of charging from two different sources, the resistors values will be studied by simulation in this section as follows:

For the case that R1is greater than R2 (100 times for example), the capacitor becomes act as perfect integrator. This can be expected as the value of the R1C is following the same rule of integrator as mentioned before in this thesis. The circuit and the waveforms of the input signals and capacitor voltage waveform are shown in Figures II-27 and II-28
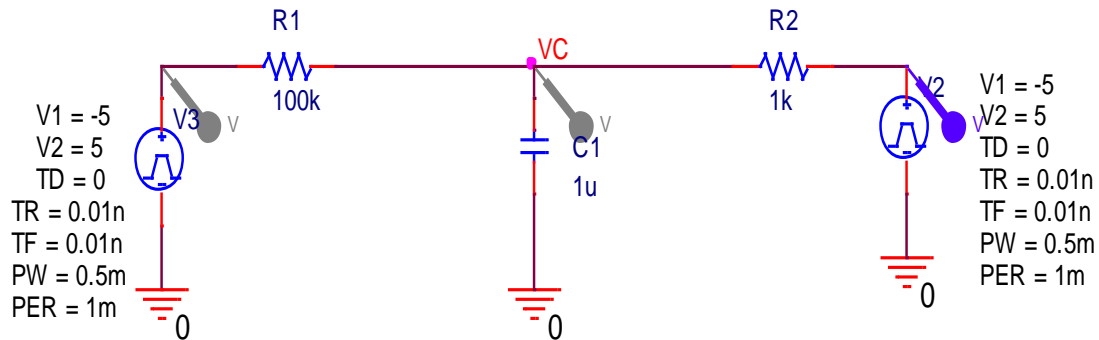
Figure II- 27 R1is greater than R2 case with two identical square wave
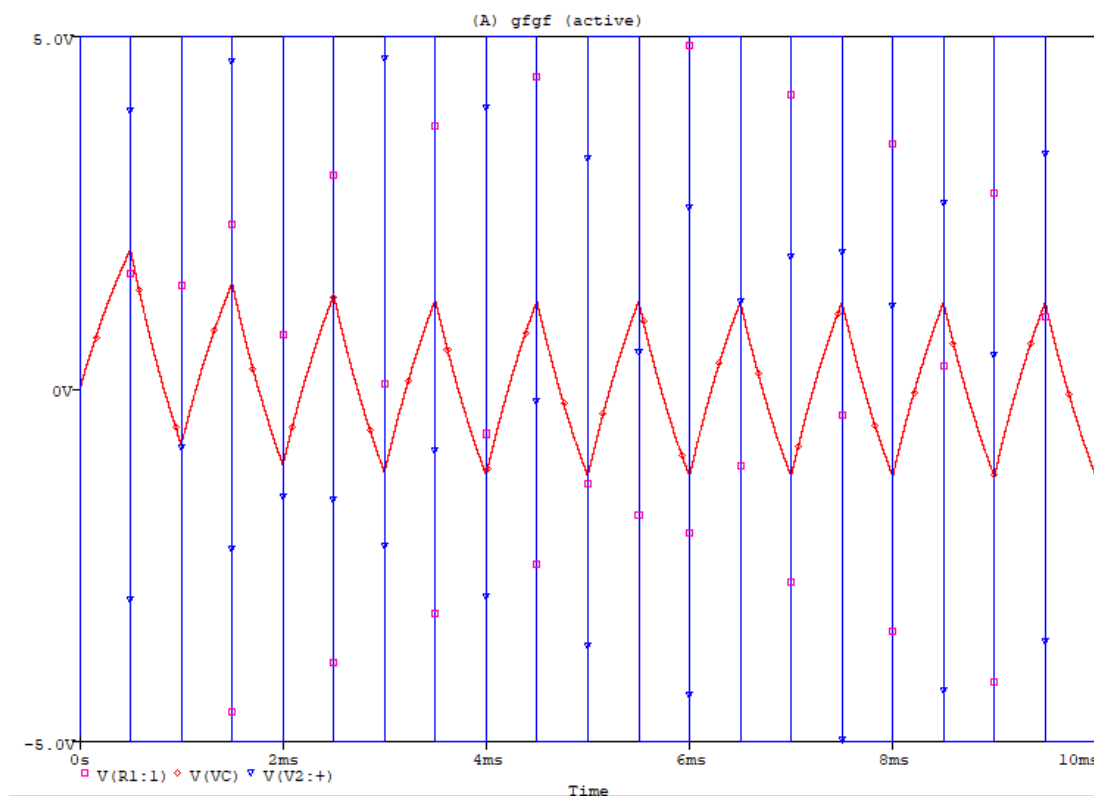
Figure II- 28 input signals and capacitor voltage waveforms

By changing the frequency only of the two sources, the capacitor voltage waveform still generates a triangle waveform which is the integration of the input signal. However, the amplitude of the capacitor voltage waveform changes according to the location of the big resistor. If the big resistor is attached to the high-frequency source, the amplitude of the capacitor voltage waveform is larger in the

comparison of the reverse case. This can be analysed if we model the circuit by laws of static mechanics.

However, the capacitor waveform follows the slowest source. On the other hand, the sides of the triangle waveform which represent the capacitor voltage waveform are not smooth. The shape is like a triangle analogue signal affected by high noise. This gives the indication that the slower frequency source is more dominant.

This can be easily explained from a static mechanics point of view. The value of the resistance can be modelled as the distance from the force source (input source) to the mass (the capacitor in our case). If the source of the force is far from the mass the resultant force is very low. Hence, as the resistor get larger, the effect of the attached source to it will be reduced. This is also shown if the large resistor attached to the slow source as shown in Figure II-29.

In this case, the capacitor frequency follows the quick source because the low resistor is attached to it which models as less distance. The amplitude of the capacitor waveform becomes attenuated following the governing equation of the capacitor which is explained before and shown in Figure II-30.

By changing the amplitude or the shape of the sources, the previous case will be the same as differing in the value of the capacitor voltage based on which source is attached to the lower resistor. Because any alternatives in the shapedwave, amplitude or frequency for the sources will follow the same concept, few cases will be selected as a proof of concept and are shown in the Figures II-31 through II-39.
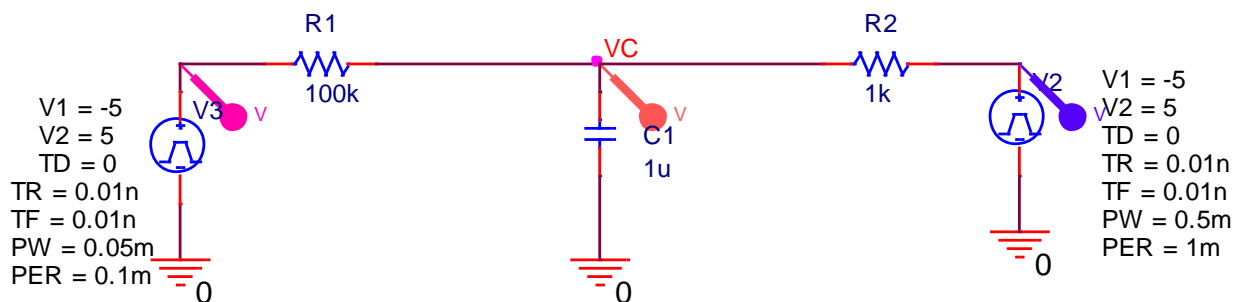
Figure II- 29 Large resistor attached to the slow source
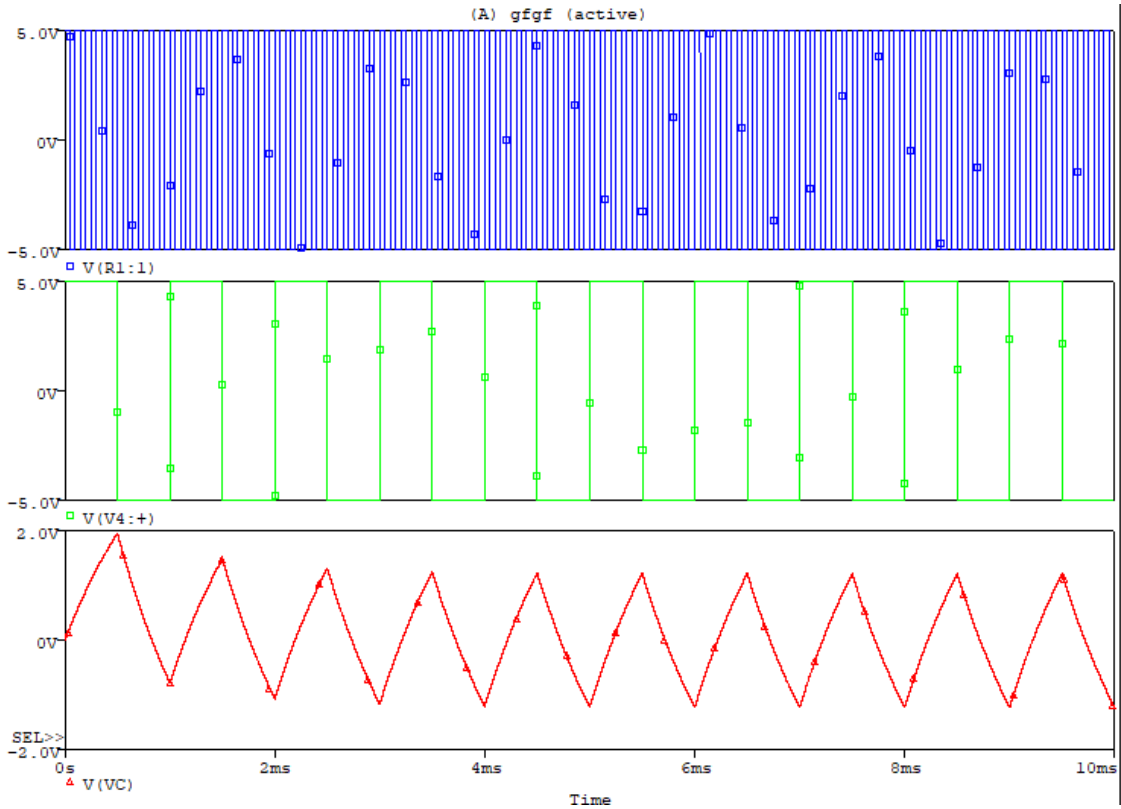
Figure II- 30 Input sources and the capacitor voltage waveform. The capacitor waveform follows the slower source as shown in Figure II-29
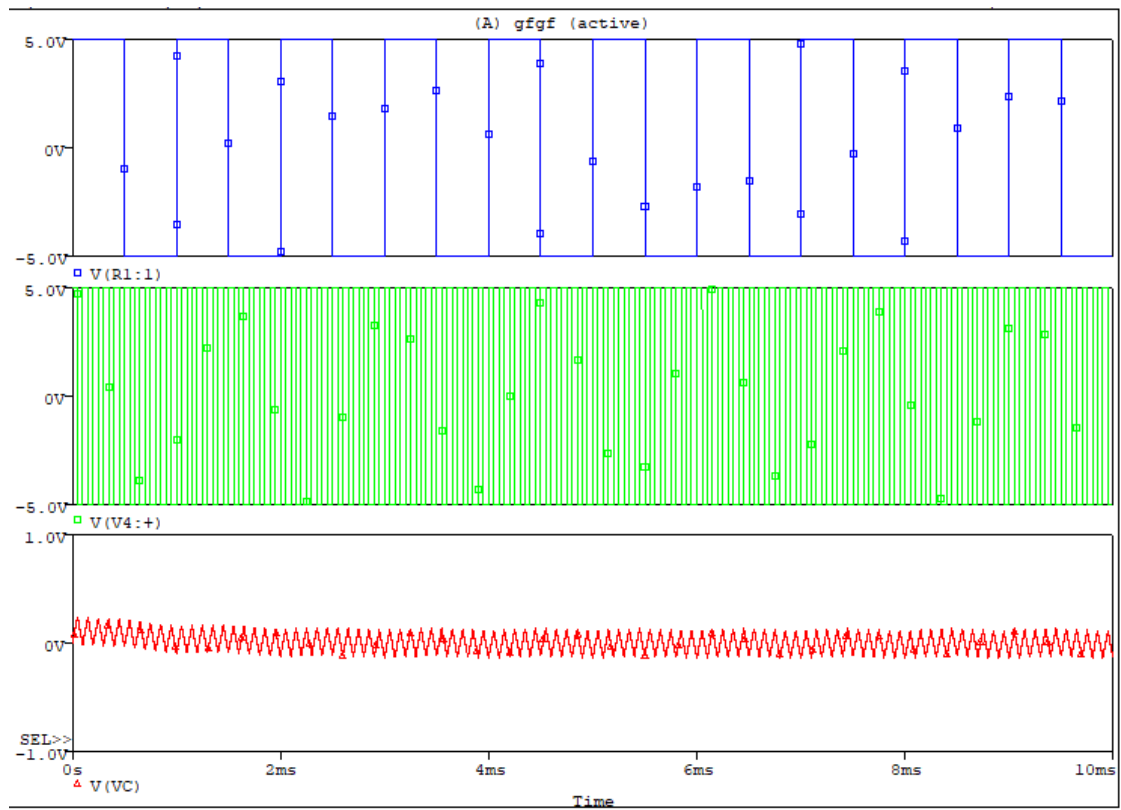
Figure II- 31 Input sources and the capacitor voltage waveform. The capacitor waveform follows the faster source because of the large resistor attached to the slower source
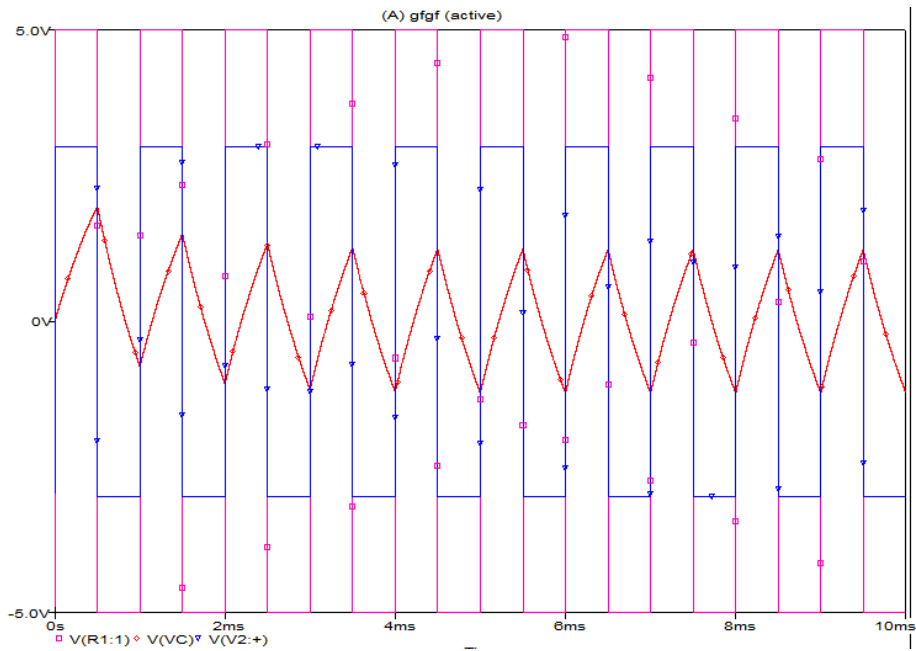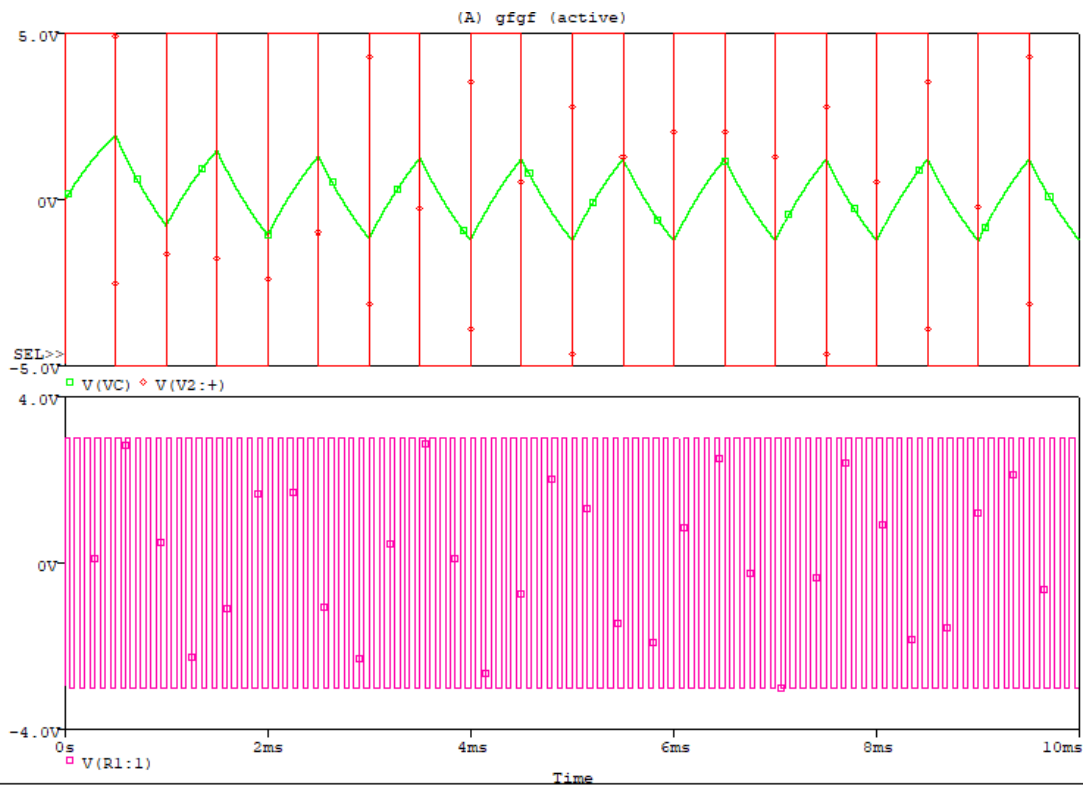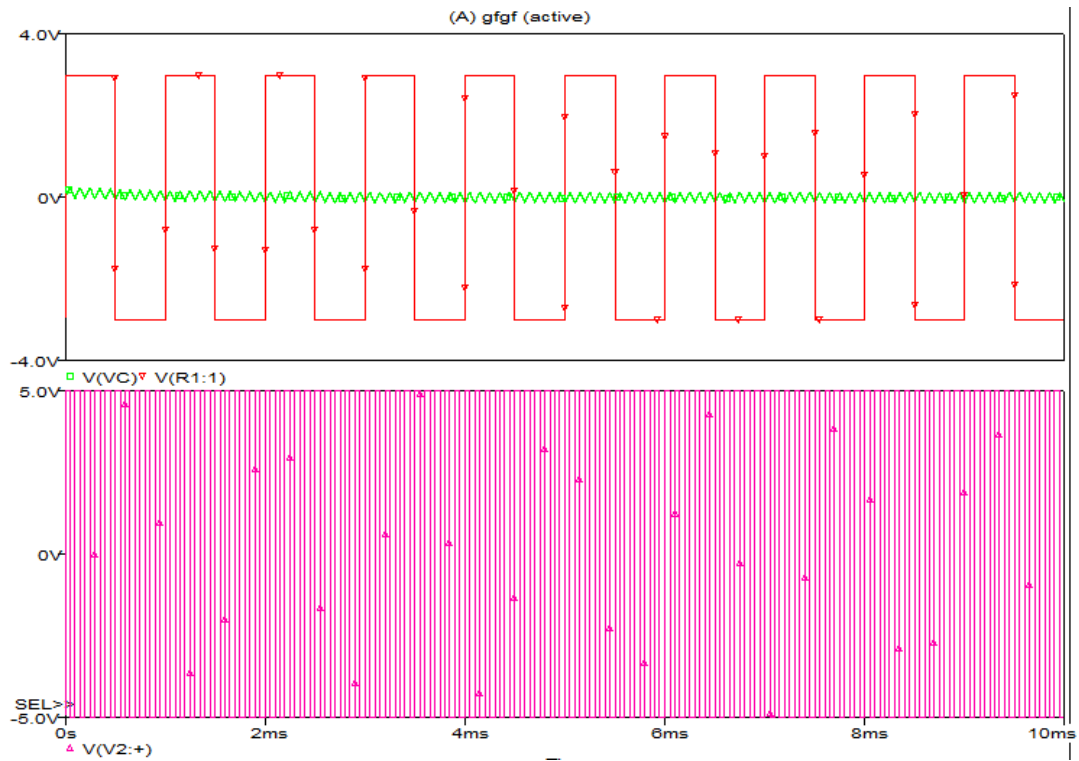
Figure II- 32 Input sources and the capacitor voltage waveform. The two sources have the same shape and frequency while the amplitude is different and the large resistor is attached to the low amplitude source
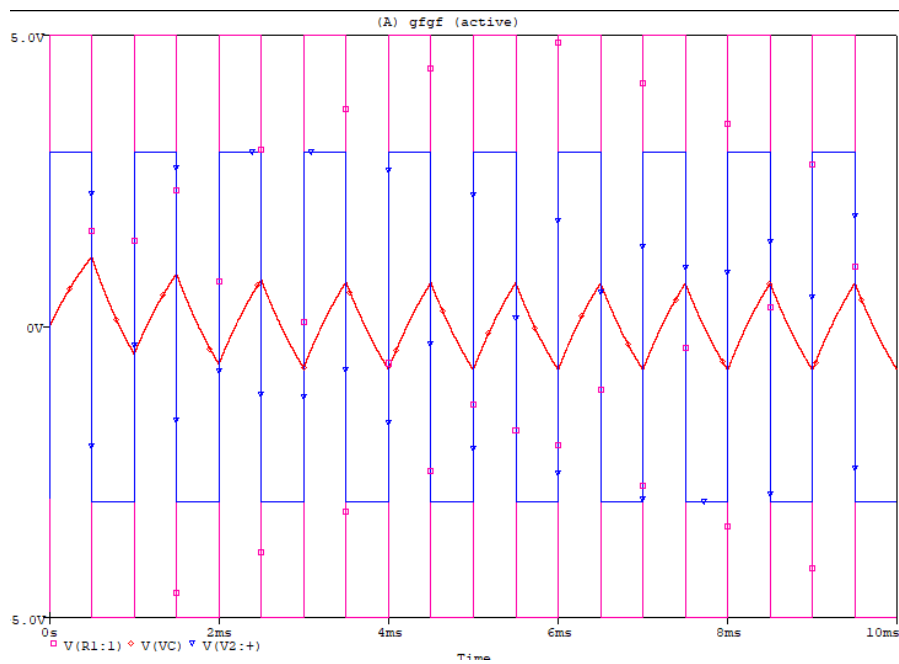
Figure II- 33 Input sources and the capacitor voltage waveform. The two sources have the same shape and frequency while the amplitude is different and the large resistor is attached to the high amplitude source
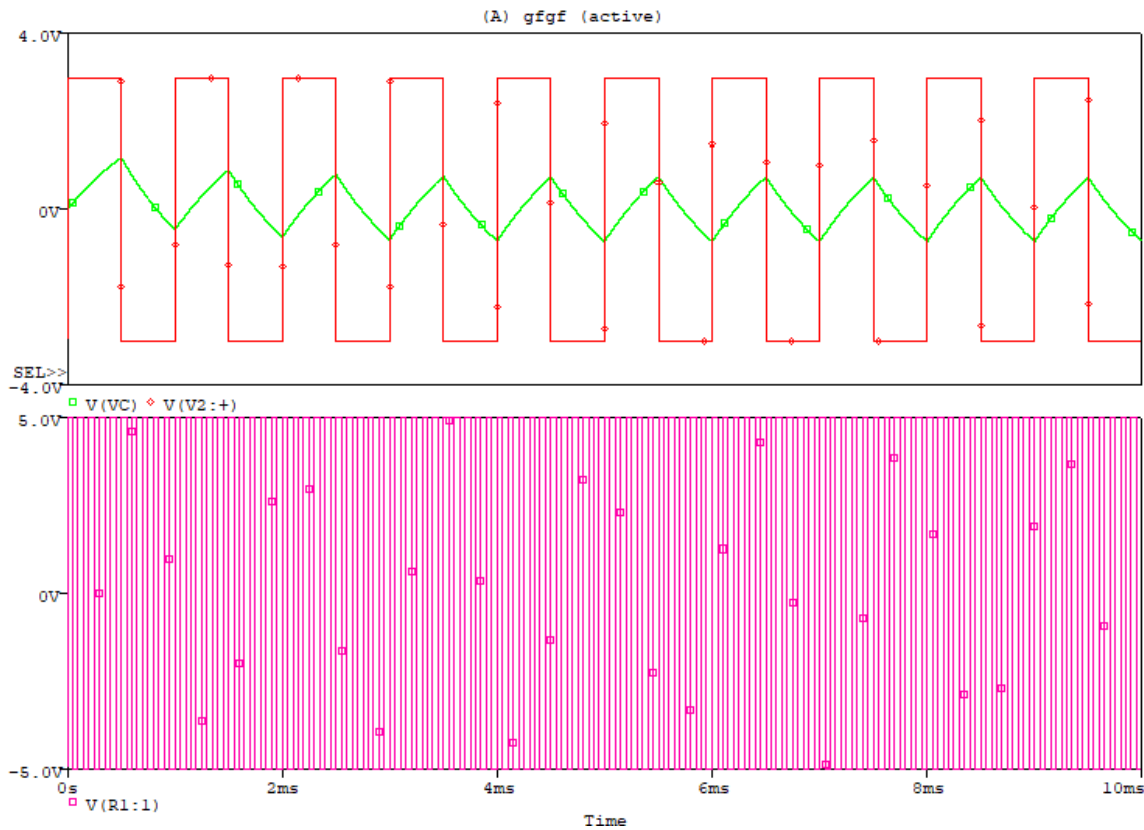
Figure II- 34 Input sources and the capacitor voltage waveform. The two sources have the same shape while the amplitude and frequency are different and the large resistor is attached to the low amplitude high-frequency source

Figure II- 35 Input sources and the capacitor voltage waveform. The two sources have the same shape while the amplitude and frequency are different, and the large resistor is attached to the high amplitude high-frequency source

Figure II- 36Input sources and the capacitor voltage waveform. The two sources have the same shape while the amplitude and frequency are different, and the large resistor is attached to the high amplitude low-frequency source
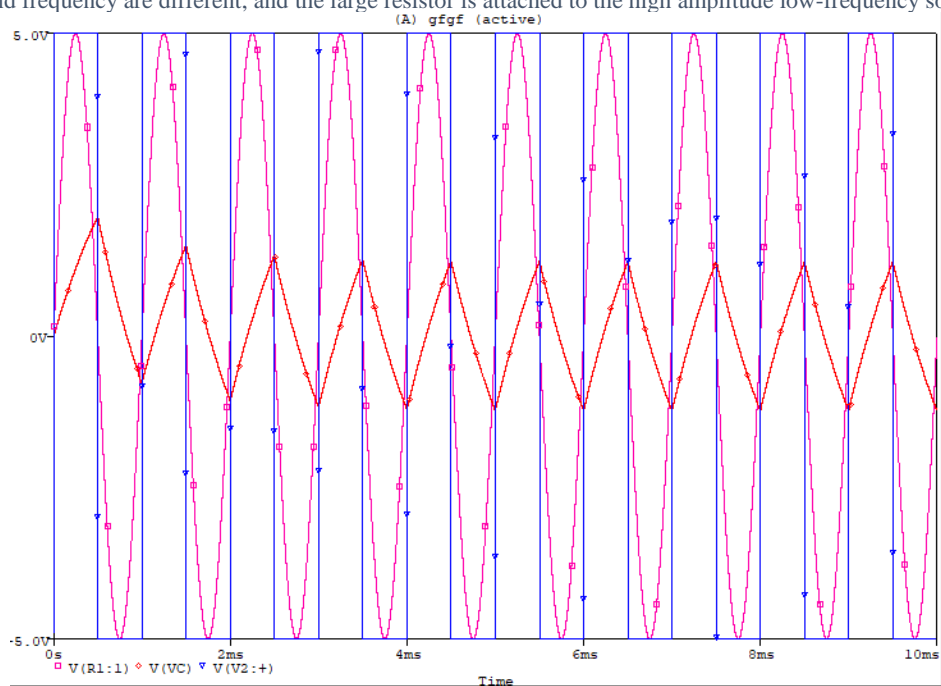
Figure II- 37 Input sources (square and sinusoidal) and capacitor voltage waveform. The two sources have the same shape while the amplitude and frequency are different, and the large resistor is attached to the sinusoidal source

211
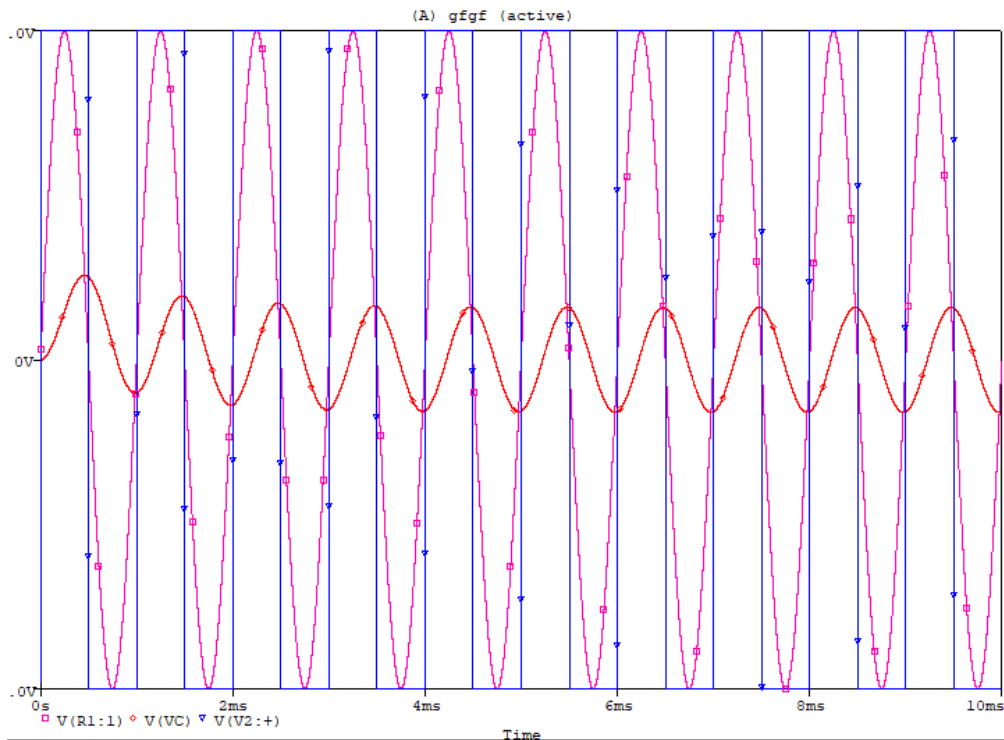
Figure II- 38 Input sources (square and sinusoidal) and capacitor voltage waveform. The two sources have the same shape while the amplitude and frequency are different, and the large resistor is attached to the square wave source
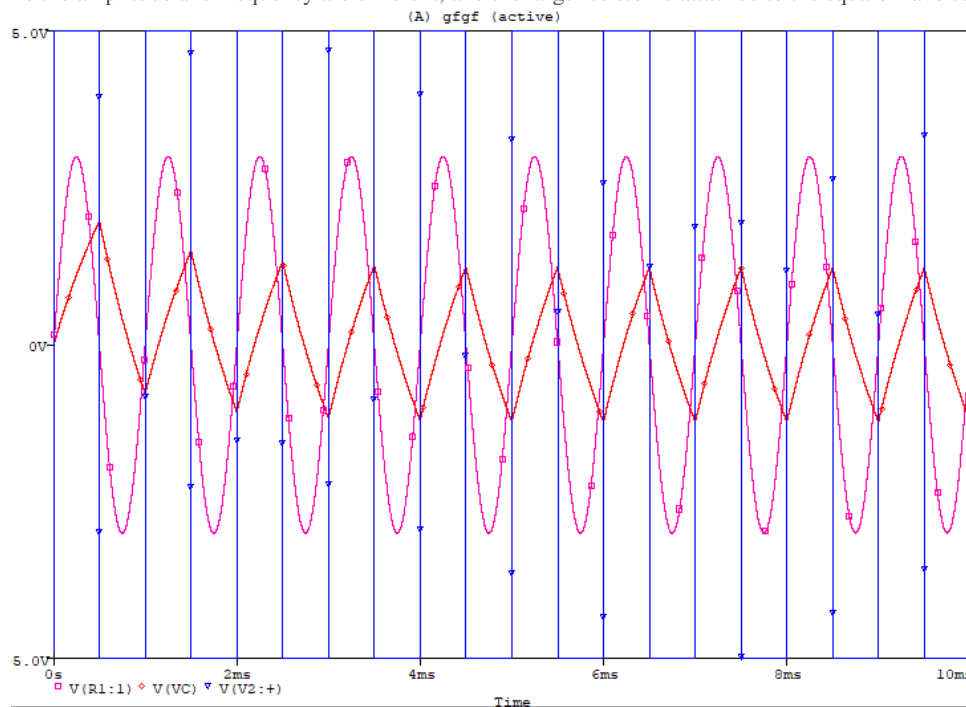
Figure II- 39 Input sources (square and low amplitude sinusoidal) and capacitor voltage waveform. The two sources have the same shape while the amplitude and frequency are different, and the large resistor is attached to the sinusoidal source

Conclusion

In this section, the RCR coupling function between two fixed oscillators has been studied. However, chaotic behaviour was not observed. This was already obvious because the oscillators are fixed and will not change their behaviour or their output waveshape. The

intention of this section is to study the effect of RCR coupling function only without any effect on the oscillators. The analysis of this type of coupling can be modelled based on the Static Physics law as it was shown and gives some requirements for designing a chaotic oscillator based on the coupling oscillator design concept.

11. APPENDIX III: THE REST OF THE CASES IN CHAPTER 5

This section continues the cases mentioned in Chapter 5, which did not show any change in the output pulse width which is based on simulation and/or hardware without mathematical analysis. The target is to show all the possibilities by coupling two oscillators: one is fixed and the other is relaxation oscillator. The results in Chapter 5 and the previous section in the Appendices guide of designing the proposed systems presented in Chapter 6. The results are for the first modification only, because it was shown from the results of the first modification and the analysis of the previous section the general conditions required to couple two oscillators to generate semi-chaotic or irregular pulse width generator by means of waveshaping.

Sinewave

Case "f"

Frequency: 1 kHz

Amplitude: 5V

As the input signal voltage increases, the opamp output follows the frequency of the input and the effect of the capacitance will not change the output frequency. While, in this case, both input and the standalone astable Schmitt trigger opamp have the same frequency, the increase of the amplitude of the input signal is dominant in equation 6 as case c. Hence, the opamp will act as a non-autonomous Schmitt trigger. However, this modification gives more advantage by generating two different waveforms (square and triangle) with one opamp as shown in Figure III-1. This yields the modification to be used for waveform generators, which are used in several applications.
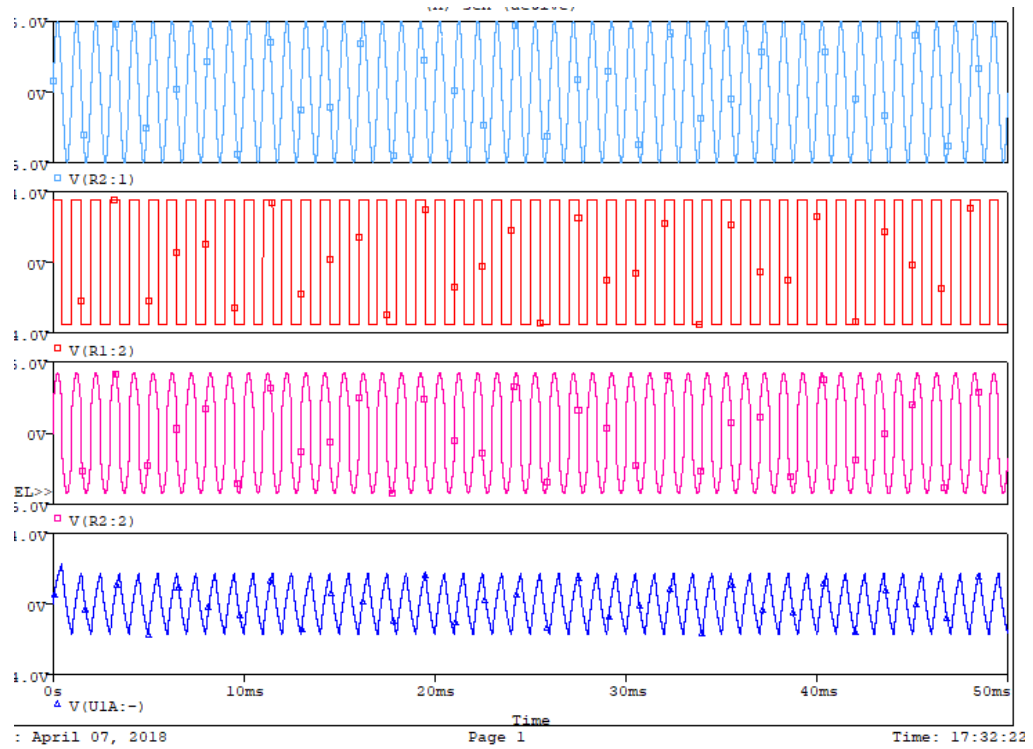
a- Simulation Results
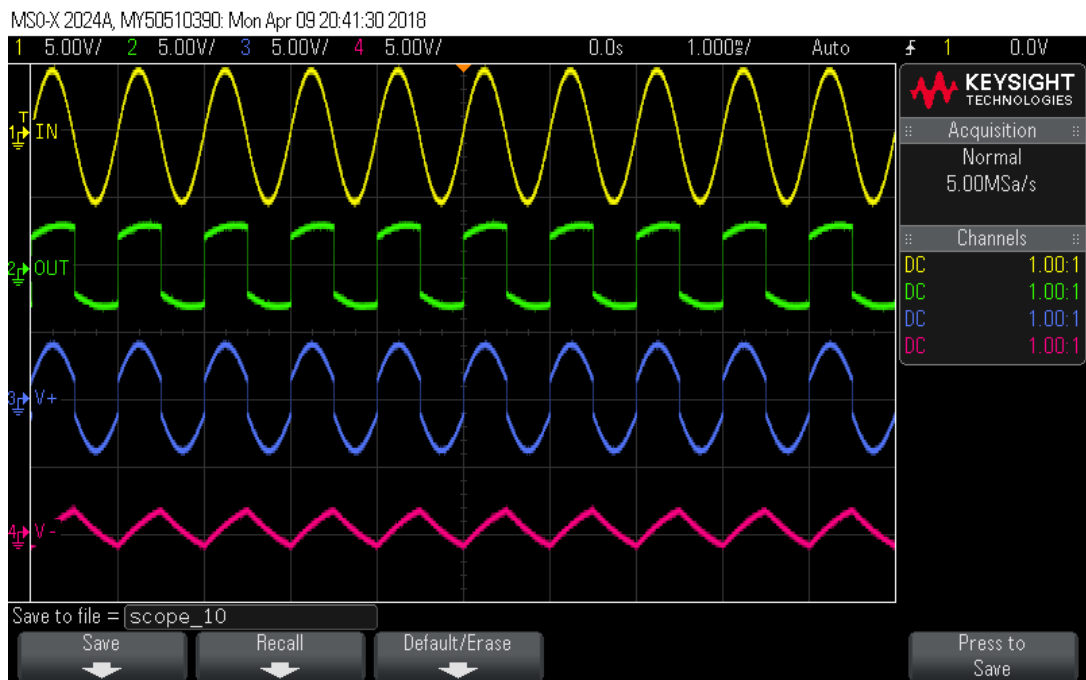
b- Hardware Results

Figure III- 1 Waveform Outputs of Case "f"

215

Case "g"

Frequency: 10 kHz

Amplitude: 1V

As shown in the previous cases, the amplitude of the input signal is very important to reshape the opamp output waveform. In this case, the input signal has less amplitude with high frequency as shown in Figure III-2.
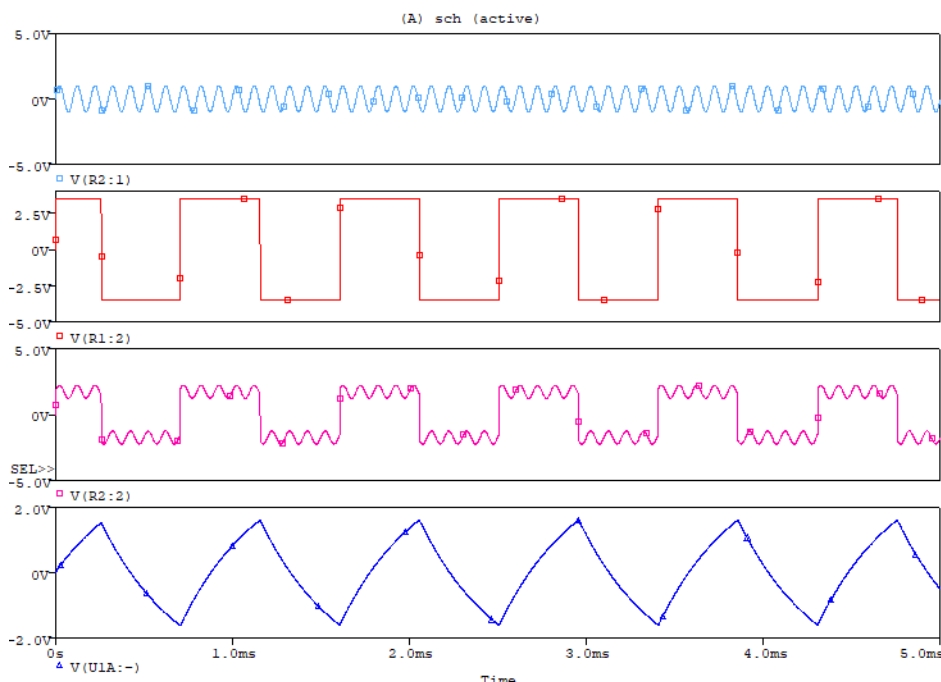
a)   Simulation Results
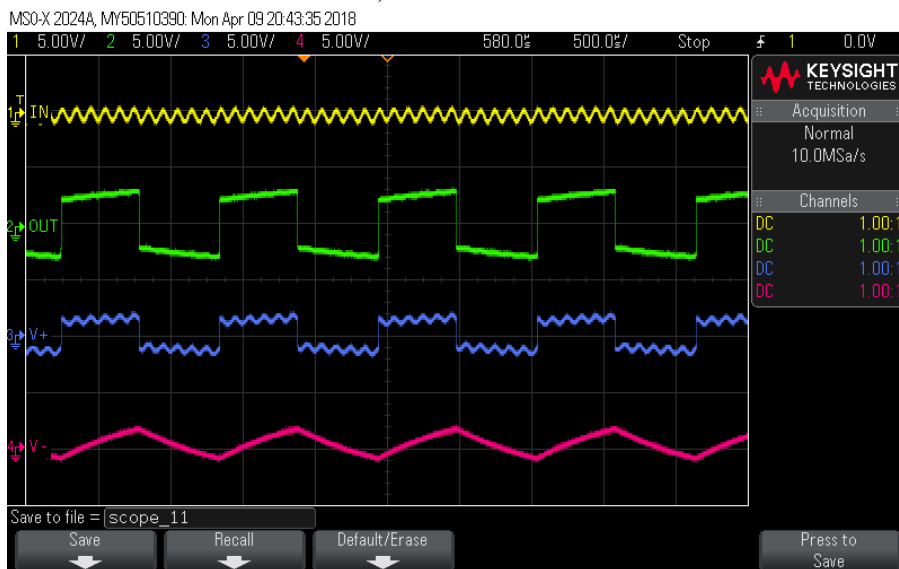
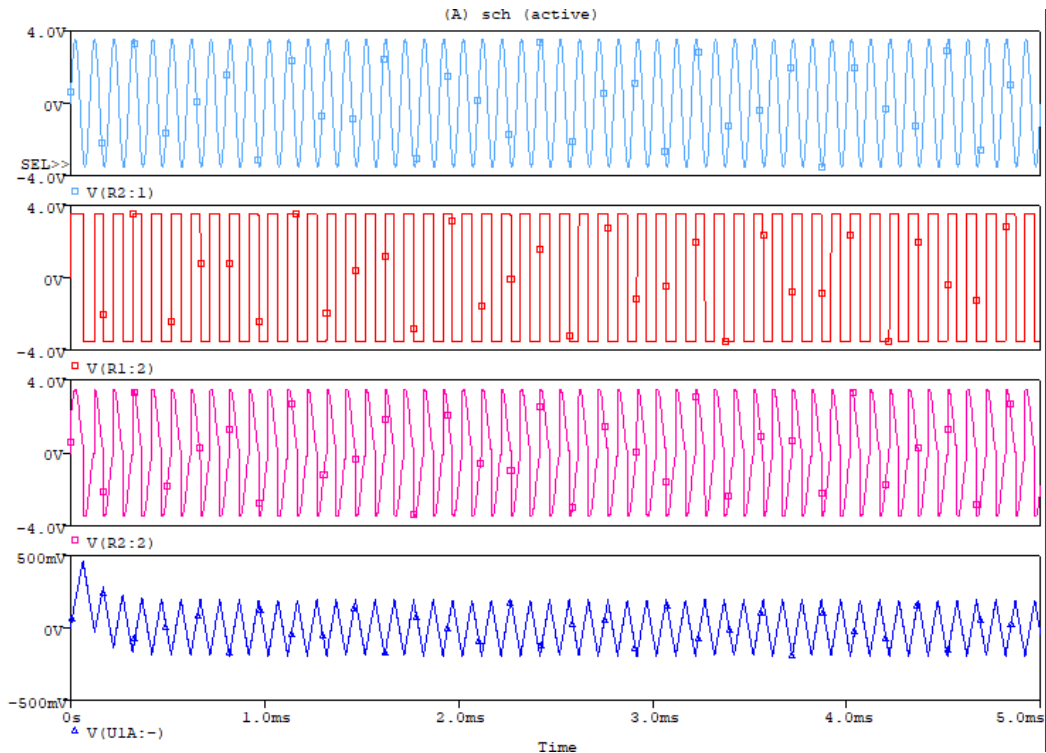a)   Hardware Results

Figure III- 2 Waveform from Case "g"

Recalling equation (6) in Chapter 5 and the observations from the previous cases, the non-inverting terminal waveform will be the same as the standalone astable Schmitt trigger and the input signal will act as a noise for this signal, which can be analysed and predicted. However,

in this case, the higher frequency of the input with low amplitude prevents the opamp output pulse from changing its width.

Case "h"
Frequency: 10 kHz
Amplitude: 3.5V

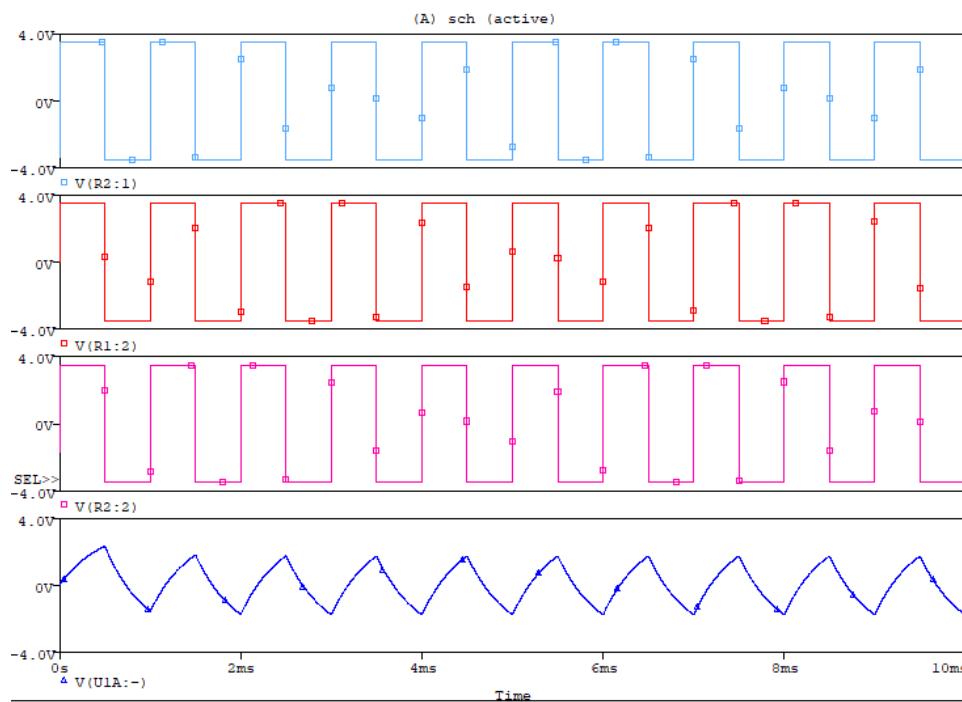a-   Simulation Results
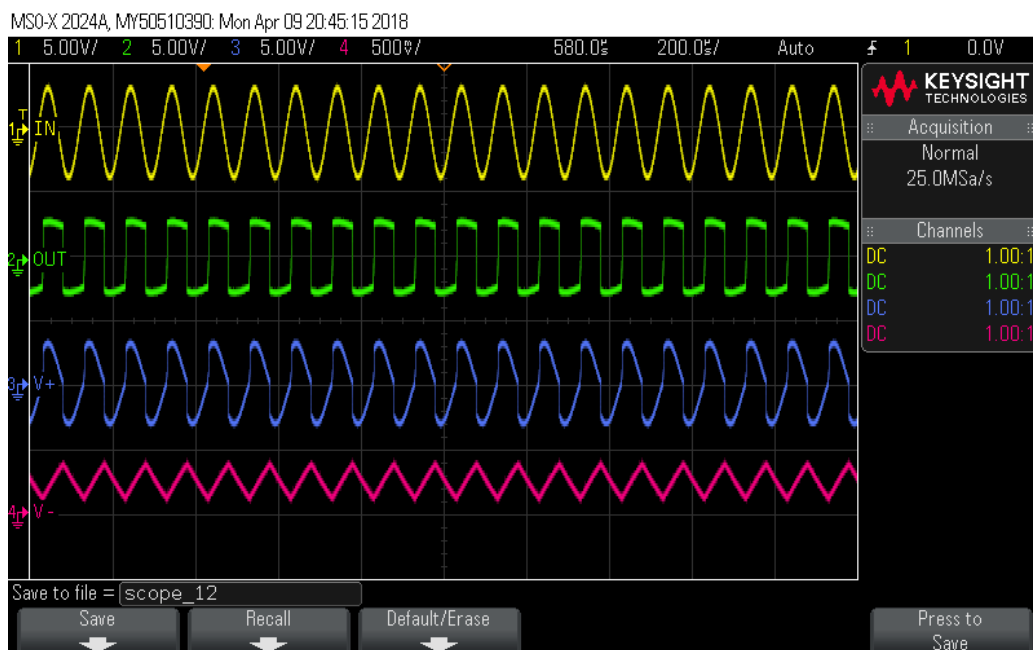
b-   Hardware Results

Figure III- 3 Case "h" results

Case "i"

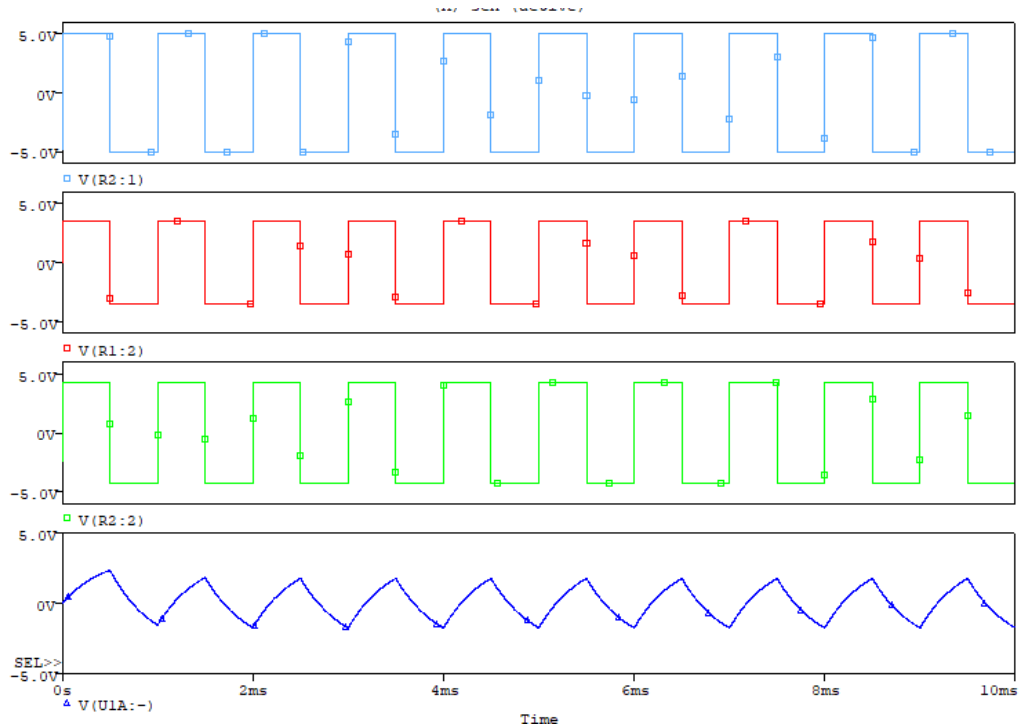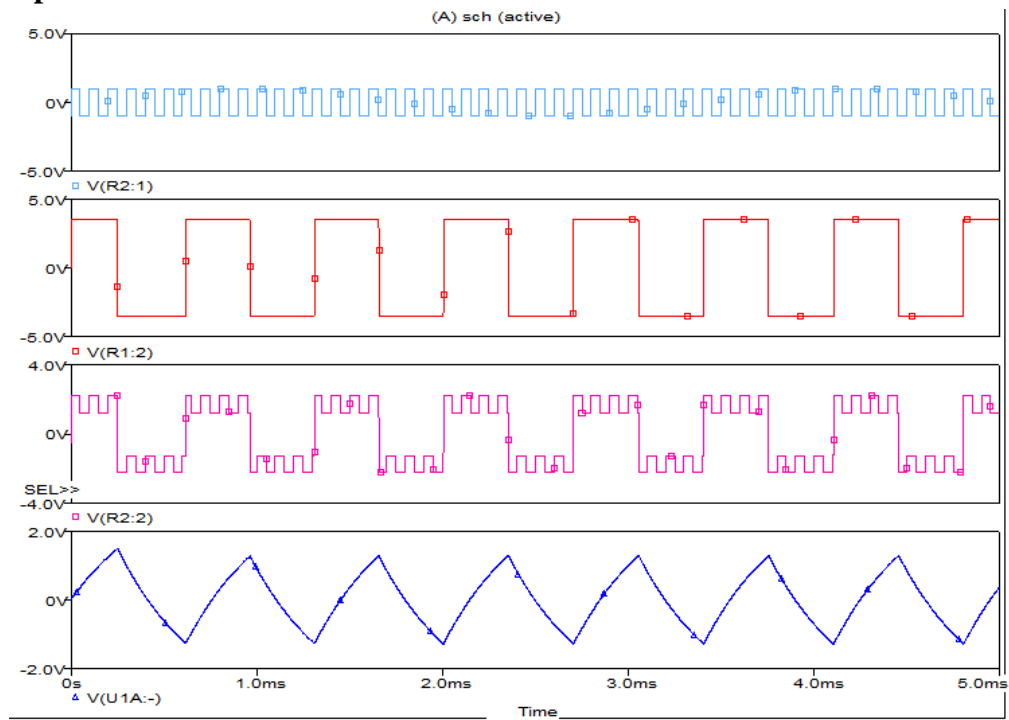**Frequency** :10 kHz
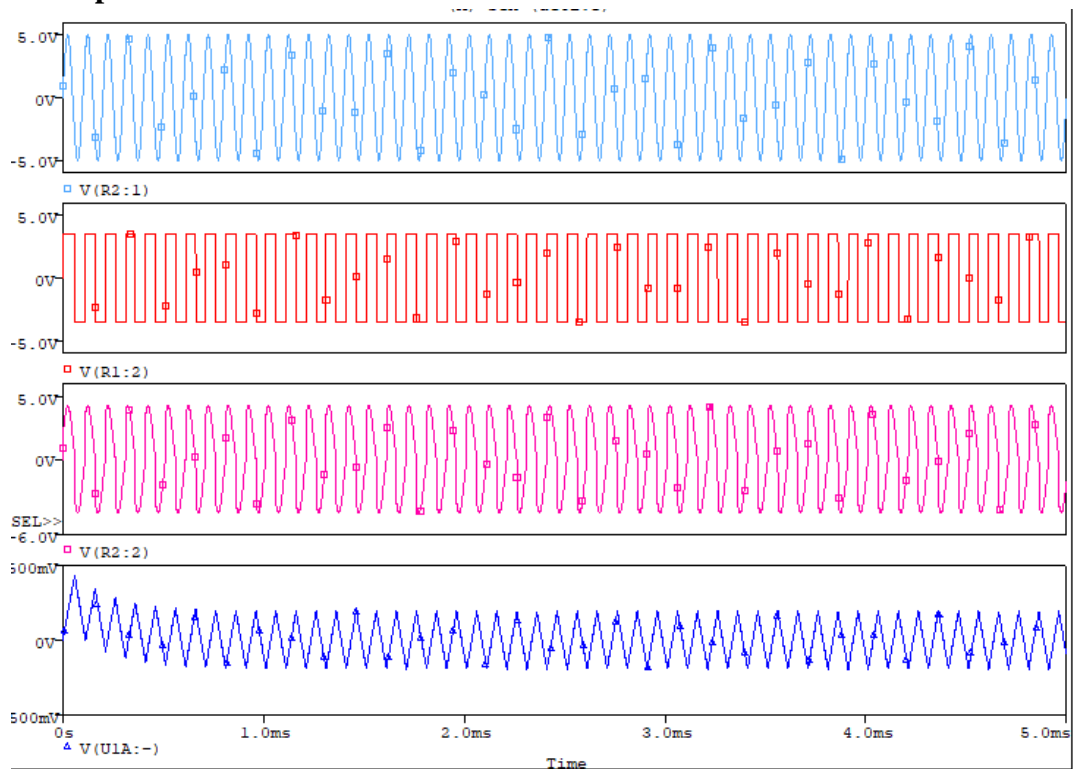
Amplitude: 5V

a- Simulation Results
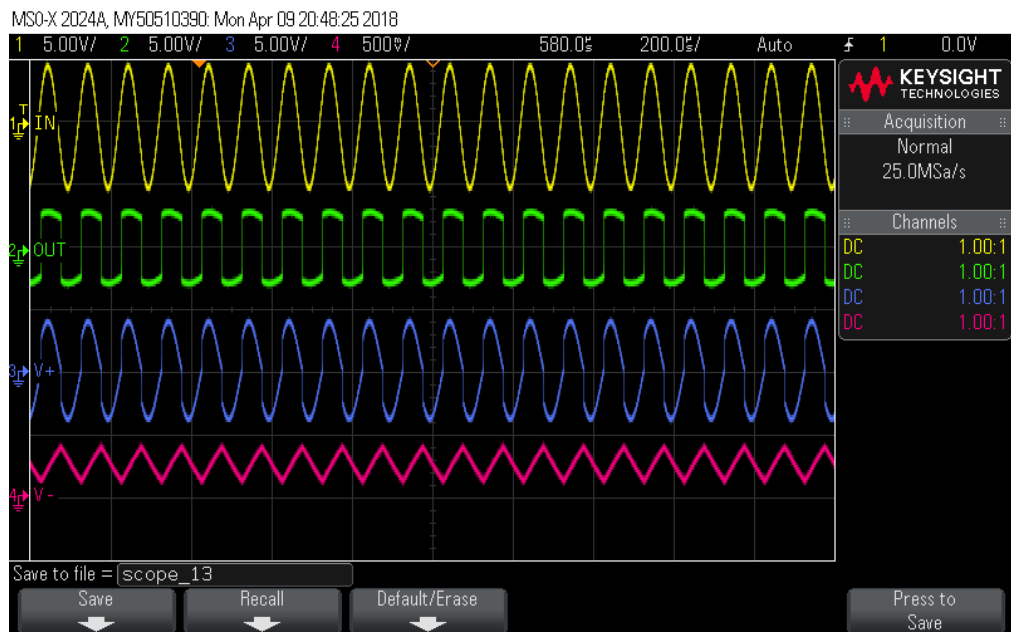
b- Hardware Results

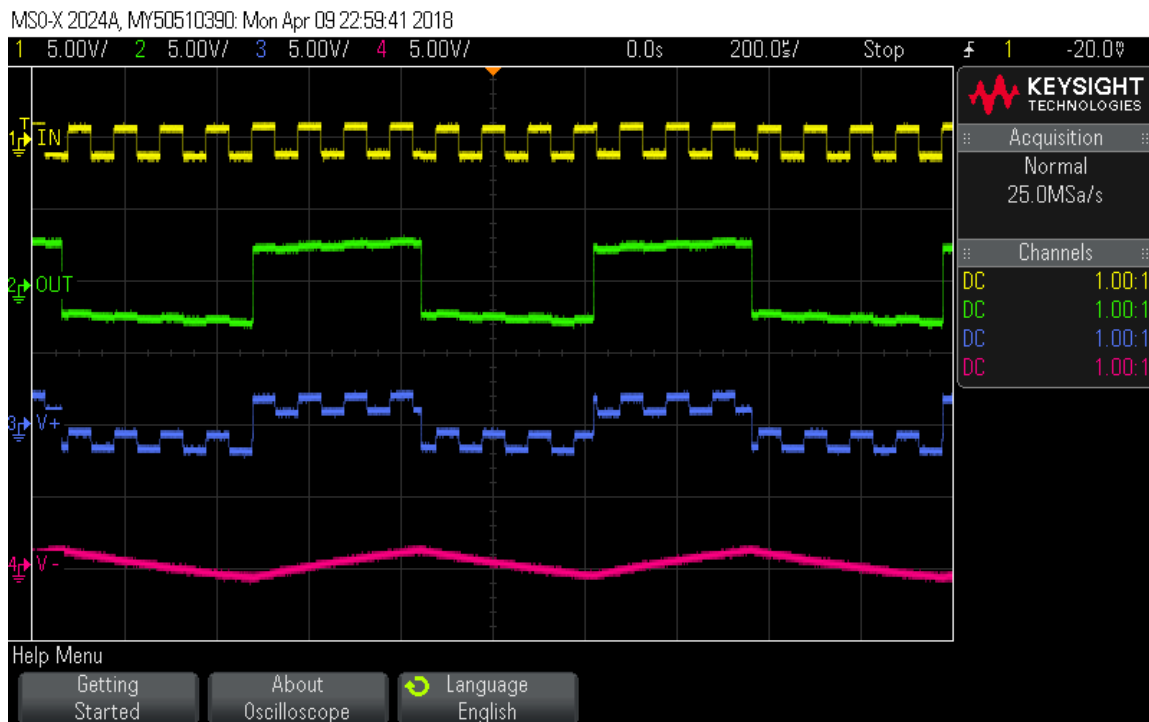Figure III- 4 Case "i" Results

Square

Case "c"

Frequency :100 Hz
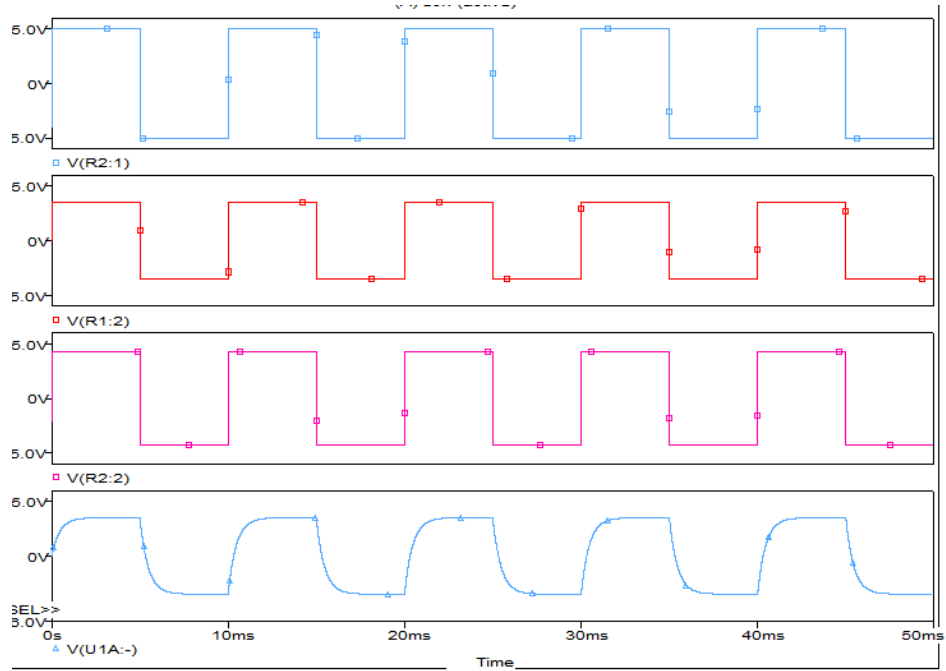
Amplitude:5V

a- Simulation Results
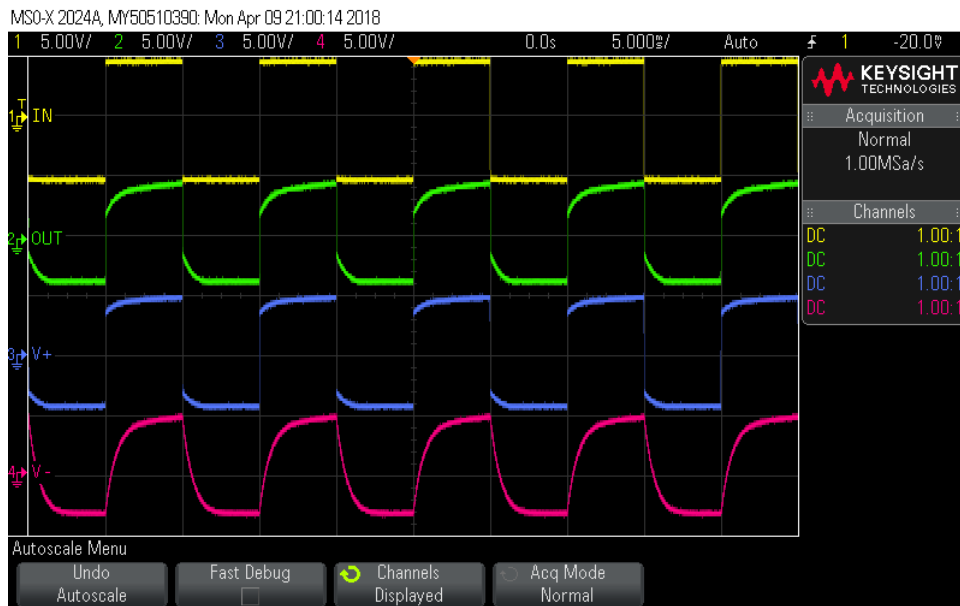
b-Hardware results

Figure III- 5 Case "c" results

Case "d"
Frequency :1 kHz
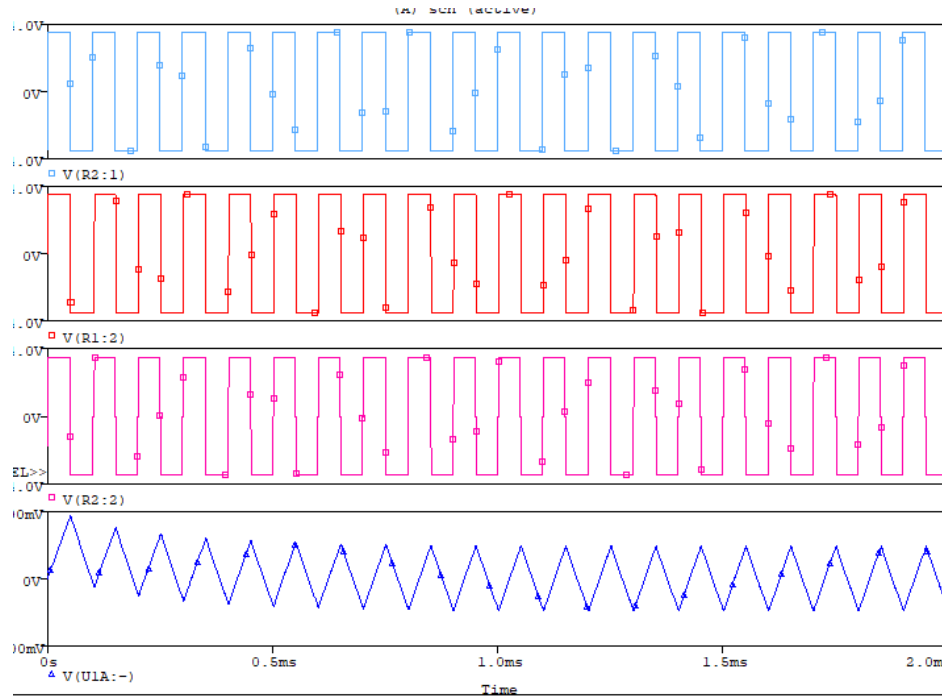**Amplitude**:1V
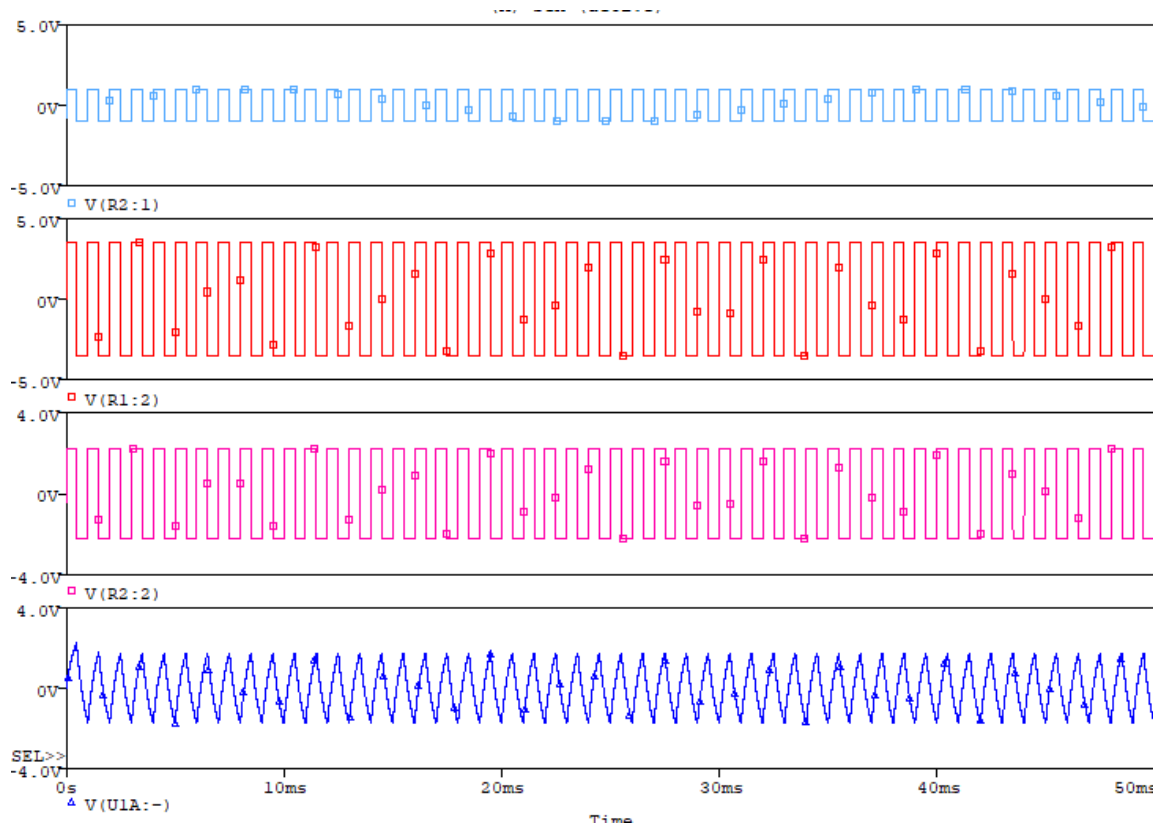
a- Simulation Results

b- Hardware Results

Figure III- 6 Case "d" results

Case "e"
Frequency :1 kHz
Amplitude: 3.5V

a- Simulation Results

b- Hardware Results

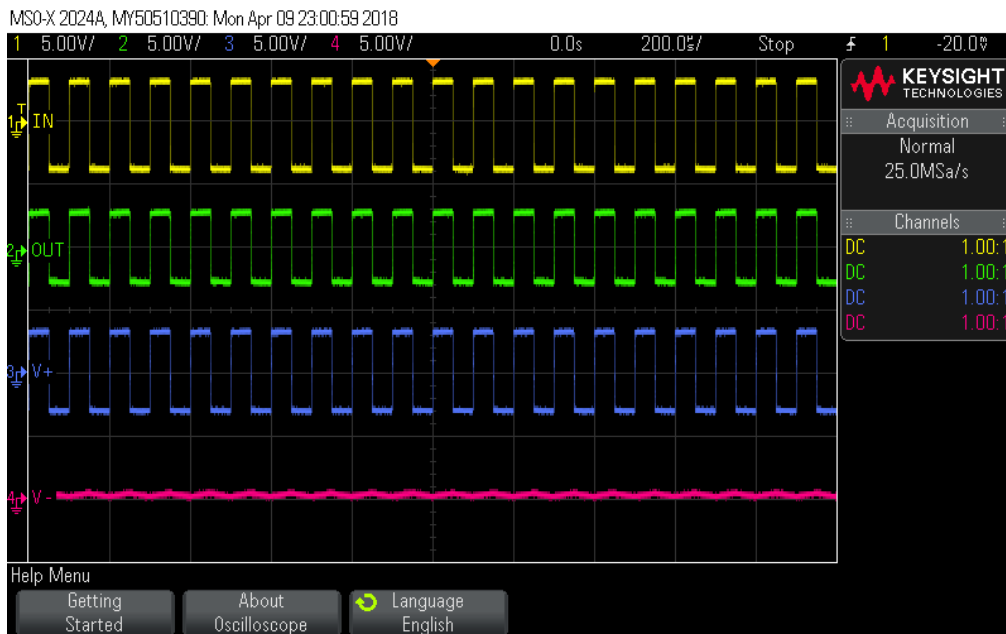Figure III- 7 Case "e" results

221

Case "f"
Frequency :1kHz
Amplitude: 5 V

a-   Simulation Results

b-   Hardware Results

Figure III- 8 Case "f" results

Case "g"

Frequency: 10 kHz

Amplitude: 1V

a- Simulation Results

b- Hardware Results

Figure III- 9 Case "g" results
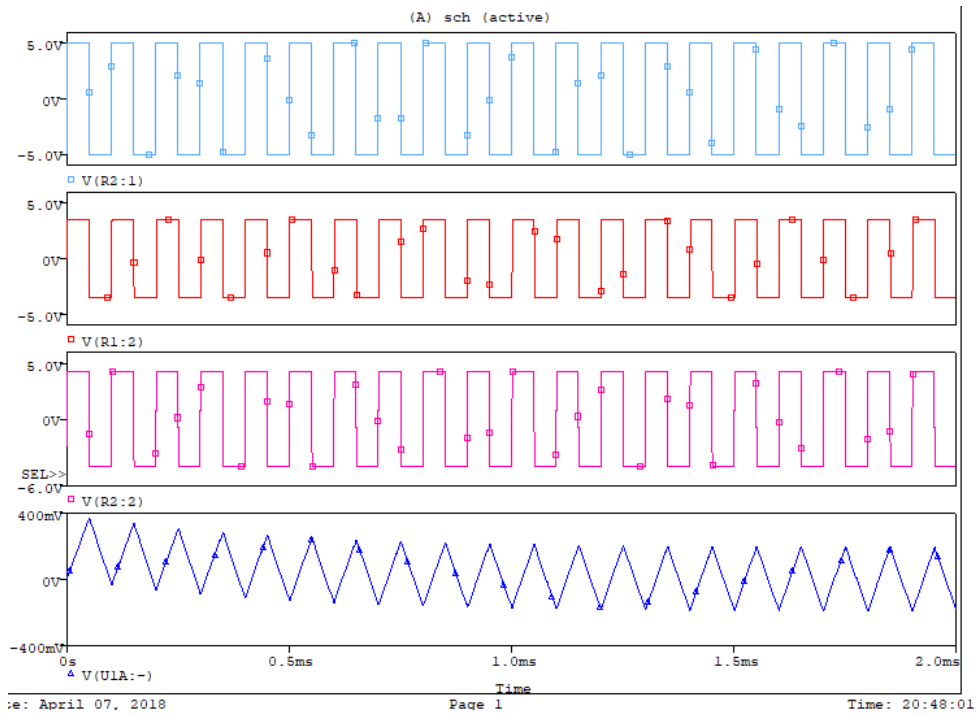
Case "h"
Frequency :10 kHz
Amplitude: 3.5 V

a- Simulation Results

b- Hardware Results
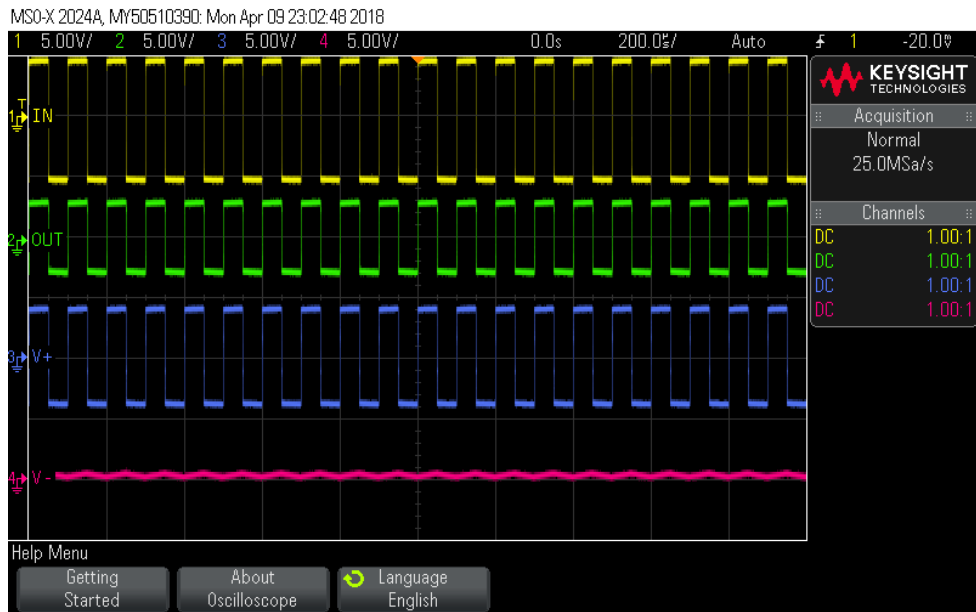
Figure III- 10 Case "h" results

Case "i"
Frequency :10 kHz
Amplitude: 5V

a- Simulation Results

b- Hardware Results

Figure III- 11 Case "i" results